SF7

Forschungszentrum Karlsruhe
Technik und Umwelt

Wissenschaftliche Berichte
FZKA 5702

Long-Term Safety of Radioactive Waste Disposal:

Chemical Reaction of Fabricated and High Burnup Spent UO_2 Fuel with Saline Brines

Final report

B. Grambow, A. Loida, P. Dressler, H. Geckeis, J. Gago, I. Casas, J. de Pablo, J. Giménez, M. E. Torrero

Institut für Nukleare Entsorgungstechnik
Institut für Technische Chemie

März 1996

Forschungszentrum Karlsruhe
Technik und Umwelt

Wissenschaftliche Berichte

FZKA 5702

Long-Term Safety of Radioactive Waste Disposal:

Chemical Reaction of Fabricated and High Burnup Spent UO_2 Fuel with Saline Brines

Final report

B. Grambow, A. Loida, P. Dressler, H. Geckeis, J. Gago[1], I. Casas[2], J. de Pablo[2], J. Giménez[2], M.E. Torrero[2]

Institut für Nukleare Entsorgungstechnik
Institut für Technische Chemie

1 Empresa Nacional de Residuos Radioactivos S.A. (ENRESA), Madrid,
2 Universidad Politecnica de Cataluna (UPC), Barcelona

Forschungszentrum Karlsruhe GmbH, Karlsruhe

1996

Als Manuskript gedruckt

Forschungszentrum Karlsruhe GmbH
Postfach 3640, 76021 Karlsruhe

ISSN 0947-8620

This work was performed in the years 1991-1995 under the contract

FI2W - CT90-0055

with the Commission of the European Communities (Brussels)

ABSTRACT

This is the final report of a large EU-research project on spent fuel stability in saline repository environments. Static dissolution experiments with high burnup spent fuel samples and unirradiated UO_2 were performed for about two years in anaerobic NaCl solutions and deionized water with and without container material (iron) being present. Experiments performed at 25 and 150°C gave similar results. Dissolution rates were similar to those measured in the Swedish, or Canadian program for granite media. Rates are strongly influenced by the specific sample surface area, probably related to the mass balance of consumption and production of radiolytic oxidants. In the competition between the oxidizing effect of radiolysis and the reducing effect of iron, the metal corrosion process dominates. Processes controlling radionuclide release are matrix dissolution, solubility, coprecipitation, sorption phenomena and colloid formation. In the absence of iron release rates of Sr90, Tc99, Np237, Sb125 and at low reaction progress Ru106 were controlled by matrix dissolution whereas concentrations of tetra-, hexa-, and trivalent actinides (U, Pu, Am, Cm) were controlled by solubility or coprecipitation. The presence of iron did effectively reduce the rates of fuel dissolution and the concentration of many, though not all radionuclides. Solubilities of U were similar for unirradiated UO_2 and for spent fuel both in the case of oxidizing and reducing conditions. In contrast, due to the effect of radiolysis, reaction rates of spent fuel were higher than UO_2 dissolution rates.

KURZFASSUNG

Reaktion von hochabgebranntem Kernbrennstoff und von unbestrahltem UO_2 in salinen Lösungen

Dieser Abschlußbericht eines umfangreichen von der EU geförderten Forschungsvorhabens behandelt die Stabilität von abgebranntem Kernbrennstoff in einem Steinsalzendlager. Hochabgebrannter LWR-UO_2-Kernbrennstoff und unbestrahltes UO_2 wurden in statischen Korrosionstests über ca. 2 Jahre unter anaeroben Bedingungen mit NaCl-Lösung und dest. Wasser in Kontakt gebracht, zum Teil in Anwesenheit von Behältermaterial (Fe-Pulver). Versuche bei 25°C und 150°C führten jeweils zu ähnlichen Ergebnissen. Die Auflöseraten des Brennstoffs waren in vergleichbarer Größenordnung wie diejenigen, die im Rahmen von schwedischen und kanadischen Programmen in granitischen Grundwässern gefunden wurden. Es hat sich gezeigt, daß die Raten sowohl von der spezifischen Probenoberfläche stark abhängig sind, als auch mit hoher Wahrscheinlichkeit von Effekten der Massenbilanz von produzierten und verbrauchten radiolytischen Oxidanten. In Konkurrenz zwischen Oxidationseffekten durch Radiolyse und Reduktionseffekten durch das Eisen dominieren die Effekte der Metallkorrosion. Zu den Prozessen, die die Freisetzung von Radionukliden kontrollieren, gehören die Auflösung der Matrix selbst, Löslichkeit, Mitfällungs- und Sorptionsphänomene und Kolloidbildung. Bei Abwesenheit von Eisen werden die Raten der Freisetzung für Sr90, Tc99, Np237, Sb125 und bei niedrigem Reaktionsfortschritt auch Ru106 vom Auflösungsverhalten der Matrix kontrolliert, dagegen werden die Konzentrationen von vier-, sechs- und dreiwertigen Aktiniden (U, Pu, Am, Cm) durch Löslichkeits- und Mitfällungsphänome bestimmt. Bei Gegenwart von Eisen sind die Raten der Brennstoffauflösung deutlich verringert und die Konzentrationen fast aller Radionuklide erheblich reduziert. Die Löslichkeit von U ist ähnlich bei unbestrahltem UO_2 und abgebrannten Brennstoff bei oxidierenden wie auch bei reduzierenden Bedingungen. Dagegen sind die Reaktionsraten für abgebrannten Brennstoff auf Grund der Radiolyseeffekte höher als bei UO_2.

LONG - TERM SAFETY OF RADIOACTIVE WASTE DISPOSAL

According to German nuclear waste management regulations, high-level radioactive waste products such as HLW-glass and /or spent fuel shall be disposed in deep geological formations. The release of hazardous quantities of radionuclides from the repository into the biosphere shall be excluded for all future. For this purpose several in part independent barriers ("multibarrier concept") shall limit the transport of ground water to and from the waste and shall also reduce the mobility of radionuclides by retention within stable waste matrices, by remineralization and sorption processes. The innermost barrier is an engineered system consisting of the waste form "high-level waste glass" or "spent nuclear fuel", the packaging material (e.g., steel container) and the backfilling material (e.g., salt chippings, clay, apatite). In addition, geoengineered barriers (e.g.,filling material, dams) and the geological barrier (host rock, overburden) contribute to safety by delaying the transport of the radionuclides (e.g., by sorption). Without comprehensive knowledge of the performance of each of the various barriers under disposal conditions long-term safety of the repository cannot be guaranteed.

Performance of the engineered barrier system

Experimental programs are currently under way at our research center (FZK-INE), aiming at performance assessment of glass and spent fuel as barriers for radionuclide immobilization. The dissolution or corrosion behavior of the waste forms and the containers is studied in order to evaluate the potential mobilization of radionuclides, the subsequent reimmobilization within newly formed mineral phases (secondary reaction products) or by sorption on surfaces of host rock or engineered materials. The waste form corrosion behavior is studied in conjunction with basic studies on the chemistry (solubility, complexation, coprecipitation...) of important radionuclides (in particular the actinides) in repository relevant aqueous solutions (deep groundwaters, brines). For assessing of the performance of the engineered barrier system, dissolution, remineralisation and migration phenomena must be analysed in the context of an integrated geochemical model. Results obtained in this research project were and will be published in a number of FZKA-reports (previously KfK-reports) related to the subject of "long-term safety of radioactive waste disposal".

The corrosion behavior of real high radioactive waste products and container materials is studied under repository relevant conditions. Waste products currently under investigation are

- high-level waste borosilicate glass R7T7, similar in composition to the COGEMA produced HAW-glass for the German base load customers,
- high burnup UO_2 fuel (burnup > 50 MWd/kg U) from the Biblis and Gösgen (Switzerland) nuclear power plants.

Principal container materials studied include

- thick fine grained carbon steels (corrosion allowance concept)
- thin Ti0.2Pd alloys (corrosion resistant concept)

The behaviour of the waste forms in contact with solutions is evaluated on the basis of the type and amount of radionuclides released to solution and gas phase and the structural change of the solid phases (e.g., decomposition of the microstructures, formation of secondary phases). Corrosion mechanisms, rate laws and processes governing release of individual radionuclides (sorption, coprecipitation, solubility, etc.) are to be determined. Container corrosion is evaluated on the basis of corrosion rates, mechanism and corrosion products. The effect of simoultaneously corroding container materials and of waste forms is investigated inserting container materials in the glass and spent fuel corrosion experiments.

Our work serves the purpose of developing models by means of which the contribution of the engineered barrier system to repository long-term safety can be assessed. The significance of individual experimental observations can only be evaluated in the general context. The relevance of laboratory findings for the natural system must be assessed as well as the validity of the models developed.

General objective and scope of the project.

The research program aims at characterization and qualification of the chemical durability of unprocessed high burnup UO_2 spent fuel as a final waste form for disposal sites in salt formations. The reaction behavior of the fuel with saline brines is going to be studied as a function of time, temperature, redox potential and surface area in order to give insight into the corrosion mechanisms and sources of radionuclide release. Additionally the solubility of unirradiated UO_2 in salt brines is studied for comparison with the reaction behavior of the irradiated material in order to identify radiolysis and burnup effects and in particular to identify and quantify solubility effects in the degradation of the fuel matrix. Eventually, the ongoing work will provide a basis for modeling, bridging over the gap between experimental results and performance assessment for long-term storage of the fuel in a repository in salt formations in case of brine intrusion.

Work program

I. General preparations, analytical techniques and sample preparation

II. Characterization of the durability of spent UO_2-fuel in saturated salt brines

III. Solubility tests with unirradiated UO_2

IV. Modeling of the reaction behavior of spent fuel with salt brines

SUMMARY

For the assessment of the potential performance of directly disposed spent fuel in a nuclear waste repository in salt formations the chemical reactions of the fuel with possibly intruding saline brines must be understood and the associated radionuclide release must be quantified. In this context a large research project has been conducted, combining experimental approaches (in particular leach or corrosion tests) with modeling techniques. It is very well known that spent fuel is a rather heterogeneous material with the degree of heterogeneity increasing with burnup and linear power rating. A rather high burnup/high linear power spent UO_2 fuel rod of 50 MWd/kgU was conservatively selected in our study representing the various LWR-fuel types expected to be disposed off in a first high level nuclear waste repository to be openend in may be 20 years. For comparison experiments were also performed with as fabricated UO_2.

Static dissolution experiments of pre-washed spent fuel samples were performed for about two years in anaerobic NaCl solutions and deionized water at room temperature. Experiments performed at 150°C gave similar results to those obtained at room temperature, clearly demonstrating the suitability of low temperature tests for assessing spent fuel behavior over large ranges of temperature, as expected in a final repository.

Important insight into the dissolution behavior of spent fuel has been achieved, applicable not only to saline media but as well to clay and granite conditions. Spent fuel dissolution rates in anoxic saline solutions were found to be similar to the rates measured in the Swedish, or Canadian program for granite media. It has been shown for the first time that there is a strong influence of the ratio of sample surface area to solution volume (S/V) on spent fuel reaction rates. This parameter must be well chosen when scaling laboratory data to repository relevant conditions. By dissolving mm sized fragments in large volumes of solution, possible saturation effects were avoided and intrinsic fuel matrix dissolution rates of 0.3% of the inventory per year were measured, corresponding to upper limits of surface area normalized rates of about 5-20 $mg/(m^2d)$. Surface area normalized reaction rates were significantly lower when using fine grained fuel powder (sample surface area to solution volume ratio (S/V) > 3000 m^{-1}).

The dependency of reaction rates on S/V was rationalized by radiolysis effects. At high S/V ratios, molar fuel dissolution rates were found to be similar to the molar rate of radiolytic production of oxidants. This indicated that the mass balance of consumption and production of oxidants may be of key concern in predicting long-term spent fuel performance in a repository. A decrease of reaction rates with time was only observed when using fuel pellets, no decrease was observed with powders or fragments. The decrease in reaction rates of fuel pellets may be explained by diffusion controlled reaction of pellet fracture surfaces.

Processes that were found to control radionuclide release are solubility and coprecipitation phenomena, sorption on sample or reaction vessels or the dissolution kinetics of the fuel matrix. It depends strongly on the chemical nature of the nuclide and on environmental conditions, which of these processes is dominant. Important parameters studied include beside S/V also pH and redox conditions. The pH in the solutions during the progress of the reaction remained neutral to slightly alkaline. Eh values were reduced with respect to air saturated waters. Eh values are lower in tests using NaCl solutions than in tests using deionized water as a leachant. Highest pH values (9.6) and lowest Eh values (<-300mV) were measured in the presence of iron as an additive to the corrosion test. No acidifying or oxidizing effect by radiolysis on the solution pH and Eh values was observed.

The formation of the radiolysis gases oxygen and hydrogen was observed, in quantities proportional to the spent fuel sample mass, independently on the surface area of the sample. We conclude that the radiolysis gases are mainly produced by gamma radiation. In the presence of iron, no oxygen was observed in the gas phase, indicating that the proceeding corrosion reaction effectively removes radiolytic oxygen. Hence, in the competition between the oxidizing effect of radiolysis and the reducing effect of iron, the metal corrosion process is dominant. Nevertheless, even in an overall reducing environment, in close vicinity to the dissolving spent fuel surface, a thin steady state oxidation fronts may persist, due to α-radiolysis.

Due to the heterogeneous nature of the fuel, radionuclide release for various locations must be described explicitly: for segregated phases (e.g. the well known metallic ε-phase), for radionuclide accumulations at grain boundaries and fracture surfaces, for the UO_2 matrix at

various radial positions (including the highly burned porous rim). Nuclide specific maximum contributions to overall radionuclide release of fracture and grain boundary surfaces, segregated phases and the rim region were determined.

As expected, preferential release of Cs134/137 was observed, representing release of Cs accumulations on fracture surfaces and grain boundaries. These data are relevant to the assessment of the long-term release behavior of Cs135 in a repository. About 2-3% of the Cs inventory of the fuel was found associated to pellet fracture surfaces in a highly mobile form and about another 2-4% was associated to grain boundary surfaces contributing to long-term Cs release rates significantly higher than those of all other elements analyzed in the corrosion solutions. It should be mentioned that this high fractions of the inventory are directly related to the high burnup and the high linear power of our fuel and are not typical for the average fuel expected to be disposed off in a first nuclear waste repository.

Sr90 release data were found to be useful in indicating the degradation of the fuel matrix. The experimental data show that only a small fraction of Sr90 (less than 0.03% of the inventory) has been accumulated at grain boundary surfaces possibly contributing to fast initial Sr release from the fuel. Release of Tc99, Np237, Sb125 and at low reaction progress Ru106 occurred in many cases with a similar rate than that of Sr90. Hence, releases of these elements are controlled by the kinetics of the degradation (oxidation, dissolution) of the fuel matrix, even though that Tc99 and Ru106 are concentrated in the metallic state in the ε-phase. We conclude that the ε-phase reacts readily with the solution.

It is sometimes discussed that preferential radionuclide release may occur from the highly burned rim region of the fuel[1]. This region shows higher nuclide inventories and porosity and specific surface area is higher. Dissolution results of a small rim sample show that the contribution of the rim region to overall radionuclide release from a fuel rod will be less of 2% of the total nuclide release from a fuel pellet.

In order to understand radionuclide release upon spent fuel dissolution one must further consider the various sinks involved. Radionuclides, initially mobilized by the

[1] Matzke, H.J., Journal of Nuclear Materials, **189** 141-148 (1992)

dissolution reaction may in many cases be reimmobilized immediately in newly formed secondary phases. For example, concentrations of actinide and rare earth elements are not controlled by the rate of fuel matrix dissolution but by a combination of sorption, precipitation and coprecipitation phenomena. At low reaction progress values, far away from solubility limits, the solution concentrations of the elements U, Pu, Am, and REE were significantly lower than anticipated from the extent of fuel matrix dissolution, indicating sorption and/or coprecipitation controls. On the other hand, at high reaction progress, the maximum concentrations of Pu and U ever reached in any of our tests are close to reported solubility limited concentrations in pure 5m NaCl solutions. Maximum concentrations of Am241/Am243 remain about five orders of magnitude lower than the solubility limit of pure $Am(OH)_3$.

The presence of iron, simulating the effect of a corroding container, did effectively reduce the rates of fuel dissolution and the concentration of many, though not all radionuclides. Fuel matrix dissolution rates were reduced by about a factor of 3-4. Pu and U concentrations in the leachate are likely controlled by tetravalent oxides or hydroxides. Concentrations of Am and other trivalent elementes were found to be controlled by sorption processes on the surface of iron corrosion products. Solution concentrations of Am and Pu became close to the ICRP61 limits of ingestion by workers.

Even in highly saline environments colloids play a certain role in controlling the mobile concentrations of safety relevant radionuclides. The largest effect of colloid formation was observed with trivalent actinides. In contrast, only a small fraction of dissolved Pu was in colloidal form. The experimental data show that the quantity of colloids present in the corrosion solution decreases with time.

The dissolution and solubility of unirradiated UO_2 under oxidizing conditions has been studied as a function of pH and initial sample treatment. Special attention was given to the U(VI)/U(IV)-ratio on the samples surface. UO_2 samples (particle sizes 100 - 300 and 900 - 1100 μm) were corroded in $NaClO_4$ solutions in Teflon vessels at room temperature and pH values at 4 and 8. The release of uranium was found to be significant lower at pH 8, compared to that obtained at pH 4. A decrease of release rates is observed in both cases after

relatively fast initial dissolution. The rather high initial release has been explained by the presence of an oxidized surface layer, which dissolves very easily.

The corrosion behavior of unirradiated UO_2 in a NaCl-rich brine has been studied also as a function of oxygen partial pressure. Under reducing conditions initially a rapid increase in the solution concentration of uranium was observed, followed by a decrease, which is attributed to the precipitation of U(IV)-hydroxides. Finally constant U-concentrations were achieved. The final value agrees with the solubility of UO_2 determined in 5 m NaCl - solutions at the same conditions. Under oxidizing conditions dissolution rates were measured in a replenishment test. Tow stages were distinguished: (1) dissolution of an oxidized layer; rate: 0.03 mg /m^2d, (2) dissolution of "less" oxidized uranium oxide; rate: 0.001 mg /m^2d. XPS analyses resulted in a surface composition of $UO_{2.4}$, which is close to that, obtained in dissolution tests with diluted solutions. This might be an indication, that the dissolution mechanism of UO_2 in brines and diluted solutions is similar. Under anoxic conditions reaction rates were significant lower than under oxidizing conditions.

Introduction

The direct disposal of spent nuclear fuel as a waste form is currently under consideration in many countries of the European Union. Our work aims at characterizing and qualifying the chemical durability of unprocessed high burnup UO_2 fuel as waste form for disposal sites in salt formations. Extensive experimental investigations worldwide[2,3] have shown that spent nuclear fuel is a very stable material, suitable for direct disposal as a waste form in a geological repository. The chemical stability is assessed by performing leach (corrosion) tests and subsequent sample surface and solution analyses. Laboratory determined fuel dissolution rates and radionuclide release fractions are known empirically for various geological media. The stability of spent fuel and its ability to retain radionuclides is not an inherent materials property but rather depends on the waste package and on surrounding hydrogeochemical constraints. Important reversible and irreversible reactions which mutually control radionuclide release are the chemically or electrochemical controlled dissolution of the fuel matrix or of segregated phases, grain boundary dissolution, sorption, and formation of new phases by (co)precipitation. Strong effects stem from radiolysis, from the corrosion products of canisters, backfill materials and repository rock. The presence of iron effectively reduces the concentration of many radionuclides.

Important processes which may control radionuclide release from the spent fuel into a contacting aqueous solution are: (1) kinetics of corrosion of the fuel matrix and of segregated phases (2) formation of secondary alteration products ((co-)precipitation processes limiting solubility), (3) sorption on surfaces of near field materials and (4) colloid formation. It depends strongly on the chemical nature of the nuclide and on environmental conditions, which of these processes is dominant. Important environmental factors controlling radionuclide release include radiation field, temperature, S/V, pH, pCO_2, redox conditions and the presence of backfill materials or of corrosion products of container materials (iron etc.). The complicated interrelationship of the various (electro)chemical reactions often hampers unambiguous interpretation of individual experimental results.

---

[2] L.H. Johnson, D.W.Shoesmith, "Spent Fuel"; in Waste Forms for the Future, Lutze, Ewing ed., Elsevier Science Publishers B.V., (1988)

[3] L. H.Johnson, L.O.Werme, MRS Bulletin, Vol.XIX, 12/1994, pp 24 - 27

Further problems arise from the heterogeneous nature of the fuel and from the presence of additional materials in the vicinity of the dissolving fuel, because measured radionuclide release data are attributable to various sources and sinks. Radionuclides are transferred to the aqueous phase simultaneously from various locations of the UO_2-matrix, from grain boundaries, from the fuel/sheath gap and fracture surfaces, from segregated phases and from the cladding and, subsequently, the nuclides may become immobilized again in secondary phases or be sorbed on solid surfaces. The uncertainties in mechanistic interpretations and in the quantification of release controlling processes can only be reduced by combining various experimental techniques and by interpretation of results consistently using modeling techniques. The interplay of various radionuclide sources and sinks must be understood, before meaningful performance assessment of spent fuel can be made.

Using powdered fuel samples, Gray et al.[16,17] succeeded recently in distinguishing matrix dissolution effects from other effects. Avoiding saturation effects under oxidizing conditions by using leach tests with fast flowing water, they obtained matrix dissolution rates of about 1 to 5 mg/(m^2d) at 25°C. Surface analyses by XPS have shown that under oxidizing and anaerobic conditions, the dissolution process of the UO_2 matrix and the associated radionuclide release is preceded by surface oxidation to U_3O_7 [2] (see also results of solubility tests with unirradiated UO_2, second part of this report). However, the rate limiting process and potential saturation (steady state or solubility) effects are still not yet known.

In order to enhance our understanding of features and parameters controlling radionuclide release, a large research project has been conducted, combining experimental approaches (in particular leach or corrosion tests) with modeling techniques. Dissolution test results of spent UO_2 fuel and UO_2 in saline waters provide data on reaction rates, rate controlling processes and in some cases the results give upper limits of release of significant radionuclides including colloidal contributions. A rather high burnup/high linear power spent UO_2 fuel rod of 50 MWd/kgU was selected in our study representing worst case phase segregation and radionuclide enrichments at the rim of the various LWR-fuel types expected to be disposed in a first final repository.

Static dissolution tests were performed under anoxic and reducing conditions with spent fuel samples of very different dimensions and consequently different surface area to solution volume ratios (S/V). Distinction is made between solubility, inventory and rate controls for releases of radionuclides. Spent fuel matrix dissolution rates are assessed mainly from release data of Sr90. Colloid formation is analyzed by ultrafiltration techniques. The behavior of a large quantity of radionuclides is analyzed in order to identify general corrosion properties of the fuel matrix and element specific secondary processes. For comparison experiments were also performed with as fabricated UO_2. Static dissolution tests of UO_2 allow to determine reaction rates in the absence of radiolysis effects, provided saturation effects with respect to U-concentrations are prevented (case UO_2).

I. General preparations, analytical techniques and sample preparation

I. 1 Characteristics of spent fuel used in the experiments.

A high burnup LWR-UO_2-spent fuel rod segment (N 0203) from the PWR power plant Gösgen, Switzerland was obtained from SIEMENS/KWU. The following data of the fuel rod were provided by SIEMENS/KWU

Table I.1: List of data from spent fuel rod SBS 1108, segment N 0203.

Discharge date	May, 27th, 1989
Burnup	50 400 MWd/tU
Irradiation time in the reactor	1226 days (1986-1989)
Average linear power (segm.N 0203)	260 W/cm
Maximum linear power (segm.N 0203)	315 W/cm
Specific activity (1-2-92)	$7.4*10^{10}$ Bq/g
Initial density	10.41 g/cm^3
Initial ^{235}U enrichment	3.8 wt.%
U_{tot}	1171.0 g
Pu_{tot}	14.0 g
Gap (fuel/cladding)	0.17 mm
Cladding	Zircalloy 4

The fuel segment contained 37 pellets (UO_2-fuel) with an initial enrichment of 3.8 weight percent ^{235}U and on top and bottom a pellet of natural UO_2 with a content of 0.7 weight percent ^{235}U, followed by isolating pellets of Al_2O_3.

With respect to the increase of heterogeneity of the fuel with burnup and temperature at reactor operations, the burnup and linear power of the fuel are realistic upper limits and are not typical for the average LWR fuel expected in a first nuclear waste repository hosting directly disposed spent fuel.

I.2. Spent fuel samples.

To obtain samples for the dissolution tests, the fuel rod was cut into pellet sized segments. Some of these segments were decladded. In order to minimize fuel oxidation prior to the start of the tests cutting and decladding operations were performed under inert

atmosphere in the hot cell facilities of the JRC Institute for Transuranium Elements. The locations inside the fuel rod from where the different kinds of samples were taken are shown in the schematics in Figure I.1. The identification of the samples used is

K :	compact pellet sized fuel segment, not decladded
P, A, S1, X-ray :	powdered pellets
F :	decladded pellet, source for spent fuel fragments with sizes between 1 - 2 mm

This first step of sample preparation in the JRC is documented by photographs shown in Figure I.2. No additional preparation was done with the compact pellets, signed with "K". These samples were photographed and weighted prior to use in corrosion studies. Preparation of spent fuel powders and corrosion tests were carried out in the hot cells of the Forschungszentrum Karlsruhe (FZK). Transport from the JRC to FZK occurred in gas tight Ar-filled containers and all preparation steps as well as sample storage at FZK were performed in an inert atmosphere (N_2).

The granulate obtained from the decladded pellet signed with "F" was passed through a set of sieves. From the fraction < 2 mm and > 1 mm individual fragments were selected. Spent fuel powders were prepared with particle sizes less than the average grain size of the UO_2 matrix of approximately 15 µm. The desired average powder fraction was obtained from various positions of the fuel rod (top, center) by decladding the pellets "A", "S 1" and "X-ray" and dividing the resulting fragments into batches of 5 - 6 g. Each of the batches was milled for 15 minutes in a ball mill. The resulting powder was passed through a sieve (< 20 µm) and the fraction > 20 µm was milled and sieved again in order to achieve a maximum amount of the desired fraction < 20 µm. Preparation of samples with this particle size usually requires the technique of wet sieving, which was not available in the hot cell. Alternatively, by inserting 10 balls of agate (10 mm) additionally with the spent fuel powder on the 20 µm sieve a throughput of more than 70 % powder was achieved. The dust fraction was removed by washing the spent fuel powder with water in an ultrasonic bath for 10 minutes and a careful removal of the supernatant liquid. After filtration, the solution was analyzed for radionuclide content. The dust free spent fuel powder was dried for 2 days at room temperature under anoxic conditions. The average particle size of the powder was between 2,5 and 4,5 µm as measured by using image analyses from reflecting optical light micrographs of an embedded, polished section of a 50 mg specimen.

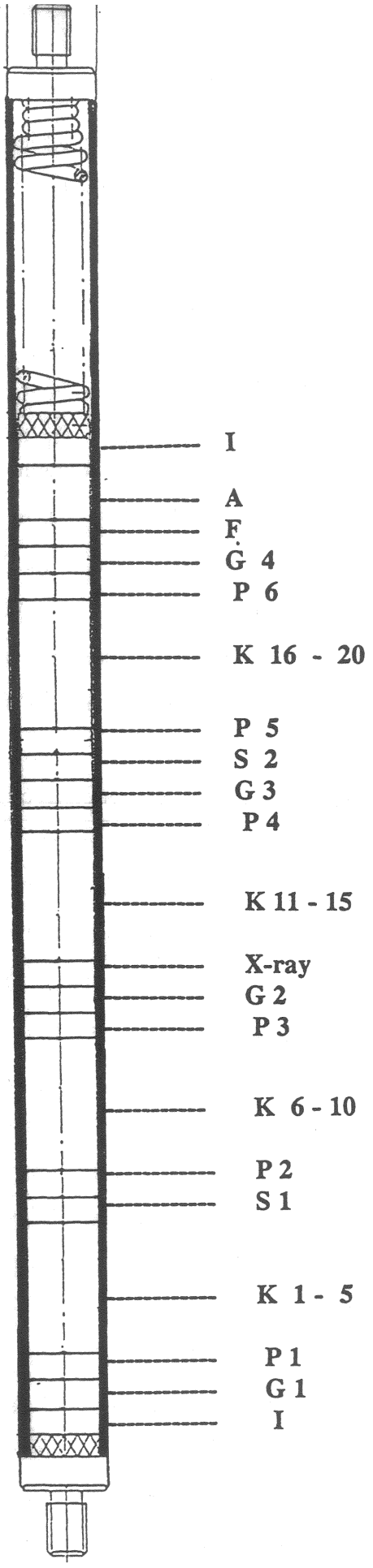

Identification of pellets:

K : compact pellet sized fuel segment, not decladded
P, A, S1, X-ray : powderized pellets
F : decladded pellet, source for spent fuel fragments with sizes between 1 - 2 mm
G: compact pellets (as reserve)
I : isolation pellet of natural UO2 (not to be used)

Figure I.1: Cutting plan of the spent fuel segment N 0203.

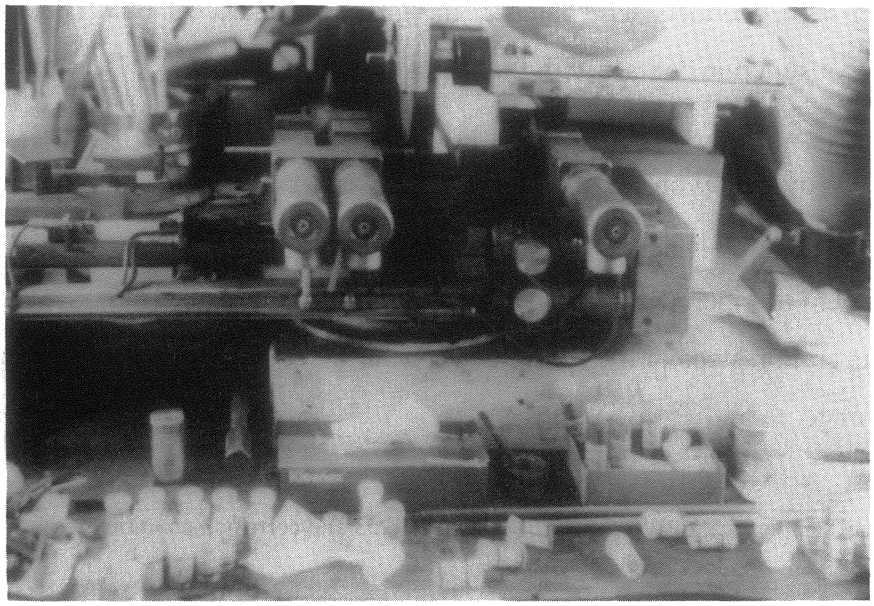

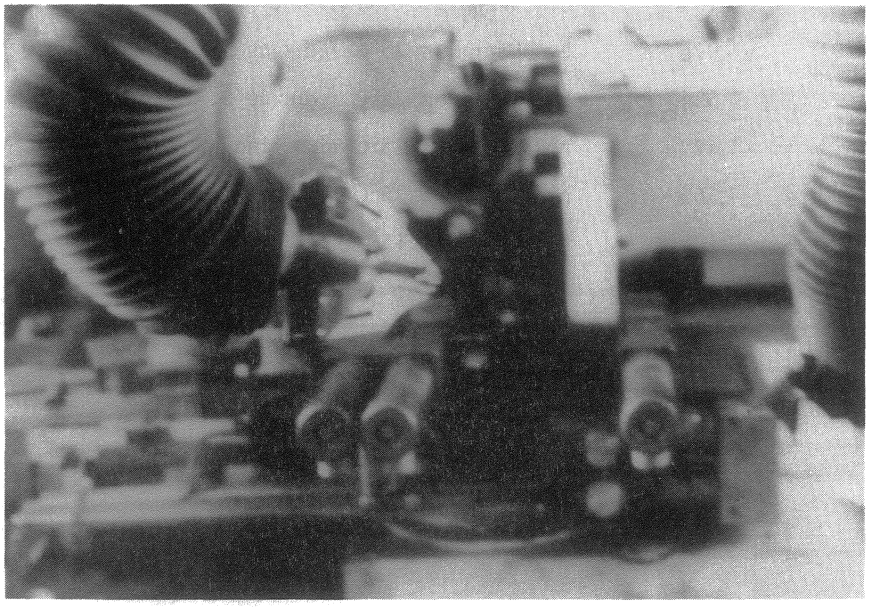

Figure I.2: Cutting of the spent fuel segment N 0203 in the hot cell facilities from JRC Institute for Transuranium Elements

As the average grain size of the fuel matrix is approximately 15 μm, most grain boundaries should be accessible to water and sufficient transgranular cracks must have been produced, that the interior of the fuel matrix could directly interact with the corrosion medium. Consequently, fission products segregated at the grain boundaries should become leachable almost instantaneously upon contact with the aqueous medium.

Table I.2 gives an overview on the different kinds of prepared spent fuel samples and their experimental use. Samples designated as "C" were investigated within this EU-contract. Other samples (duplicates) are included for comparison. Figure I.3 and I.4 show photographs from the principal preparation steps of the spent fuel powder : "milling", "sieving", "washing" and "sealing" for storage.

Table I.2: Spent fuel samples from PWR Gösgen, segment N0203 and corrosion conditions.

Sample	*Mass (g) (with cladding)*	*Mass(g) (without cladding)*	*Corrosion conditions*	*Tests,as agreed upon contract = C*
Pellets:				
K 1	8,945	7,335	dest.Water, 25°C, anaerobic	C
K 2	8,670	7,109	dest.Water, 25°C, anaerobic	
K 3	8,507	6,976	NaCl-solution, 25°C, reducing	C
K 4	9,118	7,534	NaCl-solution, 25°C, reducing	
K 9	9,060	7,429	NaCl-solution, 25°C, anaerobic	C
K 10	8,986	7,369	NaCl-solution, 25°C, anaerobic	
K 13	8,555	7,105	NaCl-solution, 150°C, anaerobic	C

Sample	*Mass (g)*	*Size (μm)*	*Corrosion conditions*	
Fragments:				
F 3	0,020	1500	NaCl-solution, 25°C, anaerobic	C
F 4	0,020	1500	NaCl-solution, 25°C, anaerobic	
Powders:				
P 1	2,90	2,5 - 4,5	NaCl-solution, 25°C, anaerobic	C
P 2	2,95	2,5 - 4,5	NaCl-solution, 25°C, anaerobic	

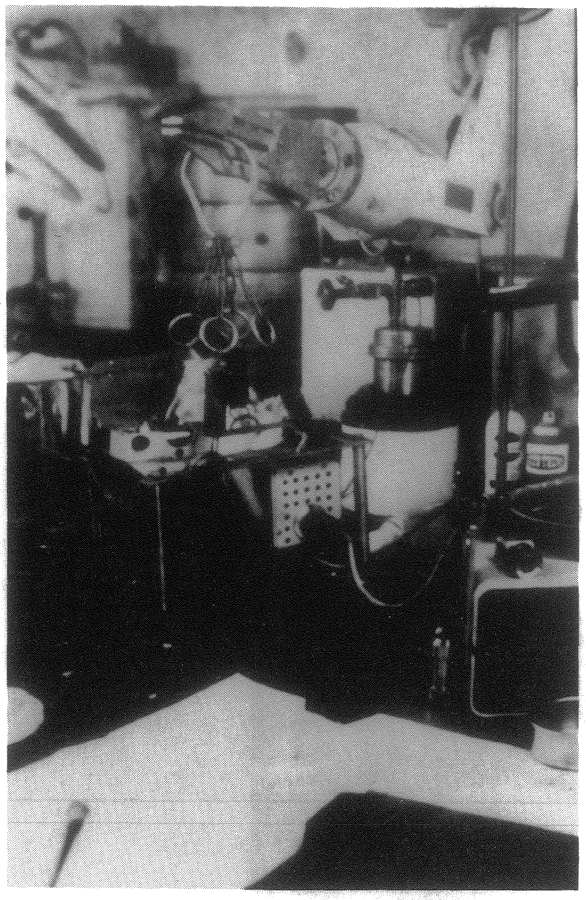

a

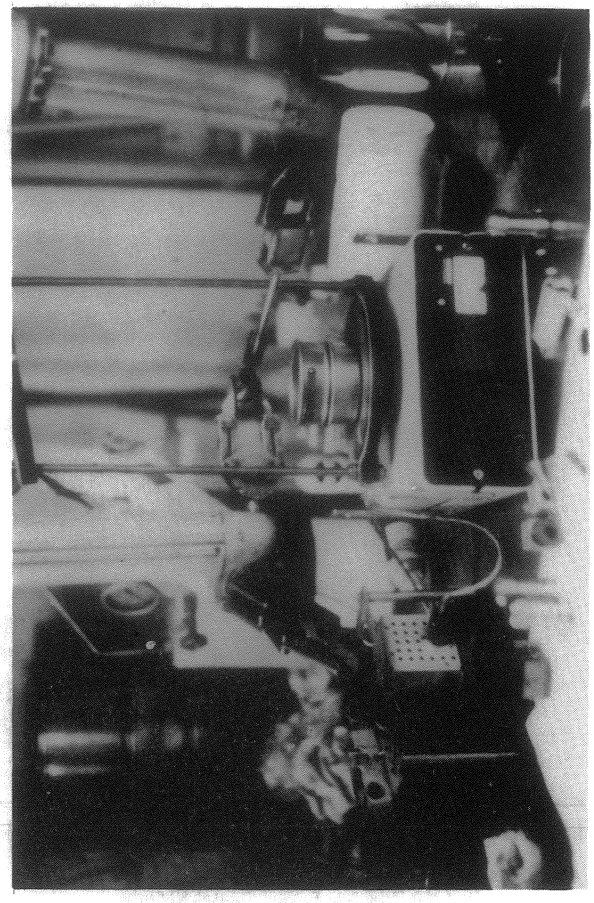

b

c

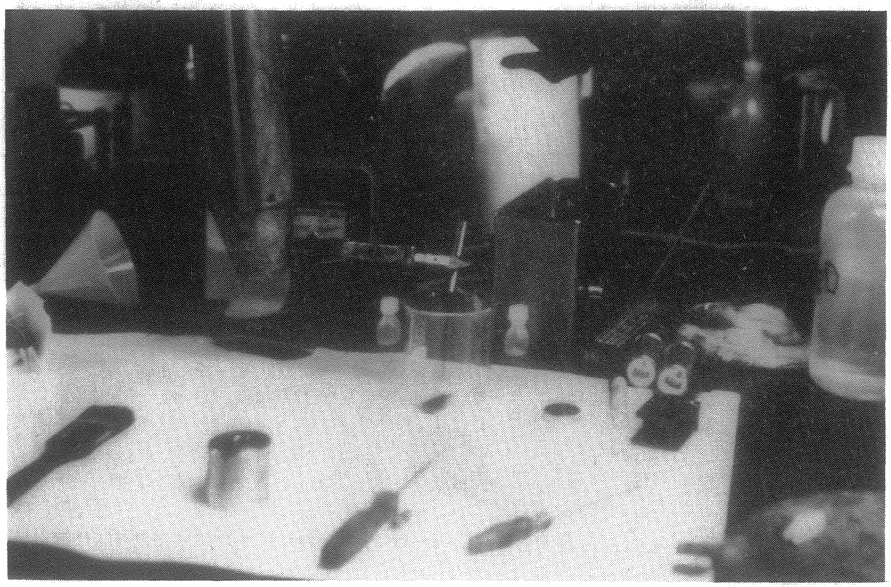

Figure I.3: Preparing of spent fuel powder samples: (a) milling in a ball mill, (b) passing through a 20 μm sieve, (c) preparation for removing dust fraction by ultrasonic cleaning.

a

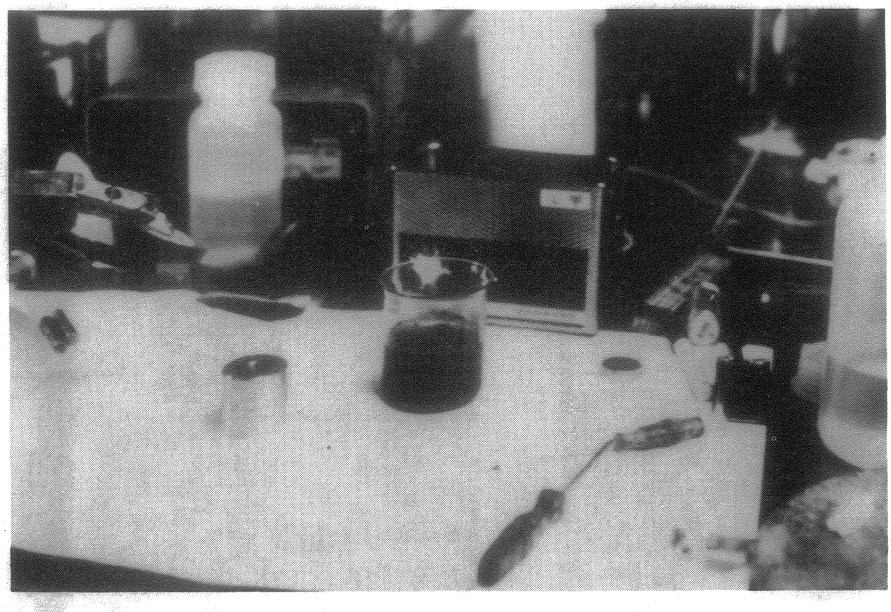

b

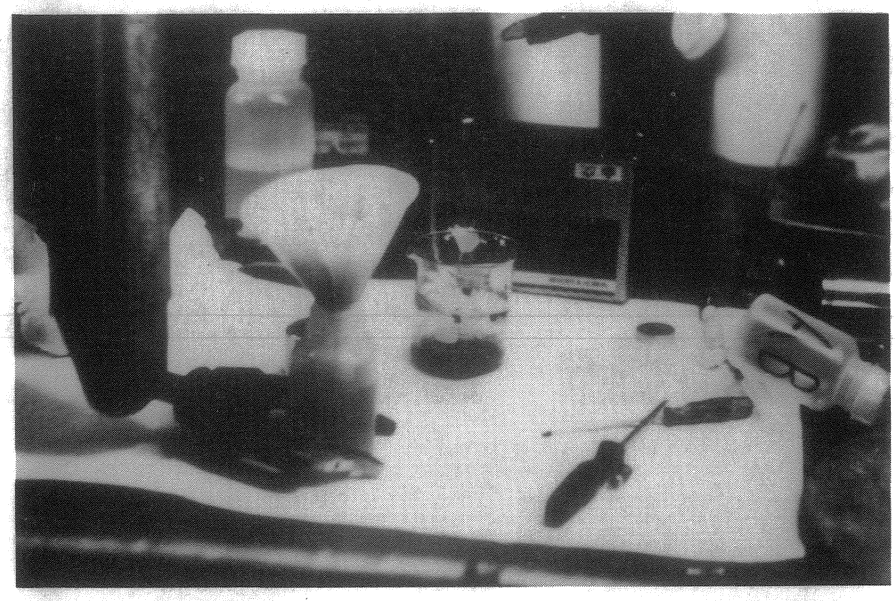

c

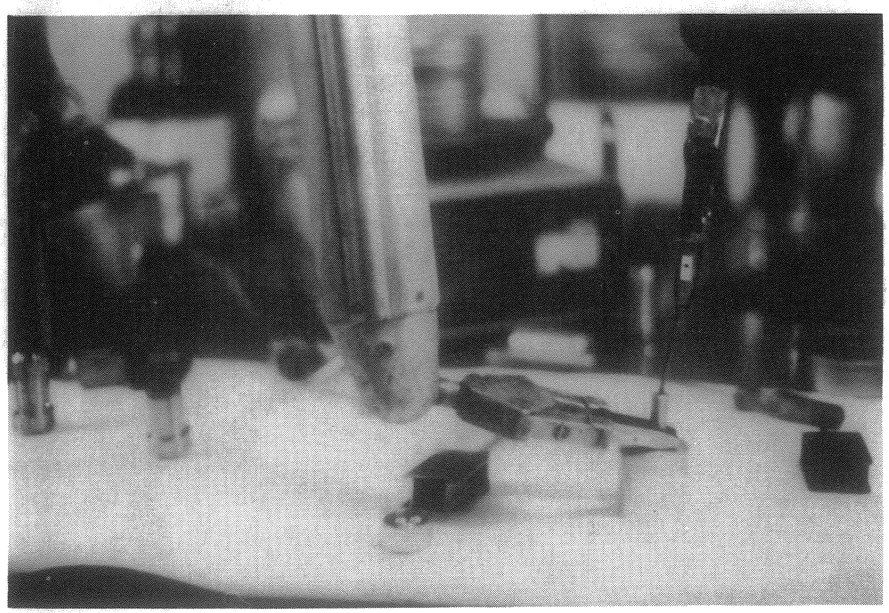

Figure I.4: Preparing of spent fuel powder samples: (a) dust fractionation in the supernatant water after ultrasonic treatment, (b) separation of dust enriched water by filtration, (c) sealing of washed spent fuel powder into gas tight capsule after drying

I.3 Radionuclide inventory in the fuel

Nuclide inventories of the fuel samples were both measured and calculated with the help of the KORIGEN code [Version 1990][4] using a neutron cross section library applicable to high burnup values. Radionuclide inventories of the samples were calculated for various reference dates (Feb.1st, 1992,1993,1994). Calculated specific nuclide radioactivity inventories are given in Table I.3 and specific elemental mass inventories in Table I.4. Considering radioactive decay and buildup of radioactive decay products, these reference data were used to calculate actual radioactivity inventories I for the respective dates of analyses. For the nuclides, which we can analyze in aqueous solution, the buildup of daughter nuclides must be considered only for the formation of Am241 by decay of Pu241 and for the formation of Cm242 from Am242. The amount of daughter nuclides present at time t was calculated by the formula

$$ {}^{D}A = {}^{P}A_0 \exp(-{}^{P}\lambda t)/(1-{}^{P}\lambda/{}^{D}\lambda) + ({}^{D}a_0 - {}^{P}A_0/(1-{}^{P}\lambda/{}^{D}\lambda))\exp(-{}^{D}\lambda t), $$

where the superscripts D and P indicate daughter and parent nuclide, A and A_0 are activities at the date of analyses and at the reference date (Feb.1st,1992) respectively, t is the time between these two dates and λ values are the decay constants. Results calculated by this method were compared with results calculated by KORIGEN for another reference date). Agreement was always better than 1% of deviation.

Measurement of nuclide inventories

The exact knowledge of the inventory is of high importance, when calculating release rates and concentrations of radionuclides in corrosion solutions. In order to evaluate the correctness of our KORIGEN calculations and to obtain data on the spatial inventory variations, the radial radionuclide distribution was analyzed radiochemically. For analyses, small fragments were selected from the central part of a fuel pellet and from the edge each about a millimeter in diameter. Additionally a piece of cladding with adhering fuel grains was selected in order to

[4] Fischer and Wiese, KfK 3014, Kernforschungszentrum Karlsruhe (1983)

Table 3: Nuclide radioactivity inventories of high burnup spent fuel in Bq/g heavy metal

	01.02.1991	01.02.1992	01.02.1993	01.02.1994
AG109M	6.9E+02	4.0E+02	2.3E+02	1.3E+02
AG110	5.5E+05	2.0E+05	7.3E+04	2.6E+04
AG110M	4.1E+07	1.5E+07	5.5E+06	2.0E+06
AM241	2.3E+07	3.2E+07	4.1E+07	5.0E+07
AM242	2.6E+05	2.5E+05	2.5E+05	2.5E+05
AM242M	2.6E+05	2.6E+05	2.5E+05	2.5E+05
AM243	1.8E+06	1.8E+06	1.8E+06	1.8E+06
BA137M	5.3E+09	5.2E+09	5.0E+09	4.9E+09
BE 10	1.3E+01	1.3E+01	1.3E+01	1.3E+01
BI212	6.7E+02	9.6E+02	1.2E+03	1.5E+03
BK249	4.2E+02	1.9E+02	8.5E+01	3.9E+01
C 14	7.5E+02	7.5E+02	7.5E+02	7.5E+02
CD109	6.9E+02	4.0E+02	2.3E+02	1.3E+02
CD113M	2.8E+06	2.7E+06	2.6E+06	2.4E+06
CE142	1.5E+00	1.5E+00	1.5E+00	1.5E+00
CE144	1.2E+10	4.9E+09	2.0E+09	8.2E+08
CF249	3.3E+00	3.8E+00	4.1E+00	4.2E+00
CF250	5.0E+01	4.7E+01	4.5E+01	4.2E+01
CF252	4.3E+01	3.3E+01	2.6E+01	2.0E+01
CM242	2.3E+08	4.8E+07	1.0E+07	2.4E+06
CM243	1.2E+06	1.2E+06	1.2E+06	1.2E+06
CM244	3.0E+08	2.9E+08	2.8E+08	2.7E+08
CM245	2.6E+04	2.6E+04	2.6E+04	2.6E+04
CM246	6.4E+04	6.4E+04	6.4E+04	6.4E+04
CS134	6.3E+09	4.5E+09	3.2E+09	2.3E+09
CS135	2.2E+04	2.2E+04	2.2E+04	2.2E+04
CS137	5.6E+09	5.4E+09	5.3E+09	5.2E+09
EU152	1.8E+05	1.7E+05	1.6E+05	1.5E+05
EU154	7.1E+08	6.5E+08	6.0E+08	5.6E+08
EU155	2.3E+08	2.0E+08	1.7E+08	1.5E+08
GD153	2.0E+05	7.1E+04	2.5E+04	8.8E+03
H 3	2.4E+07	2.3E+07	2.2E+07	2.1E+07
HO166M	1.3E+01	1.3E+01	1.3E+01	1.3E+01
I 129	1.6E+03	1.6E+03	1.6E+03	1.6E+03
KR 85	4.4E+08	4.2E+08	3.9E+08	3.6E+08
NB 93M	1.7E+04	2.1E+04	2.4E+04	2.8E+04
NB 94	5.7E+01	5.7E+01	5.7E+01	5.7E+01
NB 95	1.8E+08	3.6E+06	6.9E+04	1.3E+03
NB 95M	6.1E+05	1.2E+04	2.2E+02	4.2E+00
NP236M	1.8E+00	1.8E+00	1.8E+00	1.8E+00
NP237	1.9E+04	1.9E+04	1.9E+04	1.9E+04
NP238	1.3E+03	1.3E+03	1.3E+03	1.3E+03
NP239	1.8E+06	1.8E+06	1.8E+06	1.8E+06
PA233	1.9E+04	1.9E+04	1.9E+04	1.9E+04
PA234	1.5E+01	1.5E+01	1.5E+01	1.5E+01
PA234M	1.2E+04	1.2E+04	1.2E+04	1.2E+04
PB212	6.7E+02	9.6E+02	1.2E+03	1.5E+03
PD107	8.0E+03	8.0E+03	8.0E+03	8.0E+03

	01.02.1991	01.02.1992	01.02.1993	01.02.1994
PM147	4.8E+09	3.7E+09	2.9E+09	2.2E+09
PO212	4.3E+02	6.2E+02	7.9E+02	9.5E+02
PO216	6.7E+02	9.6E+02	1.2E+03	1.5E+03
PR144	1.2E+10	4.9E+09	2.0E+09	8.2E+08
PR144M	1.4E+08	5.8E+07	2.4E+07	9.8E+06
PU236	3.3E+04	2.6E+04	2.0E+04	1.6E+04
PU238	2.3E+08	2.3E+08	2.3E+08	2.2E+08
PU239	1.3E+07	1.3E+07	1.3E+07	1.3E+07
PU240	2.3E+07	2.3E+07	2.4E+07	2.4E+07
PU241	6.0E+09	5.7E+09	5.5E+09	5.2E+09
PU242	1.4E+05	1.4E+05	1.4E+05	1.4E+05
RA224	6.7E+02	9.6E+02	1.2E+03	1.5E+03
RB 87	1.1E+00	1.1E+00	1.1E+00	1.1E+00
RH106	1.0E+10	5.1E+09	2.6E+09	1.3E+09
RN220	6.7E+02	9.6E+02	1.2E+03	1.5E+03
RU106	1.0E+10	5.1E+09	2.6E+09	1.3E+09
SB125	3.0E+08	2.3E+08	1.8E+08	1.4E+08
SB126	6.4E+03	6.4E+03	6.4E+03	6.4E+03
SB126M	4.6E+04	4.6E+04	4.6E+04	4.6E+04
SE 79	1.6E+04	1.6E+04	1.6E+04	1.6E+04
SM151	1.6E+07	1.6E+07	1.6E+07	1.6E+07
SN119M	1.7E+06	6.1E+05	2.2E+05	7.7E+04
SN121M	1.2E+05	1.1E+05	1.1E+05	1.1E+05
SN123	3.8E+06	5.4E+05	7.6E+04	1.1E+04
SN126	4.6E+04	4.6E+04	4.6E+04	4.6E+04
SR 89	6.5E+06	4.3E+04	2.9E+02	1.9E+00
SR 90	3.7E+09	3.6E+09	3.5E+09	3.4E+09
TB160	2.0E+05	6.1E+03	1.8E+02	5.5E+00
TC 99	7.1E+05	7.1E+05	7.1E+05	7.1E+05
TE123M	2.1E+04	2.6E+03	3.1E+02	3.7E+01
TE125M	7.4E+07	5.7E+07	4.5E+07	3.5E+07
TE127	1.2E+07	1.1E+06	1.1E+05	1.1E+04
TE127M	1.2E+07	1.2E+06	1.1E+05	1.1E+04
TH228	6.7E+02	9.6E+02	1.2E+03	1.5E+03
TH230	1.9E+00	2.3E+00	2.7E+00	3.1E+00
TH231	4.4E+02	4.4E+02	4.4E+02	4.4E+02
TH234	1.2E+04	1.2E+04	1.2E+04	1.2E+04
TL208	2.4E+02	3.5E+02	4.4E+02	5.3E+02
U 232	1.5E+03	1.7E+03	2.0E+03	2.1E+03
U 233	1.6E+00	1.7E+00	1.8E+00	1.9E+00
U 234	4.5E+04	4.5E+04	4.6E+04	4.7E+04
U 235	4.4E+02	4.4E+02	4.4E+02	4.4E+02
U 236	1.2E+04	1.2E+04	1.2E+04	1.2E+04
U 237	1.5E+05	1.4E+05	1.4E+05	1.3E+05
U 238	1.2E+04	1.2E+04	1.2E+04	1.2E+04
Y 90	3.7E+09	3.6E+09	3.5E+09	3.4E+09
Y 91	2.9E+07	3.8E+05	5.0E+03	6.7E+01
ZR 93	9.7E+04	9.7E+04	9.7E+04	9.7E+04
ZR 95	8.2E+07	1.6E+06	3.0E+04	5.7E+02

Table 4: Specific elemental mass inventories of high burnup spent fuel in µg/g heavy metal

	01.02.1991	01.02.1992	01.02.1993	01.02.1994
AG	1.1E+02	1.1E+02	1.1E+02	1.1E+02
AM	4.2E+02	4.9E+02	5.6E+02	6.3E+02
AS	9.1E-02	9.1E-02	9.1E-02	9.1E-02
AU	5.2E+00	5.2E+00	5.2E+00	5.2E+00
BA	2.4E+03	2.4E+03	2.5E+03	2.6E+03
BE	1.6E-02	1.6E-02	1.6E-02	1.6E-02
BR	2.9E+01	2.9E+01	2.9E+01	2.9E+01
C	4.6E-03	4.6E-03	4.6E-03	4.6E-03
CD	1.5E+02	1.5E+02	1.5E+02	1.5E+02
CE	3.7E+03	3.6E+03	3.6E+03	3.6E+03
CM	1.1E+02	1.1E+02	1.0E+02	1.0E+02
CS	4.0E+03	3.9E+03	3.8E+03	3.8E+03
DY	1.9E+00	1.9E+00	1.9E+00	1.9E+00
ER	1.3E-02	1.3E-02	1.3E-02	1.3E-02
EU	2.2E+02	2.1E+02	2.0E+02	2.0E+02
FR	2.1E-15	2.4E-15	2.6E-15	2.9E-15
GD	2.4E+02	2.4E+02	2.5E+02	2.6E+02
GE	3.0E-01	3.0E-01	3.0E-01	3.0E-01
H	7.7E-02	7.3E-02	7.0E-02	6.7E-02
HE	1.6E+00	1.6E+00	1.6E+00	1.6E+00
HO	6.8E-02	6.8E-02	6.8E-02	6.8E-02
I	3.1E+02	3.1E+02	3.1E+02	3.1E+02
IN	1.9E+00	2.0E+00	2.0E+00	2.0E+00
KR	5.3E+02	5.3E+02	5.3E+02	5.3E+02
LA	1.9E+03	1.9E+03	1.9E+03	1.9E+03
LI	1.3E-03	1.3E-03	1.3E-03	1.3E-03
MO	5.0E+03	5.0E+03	5.0E+03	5.0E+03
NB	1.4E-01	1.4E-02	1.2E-02	1.3E-02
ND	6.0E+03	6.1E+03	6.1E+03	6.1E+03
NP	7.2E+02	7.2E+02	7.2E+02	7.2E+02
PA	5.3E-04	5.3E-04	5.4E-04	5.4E-04
PB	1.0E-05	1.9E-05	3.1E-05	4.6E-05
PD	2.4E+03	2.5E+03	2.5E+03	2.5E+03
PM	1.4E+02	1.1E+02	8.3E+01	6.4E+01
PO	6.7E-13	1.1E-12	1.7E-12	2.4E-12
PR	1.7E+03	1.7E+03	1.7E+03	1.7E+03
PU	1.1E+04	1.1E+04	1.1E+04	1.1E+04
RA	1.8E-07	2.5E-07	3.3E-07	4.0E-07
RB	4.9E+02	5.0E+02	5.0E+02	5.0E+02
RH	6.3E+02	6.3E+02	6.3E+02	6.3E+02
RN	2.0E-11	2.9E-11	3.7E-11	4.4E-11
RU	3.7E+03	3.6E+03	3.6E+03	3.6E+03
SB	2.4E+01	2.2E+01	2.1E+01	2.0E+01
SE	7.3E+01	7.3E+01	7.3E+01	7.3E+01
SM	1.1E+03	1.1E+03	1.1E+03	1.2E+03
SN	1.1E+02	1.1E+02	1.1E+02	1.1E+02
SR	1.2E+03	1.2E+03	1.2E+03	1.2E+03
TB	4.3E+00	4.3E+00	4.3E+00	4.3E+00
TC	1.1E+03	1.1E+03	1.1E+03	1.1E+03
TE	7.1E+02	7.2E+02	7.2E+02	7.2E+02
TH	3.1E-03	3.8E-03	4.5E-03	5.3E-03
U	9.4E+05	9.4E+05	9.4E+05	9.4E+05
XE	8.1E+03	8.1E+03	8.1E+03	8.1E+03
Y	6.4E+02	6.4E+02	6.4E+02	6.4E+02
ZR	5.2E+03	5.2E+03	5.2E+03	5.3E+03

analyze the composition of the highly burned fuel grains at the rim ("rim effect") and of potentially segregated phases.

The complete dissolution of these high burnup spent fuel samples requires much more efforts than for "normal" and low burnup spent fuel. The specimen were dissolved by boiling them in a mixture of 13 m HCl and 14 m HNO_3 ("aqua regia") for 20 or 135 minutes, respectively. Weights of the dissolved spent fuel samples and dissolution acids are listed below.

	"Rim"	"Center"	"Cladding"
Sample	0,119 g	0,133 g	0,826 g (mainly ZrO_2)
13 m HCl	8,84 g	9,27 g	25,201 g
14 m HNO3	3,68 g	3,98 g	11,114 g
Boiling time	20 minutes	20 minutes	135 minutes

From the resulting solutions aliquots were taken and diluted (1:100) with 1 m HNO_3. The radionuclide contents of the solutions were analyzed by radiochemical methods as described further below.

The specific activities (Bq/g HM) of the particles from the center, the edge and the rim were measured by two independent laboratories (INE, ITC). Measured activities are related to the fuel mass, either by the sample weight or, in case fuel grains adhering to the cladding, by reference to the Uranium content of the sample. Results are listed in Table I.5, together with the specific activities, calculated by the KORIGEN code. Calculations and measurements are related to the reference date February 1st, 1994. In general measurements of the two laboratories deviate by less than about 10 % from a mean value. In Figure I.5 the ratio of the measured to the calculated specific radionuclide activities is plotted as a function of radial position. Central and edge sample analyses are considered as representing an area with a diameter of about 1 mm each. As shown in Figure I.5 and Table I.5, the deviation in the composition of samples taken from the edge and the center is rather small. The deviation of the analyzed activities of these samples from the KORIGEN data is in general not very high. Slightly higher specific activities were determined for Cs-134, Cs-137, Sr-90, Tc99, Am-241, Am-243, Np-239, Cm-244, Cm-242, Pu-238, Pu-239/40 and slightly lower specific activities

were found for Eu-154, Sb-125 and Ag-110m, when compared with the KORIGEN data. The often reported "rim effect" of higher burnup and higher nuclide concentrations in the outer part of the rim (100 μm) was veryfied for the fuel grains adhering to the cladding. Enrichment factors for radionuclide inventories in the rim were calculated from the ratio of the inventories as measured in the rim sample versus the average inventory of edge and central samples. In particular, enrichment of of Ag110m and of Sb125 was observed. The data for Ag110m may be indicative for enhanced contribution of Pu239 fission in the rim. Higher actinides (Cm244, Am241) Cs134/137 and Tc99 show also rather high enrichments of about a factor 2.5. In case of Cs this high enrichment probably results from migration during reactor operation. Other fission products are enriched by less than a factor of 2, indicating an upper limit for rim burnup of about 2*50=100 MWd/kgU. Almost no rim effect is observed for the lower actinides Pu238 and Np237.

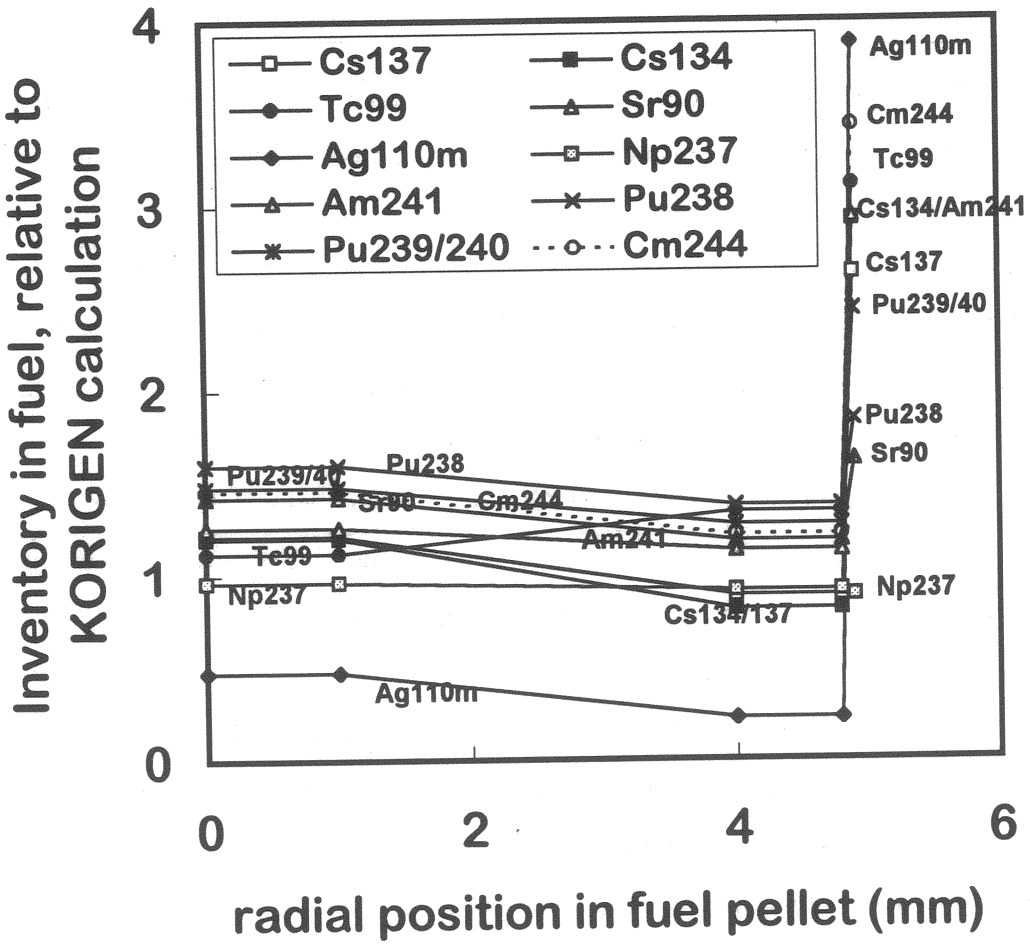

Figure I.5: Radial radionuclide inventory distribution in high burnup fuel, ratio of measured inventories to respective average values calculated with the KORIGEN code.

Table I.5: Analyzed and calculated specific activities (Bq/g HM) of high burnup spent fuel from PWR-Gösgen (* Data are related to Febr.1st,1994).

Radial radionuclide distribution in a fuel pellet: Comparison of analyses results obtained at INE and at ITC with calculations made by KORIGEN, Ref. Date: 1.2.1994

	Center			Edge			Rim			KORIGEN	Rim enrich-ment factor
	INE	ITC	mean	INE	ITC	mean	INE	ITC	mean	calc.	
Cs137	5.0E+9	6.1E+9	5.6E+9	3.9E+9	4.2E+9	4.1E+9	1.2E+10	1.2E+10	1.2E+10	4.6E+9	2.5
Cs134	2.2E+9	2.8E+9	2.5E+9	1.6E+9	1.8E+9	1.7E+9	6.1E+9	6.2E+9	6.1E+9	2.1E+9	2.9
Sb125	1.0E+8	1.0E+8	1.0E+8	8.9E+7	8.9E+7	8.9E+7	1.7E+9	2.0E+9	1.8E+9	1.3E+8	19.1
Ce144	8.2E+8	8.4E+8	8.3E+8	7.5E+8	6.8E+8	7.1E+8	1.2E+9	1.2E+9	1.2E+9	8.0E+8	1.5
Eu154	3.1E+8	3.3E+8	3.2E+8	2.8E+8	2.7E+8	2.7E+8	5.1E+8	4.9E+8	5.0E+8	5.0E+8	1.7
Eu155	1.4E+8	1.6E+8	1.5E+8	1.2E+8	1.3E+8	1.3E+8	2.5E+8	2.7E+8	2.6E+8	1.4E+8	1.9
Ru106	1.2E+9	1.3E+9	1.3E+9	9.8E+8	8.8E+8	9.3E+8	2.3E+9	2.6E+9	2.4E+9	1.2E+9	2.2
Ag110m		9.3E+5	9.3E+5		4.4E+5	4.4E+5	0.0E+0	7.6E+6	7.6E+6	2.0E+6	11.1
Sr90	4.6E+9	3.9E+9	4.3E+9	4.0E+9	3.2E+9	3.6E+9	5.5E+9	4.2E+9	4.9E+9	3.0E+9	1.2
Tc99	7.0E+5		7.0E+5	8.4E+5		8.4E+5	2.0E+6		2.0E+6	6.3E+5	2.5
Pu238	3.1E+8	3.2E+8	3.1E+8	2.9E+8	2.5E+8	2.7E+8	4.0E+8	3.3E+8	3.6E+8	2.0E+8	1.2
Pu239	4.6E+7	5.0E+7	4.8E+7	4.2E+7	4.0E+7	4.1E+7	8.1E+7	7.7E+7	7.9E+7	3.2E+7	1.8
Pu241	7.6E+9		7.6E+9	6.5E+9		6.5E+9	1.3E+10		1.3E+10		1.8
Am241	5.4E+7		5.4E+7	4.8E+7		4.8E+7	1.3E+8		1.3E+8	4.3E+7	2.5
Cm242	3.4E+6	4.7E+6	3.4E+6	1.8E+6	3.8E+6	2.8E+6	6.1E+6	9.6E+6	6.1E+6	2.3E+6	2.0
Cm244	3.4E+8	4.3E+8	3.4E+8	2.7E+8	3.1E+8	2.9E+8	8.1E+8	8.9E+8	8.1E+8	2.4E+8	2.6
Np237		1.6E+4	1.6E+4		1.5E+4	1.5E+4		1.5E+4	1.5E+4	1.7E+4	0.9

I.4 Preparation of laboratory space, reaction vessels and auxiliary tools.

Due to the high radiation doses, experiments with spent fuel samples had to be performed permanently in specially equipped hot cells. Since the shielded cells of the INE were presently in a long course of reorganization, the entire corrosion test program was performed into the Hot Cell department (mainly cell 5) of our research center. In order to install the spent fuel corrosion tests in these cells, time consuming technical work was performed with emphasis on availability of locations for the reaction vessels, modification of stainless steel autoclaves (500 ml volume) and modification of the heating cabinets.

Autoclaves.

The spent fuel corrosion tests were performed in Ta (for tests at 150°C) or Ti(99.8)/Pd(0.2) (tests at room temperature) lined stainless steel autoclaves (500 ml volume). Both Ti/Pd and Ta are known to be very corrosion resistant to saline and slightly alkaline solutions. Ti is known to form thin oxide films (few nm) with rather low permeability to H_2 gas. The autoclaves were equipped each with two ball valves (Ti) in the lid, which allowed sampling of fission and radiolytic gases as well as solution sampling during the experiment. In case of solution sampling, inert gas (Ar) was flushed through one of the valves, the solution sample was taken by using a syringe passing through the other valve. By this method contamination by air during sampling was avoided. Figure I.6 shows a schematics of the autoclave.
The autoclaves were adapted for remote operation conditions. For loading and sampling tools were developed for clamping the autoclave, for opening and closing the autoclave by electrical screw drivers and for centering the sealing rings. An automatic solution sampling device was developed, based on a robot driven syringe technique. Figures I.7 and I.8 show a selection of these devices.

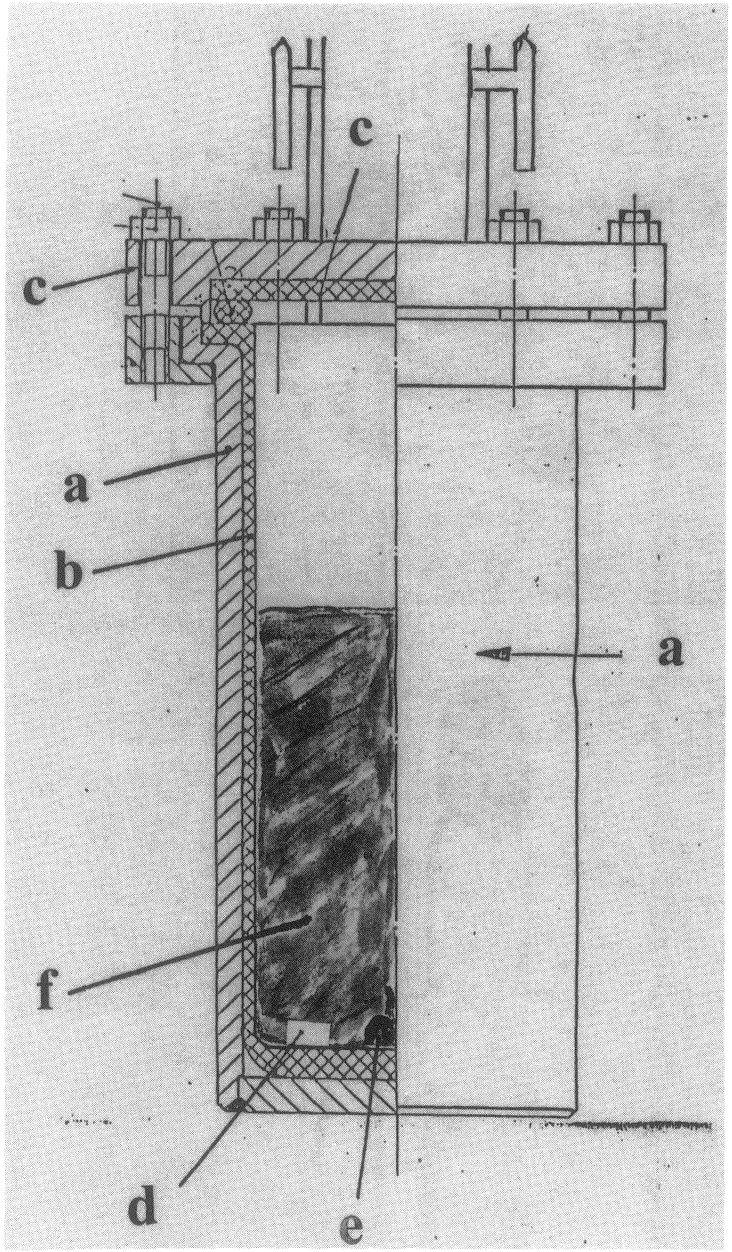

Figure I.6: Schematics of the autoclaves used

Static spent fuel corrosion tests:
Design of the autoclaves

(a) stainless steel container,

(b) tantalum liner,

(c) lid with two ball valves for sampling (solutions, gases),

(d) tantalum disc,

(e) spent fuel sample (pellet, mm-fragment, µm-powder),

(f) corrosion solution ($NaCl$-, $MgCl_2$- solution, DI-water)

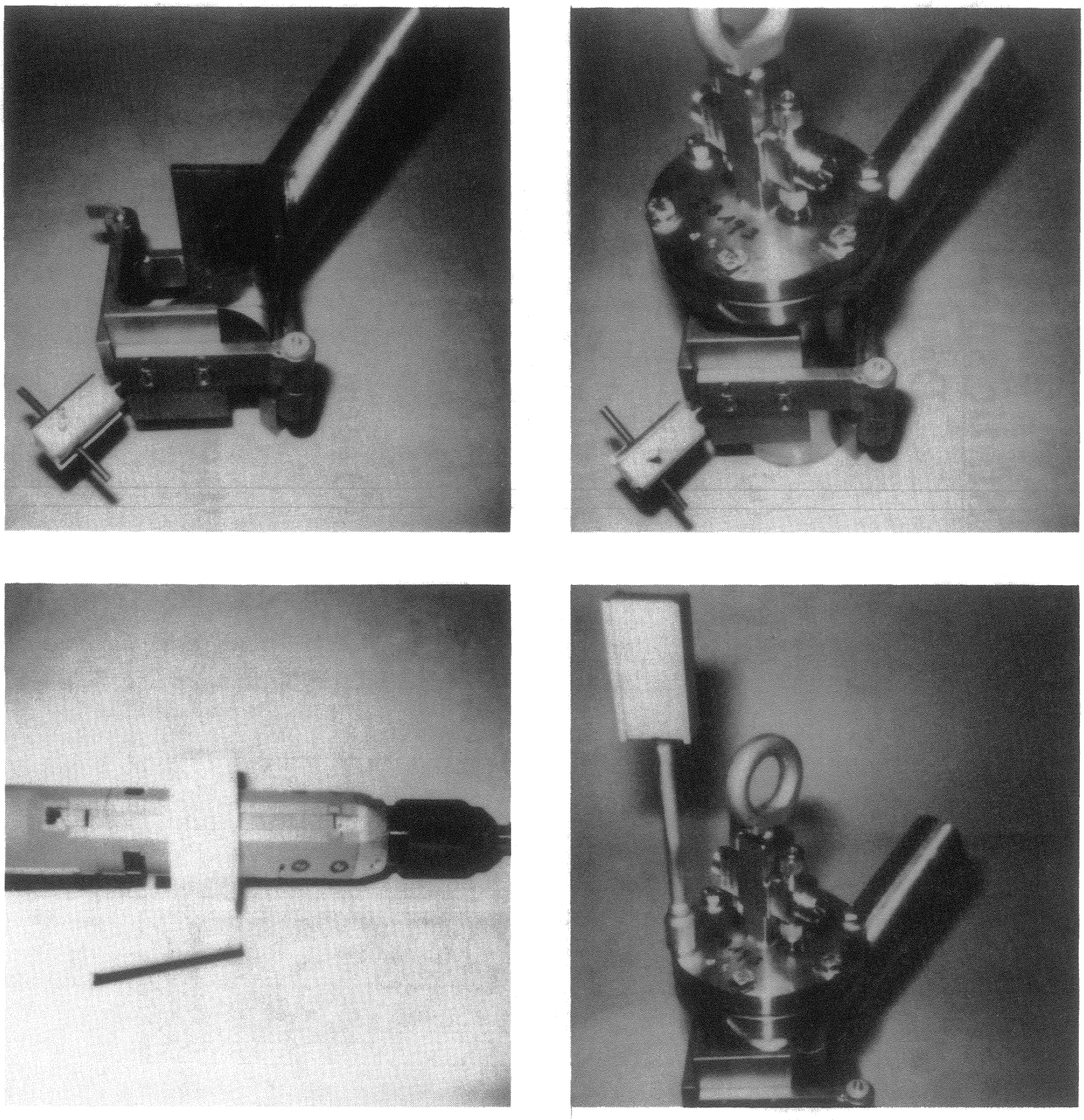

Figure I.7: Auxiliary tools, adapted for remote operation for sealing and opening the autoclaves: equipment for clamping the autoclave (top); remote operating electrical and mechanical screw driver (below)

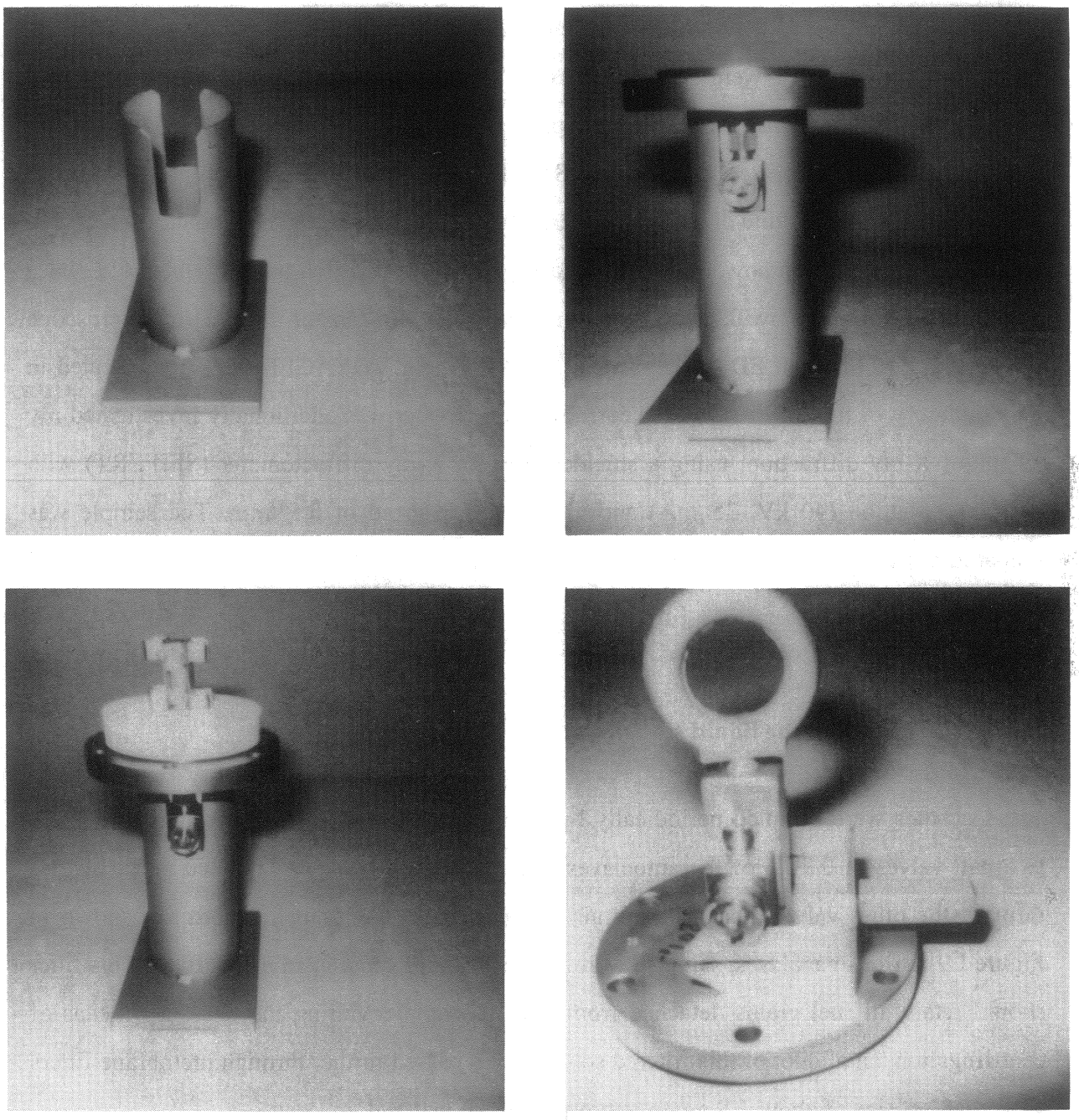

Figure I.8: Auxiliary tools, adapted for remote operation for sealing and opening the autoclaves: support for keeping the lid, when mounting the sealing ring (top), teflon disc for centering the sealing ring, handle for the lid (below)

I.5 Characterization of samples and sampling procedures.

I.5.1 Characterization of solid samples

Spent fuel samples were analyzed by optical microscopy prior and after the tests. Spent fuel samples with ß/γ - dose rates below 2 mSv/h, such as the fragment F 3 or some grains from powder P 1 were studied by using X-ray diffraction pattern and by a shielded electron microscope (PHILIPS 500 X), equipped with EDX microanalyzer, located in the Hot Cell department of our research center. Samples were mounted on a sample holder of aluminum by using araldite and were sputtered with gold. The reaction of container material and added corroded iron powders were also analyzed. Corroded iron powder and Ti/Pd-plates with ß/γ - dose rates below 0,8 mSv/h were investigated by means of the electron microscope CAMSCAN 44 FE with EDX analyzer (NORAN-System; VOYAGER software), located in the laboratory of the INE(FZK). The corroded iron powder was additionally investigated my means of X-ray diffraction, using a shielded 2-circle X-ray diffractometer (SEIFERT) with CuKα - radiation (40 kV, 35 mA) and a goniometer speed of 0,5°/min. The sample was prepared by embedding into araldite and then polished.

I.5.2 Investigation of the liquid samples

The leachates were sampled periodically by means of a syringe passing through one of the two ball valves in the lid of the autoclaves. During sampling, water saturated Ar is flushed through the other valve, thus avoiding air contamination. Sampling methods are shown in Figure I.9. Prior to analyses, samples were filtered through a 0.45 µm micro filter. This filter should retain all fuel grains detached from the fuel samples during the tests. By means of centrifugation, an aliquot of this filtered solution was passed further through membrane filters with a cut off size of about 1.8 nm to remove colloidal material.

I.5.2.1 Eh/pH analyses

In order to avoid air contamination (oxidation, CO_2-uptake) Eh and pH values were determined only few minutes after solution sampling. Measurements were performed under N_2 -atmosphere inside the hot cell. This technique was developed during the test and was used only for the last two solution sampling intervals. In the first three solution sampling intervals samples were analyzed few days sampling in a glove box outside of the hot cells. It is quite possible that Eh values of these samples are augmented by the presence of oxygen uptake, and carbonate uptake may have acidified the pH values. For 95% saturated NaCl solutions measured pH and Eh data were corrected for liquid junction potential. The liquid junction potential of the pH electrode (system Ross) was obtained by measuring the pH value of the NaCl solution after adding HCl with a resulting known activity a_{H+} (see [5]). The liquid junction potential of the Eh-electrode (Pt) was determined by measuring the potential of the electrode in H_2-saturated (1 atm) NaCl solutions at a known activity a_{H+}. Reported pH and Eh values are consistent with Pitzer's ionic splitting convention.

[5] Grambow B., R. Müller, Mat. Res. Soc. Symp. Proc. Vol. 176 (1990), pp 229 - 240

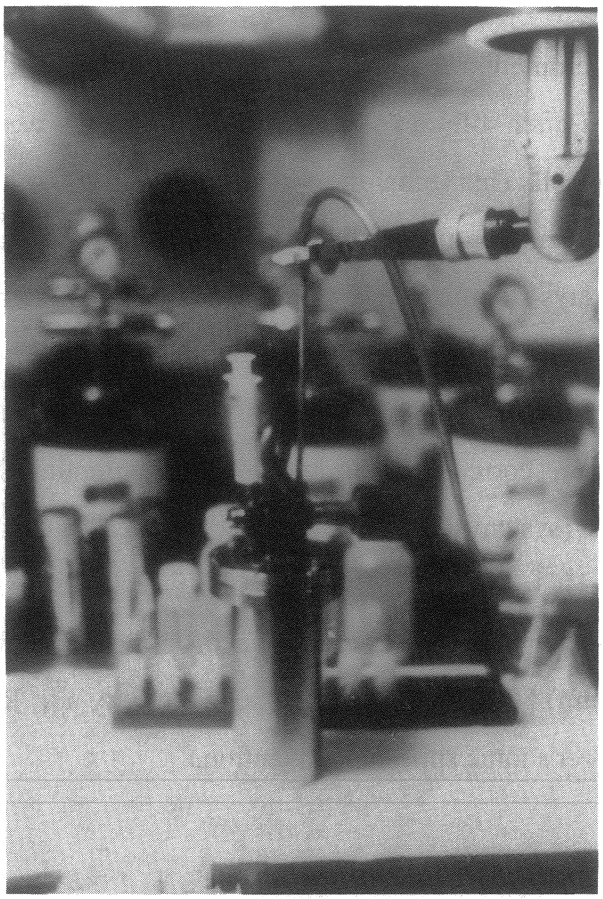

Figure I.9: Sampling methods of leach solutions: Top: Flushing of an autoclave with water saturated Ar during solution sampling. Solution samples are taken by means of a syringe; Bottom: inserting a solution samples filtered by a 0,45 µm micro filter into a vial with an 1,8 nm ultra filteration membrane, prior to centrifugation.

I.5.2.2 Details of the radiochemical separation and analyses procedure.

Prior to the analysis of the solution, samples were filtered through 0,45 μm filters in order to remove coarse fuel particles. An aliquot of some samples was passed through an ultrafiltration membrane (pore size 18 A) to check for colloid formation. Filtrates were preserved by adding 1 M HNO_3.

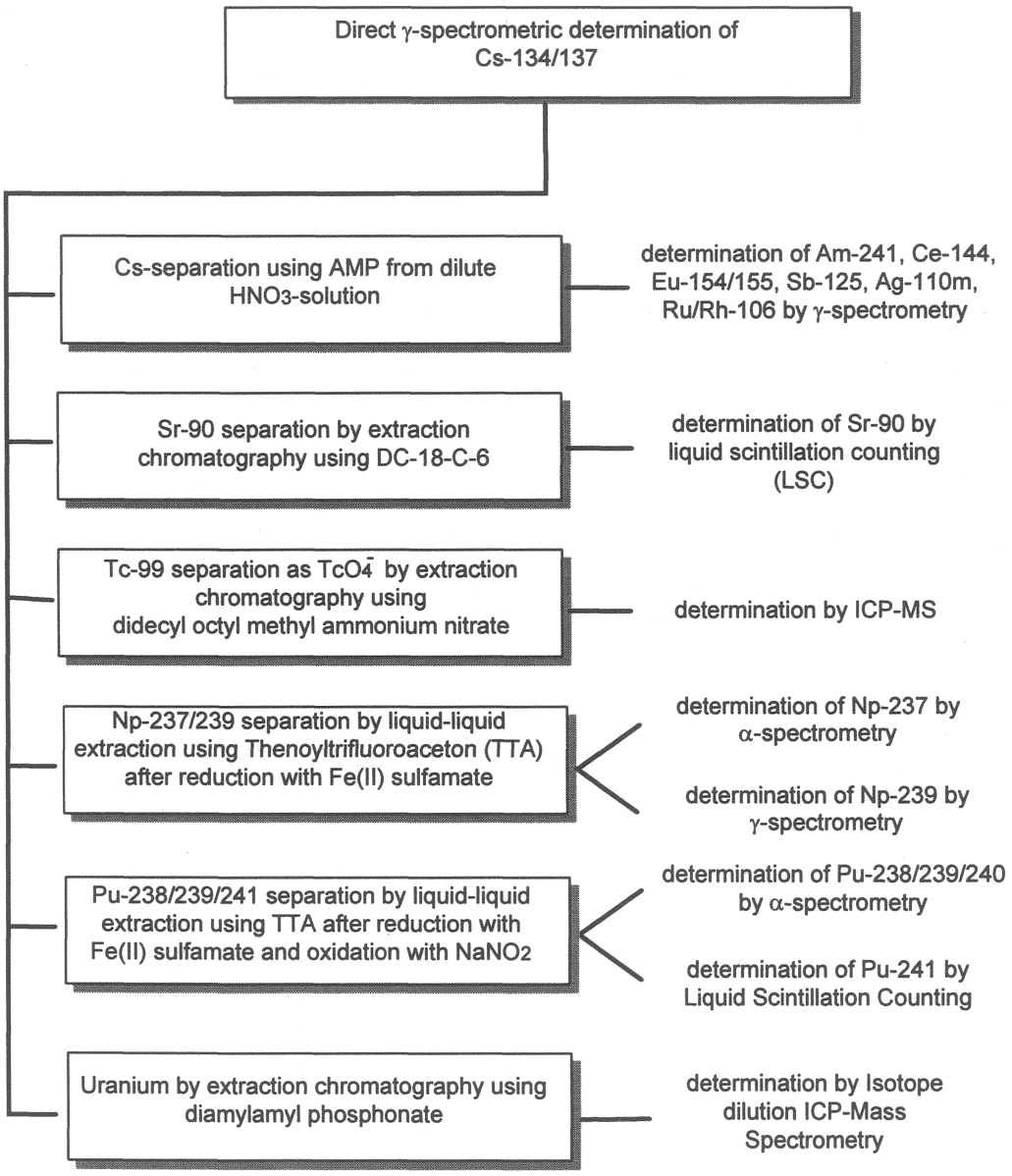

Figure I.10: Flowsheet of the radioanalytical procedure

For the determination of almost all radionuclides a prior isolation by radiochemical separation steps was necessary. This was done by either liquid-liquid extraction or extraction

chromatography procedures. For the final determination of nuclide concentrations nuclear analytical methods as α-, γ-spectroscopy and liquid scintillation counting (LSC) were used. For the long-lived radionuclides U-238 and Tc-99 ICP-MS prooved to be more sensitive. An overview over the complete analytical procedure is shown in Figure I.10.

Only Cs-134 and Cs-137 were determined directly by γ-spectrometry in diluted sample solutions (dilution factor: 1000). Other γ-emitting nuclides such as Am-241, Ce-144, Eu-154, Eu-155, Ru-106, Ag-110m and Sb-125 could be detected after separation of the Cs-isotopes being present in high excess. Cs is removed by specific sorption on the inorganic cation-exchanger ammonium molybdophosphate (AMP). Due to the high γ-doserate of some sample solutions the separation is carried out by adding 3 g AMP to 10 ml of the 1:10 diluted solution in a shielded alpha-box with remote handling. Cs is effectively removed from solution with decontamination factors of about 10^3-10^4. After filtration through a membrane filter with pore diameters of 0,45 µm, all other radionuclides were determined subsequently in the filtrate. Recovery rates for other nuclides after Cs-separation in the filtrate were determined to range from 95 to 100 %.

Due to the Cs-separation the Compton-background of the γ-spectrum decreased to such an extent, that other γ-emitting isotopes like Ce-144, Eu-154/155, Am-241, Sb-125, Ag-110m and Ru-106/Rh-106 could be detected. γ-spectra of a sample solution before and after Cs-separation are shown in Figure I.11.

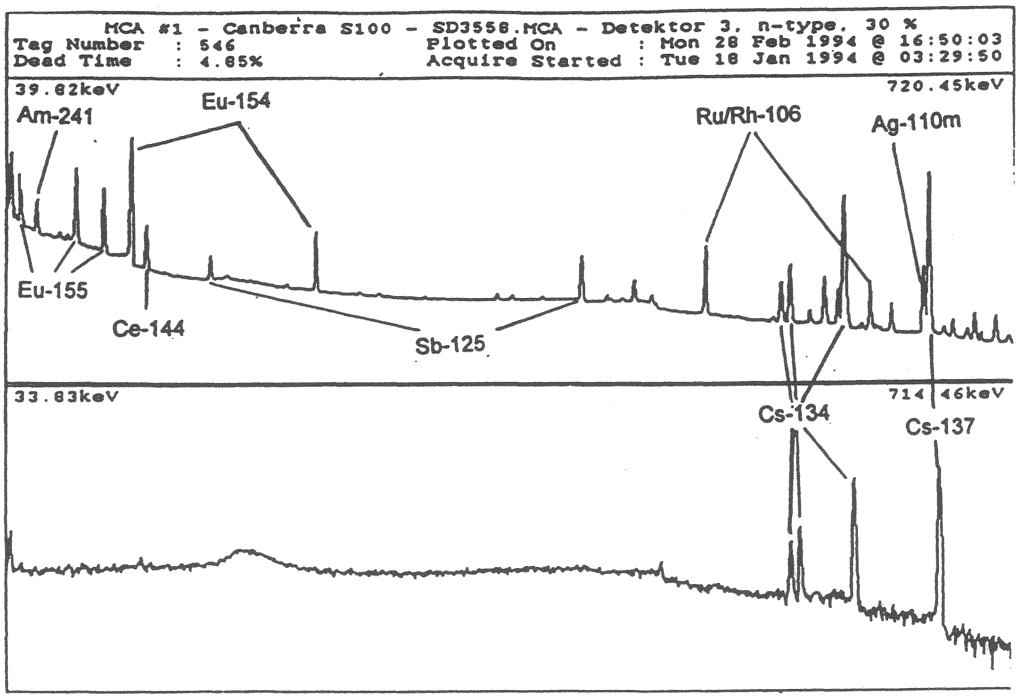

Figure I.11: γ-spectra of the same sample solution before (lower spectrum) and after (upper spectrum) Cs-separation

The radiochemical separation of Sr-90 is carried out using a chromatographic material consisting of an inert support and di-tert-butyl-cyclohexyl-18-crown-6 as a selective extractant for Sr. After Cs-separation 1ml of the sample solution was adjusted to 8 M HNO_3 and non-radioactive Sr-tracer was added. The sample was passed through a 1 ml column and Sr eluted with 10 ml 0,05 M HNO_3. An aliquot of the elute was measured immediately by LSC. The result of this measurement is verified by a second LSC-measurement after ingrowth of the daughter nuclide Y-90. Thus, it is possible to eliminate errors due to other co-extracted radionuclides. The separation yield was determined by ICP-AES analysis of the non-radioactive Sr and varied between 83% to 93%. Care had to be taken for cross-contamination effects from one sample to another, due to a slow kinetic of the Sr-desorption from the column. Therefore it has been necessary to wash the column after and before each separation extensively.

The analysis of Tc-99 by solvent extraction of the ion-pair complex of TcO_4^- with tetraphenylarsonium (TPA) and subsequent determination by LSC proved to be not satisfactory. Even after excessive washing of the organic phase the β-spectra recorded by LSC revealed the non-purity of the sample. Interferences were mainly due to high concentrations of coextracted Ru/Rh-106 and Pu-isotopes. Therefore a new procedure was applied consisting of a separation step using didecyl octyl methyl ammonium nitrate immobilized on an inert carrier and subsequent determination by ICP-MS. The sample aliquot (1-2 ml) had to be adjusted to 0,5 M HNO_3 and then was passed through a column filled with approx. 1 ml of the resin. Tc-99 was sorbed as TcO_4^- and subsequently eluted with 8 M HNO_3. After evaporation to near dryness the residue was dissolved in 0,5 M HNO_3 and analyzed by ICP-MS. The chemical yield over the whole procedure was controlled γ-spectrometrically using Tc-95m as a tracer. To verify Tc to be present as TcO_4^- the sample was treated with H_2O_2 before separation. Possible interferences due to the high concentrations of Mo in all samples could be excluded. No overlap of the peaks at 98 and 100 AMU to the peak of Tc at 99 AMU was observed. Mo is inferred by the Cs-separation step using AMP. On the basis of the 3 σ error of the background count rate a detection limit of $1,3 \cdot 10^{-3}$ ng/ml (= $0.83 \cdot 10^{-3}$ Bq/ml) can be calculated for the ICP-MS analysis. For comparison LSC-analysis of a pure Tc-99 solution shows a detection limit of $7,3 \cdot 10^{-2}$ Bq/ml (1 ml sample solution measured / 68,5 % efficiency / measuring time: 60 min). Under real conditions Tc-99 samples are always

contaminated after separation. Consequently real detection limits for LSC-analysis strongly depend on the sample composition and are even higher. A typical mass spectrum in the range 96 to 101 AMU of a separated Tc-sample is shown in Figure I.12.

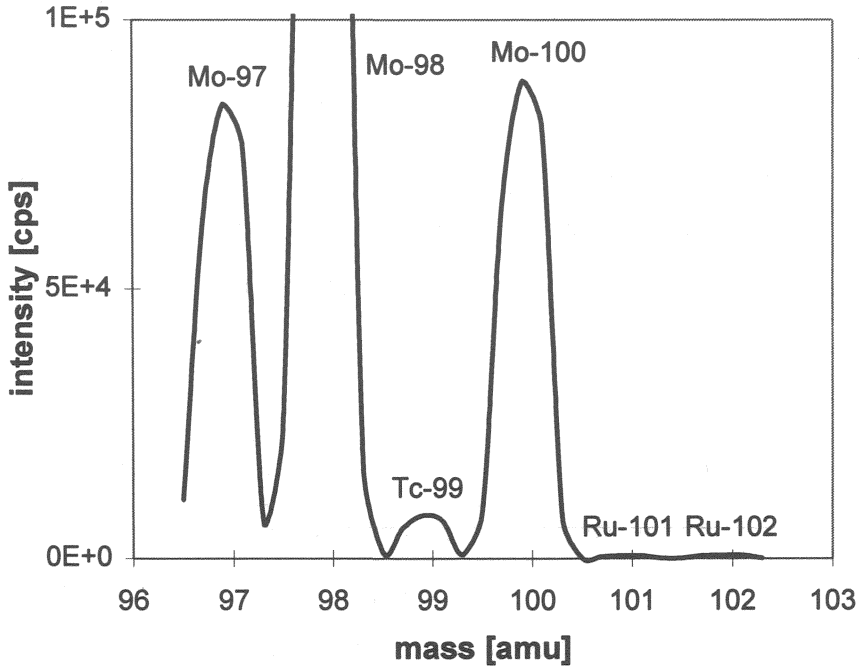

Figure I.12: Mass spectrum of a separated Tc-99 sample (c (Tc-99) = 0,49 ng/ml ± 1% / c (Mo) = 420 ng/ml)

1 ml aliquots of the sample solution were submitted to solvent extraction with thenoyltrifluoracetone (TTA) in order to separate Np and Pu from the samples. A selective extraction of both elements separately is possible by adjusting different oxidation states. Firstly Np was reduced from V to IV using Fe(II)sulfamat and then was extracted by TTA from 1 M HNO_3. Pu exists under these conditions in the oxidation state (III) and therefore remains in the aqueous phase. After washing the organic phase and stripping Np into 8 M HNO_3, the aqueous solution was evaporated on a stainless steel dish and analyzed by α-spectrometry. In a second aliquot of the solution Pu was reduced as described before and reoxidized to the oxidation state (IV) with $NaNO_2$. After re-extraction of Pu into 8 M HNO_3-solution Pu-238 and Pu-239/240 were determined by α-spectrometry and Pu-241 by LSC. The separation yield for the Pu-separation was taken into account by using Pu-236 as an isotopic tracer. It was found that NaCl-concentrations have almost no influence on the Pu-extraction yield until 2 M.

The separation of Am-241 and Cm-242/244 was modified compared to the procedure described in the last progress report. Instead of a cation exchanger an extraction chromatographic resin containing CMPO/TBP as extractant was used. Tri-, tetra- and hexavalent actinoids are sorbed from 3 M HNO_3, but only the trivalent actinoids are eluted by 4 M HCl. After evaporation of the HCl-solution the residue was dissolved in HNO_3 and analyzed by α-spectrometry.

The analysis of uranium was not possible by radiometric methods due to the low specific activity of the uranium isotopes and low concentrations in sample solutions. Therefore two methods - a compact laser fluorescence spectrometer (LFS) (SCINTREX, UA-3) and ICP-mass spectrometry (ICP-MS, Perkin-Elmer) - have been tested for their suitability of uranium trace analysis. For both methods it is necessary to separate uranium from an excess of matrix components. Especially in the case of LFS, uranium fluorescence is heavily influenced even by low salt or acid concentrations. Uranium separation has been carried out in 3 M HNO_3-solution by extraction chromatography using diamyl amylphosphonate sorbed on an inert support. For LFS-analysis uranium is desorbed from the column by a buffer containing 0,5 M H_3PO_4/0,04 M $Na_4P_2O_7$. The phosphate/pyrophosphate buffer additionally serves as a fluorescence amplifier. After neutralization of the acidic solution the sample was filled into a quartz cuvette and fluorescence intensity was measured. The uranium concentration was quantified by the standard addition method. From the 3 σ-error of the background a detection limit of 0.6 ppb was calculated.

ICP-MS offers two advantages over LFS: 1) isotope dilution analysis can be applied using U-233 as a tracer and 2) isotope ratios of uranium can be determined. After addition of U-233 as an isotopic tracer the separation from the matrix was done as described before. With 0.5 M $H_2C_2O_4$ uranium was eluted and the solution directly submitted to ICP-MS analysis. A detection limit 0,01 ppb was calculated for the analytical conditions used, thus being one order of magnitude lower than LFS. Separation yields varied from 92 to 100 %. Figure I.13 shows a comparison of uranium concentration measured by LFS and ICP-MS.

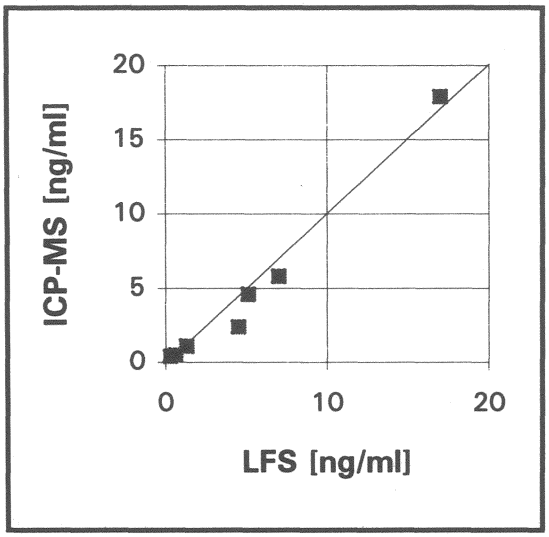

Figure I.13: Comparison of uranium concentrations determined by laser fluorescence and ICP-MS after chemical separation of uranium

Considering the low uranium concentrations in the lower ppb range the conformity of the results is quite satisfactory. Due to the lower sensitivity of ICP-MS against matrix effects and the possibilities to apply isotope dilution analysis and to determine isotope ratios the latter method was favored over LFS analysis.

Analytical quality control

In order to get a feeling for the reliability of the analytical procedure the quality of the applied methods has been validated, where possible, by internal standardization using isotopic tracers and additionally by intercomparison runs with the radiochemical laboratory of the institute of hot chemistry (IHCH). A flowsheet of the analytical steps is shown in Figure I.10.

In order to guarantee a high confidence level in the analytical results two kinds of quality control methods were applied:

- internal quality control

For most of the radiochemical separations isotopic tracers were added to the sample solution in order to verify the chemical yield of the whole procedure. This has been done for Sr-analysis using non-radioactive Sr, for Tc-analysis using Tc-95m, for Pu-analysis using Pu-236 and for U-analysis using U-233.

Pu-analysis was checked for plausibility by comparing the total α-activity of all Pu-isotopes determined by α-spectrometry with gross α-activity measured by LSC (Figure I.14).

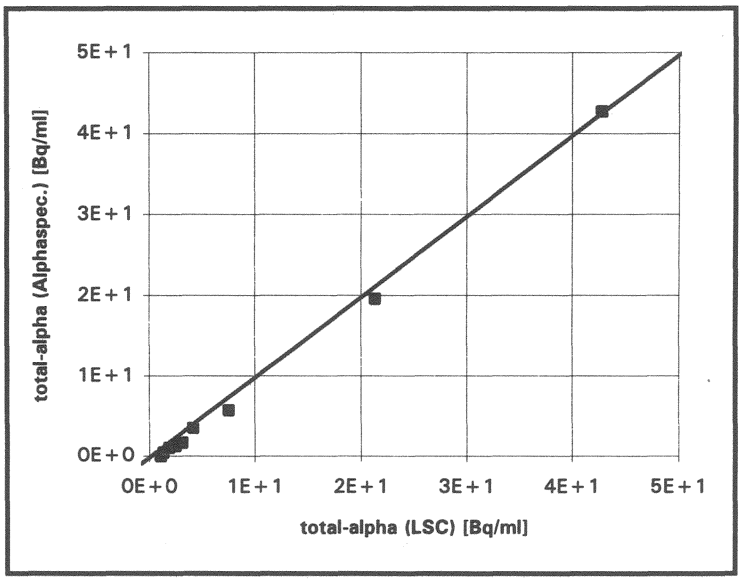

Figure I.14: Quality control of Pu-analysis by comparison of total α-activity determined by α-spectrometry with total α-activity determined by LSC

Am-241 analysis additionally was verified by comparing direct γ-measurement after Cs-separation and determination after selective separation of the trivalent actinides and alphaspectrometric analysis.

- external quality control

An intercomparison was organized with the radioanalytical laboratory of IHCH. As an example the results of Pu-238 analysis, Sr-90-analysis and determination of Am-241 were compared in Figure I.15. In general the results agree satisfactorily and show scattering only in the lower concentration range, thus demonstrating the limits of the analytical methods.

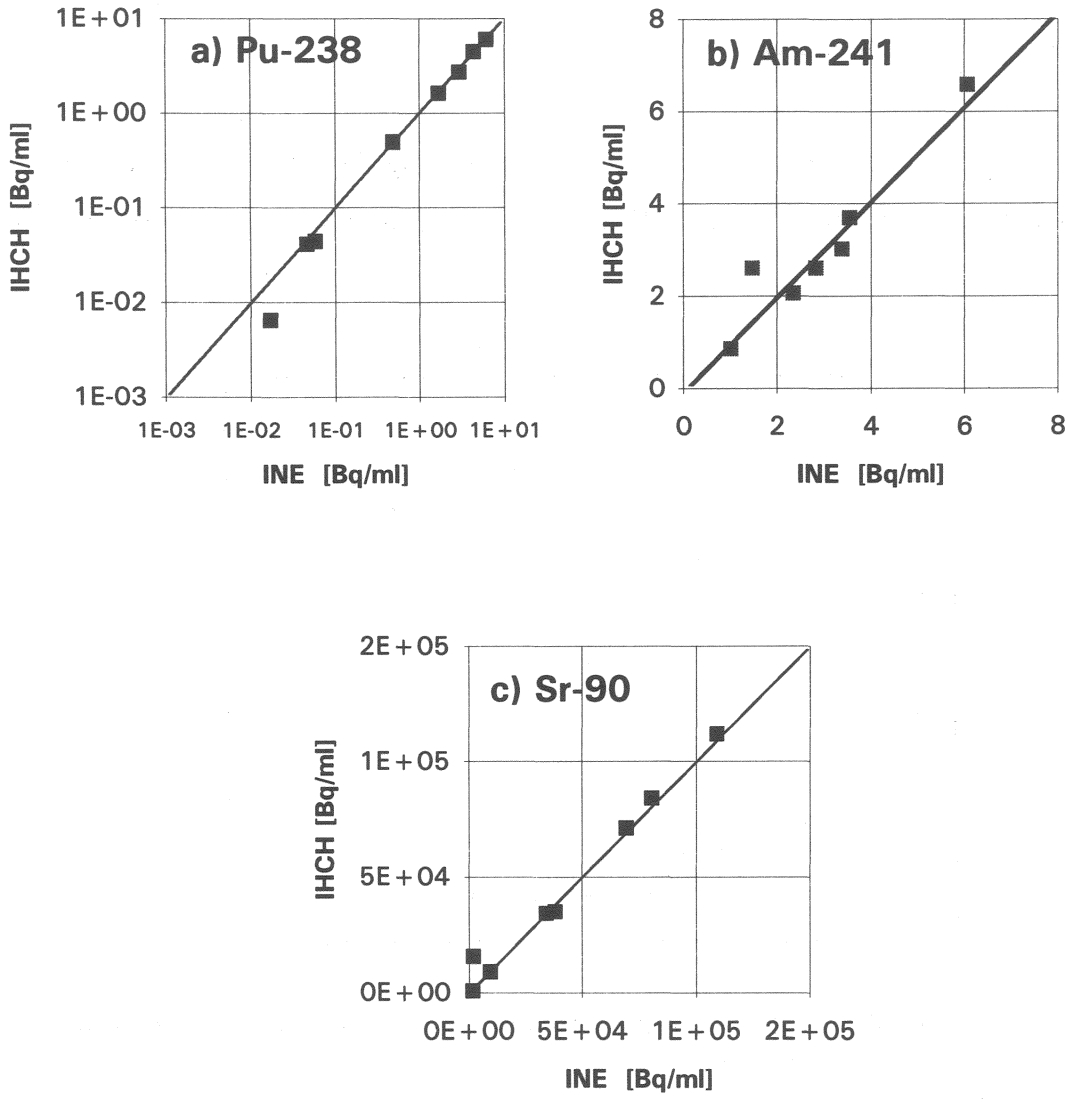

Figure I.15: Intercomparison test run for the determination of a) Pu-238, b) Am-241 and c) Sr-90 after radiochemical separation methods by INE and IHCH laboratory

I.5.3 Analyses of radiolytic and fission gases.

Using an evacuated (10^{-6} bar) gas collection cylinder (V=50 cm^3), the atmosphere inside of the reaction vessels was sampled. The gas collection vessel was connected to the

autoclaves by a stainless steel tubing. Prior to opening the valves of autoclave and gas collection vessel, the tubing was evacuated for about 5 minutes by a pump (ca. 1 mbar). Gas composition was analyzed quantitatively by a quadrupole mass spectrometer (GAM 445, Balzers, Lichtenstein). Calibration was performed, using a gas mixture of known amounts of H_2, N_2, O_2, Kr and Xe in Ne. The gas sampling scheme is shown in Figure I.16.

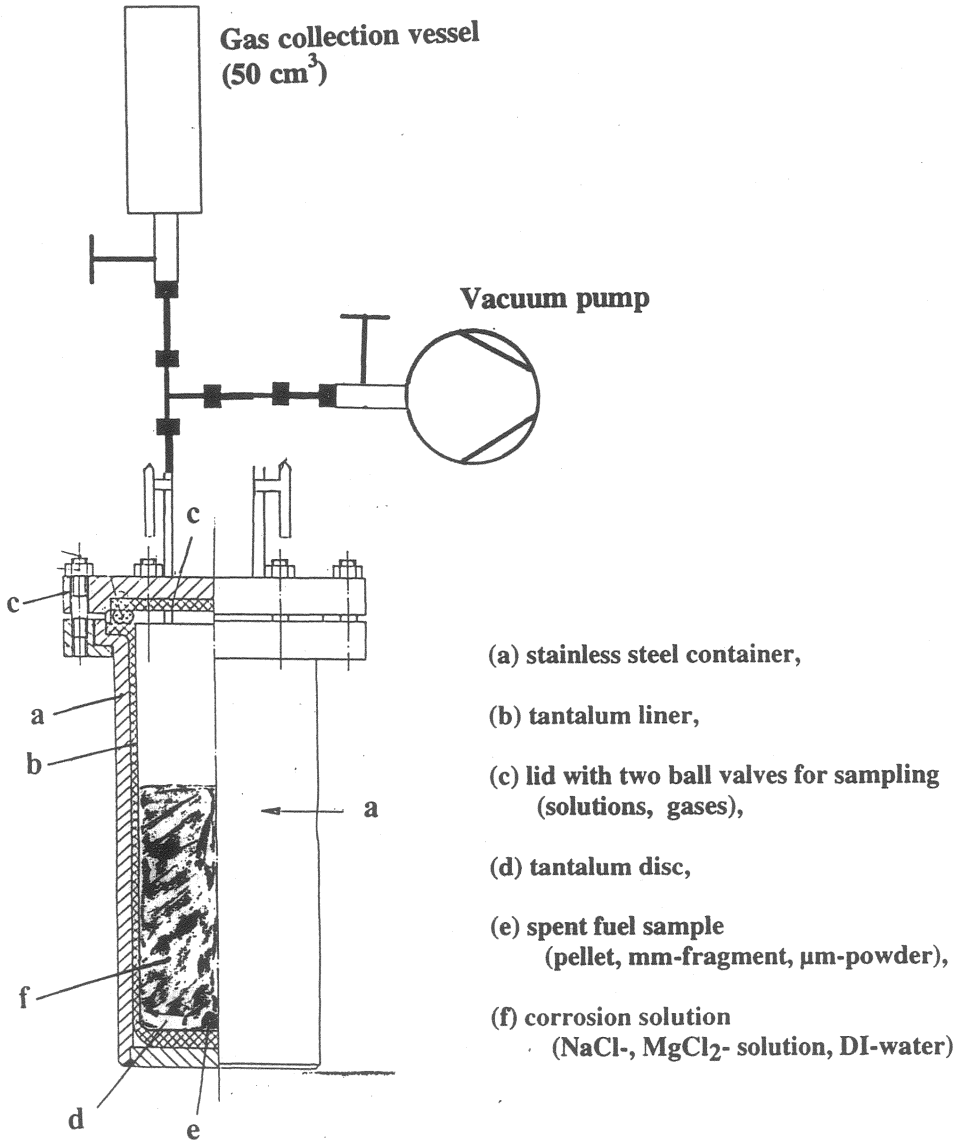

Figure I.16: Scheme for taking of gas samples from autoclaves containing spent fuel.

II. CHARACTERIZATION OF THE DURABILITY OF SPENT UO_2 FUEL IN SATURATED NACL BRINES

The corrosion tests are designed in such a way, that fundamental mechanism of spent fuel dissolution and associated radionuclide release in saline solution could be evaluated in the context of requirements of long-term performance assessment of spent fuel in a repository. The test plan is guided by two criteria: the tests should be as simple as possible to facilitate interpretation and they should be relevant to a repository in salt formations. The following parameter were studied, influencing fuel dissolution mechanism and rates: redox potential, radiolysis, surface area to solution volume ratio, temperature, time and salinity. It has been shown in the literature that the redox potential is the most sensitive parameter in the stability of uranium minerals in natural environment as well as of spent fuel and UO_2 under experimental corrosion conditions. In a repository, free and dissolved oxygen will be rapidly consumed by metallic engineered barrier materials, leaving the geochemical environment anoxic or even reducing. Consequently, the effect of anoxic versus reducing environment is tested. Very much care was taken in our tests to control and avoid oxygen access into the autoclaves, to maintain anoxic conditions for test durations of about 2 years, even under conditions of periodical solution sampling. Reducing conditions were achieved in a very realistic manner by codissolving the fuel with added metallic iron in some of the autoclaves. Most tests were performed at room temperature to facilitate comparison of our results for saline solution with internationally reported data on spent fuel behavior in deionized water and granite groundwaters. This comparison has two objectives: it should identify specific effects of saline solutions on the dissolution mechanism, if present, and it should identify burnup effects, as the fuel used in our study had significantly higher burnup (50MWd/kgU, see chapter I) than those used in most other studies (typically a value of 33 MWd/kgU is used). One test were performed at higher temperature (150°C) to confirm that temperature is not of primary concern in spent fuel dissolution studies.

Radionuclide release resulting from fuel dissolution and grain boundary leaching is analyzed in such a way that the release controlling processes could be distinguished: coprecipitation, solubility, sorption, sources of release and rate controls. Pure NaCl solutions, 95% saturated with respect to halite, were used in most tests, instead of one of the various solutions of the quinary or hexary system of oceanic salts which might be expected in a repository in salt formations. The close deviation from halite saturation should prevent halite

formation in the experiments and during sampling. The choice of this leachant allowed to compare radionuclide release properties from our tests with actinide solubilities reported in the literature. It will been shown further below that the choice of such a simplified leachant did not alter the fuel dissolution mechanism.

II. 1 Test description.

Experiments are performed under static conditions in 200 ml 95% halite (NaCl) saturated, anaerobic (Ar), carbonate and nitrogen free solutions at 25°C and at 150°C. Air influx during the experiment was avoided by using Ti99.8Pd0.2 or Ta lined tight autoclaves as reaction vessels. Pellet sized fuel segments, individual fragments and powdered fuel were used as spent fuel samples. A detailed sample description is given in Table I.2. Cladding was present in tests with pellets and with fuel powders but not with fuel fragments. Prior to static testing, the samples were "washed" twice in NaCl solution under Ar-atmosphere, for periods each of one month duration, to remove the gap inventory of Cs and possibly oxidized surface layers. Thereafter, the experiments were continued under static conditions. In all autoclaves a metal plate of Ti99.8Pd0.2 was added to allow analyses of reactions a the walls of the reaction vessels at test termination. In two tests 8.5 g iron powder (Merck 3819, average grain size 10 μm) was inserted after starting the static test. The leachates were sampled 5 times during about two years of static tests. At the end of the static tests sorbed material on reaction vessel or iron corrosion products is analyzed. Table II.1 and Figure II.1 summarize the various tests and sampling conditions used. A detailed description of the reaction vessel, the materials used, the sampling methods and sample characterization is given in Chapter I.

Sample surface area to solution volume ratios (S/V) and specific surface areas used in the tests

Certain aspects of the spent fuel dissolution process and associated radionuclide release will depend strongly on the geometric constraints in a repository. Among those are processes which depend on the accumulation of dissolved material or radiolysis products in solution (saturation effects etc.) or processes which depend on the depletion of reactants (i.e. trace levels of residual dissolved oxygen). Moreover, the specific surface area of the fuel (i.e. the "particle size") has a significant influence on the contribution of alpha decay to overall radiolysis effects. In order to consider these effects in spent fuel performance assessment, specific care must be taken on the scale up of experimental set-up to repository geometry.

Table II.1: Test and sampling conditions used in spent fuel corrosion experiments

Sample	Mass (g)	Solution	T	Wash cycles(d)		Corrosion tests under static conditions						
				Duration (d) of		Accumulated corrosion time (d) and dates of sampling solutions (S 1 - S 5) and gases (G 1 - G 2)						
				Cycle 1	Cycle 2	S 1	S 2	S 3	G 1	S 4	G 2	S 5
*K 1	7,335	DI-Water	25°C	31	45	45	107	199	418	437	750	750
K 2	7,109	DI-Water	25°C	31	45	45	107	199	418	437		running
K 3	6,976	NaCl - sol.	25°C	30	41	a) 52	114	206	344	438	745	745
K 4	7,534	NaCl - sol.	25°C	31	42	b) 50	112	207	284	438		running
K 9	7,429	NaCl - sol.	25°C	31	42	53	116	207	390	441		running
K 10	7,369	NaCl - sol.	25°C	32	42	52	115	206	390	442	752	752
K 13	6,937	NaCl - sol.	150°C	63	0,16	61	173					
**F 3	0,02	NaCl - sol.	25°C	33	43	49	112	203	n.m.	437		749
F 4	0,008	NaCl - sol.	25°C	33	43	49	112	203	n.m.	440		running
***P 1	2,9	NaCl - sol.	25°C		42	c) 40	83	201	385	409	657	657
P 2	2,95	NaCl - sol.	25°C		42	c) 42	83	201	385	409		running

*K: compact pellet with cladding

**F: fragment

***P: powder (O< 5μm)

Addition of:

a) 8,5 g Fe-powder (Ø < 10 μm)

b) 9,5 g Fe-powder (Ø < 10 μm)

c) 0,65 g Zircaloy - cladding

Fig. II.1: Sampling intervals in spent fuel corrosion experiments

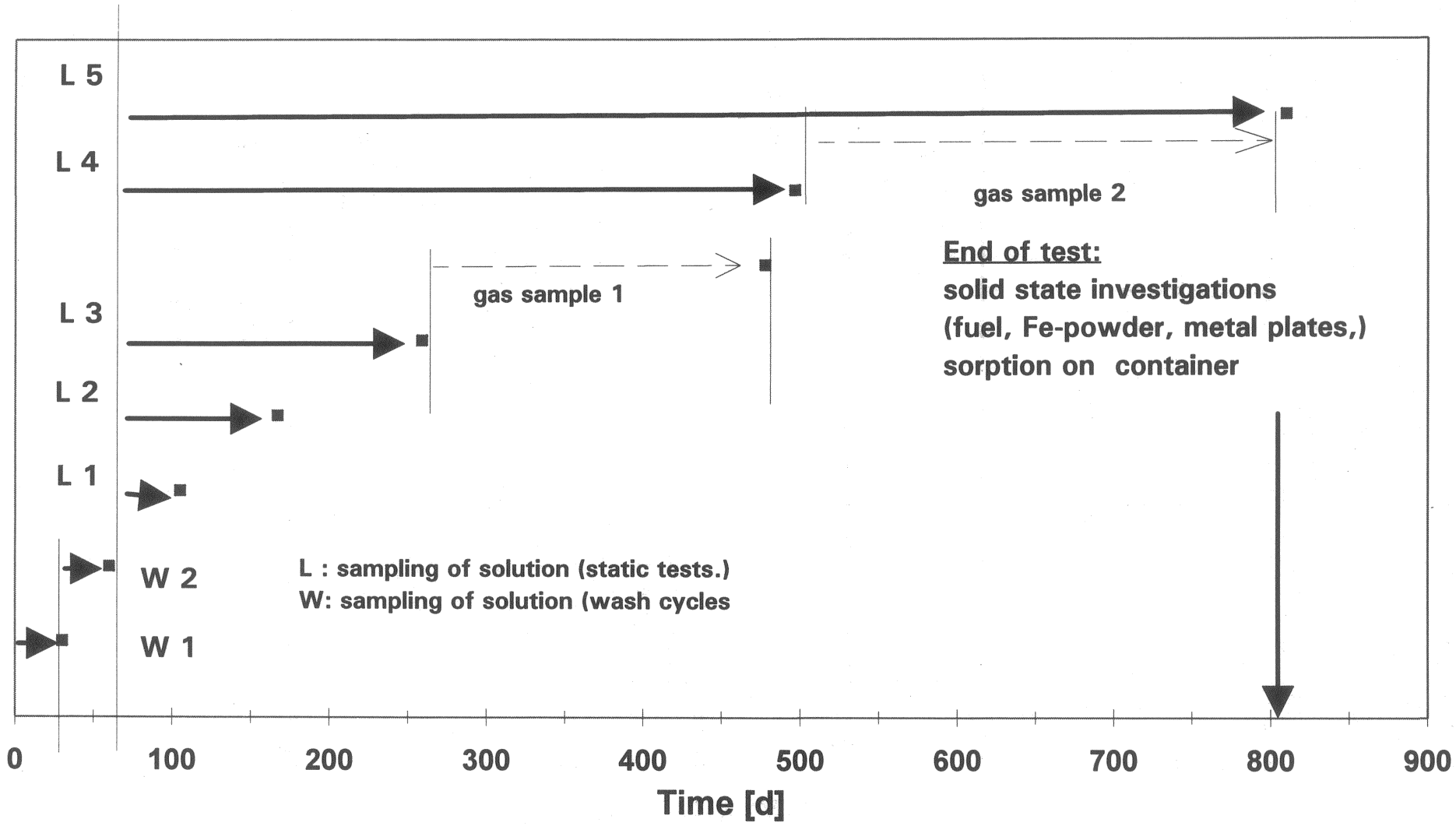

For this purpose the ratio of the sample surface area to the solution volume (S/V) was varied by many orders of magnitude. The surface area of the fuel samples used in our tests is not known exactly but minimum values may be estimated from geometrical considerations. Due to surface roughness, effective surface areas may be 2-3 times higher (typical surface roughness factor: 2.5) and effective surface areas may be further increased by water accessible grain boundaries.

The geometrical relations between specific sample surface areas and the ratio of surface area to solution volume encountered in our tests are compared in Figure II.2 to the geometric relationships expected in a repository.

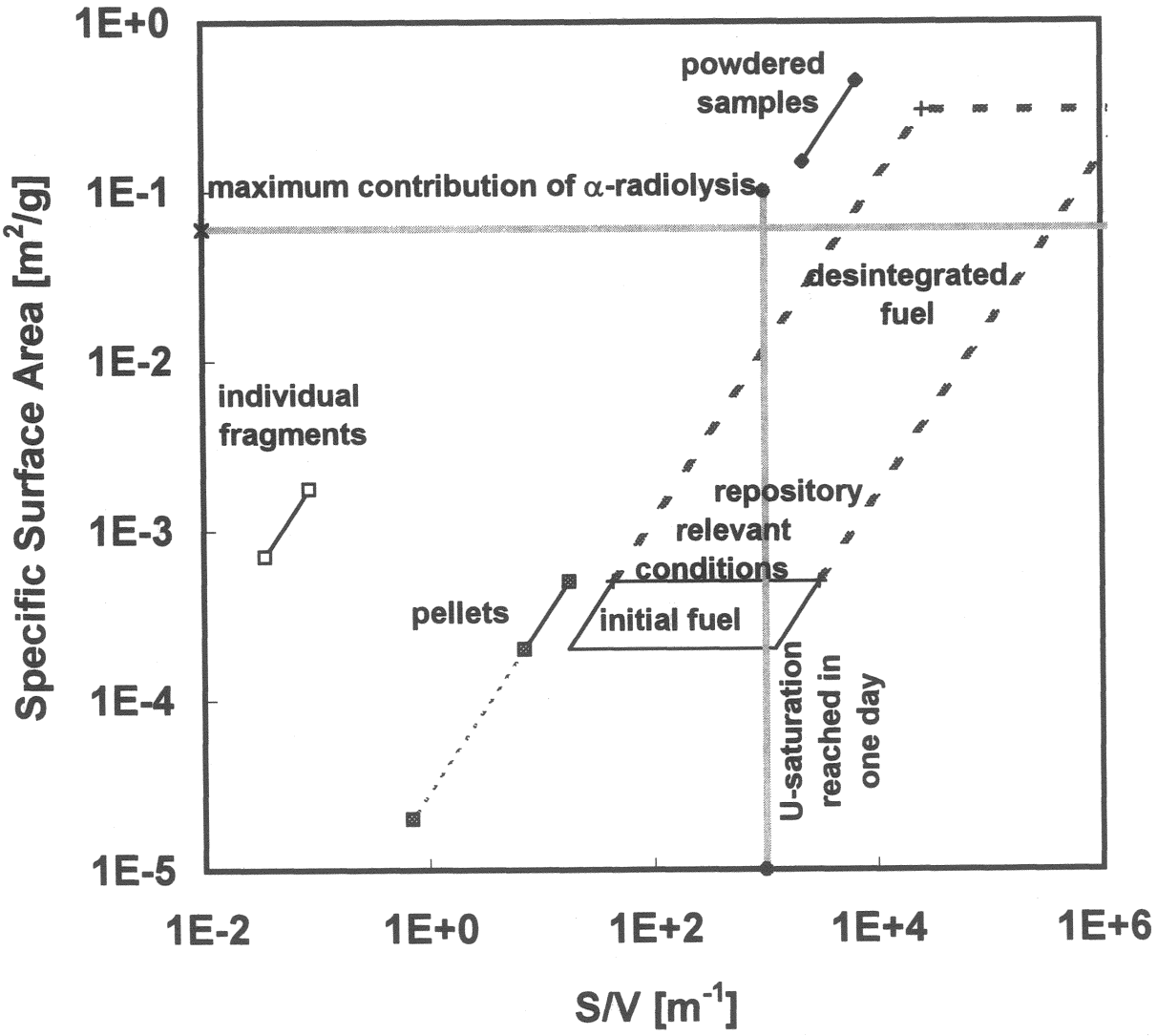

Figure II.2: Relations between specific sample surface areas and the ratio of sample surface area to solution volume (S/V) in our tests, compared to expected values in a repository

For all experiments a solution volume of 200 ml was used. Surface areas and their uncertainties are estimated as follows. Pellets: With a typical fragment diameter of about 2-3 mm, the specific surface area of a pellet sized fractured fuel segment (fuel not decladded) is at least $2*10^{-4}$ m^2/g (fragments idealized as cubes) corresponding to $1.4*10^{-3}$ m^2 for the surface area of a pellet sized fuel segment. However, if only the two cross sections of the segment are considered exposed to the solution, the effective surface area may be as low as $1.4*10^{-4}$ m^2 (broken line in Figure II.2). Fragments: The individual fragments used have a diameter of about 1 mm, corresponding to a specific surface area of at least $7*10^{-4}$ m^2/g and a sample surface area larger than $6*10^{-6}$ m^2. The effect of surface roughness on specific surface areas and S/V ratios is calculated for fragments and pellets with a surface roughness factor of 2.5. Though, this is only an estimation of the absolute effective surface area, we know in relative terms that the surface area of an individual fragment is about 200 times smaller than that of a fractured pellet as surface roughness will be the same for an individual fragment as for a whole pellet composed out of these fragments. Powders: For the powdered fuel with an average grain diameter of about 3 μm the specific surface area is about 0.3 m^2/g and the sample surface area is 0.9 m^2. We assume an uncertainty in the effective surface area of at least 100%.

The data in Figure II.2 show that despite the uncertainty in the actual values of the effective surface areas our tests could cover both large variations in the sample surface area to solution volume ratio (S/V) as well as in specific surface area. S/V values were >1000 m^{-1} for powders, >10 m^{-1} or 1 m^{-1} for pellets, and >0.01 m^{-1} for fragments. Also included in Figure II.2 is a line, designating the specific fuel surface area at which almost all α-decay events lead to α-radiolysis effects, i.e. a line at which the average particle radius is smaller (5 μm) than the average escape depth of α-particles. Maximum contribution of α-radiolysis to overall radiolysis will be expected beyond this line. We may also describe saturation effects in this diagram. For a given dissolution time, saturation effects will occur at a fixed S/V ratio. As an example the S/V ratio is calculated, necessary to reach schoepite solubility (a arbitrary value of 10^{-5} mol U/l was used) within a day of spent fuel dissolution with a typical dissolution rate of 0.002 $g/(m^2 d)$.

For comparison the range of repository relevant data are calculated for a single waste package (German concept of drift emplacement of Pollux containers) assuming that either a maximum volume of an intruding brine ($50m^3$) filling an emplacement gallery of 20 waste

packages is contacting a single waste container (4300 kg UO_2 fuel), or, alternatively, a solution volume representing only the void space of the filled Pollux cask (ca. 1 m^3) was considered. Specific surface areas were similar as those used for pellets in our experiments (geometric area: $2*10^{-4}$ m2/g or $5*10^{-4}$ m^2/g when considering surface roughness). Additionally, potential oxidative disintegration of the fuel into powder was considered (0.3 m^2/g, broken line in Figure II.2), an effect which is a quite well known result of U_3O_8 formation. The comparison of the geometrical constraints of the experiments with repository relevant conditions show that realistic S/V ratios could be achieved in powder tests, and realistic specific surface areas were achieved both by tests with fuel powders and pellets. However, none of the tests covered the expected combination of S/V and specific surface area, because such tests would require solution volumes, too small to be useful in long-term laboratory experiments. Considering the effects of α-radiolysis and saturation effects, tests using powdered fuel samples seems to resemble most closely conditions of relevance for the performance assessment of spent fuel in a repository.

II. 2 Useful units for data evaluation.

The corrosion behavior of the fuel and associated mobilization of radionuclides is deduced mainly from radiochemical solution analyses, but also from analyses of the gas phase, being present in the autoclaves and to a certain extent from solid state investigations, with respect to the spent fuel samples, the container material and the iron powder, which was corroded simultaneously with the spent fuel pellet K 3 in NaCl-solution. Methods for data evaluation are described as follows.

II. 2.1 Fractions of radionuclide inventories of samples in the aqueous phase.

In order to be able to evaluate the mobilization behavior of various radionuclides in a relative manner, the measured activities of the nuclides i in the aqueous phase are normalized to the inventory of this nuclide i in the fuel sample. A fraction of inventory in the aqueous phase ($FIAP_i$) is calculated as

$$FIAP_i = A_i * V \ / \ (W * f_{HM} * AI_i)$$

where A_i is the specific activity in the aqueous phase (Bq/L), V is the solution volume (L) and AI_i is the specific nuclide activity inventory in the fuel (Bq/g heavy metal, see Table I.3); W is the sample weight and f_{HM} is the fractional mass of heavy metal in the fuel. f_{HM} is calculated by $f_{HM} = MG_U/MG_{UO2}$ where MG_U and MG_{UO2} are the molecular weights of uranium and uranium dioxide (for initially 3.8% enriched $MG_U = 237,9$ and $MG_{UO2} = 269,9$). If the FIAP values of two elements are the same, they are released congruently from the fuel, i.e. the ratio of activities in solutions matches the ratios of the nuclide inventories in the fuel. This unit is rather useful of distinguishing controls of radionuclide release by fuel matrix dissolution from selective release of radionuclides from grain boundaries or selective retention of radionuclides due to precipitation processes.

Everything is considered part of aqueous phase, which can be transported by water, this comprises truly dissolved and colloidal species. In this way, we can define the FIAP as a sum of the fraction of inventories in colloids (FIC) and truly dissolved fraction (FIS)

$$FIAP = FIS + FIC.$$

Arbitrarily, a cut-off boundary between mobile and immobile (solid) phase is set at the filter size of 0,45 μm. Fuel grains, detached from the fuel sample during the experiment would be retained on the 0.45 μm filter and are not considered in the FIAP value. For calculating the total release R(tot) of non-gaseous radionuclides from the fuel samples during the experiments, the fraction of inventory sorbed onto the liner of the reaction vessel (FIV) and if present on iron corrosion products (FIFE) must be considered:

$$R(tot) = FIAP + FIFE + FIV$$

and the total inventory fraction of a radionuclide participating in any alteration reaction is A(tot) given by

$$A(tot) = R(tot) + FIRP + FIZr$$

where FIRP and FIZr are the fractions of inventory immobilized in secondary solid alteration products or on the zircalloy cladding respectively. For all radionuclides, which are contained exclusively in the fuel matrix, the A(tot) values should be the same. However, A(tot) values of elements such as Cs or J released also from grain boundaries or from the fracture surfaces may be significantly higher. Values for FIRP and FIZr could not be measured directly, as any mechanical or chemical procedure of removing solid reaction products from the fuel samples would inevitably also remove simultaneously certain quantities of non-altered fuel. Nevertheless, since A(tot) values should be the same for all matrix bound elements, one may use the A(tot) value of a rather soluble nuclide for estimations. It will be shown further below, that Sr90 data are often very useful in indicating the total degree of fuel matrix alteration. Then we can use the following relation for a given soluble or insoluble nuclide i

$$(FIRP + FIZr)_i = A(tot)_{Sr} - R(tot)_i$$

to estimate the fractions of inventories remaining on the fuel samples.

II.2.2 Elemental solution concentrations

In order to interpret the radiochemical analyses data in terms of solution chemistry and solubility constraints it is necessary to transform radioactivity data of individual nuclides to concentration data of a given element. If the element consists of only one isotope, or if all isotopes are measured, this transformation can simply been done using specific activity values. However, in many cases not all isotopes could be measured.

Solution concentrations of the various elements can be calculated if we assume that there are no specific isotopic fractionation processes, and if we further assume that KORIGEN calculates the correct mass fraction of each active and inactive isotope. In case of Pu, isotopes with the masses 239, 240 and 242 were measured alpha-spectroscopically only as one peak. Pu concentrations can be obtained from this peak, if the mass fractions of the various isotopes are known. Considering that the predicted ratio of Pu238 to Pu239/40/42 matches rather well the experimental observations (Table I.5) we can assume that the results calculated by

KORIGEN (Table I.3) can reliably be used to obtain the required individual isotopic mass fractions. For Curium four years after discharge from the reactor, we measure mainly Cm244, however half of the Cm mass fraction is not measured: Cm245/246. In case of Cerium we measured Ce144. However, already four years after discharge from the reactor 99,5% of Ce is inactive and could not be measured by radiochemical techniques.

Using these assumptions, concentrations C_e of elements e in the aqueous phase (truly dissolved and colloidal) can generally be calculated by the formula

$$C_e = FIAP_i * MI_e * W * f_{HM} / V$$

or alternatively

$$C_e = A_i * MI_e / AI_i$$

where MI_e is the specific elemental mass inventory in the fuel (µg/g heavy metal, Table I.4)

II.2.3 Normalized mass loss

The extent of matrix dissolution may be expressed as "normalized mass loss, NL_i" of the nuclide i. This unit is frequently used to describe the dissolution behavior of nuclear waste borosilicate glasses. If the NL_i values of uranium and of the nuclide i are the same, than the nuclide i is released congruently with the dissolution of the matrix. Upper limits for NL values can be calculated from FIAP values, using the estimated minimal geometric sample surface areas S_{min} and the sample mass m.

$$NL_i = FIAP_i * m/S_{min}$$

Using the formula

$$d_i = NL_i/\rho$$

with the density ρ of the fuel (10.4 g/cm3) one obtains a depth d_i from which the nuclide i is released. In case of glass this depth is known as a "equivalent depletion depth". NL and d values are upper limits as the effective surface area is higher than the geometric.

II. 3 Results

II. 3.1. Solid phase investigations

Spent fuel pellets.

Figures II.3-II.5 show optical micrographs of cutting planes of spent fuel pellets K1, K3, K10 before and after corrosion at room temperature in deionized water and in NaCl solution with and without iron present. All samples show clear signs of solid/solution interactions.

Pellet K1, corroded in deionized water for 740 days, was found coated by a not yet identified white surface layer, preferentially accumulated along the fractures and the fuel sheet gap (Figure II.3). The white color of the layer indicates that it is not a U(VI) containing secondary alteration product, as this would either be yellow or orange. SEM analyses showed that the added Ti/Pd metal plate was covered by a similar white layer. Here it could be identified as Ti-oxide, indicating that this phase may have been precipitated as well on the spent fuel sample.

Pellet K3, corroded for 745 days in 95% saturated NaCl - solution at room temperature in the presence of 8,5 g metallic iron is shown in Figure II.4. One of the corroded cutting planes (left side, bottom in autoclave) is coated by a concentric ring of accumulated iron powder, ca. 1 mm near to the edge of the sample. The central part shows a similar degree of darkness as observed prior to corrosion. The opposite cutting plane (top in autoclave) was probably less in contact with the iron powder during the corrosion test as only small amounts of iron powder were visible. This surface was brighter than the other one.

Cutting planes of the pellet K10 before and after 752 days of corrosion in NaCl-solution at room temperature are shown in Figure II.5. Despite the specimen was rinsed with deionized water, white layers, surface layers probably of precipitated NaCl crystals were observed on both surfaces.

Spent fuel fragment (F3)

SEM-micrographs of spent fuel fragment F3, corroded for 740 days in NaCl-solution are shown in Figure II.6. This sample originated from the outer part of the fuel pellet, contacting the cladding (micrograph at the top). Therefore, results from corrosion tests with fragment F3 should allow to assess the contribution of the rim region to overall radionuclide release in contact with the NaCl -solution. Additionally, SEM-images are shown, with details of the microstructure of the corroded sample in comparison with a non-corroded similar type of spent fuel sample. After corrosion, individual grain boundaries of the matrix became clearly visible, indicating preferential grain boundary corrosion. Grains are characterized by a rounded shape, resulting from the corrosion process. Secondary phase formation could not be identified.

Iron powder (K 3)

From the autoclave with experiment K3 (experiment in NaCl solution in presence of Fe), samples of corroded iron powder were taken both during the test and after test termination. After a total corrosion time of 478 days, 2 ml of an iron containing suspension were sampled by means of a syringe. The iron powder was separated from the solution by passing the suspension through a paper filter. The filter was dried and treated partially with DI-water in order to remove precipitated NaCl - crystals. A sample of the iron powder was analyzed by SEM-EDX and an aliquot was dissolved in concentrated nitric acid, for determining the adsorbed quantities of radionuclides. At test termination, after a total corrosion time of 674 days, the entire corroded iron powder was recovered, a defined amount of 99 mg was dissolved in concentrated HCl another samples were used for SEM-EDX and X-ray diffractometry.

In the course of corrosion, the iron powder reacted with oxygen, produced by radiolysis, as well as with chlorine, supplied from the NaCl-solution. Figure II.7 shows SEM micrographs of the original metallic iron powder (Merck No. 3819) and the iron powder at test termination after 674 days of corrosion. The results of sampling after 478 days were

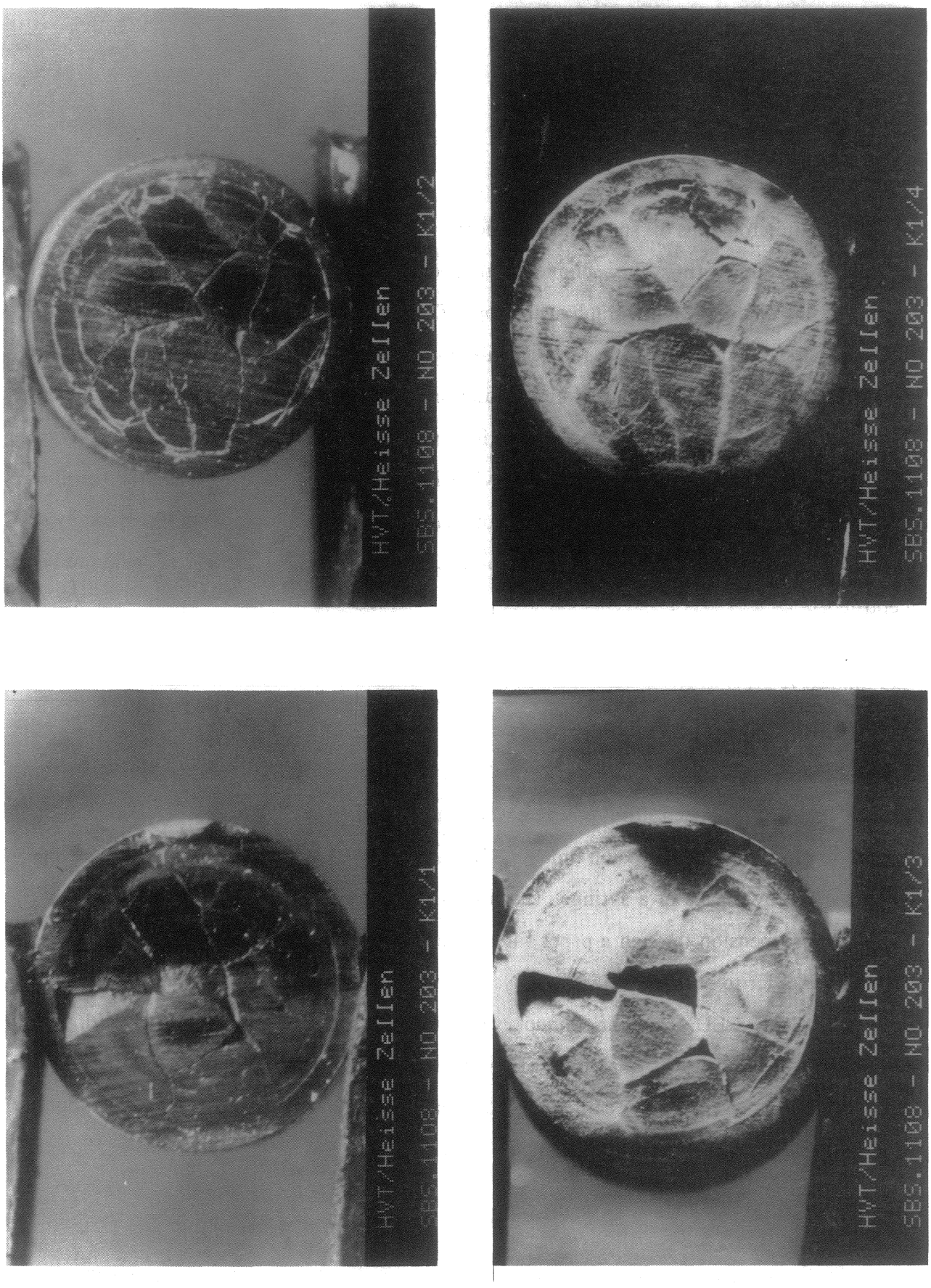

Figure II.3: Optical micrographs of sample K1 cut surfaces prior and after two years of corrosion at room temperature in deionized water

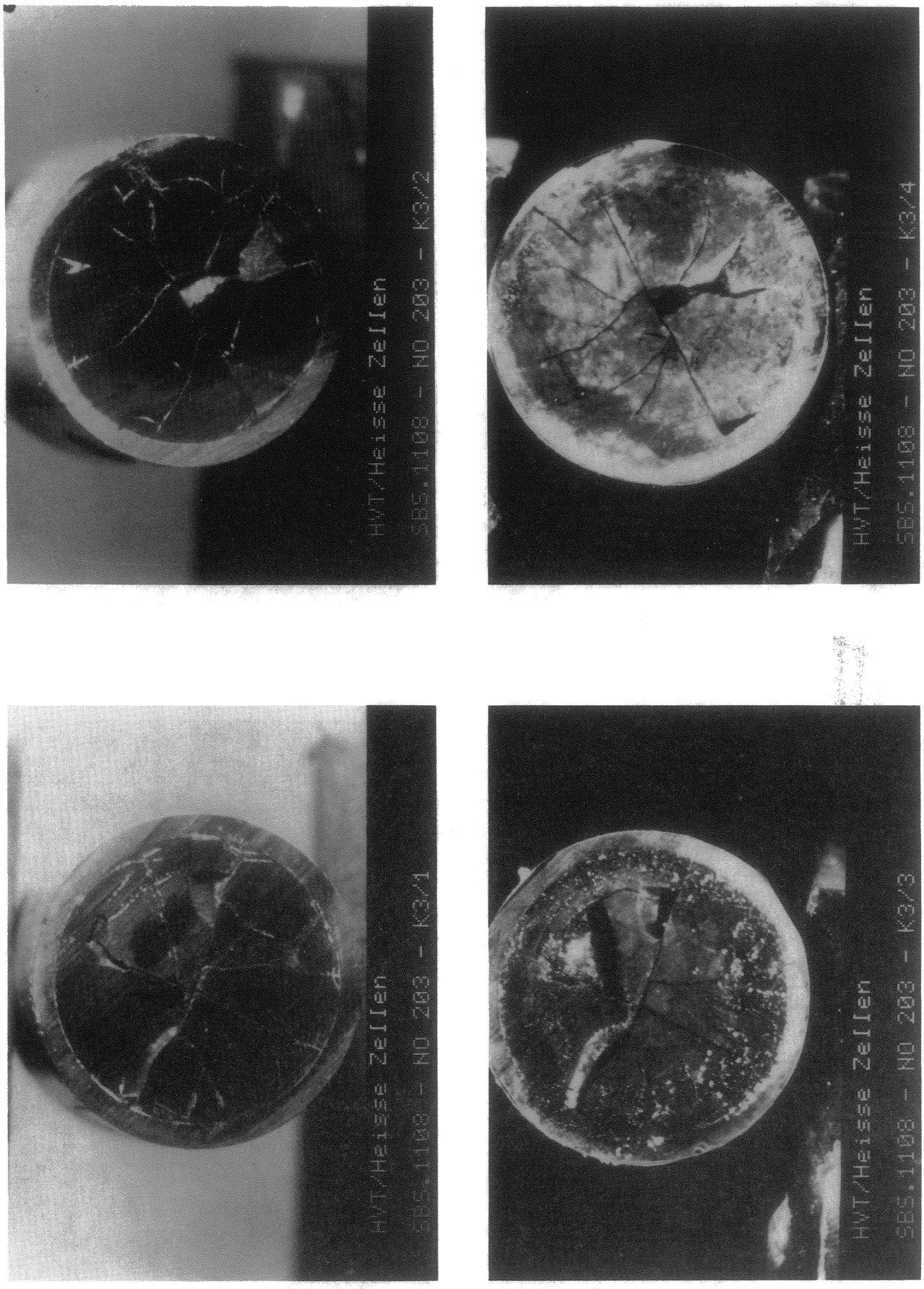

Figure II.4: Optical micrographs of sample K3 cut surfaces prior and after two years of corrosion at room temperature in 95% saturated NaCl solution in presence of 8.5 g of iron powder

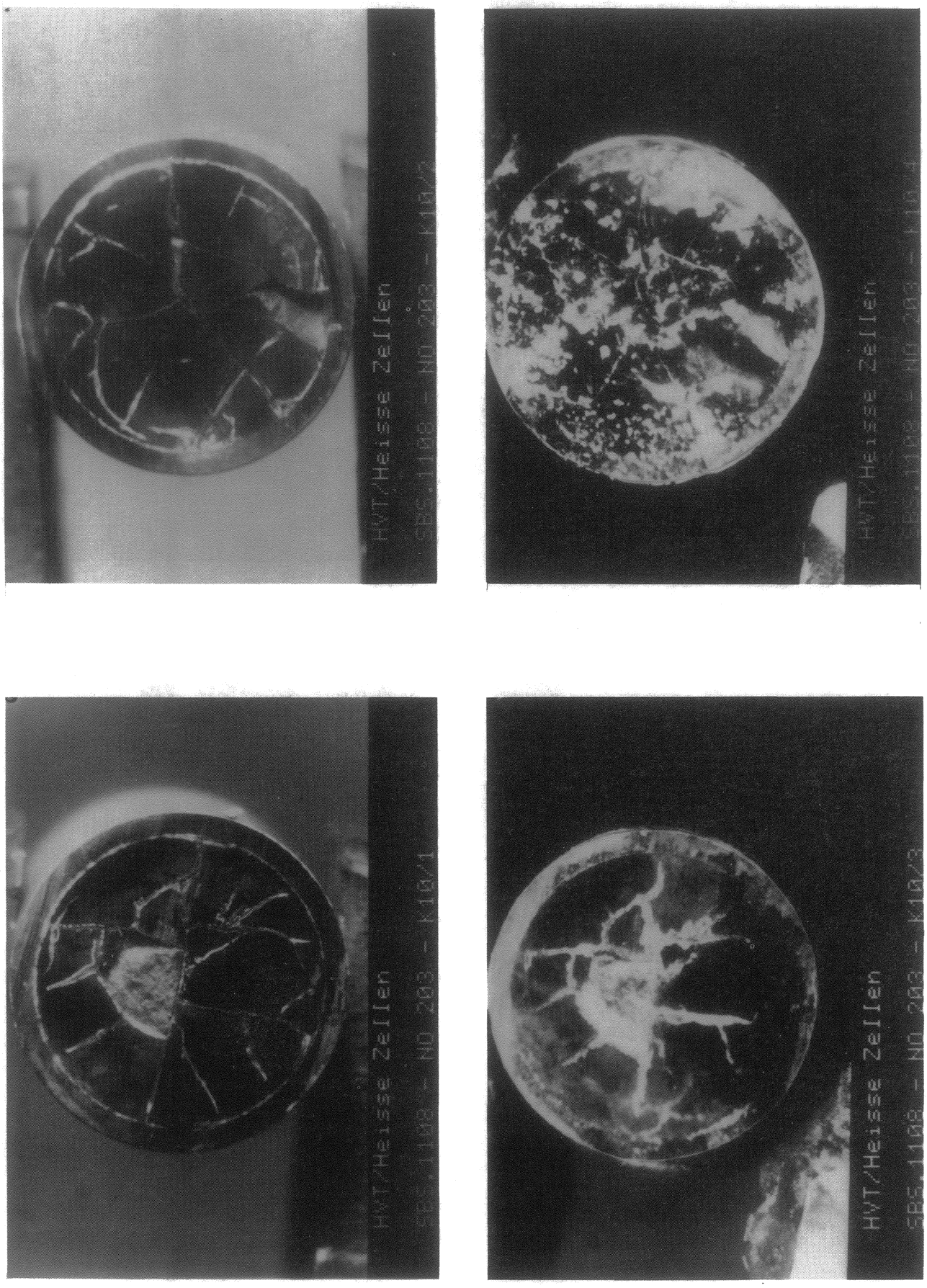

Figure II.5: Optical micrographs of sample K10 cut surfaces prior and after two years of corrosion at room temperature in 95% saturated NaCl solution

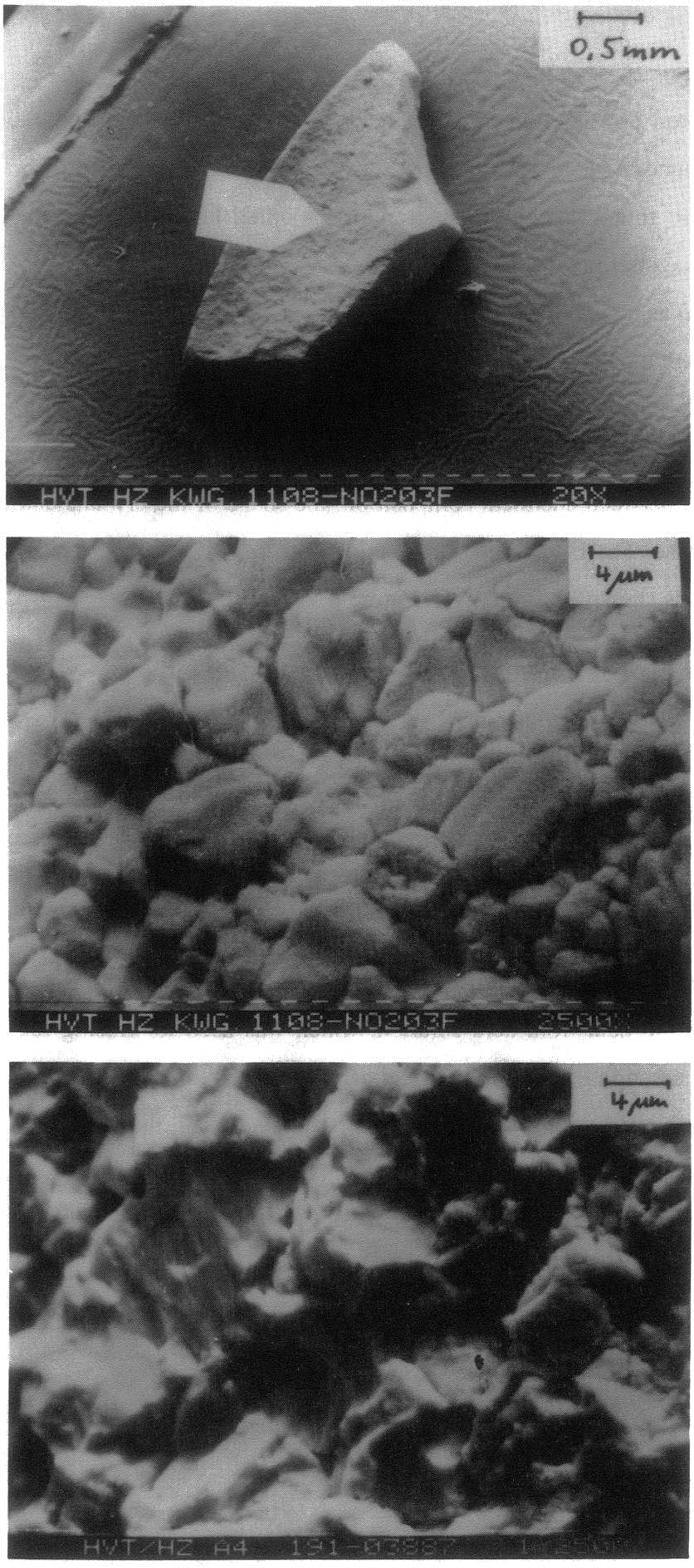

Figure II.6: SEM micrographs of sample F3 after two years of corrosion at room temperature in 95% saturated NaCl solution, top: overview showing fuel rim, center: corroded fuel grains, bottom: uncorroded fuel grains

similar. The initial iron powder was not completely oxidized, because metallic, as well as oxidized iron were found. As analyzed by EDX, spherical metallic iron particles from the starting material were found coated by an iron (hydr-)oxide layer. Additionally, a newly formed phase of hexagonal crystal plates of up to 8 μm in size was found. EDX analysis revealed Fe, Cl and O as main compounds. By means of X-ray powder diffraction α-Fe and a magnetite (Fe_3O_4) were identified as crystalline phases. Two remaining reflections at d-values of 3,94Å and ca. 7,9Å may be related to the main reflections of the hexagonal Fe-O-Cl phase and are tentatively identified as indications for the presence of green rust I. A relative good agreement was found between chemical composition, the shape of the crystals and the X-ray reflections of this phase. The EDX spectrum of this phase, labeled by the white rectangle in the SEM-micrograph is shown additionally in Figure II.7.

Sorption effects on the Fe powder

The extent of sorption of radionuclides on the iron was determined by dissolving an amount of 99 mg corroded iron powder, taken at test termination, in 20 ml boiling concentrated HCl. An aliquot was analyzed radiochemically. Results are listed in Table II.2, related to activity values of the entire amount of 8,5 g iron powder, which was inserted. Additionally nuclide activities of the remaining corrosion solution (164 ml) from the end of the test are included and data from acid solution, which was used for rinsing the container wall. Results are discussed in Chapter II.4 (Effect of iron) in the context of the distribution of various radionuclides between the aqueous phase, the container wall, the surface of the spent fuel sample and the iron powder (corrosion products).

Table II.2: Radionuclide activities of 164 ml corrosion solution (after 674 days of corrosion), of the container wall and from 8,5 g iron powder after 674 days of corrosion (dissolution of 99 mg Fe in boiling concentrated HCl).

Nuclide	Activity in 164 ml NaCl-solution	Activity on the container wall	Activity on 8,5 g Fe-Powder
Ru106	< 3,03 E 3 Bq	n.d.	1,03 E 5 Bq
Cs134	2,94 E 8 Bq	n.d.	6,56 E 5 Bq
Cs137	8,02 E 8 Bq	n.d.	2,52 E 6 Bq
Eu154	< 4,25 E 2 Bq	n.d.	1,30 E 5 Bq
Eu155	< 6,04 E 2 Bq	n.d.	5,78 E 4 Bq
Sb125	< 2,25 E 3 Bq	n.d.	5,36 E 4 Bq
Sr90	2,21 E 6 Bq	1,42 E 5 Bq	2,18 E 5 Bq
Ce144	< 1,56 E 3 Bq	n.d.	9,44 E 4 Bq
Am241	2,43 E 1 Bq	6,95 E 3 Bq	3,57 E 4 Bq
Np237	<7,59 E 0 Bq	7,43 E 0 Bq	< 7,1 E-1 Bq
Cm244	<1,21 E 1 Bq	5,98 E 4 Bq	n.d.
Cm242	<2,43 E 0 Bq	9,46 E 1 Bq	n.d.
Pu238	< 9,59 E 1 Bq	4,86 E 3 Bq	4,09 E 4 Bq
Pu239/40	< 7,79 E 1 Bq	6,16 E 2 Bq	4,62 E 3 Bq
Pu241	< 2,30 E 3 Bq	6,56 E 4 Bq	4,66 E 5 Bq
U	3,03 E 0 ng	1,37 E 1 ng	2,12 E 2 ng

Sorption on the Ti/Pd-liner

In order to investigate whether radionuclides where either sorbed or precipitated on the Ti/Pd-liner of the reaction vessels, the acid strip solutions of the liners taken at test termination were analyzed radiochemically. Nuclide specific results are found in the Appendix for each experiment. In order to better understand how the Ti/Pd liner participated in the reaction, metal plates consisting of the same liner material were inserted into the autoclaves at test begin. At the end of the experiment the metal plates were investigated by means of SEM/EDX.

SEM investigations of the Ti/Pd metal plate from the test **K1** (pellet corroded in DI-water) showed the formation of a Ti-oxide phase. Few prismatic crystals (ca. 10 µm x 2 µm x 2 µm) of an uranium oxide phase, were also present. Figure II.8 shows the SEM micrographs of the surface and the element distribution images for O, Al, C, Ti, U and Mo. Figure II.9

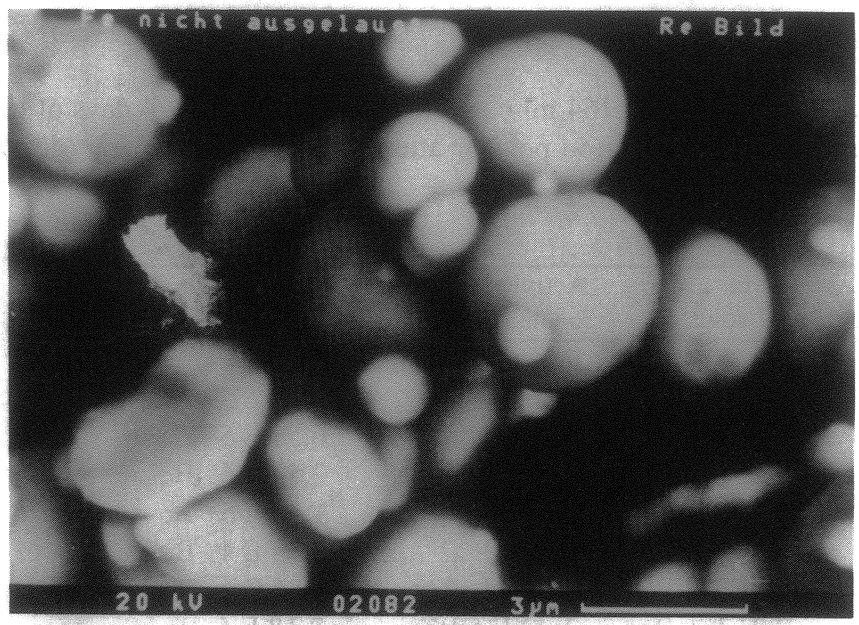

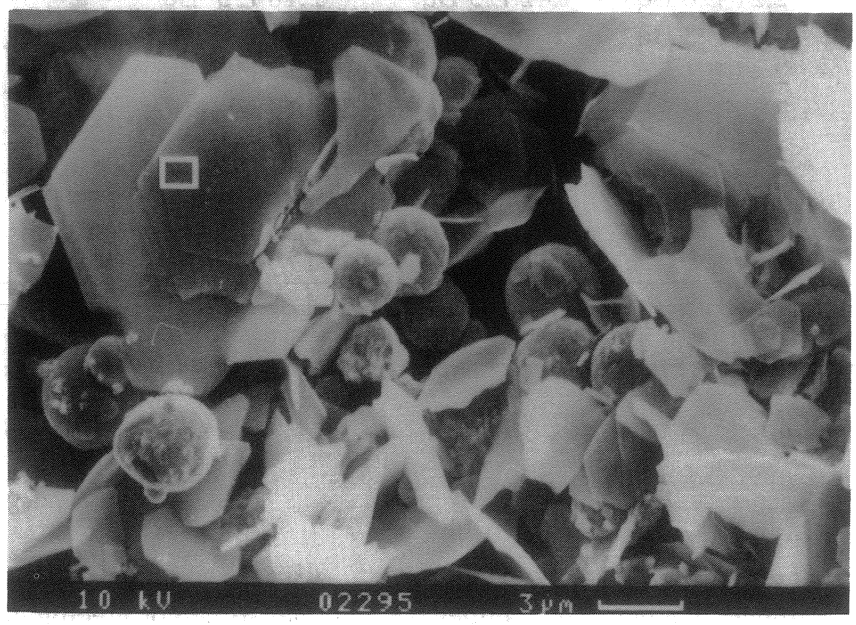

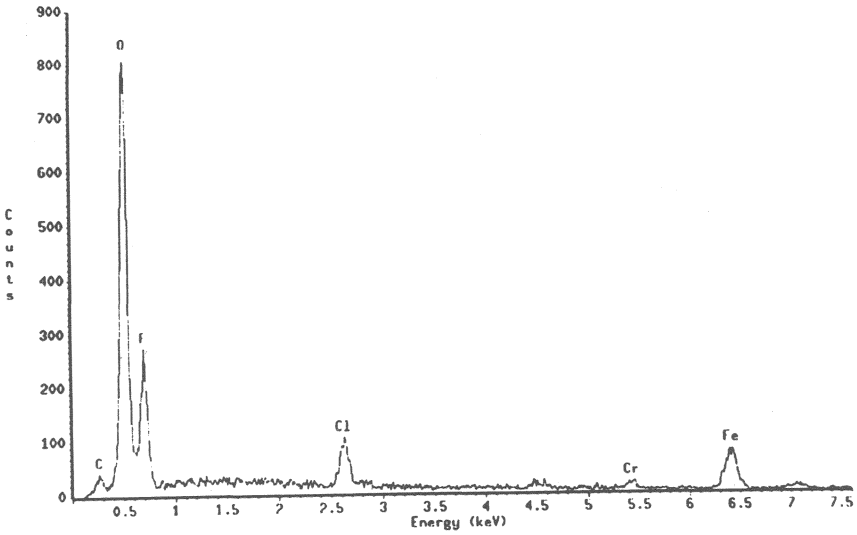

Figure II.7: SEM micrographs and corresponding EDX images of non-corroded (top) and corroded (center) iron powder from test K3 (fuel pellet sample corroded for two years at room temperature in 95% saturated NaCl solution) and EDX-spectrum of the crystal, labeled with the white rectangle.

displays an SEM micrograph of an uranium oxide crystal, as analyzed by EDX, together with the corresponding EDX spectrum.

The surface of the Ti/Pd metal plate from the test **K3** (pellet and iron powder in 95% saturated NaCl-solution) is covered by a layer, consisting only of grains of iron powder and their corrosion products. Figure II.10 shows a SEM micrograph of this layer and the corresponding integral EDX spectrum.

After the corrosion of pellet **K10** in 95% saturated NaCl-solution, on the surface of the Ti/Pd metal plate NaCl crystals of up to 200 μm in size have formed. Figure II.11 shows a typical SEM micrograph with newly grown NaCl crystals and the EDX determined integral element distribution image for O, Na, Cl, Ti. Except of the uranium oxide phase formed upon corrosion in deionized water, no further compound of the fuel was found precipitated on any of the Ti/Pd metal plates.

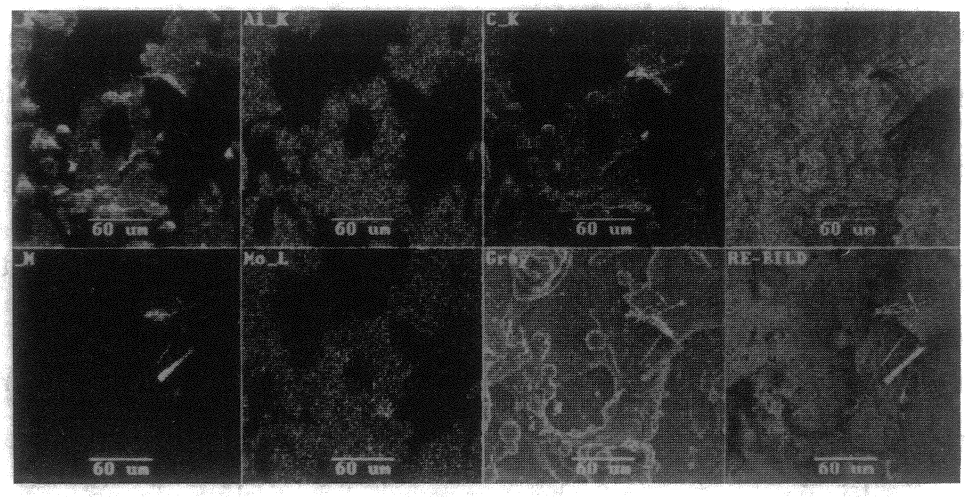

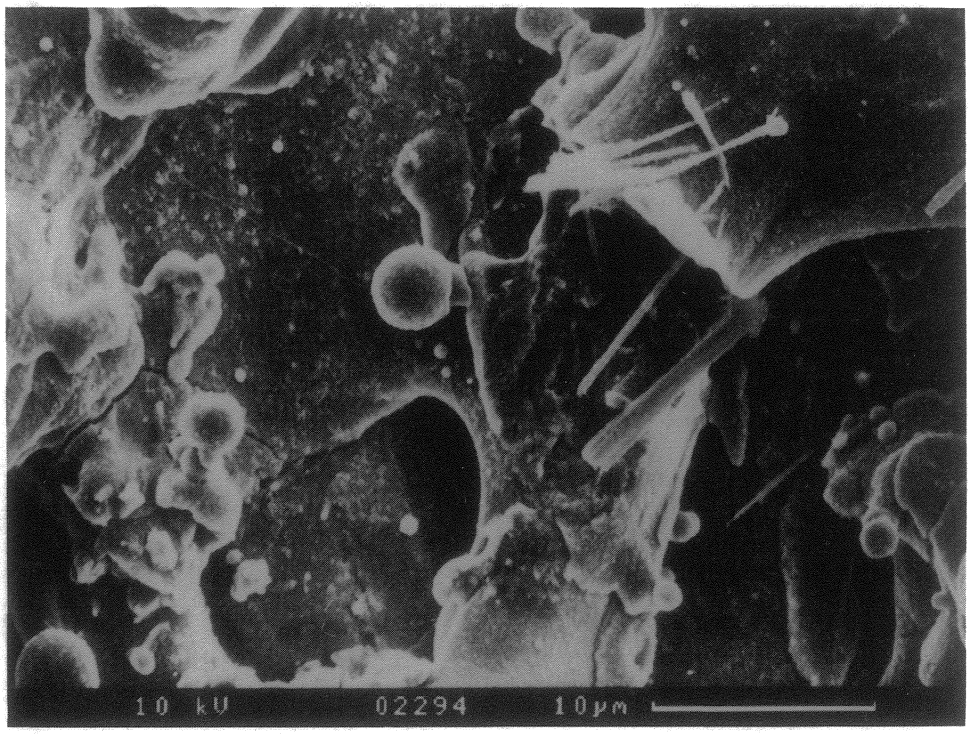

Figure II.8: SEM micrographs of the Ti/Pd plates of test K1 after two years of corrosion at room temperature in deionized water

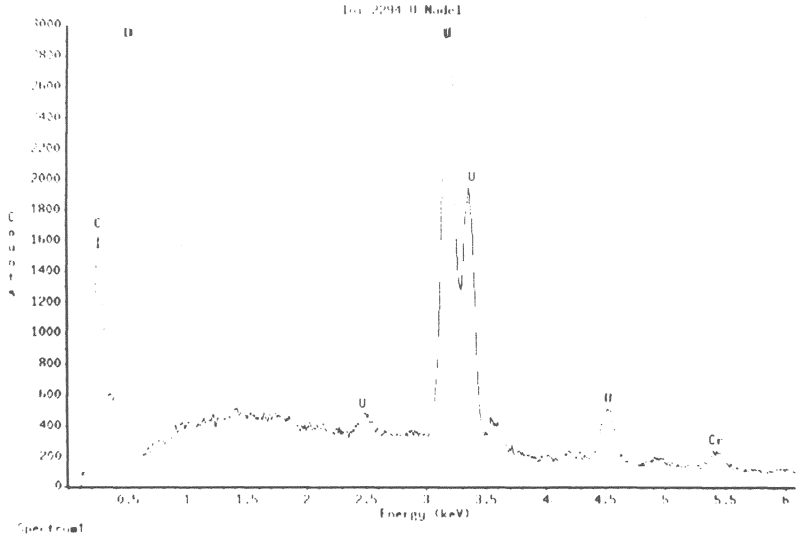

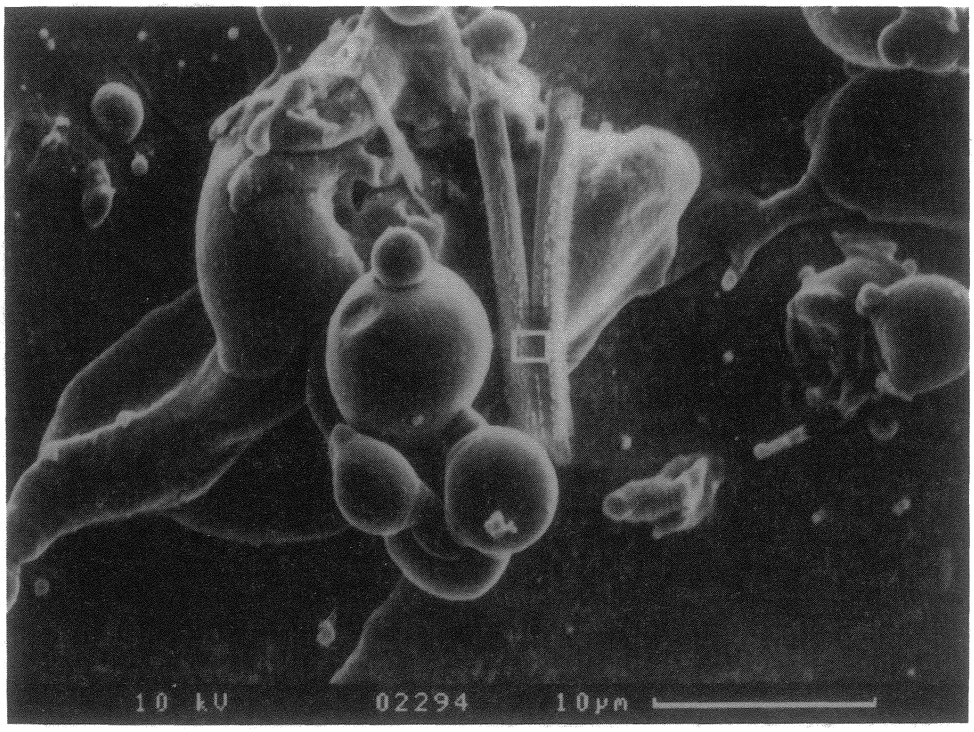

Figure II.9: SEM micrographs and EDX analyses results of the uranium oxide phase formed on Ti/Pd plates from experiment K1 after two years of corrosion at room temperature in deionized water

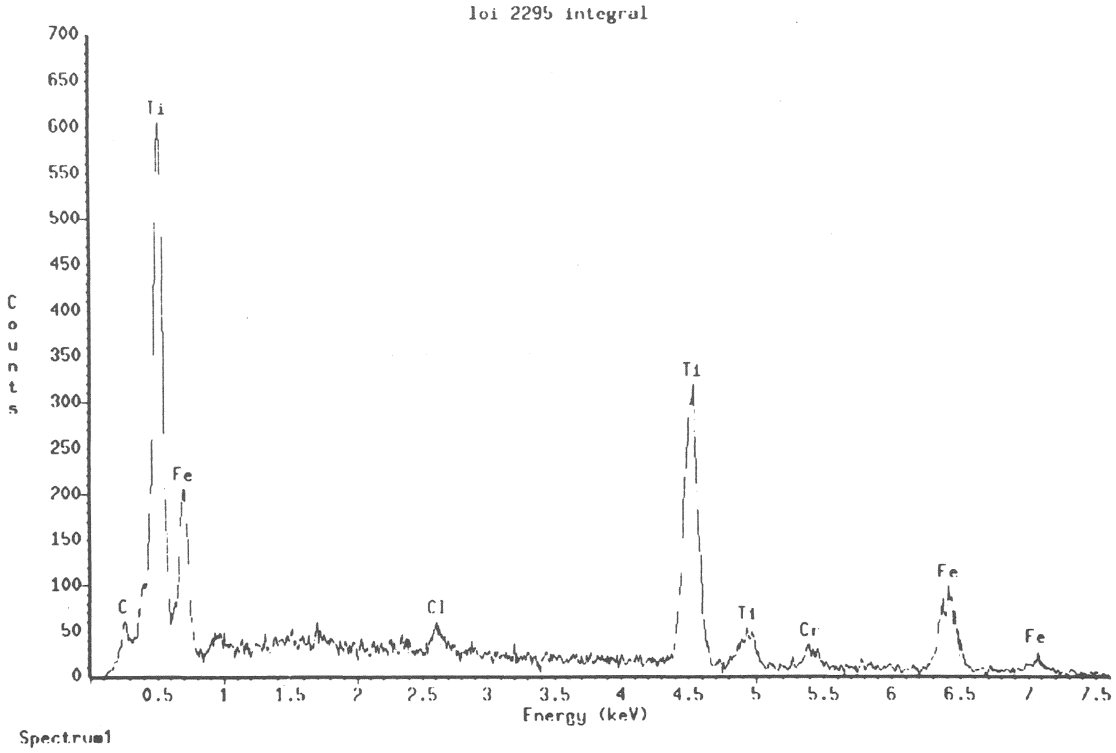

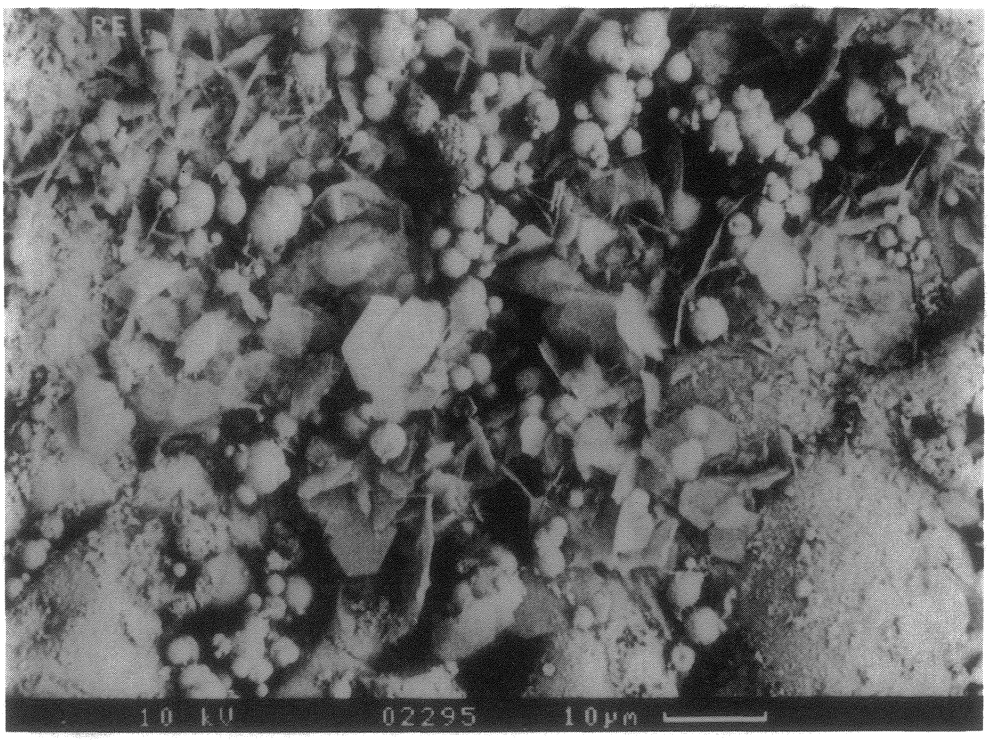

Figure II.10: SEM micrographs of the Ti/Pd plates from experiment K3 after two years of corrosion at room temperature in 95% saturated NaCl solution in presence of Fe

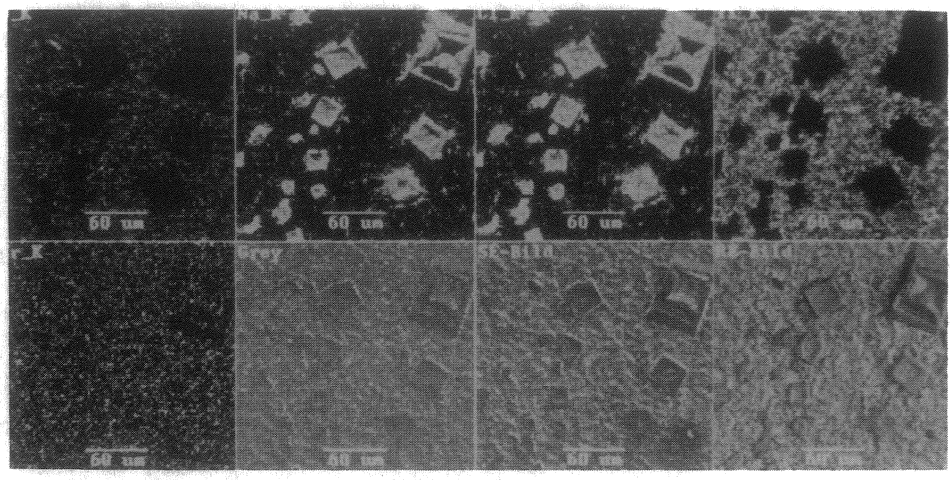

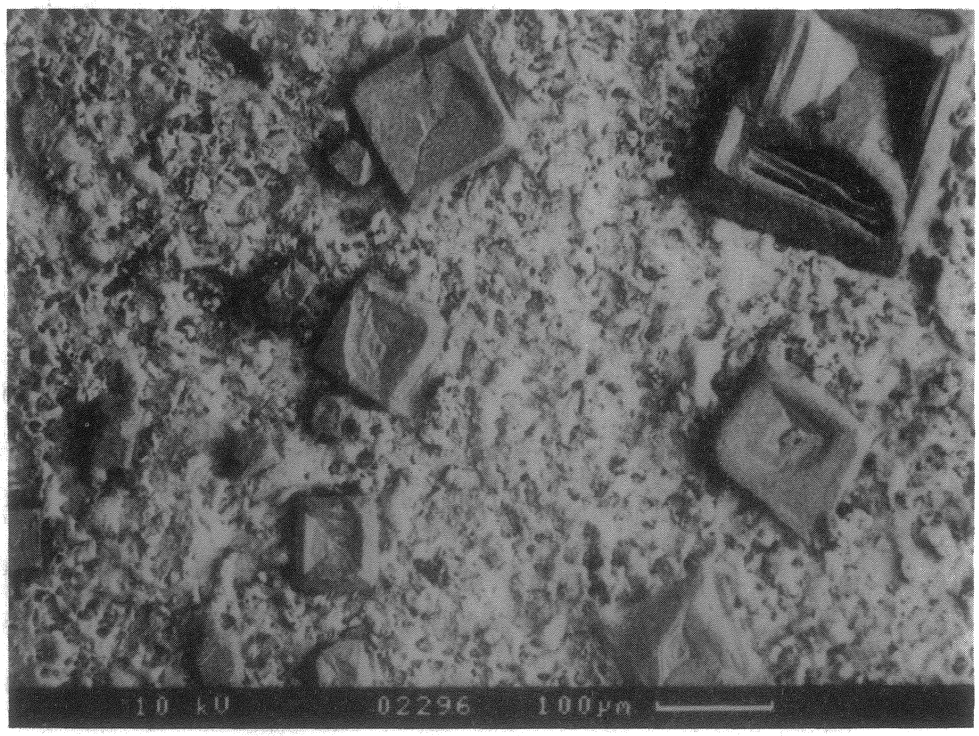

Figure II.11: SEM micrographs of the Ti/Pd plates of the experiment K10 after two years of corrosion at room temperature in 95% saturated NaCl solution

II.3.2 Liquid phase analyses

Individual results of solution analyses of all experiments are given in the Appendix. The data are represented in terms of Eh, pH, Bq/ml, FIAP, molality and incremental release rates. Results of analyzing sorbed radionuclides on reaction vessel and iron corrosion products are included.

Eh/pH

The measured Eh and pH data are given in the Pourbaix type diagram in Figure II.12 and are included in the Appendix. The diagram additionally shows the stability field of water and the UO_2/U_4O_9 phase boundary. The pH value remained neutral to slightly alkaline during the tests. Radiolysis obviously did not lead to acidification in nitrogen and carbonate free chloride media. Eh/pH data for pellets and powders corroded in NaCl solutions are located on a line parallel to the stability field boundaries UO_2/U_4O_9, outside of the stability field of UO_2. Eh values of blank samples (95% saturated NaCl solution left for more than 100 days in an Ti/Pd lined autoclave under Ar atmosphere) were found to be similar to those measured in the corrosion tests, indicating that Eh-values are not altered by the radiolysis process. As expected, lowest Eh values are observed in the presence of iron powder (one exception seems to be an artifact). Highest Eh values were observed for the experiments performed in deionized water. The differences between the Eh values measured in deionized water and Eh-values measured in saline solutions are not yet understood, but since this effect cannot be explained based on radiolysis effects (see analyses of the blank) it be related to differences in the reaction behavior of the Ti/Pd vessel with the solution.

One should be careful of using our measured Eh values as a measure of the redox state in the corrosion vessels. High simultaneous concentrations of hydrogen and oxygen show that we are dealing with an disequilibrium system. The kinetics of redox reactions is important. The Eh-electrode (Pt) reacts well with hydrogen, but UO_2 reacts much faster with oxygen or even with species such as H_2O_2. We may have radiolytically catalyzed oxidizing conditions as far as the dissolution of spent fuel is concerned and we have rather reducing conditions as far as Eh measurement is concerned.

Radionuclide release into the aqueous phase

Radionuclide release is assessed (1) in relative terms by calculating from the measured radioactivities of the fraction of the nuclide inventory of a fuel sample found in the aqueous phase (FIAP) and (2) by calculating elemental solution concentrations. Detailed results are included in the Appendix.

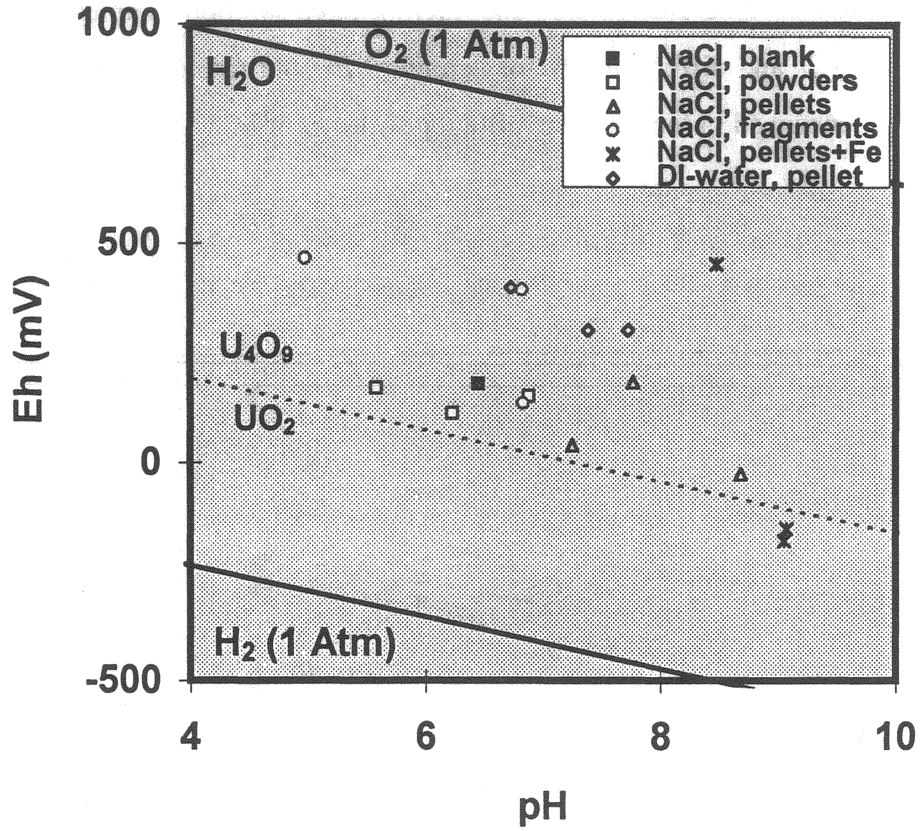

Fig. II.12: Eh/ pH values in NaCl-solutions or DI-water contacting spent fuel pellets, powders and fragments. Phase boundaries of the uranium/ oxygen water-system from[6]. Shaded area: UO_2 solubility con-troll. $Fe(OH)_2$ /$Fe(OH)_3$ boundary according to Stumm and Morgan[7]

For the various radionuclides, the results (FIAP values) from dissolution of powdered fuel, a fuel pellet and an individual fragment in 95% saturated NaCl solutions at room temperature are given in Figures II.13-II.15. Respective data for a fuel pellet dissolved at 150°C are shown in Figure II.16. Data of dissolving a fuel pellet in deionized water are given

[6] N.C.Garisto, F. Garisto, Nucl. Chem. Waste Management, Vol. 6 pp. 203-211 (1986)
[7] Stumm, W. and J.J.Morgan, "Aquatic Chemistry"; John Wiley & Sons, New York (1981)

in Figure II.17 for comparison. The released fractions of matrix bound radionuclides Sb125, Eu154, Am241, Pu239/240, Sr90, Ru106 and Ce144 are in most cases between $3*10^{-4}$ and $3*10^{-6}$ of the inventory. Except for Cs, Sr and for Sb, the rating of radionuclides with respect to their FIAP values changes with the sample geometry. The sequence is Cs>(Sr,Sb)>(Am, Eu)>(Ce,Pu,Ru) for powder (Fig. II.13), whereas it is Cs>(Sr,Sb,Ru)>(Pu,Eu)>Ce with fragments (Fig.II.15). Lowest release rates are observed when dissolving fuel pellets in presence of metallic iron (Fig.II.18).

Results from analyzing ultra filtered and micro filtered solution samples were the same for Ag, Sr, Sb, and Cs and differ slightly for actinides, Ru and rare earth elements. Colloid formation was not enhanced in the presence of fuel powder or of iron.

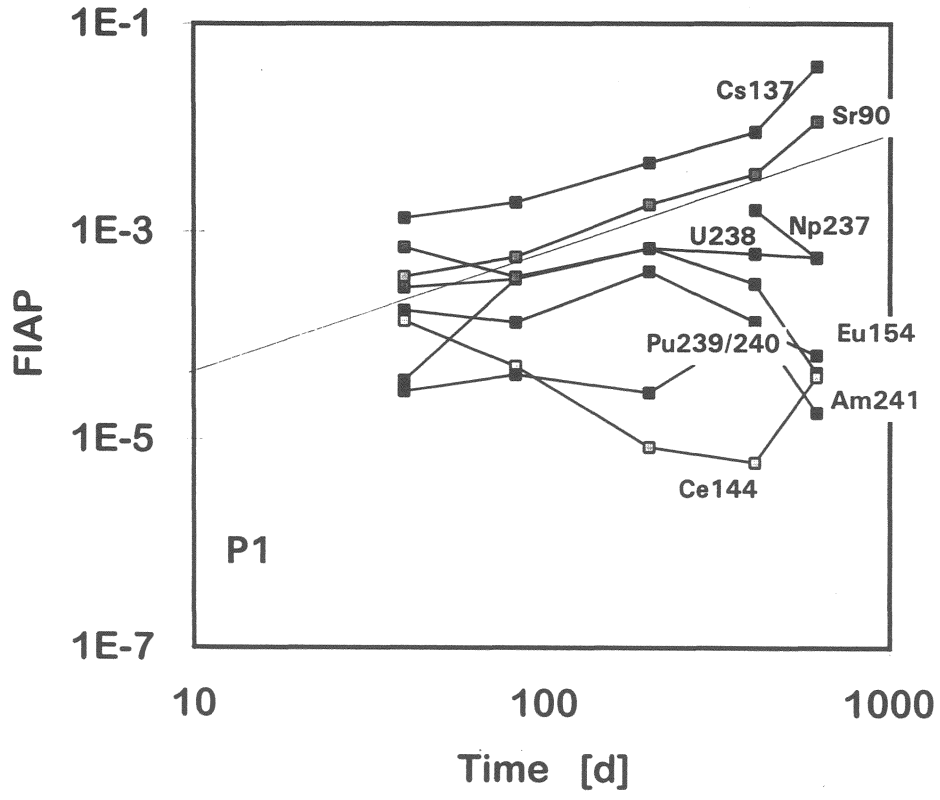

Figure II.13: Dissolution of fuel powder (P1) for two years in 95% saturated NaCl solution under anaerobic conditions at 25°C. Fraction of inventory (FIAP) of various nuclides found in the aqueous phase (0.45 µm filtrate)

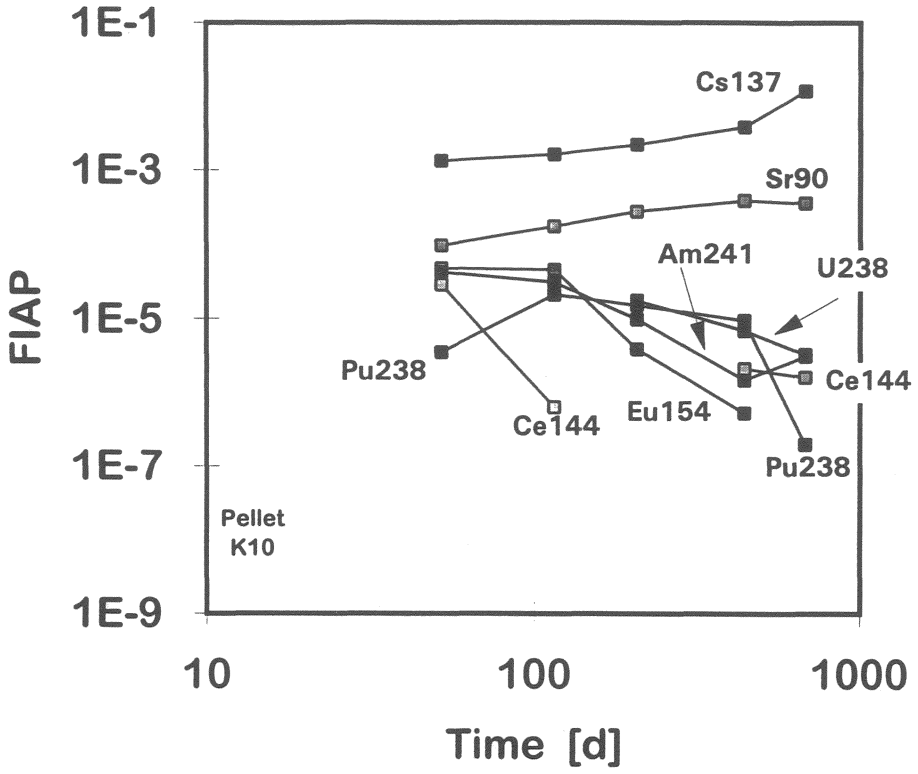

Figure II.14: Dissolution of fuel pellet (K10) for two years in 95% saturated NaCl solution under anaerobic conditions at 25°C. Fraction of inventory (FIAP) of various nuclides found in the aqueous phase (0.45 μm filtrate)

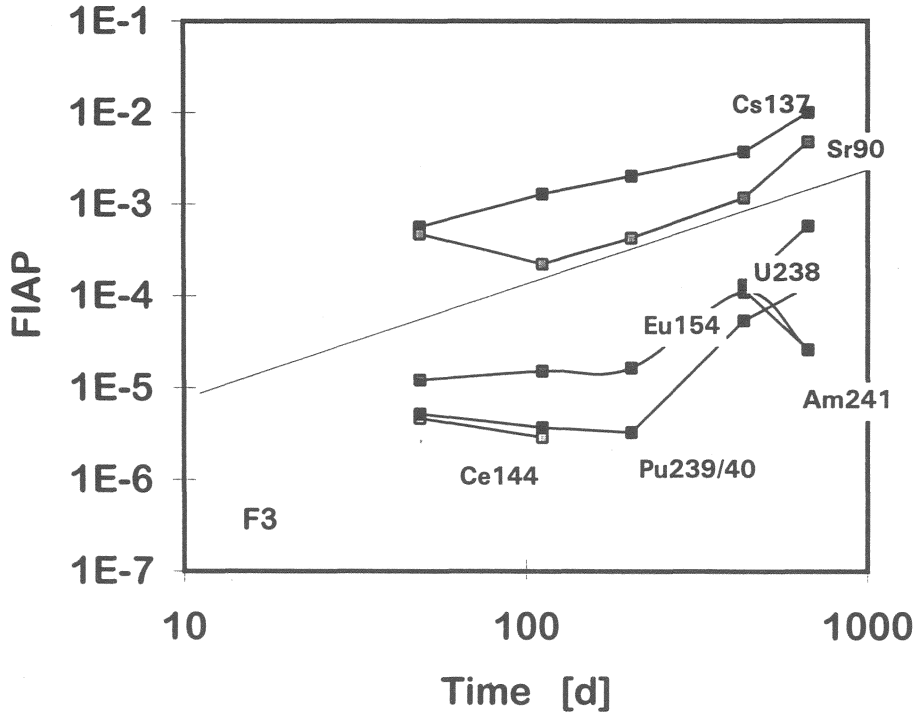

Figure II.15: Dissolution of fuel fragment (20 mg size) (F3) for two years in 95% saturated NaCl solution under anaerobic conditions at 25°C. Fraction of inventory (FIAP) of various nuclides found in the aqueous phase (0.45 μm filtrate)

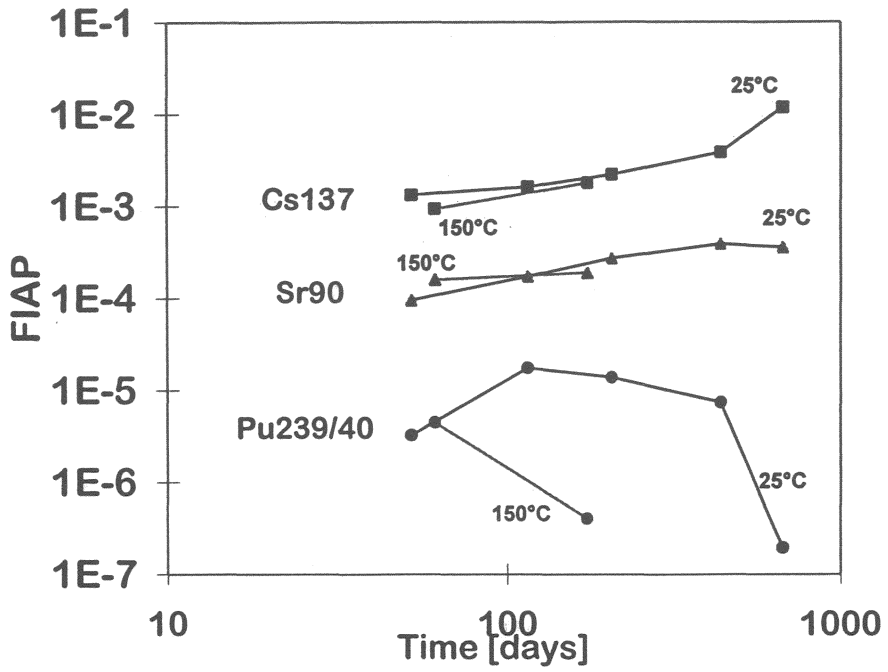

Figure II.16: Dissolution of fuel pellet (K13) for 1/2 year in 95% saturated NaCl solution under anaerobic conditions at 150°C. Fraction of inventory (FIAP) of Cs137, Sr90 and Pu239/40 found in the aqueous phase (0.45 μm filtrate) in comparison with data obtained at 25°C (K 10)

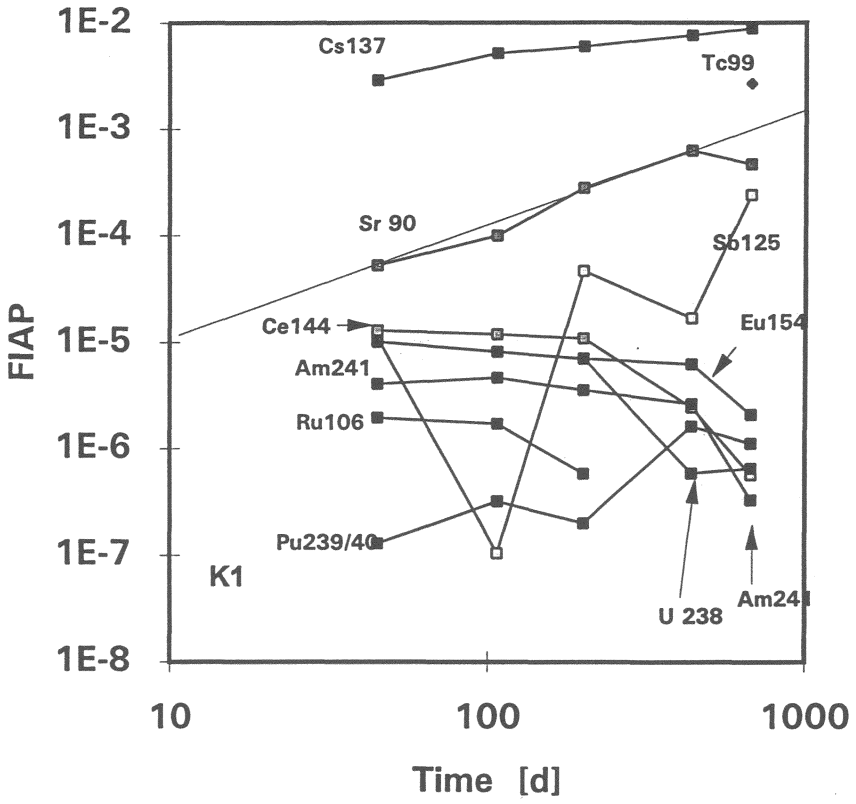

Figure II.17: Dissolution of fuel pellet (K1) for two years in deionized water under anaerobic conditions. Fraction of inventory (FIAP) of various nuclides found in the aqueous phase (0.45 μm filtrate)

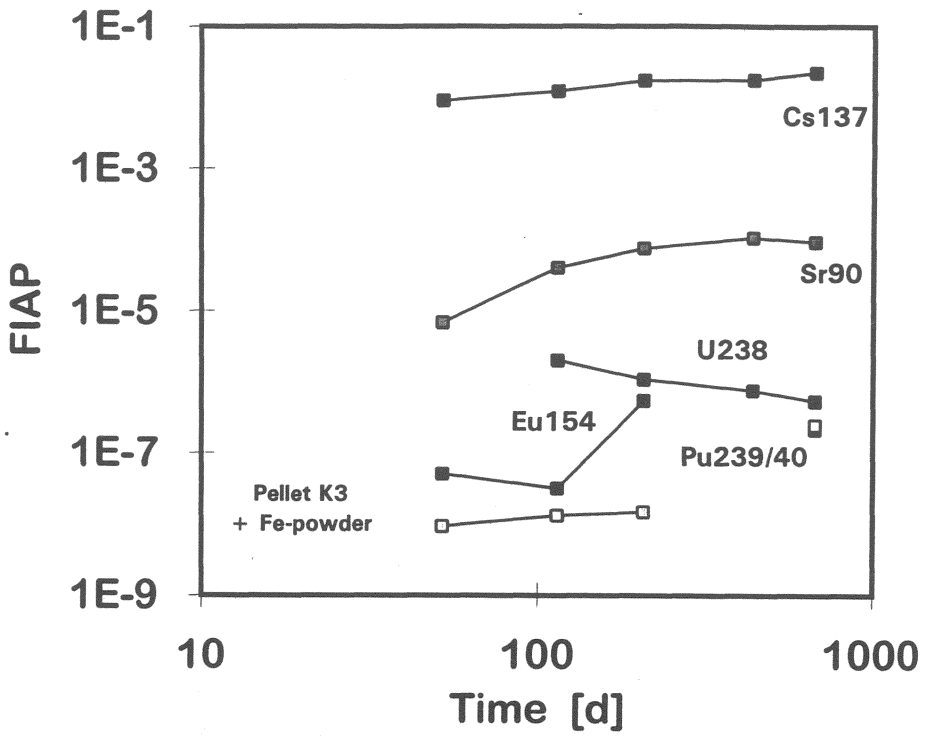

Figure II.18: Dissolution of fuel pellet (K3) for two years in 95% saturated NaCl solution under anaerobic conditions at 25°C in the presence of 8.5 g metallic Fe. Fraction of inventory (FIAP) of various nuclides found in the aqueous phase (0.45 μm filtrate)

II.3.3 Gas phase analyses

Radiolysis products

Specific formation rates of radiolysis gases are given in Table II.3, together with fuel alteration rates calculated from Sr release. Most autoclaves were extremely tight as indicated by the quantity of less than 0.2 vol% of N_2 after about 200 days of testing. However, autoclaves with fuel powder were not tight: about 10 to 50% of the atmosphere has been exchanged with air. In these tests oxygen production cannot be analyzed and only lower limits of hydrogen generation may be estimated from the analyzed H_2 content of the remaining atmosphere.

The formation of the radiolysis gases, oxygen and hydrogen, was observed, in quantities proportional to the spent fuel sample mass. Even with powdered fuel (grain size about 3 μm) gas generation is not enhanced, despite α-radiation contributes much more to

overall radiolysis (escape depth in fuel about 5 μm). We conclude that the radiolysis gases are produced by γ- and not by α-radiation. In the presence of iron, only traces of oxygen were observed in the gas phase, indicating that oxygen uptake by iron corrosion effectively removes oxygen formed by radiolysis.

Table II.3: Specific generation rates of radiolysis gases during spent fuel dissolution (ca. 200 ml solution, 250 ml head space) and comparison with corresponding Sr90 based spent fuel alteration rates. HM = heavy metal, DIW = deionized water, NaCl = 95% sat. NaCl solution, Fe = iron powder added. ? = air influx. In the presence of Fe, hydrogen generation rates mainly reflect iron corrosion rates.

sample	medium	sample mass [g_{HM}]	test duration [d]	gas sample interval [d]	gas generation rate [mol/(g_{HM}.d)]		fuel alteration [mol_{UO2}/(g_{HM}d)]
					H_2	O_2	
pellet K1	DIW	6.45	412	213	1.4e-7	9.4e-8	3.8e-8
pellet K1	DIW	6.45	650	220	5.4e-8	5.6e-8	3.8e-8
pellet K2	DIW	6.35	412	213	1.8e-7	1.1e-7	4.7e-8
pellet K10	NaCl	6.49	389	183	2.2e-7	8.8e-8	1.3e-8
pellet K10	NaCl	6.49	650	220	1.6e-7	8.4e-8	1.3e-8
pellet K9	NaCl	6.49	389	183	2.0e-7	8.0e-8	1.3e-8
powder P1	NaCl	2.5	414	213	2.7e-7	<1.5e-7	8.8e-8
powder P1	NaCl	2.5	650	220	3.0e-7	?	8.8e-8
powder P2	NaCl	2.5	414	213	2.1e-7	?	2.8e-7
pellet K3	NaCl/Fe	6.19	345	139	8.0e-7	<1e-8	3.6e-9
pellet K3	NaCl/Fe	6.19	650	220	1.5e-6	5.3e-10	3.6e-9
pellet K4	NaCl/Fe	6.0	267	60	8.4e-7	<1e-7	2.7e-9

Fission gases

A certain percentage of fission gases Xe and Kr is released during reactor operation into open voids in the fuel rod and was released instantaneously upon cutting the rod. This fraction has not been measured for the present fuel. For some samples we measured the further release of these fission gases occurring with smaller rates from grain boundaries and from the fuel matrix. The fission gases were measured in isotopic ratios given in the Figure II.19. The measured ratios are practically the same for all samples. Similarly, in all cases measured and calculated release ratios of Xe to Kr agree within 20% to the respective ratios calculated by KORIGEN. Results of gas release rates are compared with Cs- and Sr-release data in Figure II.20 and II.21 below.

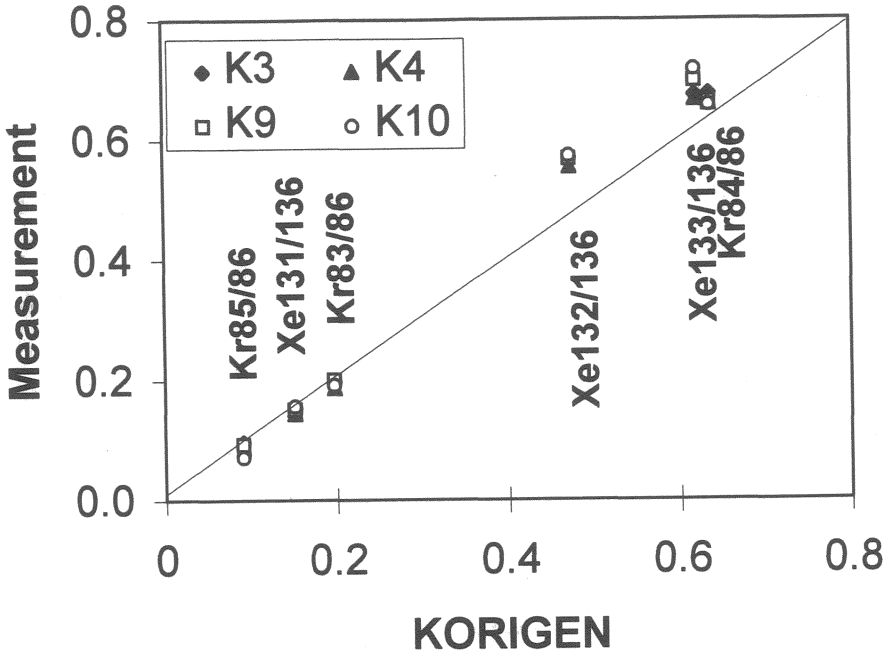

Figure II.19: Isotopic ratios of fission gases measured in various tests

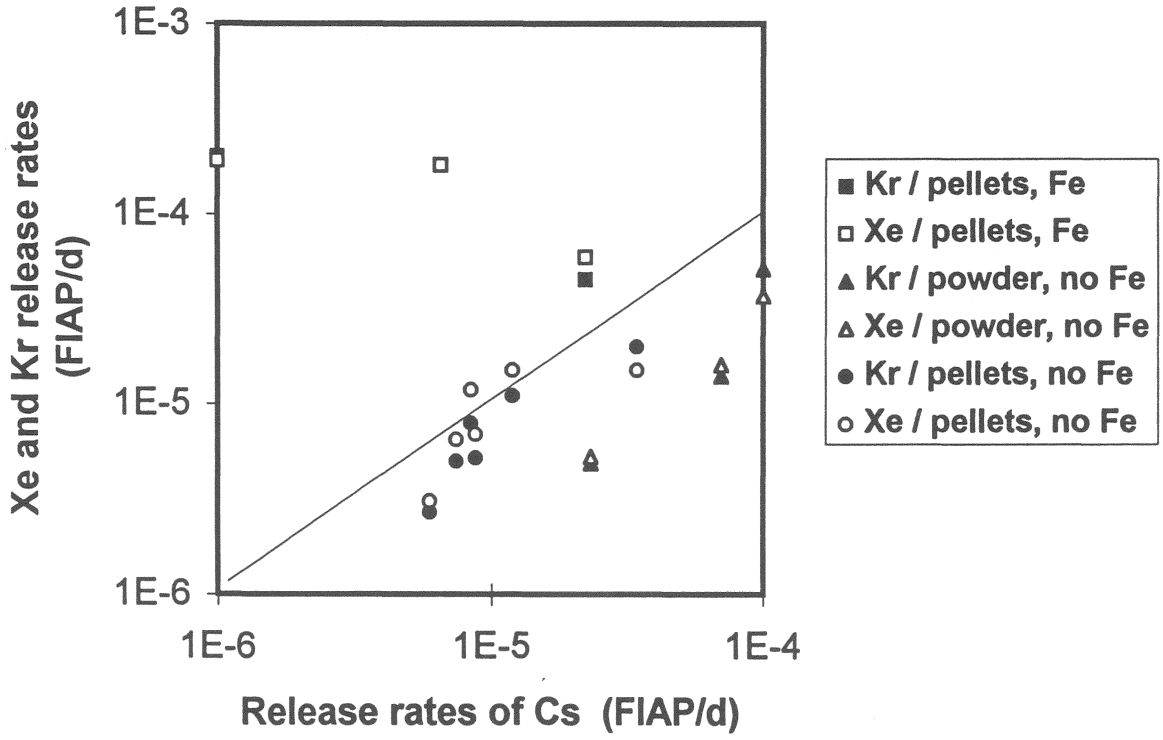

Figure II.20: Comparison of measured rates of fission product release with rates of Cs release from various fuel samples

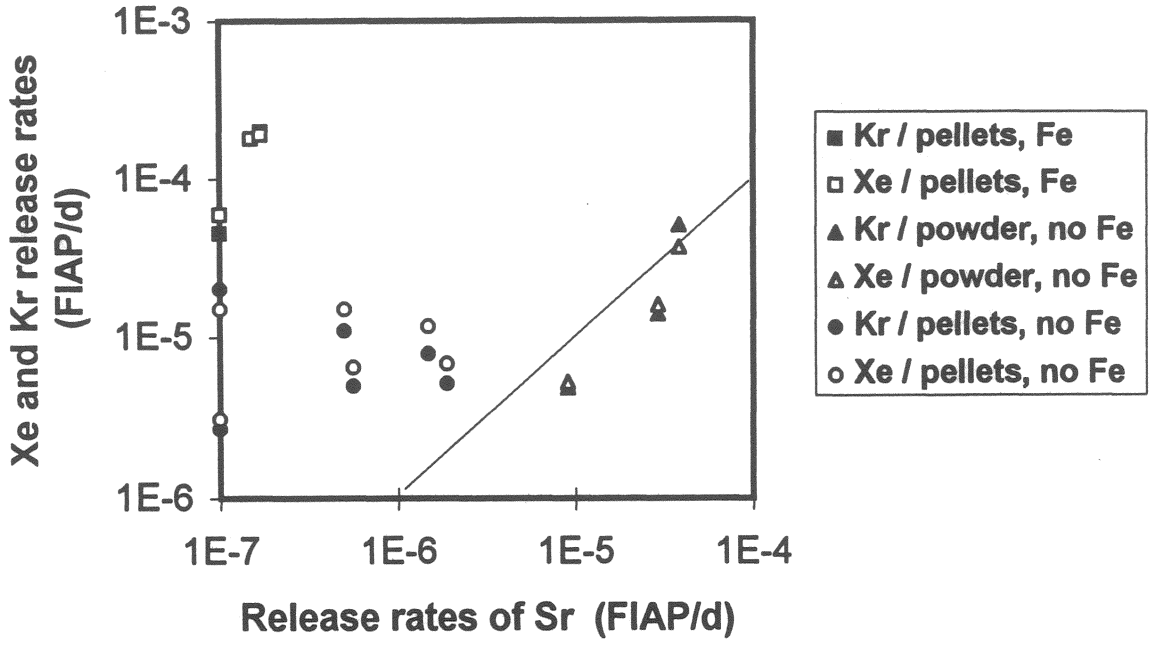

Figure II.21: Comparison of measured rates of fission product release with rates of Sr release from various fuel samples

II.3.4 Sorption at container wall.

Sorption of radionuclides at the container wall (Ti/Pd) was analyzed by acid stripping the container after ultrasonic cleaning in deionized water. Both deionized water and acid strip solution were analyzed. Details on analyzes results are to be found in the Appendix. Some analyses are hampered by fuel grains dissolved by the acid. Fuel grains were identified by radionuclide ratios identical to inventory ratios. For container walls where no fuel grains were observed, Table II.4 shows the percentages of the radionuclide inventories of the altered fuel mass (calculated from Sr90 release to solution and vessel) which are sorbed on the reaction vessel, in solution and on the fuel sample. Only small quantities of radionuclides are sorbed on the container wall and a significant amount in particular of tri-tetra- and hexavalent actinides remain on the fuel sample.

Table II.4: Percentages at test termination of radionuclide inventories of the altered fuel masses (Sr90 based) sorbed on the reaction vessel (Ti), in solution and on the fuel sample or the cladding (experiments with pellets). Radionuclide fraction remaining on sample deduced from solution and vessel analyses. (* Sr and Cs data on sample are not deducible as Cs release is larger than Cs inventory of altered fuel mass and altered fuel mass value is based on Sr data)

leachant	DI-water			NaCl soln		
pH	7			9		
	vessel	soln	sample	vessel	soln	sample
Cs137	0.02	99.98	0.0*	0.02	99.98	0.0*
Sr90	6.3	93.7	0.0*	13.5	86.5	0.0*
Pu238/239/240	4.7	0.2	95.1	7.0	1.8	91.2
Am241	11.1	0.4	88.5	5.4	0.3	94.3
Cm244	5.2	0.2	94.6	15	0.15	84.9
U238	3.7	0.1	96.2	6.1	1.5	92.4

II. 4 Discussion

II. 4.1 Dissolution behavior of the fuel matrix

II. 4.1.1 Indicators for matrix behavior

Provided there is no segregation on fracture surfaces and grain boundaries, one may use the fastest dissolving nuclide as an indicator for fuel matrix dissolution and interpret lower values of other elements as being controlled by secondary effects (i.e. sorption, (co-)precipitation). This procedure would gain plausibility if more than one element could be used as indicator for matrix degradation. Certain elements, like Cs, may only serve this purpose after the gap and accessible grain boundaries are washed out. After Cs134/137, in all tests Sr90 and thereafter Sb125 showed highest release values.

Sr data are sometimes considered as measure for the degradation of the fuel matrix[8], due to homogeneous distribution in the fuel[9], but there are indications at least for high power fuel that Sr may become segregated in part (<5%) in perovskite phases[10]. A discussion of Sr behavior during fuel dissolution is given in[11]. Recent measurements for LWR fuel samples by Gray et al.[12] indicated that not more than 0.1% of the total inventory of Sr90 was associated to grain boundaries, whereas measurements for CANDU fuel (high linear power)[13] indicate that the sum of gap and grain boundary inventories of Sr may become as high as 0.5 %. Our tests with fuel powders may provide additional insight because grain boundaries are exposed to the solution and grain boundary contents can be dissolved instantaneously. Except during initial ultrasonic cleaning, initial Sr and U releases in the static tests are rather similar. This indicates that Sr is released from the matrix. With time the difference between the Sr and the U release data increases. This can be interpreted as resulting from a dissolution (Sr,U) /

---

[8] Grambow B., "Spent Fuel, Dissolution and Oxidation - an Evaluation of Literature Data", SKB Technical Report 89-13, Stockholm, 1989

[9] Kleykamp H., "The Chemical State of the Fission Products in Oxide Fuels", J. Nucl. Mater. 131, 1985, pp. 221-246

[10] Jefferey, B.M., J. Nucl. Mater. **131**, 33-40 (1967)

[11] Grambow B., L.O. Werme, R.S. Forsyth and J. Bruno, Mat. Res. Soc. Symp. Proc. Vol. 176, Materials Research Society, Pittsburgh (1990b)

[12] Gray, W.J., D.M. Strachan, C.N.Wilson, Mat Res. Soc. Symp. Proc. **257**, 353-360 (1992)

[13] Stroes-Gascoyne, S. et al., Mat Res. Soc. Symp. Proc. **294**, 41-46 (1993)

precipitation (U) mechanism. Hence, with time, data of Sr are indicative of fuel matrix dissolution. Initially mobilized Uranium may be bound to secondary precipitates (see below). From the difference in the initial fractions of inventories, released from Sr and U during ultrasonic cleaning, we may estimate an upper limit for the sum of gap and grain boundary inventories of Sr. This is not higher than 0.03 % of the total Sr inventory.

II.4.1.2 Fuel matrix dissolution rates based on Sr90 release

Using Sr90 as an indicator, matrix dissolution rates for the various experiments are given in Figure II.22 as a function of time. Fractional release rate values were calculated from

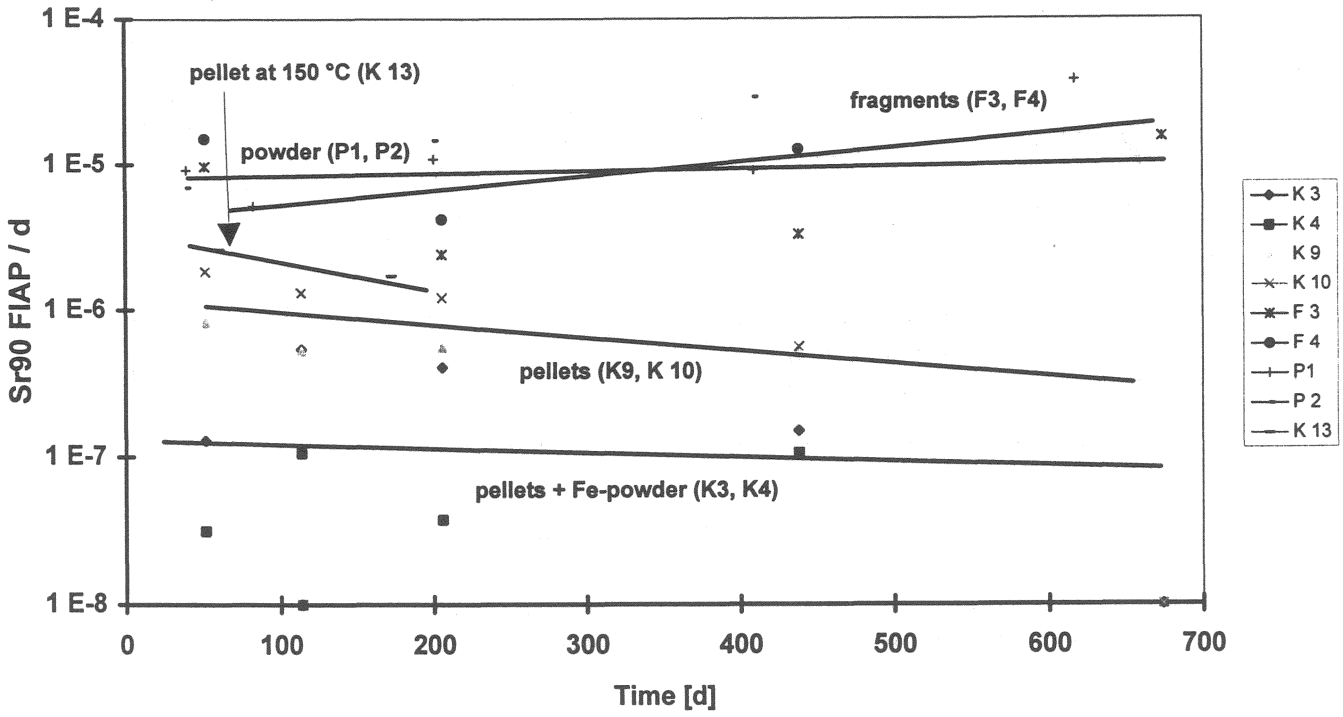

Figure II.22: Influence of sample size and salinity on incremental fractional release rates of Sr90 from high burnup spent fuel at 25°C and 150°C.

the augmentation of the Sr90 activities in solution between two subsequent solution sampling intervals. Individual rate data are included in the Appendix for each radionuclide and experiment. In general Sr90-release rates remain constant with time. The decrease of release

rates of Sr with time, as observed by Forsyth[14], has only been observed in few experiments with fuel pellets. Nevertheless, a comparison of our Sr release rates from fuel pellets in the absence of iron with respective data from various international programs show close agreement (Figure II.23). This Figure is based on a previous comparison[15] of the corrosion behavior of CANDU fuel under oxidizing conditions in granite water with data from the SKB corrosion program of LWR fuel (33MWd/kgU) in granite water and in deionized water and data from the US American NNWSI program, also from using LWR fuel of about 30 MWd/kgU.

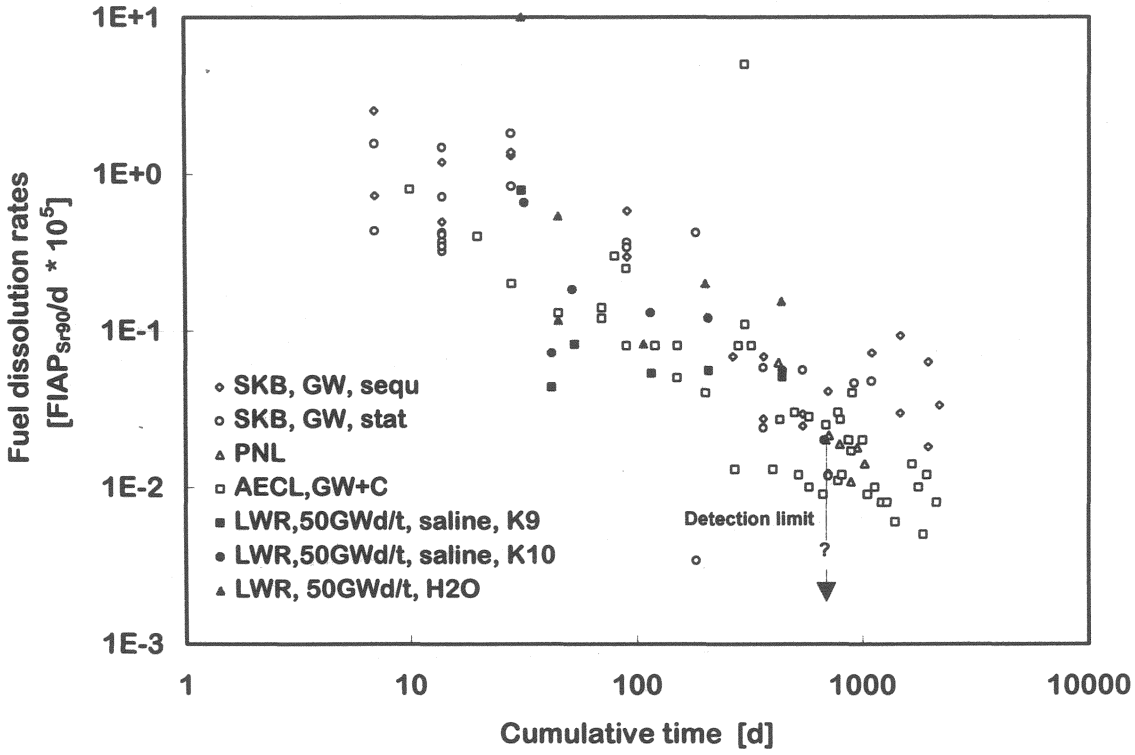

Figure II.23: Comparison of Sr90 based dissolution rates of spent fuel samples from various international programs (see text) with dissolution rates of LWR fuel pellets measured in this project

II.4.1.3 Conservative estimates for surface area normalized intrinsic fuel matrix dissolution rates

Surface area normalized reaction rates may be estimated from the fractional Sr90 release rates using the surface area considerations discussed above. Upper limits for intrinsic fuel dissolution rates ("forward reaction rates") may be obtained from tests with individual

[14] Forsyth, R.S. Mat. Res. Soc. Symp. Proc. **212**, 177-188 (1991)
[15] Grambow B., L.O. Werme, R.S. Forsyth and J. Bruno, Mat. Res. Soc. Symp. Proc. **176**, Materials Research Society, Pittsburgh, pp 465 - 498 (1990)

fuel fragments where saturation effects are negligible. With a geometric surface area, we obtain a "forward" dissolution rate of about 5-7 mg/(m^2d) in 95% sat. NaCl solutions at 25°C or about 2-3 mg/m^2d if a surface roughness factor of 2.5 is considered. Our rate values are rather similar to the value of about 2 mg/(m^2d) measured for spent fuel (ATM105, ATM106) in deionized water[16], [17] using the same surface roughness factor. Considering an effective geometric pellet surface area of 14 cm^2 and the same surface roughness factor Sr is released by similar rate from fuel pellets of about 1 mg/(m^2d) in NaCl solutions and 2 mg/(m^2d) in deionized water.

II.4.1.4 Matrix dissolution rates lower than intrinsic rates: „Saturation effects" vs. „Radiolysis effects"

Saturation effects may provide additional long-term stability for the fuel[18]. Under reducing conditions, models for release of radionuclides from spent fuel assume that the rate of release of matrix bound radionuclides is given by the product of the solubility of the UO_2 matrix and the flow rate of groundwater. However, it is not clear whether these effects can occur under oxidizing conditions, since UO_2 is unstable with respect to secondary U(VI) solid phases such as uranyl oxide hydrates (schoepite, Na-polyuranates, becquerellite etc.). Our tests with powdered fuel may provide some more insight into this question. Table II.5 contains radionuclide release data of sample P1, expressed as normalized elemental mass loss values (NL_i, see above Chapter II.2.3) obtained after two years of reaction. Considering the incremental rates of Sr and Tc release (The corresponding upper limits for surface area normalized rates are about 0.1 mg/(m^2d), much lower than intrinsic dissolution rates published in the literature [16,17] or estimated above from the present work with fuel pellets and fragments. Corresponding equivalent depletion depth values were calculated for each radionuclide (see Chapter II.2.3). Considering that a monolayer of UO_2 may have a thickness of the minimum U-U distance of 3.87 Å in the crystal lattice (fluorite structure), for each nuclide it was calculated, how much monolayers would have to be dissolved to account for the observed radionuclide release, or, if this would be less than a monolayer, which fraction f_i of the monolayer must be dissolved to accounted for the radionuclide release. For all actinides less

[16] Gray,W.; D.M. Strachan, Mat. Res Soc. Symp. Proc. **212,** 205-212 (1991)
[17] Gray, W., L.E. Thomas, R.E. Einzinger, Mat. Res. Soc. Symp. Proc. **294**, 47-54 (1993)
[18] Grambow et al.;Nucl. Technology 92 (2) (1990) pp.204-13

than a monolayer inventory is released into solution. The results show that for example only 5% of the Pu content of a monolayer is found in the aqueous phase.

The pronounced decrease in the surface area normalized reaction rate with an increasing S/V ratio may be explained either by accumulation of dissolved reaction products in solution (saturation, solubility) or by enhanced depletion of reactants (dissolved oxygen, radiolytic products, i.e. H_2O_2, radicals, ClO^-, etc.) from solution. If, hypothetically, fuel powder would be able to dissolve oxidatively with an intrinsic dissolution rate of 2 mg/(m^2d), it can be shown that this hypothetical process would consume radiogenic reactants faster than they are produced (generation rate of radiolysis products estimated from H_2 gas measurements). Hence, in the absence of other sources of oxidizing species, such high rates are impossible. In contrast, it could be that reaction rates in tests with powders are limited by the generation rate of oxidizing radiolysis products.

Table II.4 Normalized mass losses NLi [mg/m^2], and fraction f_i of a monolayer after two years of static corrosion of 2.9 g of spent fuel powder (P1) in 200 ml 95% sat. NaCl solution at 25°C

	NL	f		NL	f
Cs137	130	33	Cm244	0.04	0.01
Cs134	100	27	Am241	0.07	0.02
Tc99	38	10	Pu238	0.2	0.05
Sr90	38	10	Pu239	0.2	0.05
Eu154	0.1	0.04	U	1.9	0.5
Sb125	4	1.2	Np237	1.8	0.5
Ru106	0.8	0.2	Ce144	0.1	0.04

II.4.1.5 Correlation of fuel dissolution rates and rates of radiogenic oxidant production

In chapter IV measured fuel dissolution rates were compared with corresponding data for unirradiated UO_2. This comparison shows that radiolysis may be important for controlling fuel dissolution rates. Various attempts have been described in the literature to correlate experimentally measured spent fuel dissolution rates with radiation dose rates[19] or alpha activities[20] but the authors are not aware of any mass balance calculations, identifying

[19] D.W. Shoesmith, S. Sunder, SKB Technical Report 91-63, (1991)
[20] S. Sunder et al. Mat Res. Soc. Symp. Proc. Vol 353 , pp 617 - 624(1995)

whether radiolysis may indeed be rate limiting. Based on a comparison of our measured intrinsic fuel dissolution rates of about 2-3 mg/(m^2d) with the rate data measured in this project for unirradiated UO_2 (see Chapter III) we have concluded, that the even under initially anoxic conditions the dissolution process is oxidative (see chapter IV). With respect to mass balance, this means that an upper limit for fuel alteration rates is always given by the availability of oxidative reactants such as O_2, radiolytically produced H_2O_2 etc. according to reactions such as

$$UO_2(s) + H_2O + ½\ O_2 \leftrightarrow UO_2^{2+}(aq) + 2\ OH^-,$$

or for example

$$UO_2(s) + H_2O_2 \leftrightarrow UO_2^{2+}(aq) + 2\ OH^-,$$

Under anoxic conditions O_2 only comes from radiolysis and also other radiolysis products will act as electron donor. In the absence of non-radiolytic oxidants, oxidative dissolution rates may be lower, but never higher than the rates of radiolytical oxidant generation. The present data do not allow to identify the rate limiting oxidative reactant. In the absence of a full analyses of all dissolved radiolysis products we can only estimate upper limits for fuel dissolution rates based on the total amount of oxidative radiolysis products. Except for tests in presence of iron, we can use the hydrogen data to estimate the total amount of oxidizing species, assuming that hydrogen reacts slower with the fuel than oxidative species and assuming a closed system i.e. presence of equivalent amounts of oxidizing and reducing radiolysis species. Hydrogen is the only significant reducing species and for the geometric set-up of our reaction vessels, more than 98% of the generated hydrogen is expected in the gas phase. If oxygen is the only oxidizing product, its concentration in the gas phase should be about half of that of hydrogen, as also about 98% of the oxygen produced should be in the gas phase.

The data in Table II.3 show that fuel dissolution rates are up to a factor of 15 lower or of similar order of magnitude than the rates of radiolysis gas production. This similarity may indicate control of dissolution kinetics by radiolytical production of oxidants, i.e. the rate of formation of the total amount of oxidative radiolytic species may become equal to their consumption rate by fuel oxidation/dissolution. Limitation in the production of oxidative

species may explain the observed (see Chapter II.4.1) decrease in surface area normalized reaction rates with increasing S/V ratio: In first approximation (γ-dose is higher than α-dose!) the generation rates of radiolysis products depend only on fuel mass (H_2 production rates normalized to fuel mass are similar for fuel powder and fuel pellets in NaCl solution, see Table II.3) but the consumption rate by oxidation/dissolution depends on surface area.

For fuel pellets in NaCl solutions, the generation rate of oxidative radiolytic species appears to remain more than ten times faster than the rate of their consumption by oxidative fuel dissolution (Table II.3), whereas, by using fine grained fuel powder, the high sample surface area may lead to fast consumption of oxidative radiolysis products and fuel corrosion rates approaches the estimated H_2 gas generation rates. H_2 gas generation rates from fuel pellets in deionized waters are about 30% lower than the corresponding rates in NaCl solution, though the corresponding fuel dissolution rates of the fuel are about three times higher in deionized water than in NaCl solution. Together with the fact that H_2-generation rates for fuel pellets are higher than their dissolution rates, this means that the dissolution rates are not controlled by mass balance of oxidant production and consumption.

It has been shown in this project (Chapter III, Fig. III.1.8) that the dissolution rates of unirradiated UO_2 depends mainly on the concentration and not on the nature of the various oxidants (H_2O_2, CLO^-, etc.). Consequently, in the absence of mass balance constraints, the bulk or local steady state or transient concentration of oxidants at the fuel surface are probably of key importance. Local concentration in the solution adjacent to the dissolving fuel surface may as well be governed by α as by γ radiation. For scale up of radiolysis effects to relevant geometric disposal configurations much more understanding of the basic phenomena is necessary, considering the interplay of α and γ radiation and the interdependency of hydrodynamic constraints in fractures, grain boundaries, and diffusion processes of oxidants in the solution adjacent to the fuel surface as well as S/V-effects and head space in the autoclaves or free gas space in the repository.

II.4.2 Gap and grain boundary release of Cs and of Fission Gases

Release data of Cs137 are of significance for performance assessment of spent fuel as it allows to assess the behavior the safety relevant slow decaying nuclide Cs135. It is well known that the initial Cs release is much higher than that of any other non-gaseous nuclide (may be except of I129) due to accumulation of Cs along fracture surfaces and at grain boundaries. Initial Cs-release fractions from the fuel sheet gap and from fracture surfaces, often termed "gap release" are similar to the fractional fission gas releases measured when cutting the fuel[21] .

The cumulative Cs release data measured in our experiments are shown in Figure II.24. The data show rather large scatter. Maximum release values are about 2-7%. Highest initial Cs release is observed when dissolving fuel powders. With powdered fuel, all fracture surfaces and most grain boundaries are expected to be exposed to the solution and the major Cs release occurs within few minutes during ultrasonic cleaning. Thereafter further Cs-release occurs with rather slow rates, originating both from the remaining Cs-inventory of the slowly dissolving UO_2 matrix and from some few non-exposed grain boundaries. The increase in Cs-release after about 1 year of exposure is not yet understood. A possible explanation would be that the fuel powder formed certain agglomerates in solution, preventing water access to their interior surfaces. With time, these agglomerates may disintegrate. A consequence of this explanation would be that the sum of gap and grain boundary inventories would be as high as 4-7 %. Considering that these Cs inventories are normally similar to the percentages of gas release such high values are very untypical for normal LWR fuel and are probably associated to the high burn-up, the high linear power and the relative large fuel/sheet gap of this type of fuel. The Cs releases from pellet sized fuel segments approaches much more slowly (100-300 days) a plateau value of 2-3%. Probably, this "retardation" results from hydrodynamic constraints (diffusion processes, blocking of water access by gas inclusions etc.) for Cs-release from interior fracture surfaces. Differences in the plateau values of the various samples likely reflect heterogeneous distribution of Cs on fracture surfaces at various

[21] Stroes-Gascoyne,S.; L.H.Johnson, D.M.Sellinger, Nuclear Technology 77, 320 (1987)

axial positions within the fuel rod. Release from individual fragments surfaces is similar (about 2% of the total inventory), than that of the pellets confirming a total gap inventory of about 2-3% of this type of fuel. Subtracting this gap inventory from the total sum of gap and grain boundary inventories we obtain a value for the grain boundary inventory of Cs of 2-4%).

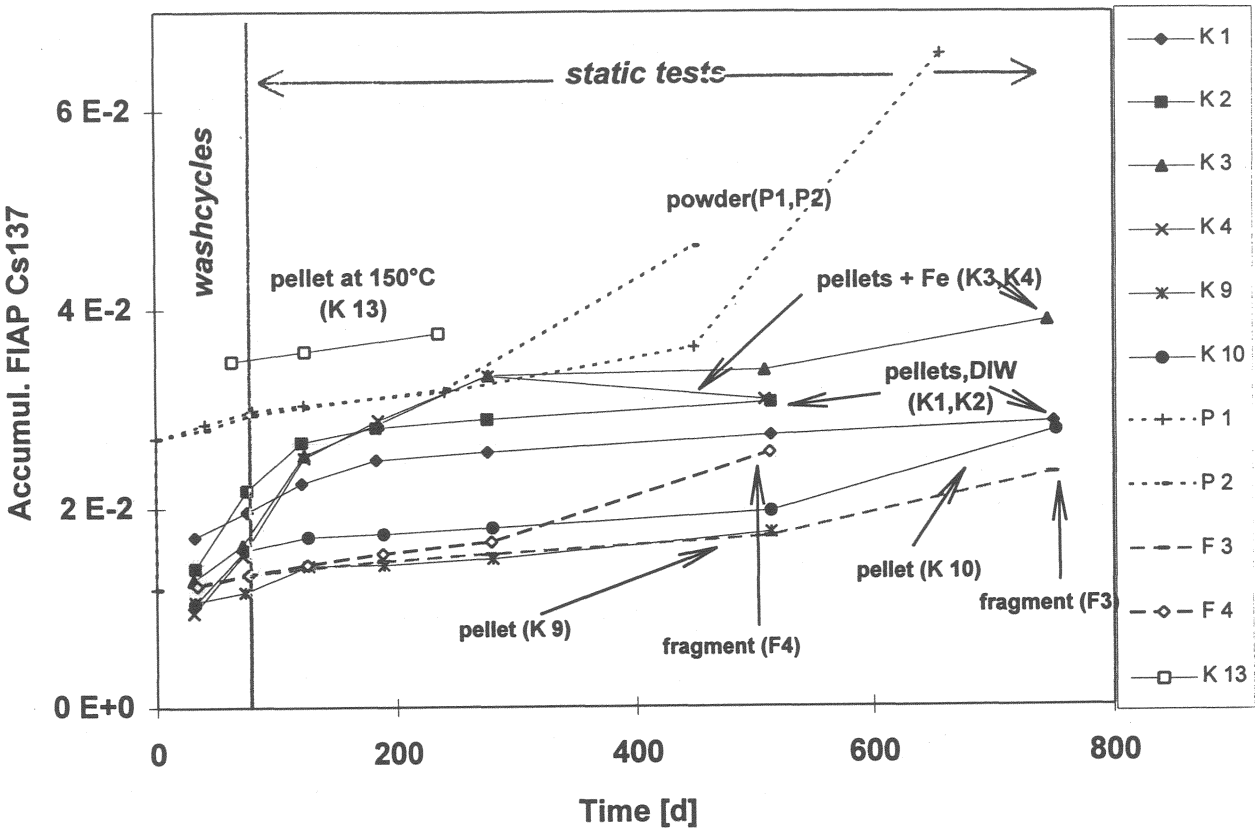

Figure II.24: Release of Cs137 from various spent fuel samples. Cs-concentrations in the initial washing or ultrasonic cleaning (powders) solutions are included.

Further understanding of the release behavior of Cs may be attained by comparing the release rates of Cs137 and of Sr90 with the corresponding fission gas release rates, measured in our experiments (see Figures II.20 and II.21) after about 450 to 800 days. For corrosion experiments with fuel pellets (NaCl solution and deionized water) in the absence of iron, the data show close agreement of Cs release rates with gas release data. Release rates are significantly higher than release rates of Sr, indicating that gas release as well as the release of

Cs is governed mainly by grain boundary attack. In the presence of iron, fission gas release rates are significantly enhanced as discussed further below. For fuel powders the data in Figures II.20 and II.21 show that gas release rates are much lower than the rates of Cs release and match the release rates of Sr90, i.e. there is no more gas release from grain boundaries, and fission gas release rates are controlled by fuel matrix dissolution rates. This clearly shows that the grinding process effectively opened essentially all grain boundary surfaces.

II.4.3 Reactivity of the highly burned fuel rim

Recently the so called "rim effect" has drawn substantial attention in post-irradiation characterization studies of high burnup nuclear fuel. In high burnup fuel, the rim region has a thickness of about 100 μm. The porosity is rather high. The enrichment of fission products indicates higher localized burnup. For the present fuel the enrichment factor is about a factor of 2 (see chapter 1). On the other hand, fission gases are normally depleted in this region (not measured in the present study). High porosity, high fission gas mobility and higher nuclide inventories may lead to much higher reactivity of the fuel rim when compared to the average reactivity of the fuel matrix. The contribution of the rim to the overall fuel dissolution behavior may best be studied by comparing the Sr-release rates of the rim fragment F3 with those of fragment F4 (Appendix). Sr90 is only slightly enriched in the rim and has been shown to be a good indicator for the reactivity of the fuel matrix. Sr-release rates are similar for the two fragments. Consequently, when compared to the behavior of fuel pellets in NaCl solution, the higher rates of Sr-release from the two fragments is probably not associated to a rim effect but to the S/V effects discussed above. The present data show no enhanced contribution of the pellet rim to overall release.

II.4.4 Effect of iron

Throughout the experiments, metallic iron and its corrosion products (magnetite, possibly green rust I etc.) were present simultaneously. This means that the reducing capacity of the iron powder as well as the sorption capacity of the corrosion products remained unexhausted in the course of the tests. The effect of iron and/or iron corrosion products on the mobility of radionuclides is illustrated by a comparison of the data given in Figures II.18 with data obtained under similar experimental conditions in the absence of iron (Figure II.14). In

the presence of iron the solution concentration of all radionuclides except of Cs were reduced. The strongest effect is observed for the actinide elements. Np237 was not anymore detectable in solution. Pu concentrations decreased by more than a factor 100, and essentially all dissolved Am was present in solution in colloidal form. In contrast, fission gas release rates are enhanced in the presence of Fe (see Figure II.20 and II.21). The cumulative release of Cs was more than 4% of the inventory after 200 days, a value higher than the sum of gap and grain boundary inventories of fuel powder leached during the same time period.

A similar decrease in the release of radionuclides has been observed by Stroes-Gascoyne[22] and was explained by increased stability of the fuel matrix under reducing conditions. However, low release of fission products and of actinides may alternatively be a result of sorption on iron corrosion products. A mass balance analyses (Table II.6) of (1) the amounts of radionuclides in solution, (2) sorbed on iron or on its corrosion products or (3) on the Ti-container or (4) remaining on the fuel samples give indications for significant sorption on iron or its corrosion products. For example, the quantities of Eu, Ce, Pu sorbed on Fe are

Table II.6 : Release of radionuclides in the presence of iron (8.5 g powder, grain size < 10 µm) from a fuel pellet (7 g) in 200 ml 95% saturated NaCl solution. Relative distribution of various radionuclides in the aqueous phase, on the container wall , on iron and its corrosion products and on the fuel sample. *values set to zero, to avoid negative values. ** Content on the fuel sample is calculated by difference, assuming that the total Sr release is given by the quantities found on iron, on the container and in solution (see Chapter II.1.1)

	% on Fuel surface**	% in solution (0.45µm)	% on container	% on iron or iron corrosion products
Ru106	n.d.	0,669	n.d.	29,910
Cs134	0*	99.733	n.d.	0,267
Cs137	0*	99,665	n.d.	0,365
Eu154	n.d.	0,200	n.d.	68,411
Eu155	n.d.	0,621	n.d.	67,717
Sb125	0	<3,45	0	>96,55
Sr90	0*	85,305	5,445	9,250
Ce144	n.d.	0,581	n.d.	48,923
Am241	14,912	0,046	13,512	71,530
Np237	0	48,012	47,027	4,952
Cm244	n.d.	0,05	11,120	n.d.
Cm242	n.d.	0,288	17,608	n.d.
Pu238	76,699	0,045	2,269	20,987
Pu239/40	83,086	0,229	1,811	14,874
Pu241	87,673	0,049	1,375	10,939
U	59,406	0,495	2,230	37,868

about 100 times (Am ca. 1000 times) as high than their amount in solution. Nevertheless, most of the Pu (ca. 80%) and U (ca. 60%) remains directly on the fuel sample (Am ca. 15%).

[22] Stroes-Gascoyne, S., et al., Mat. Res. Soc. Symp. Proc. **50**, . 317-326 (1985)

The data on the distribution of Sr90 show that about 85% stays in solution, ca. 5% was found on the container wall and ca. 9% of the mobilized Sr is reimmobilized on the Fe. As expected, the distribution factor between Sr on iron corrosion products and Sr in solution is much smaller than the respective value for the trivalent actinides and rare earth elements. Considering that the total release of Sr $A(tot)_{Sr}$ is given by the sum of the fraction of inventories in solution (FIAP), on the container wall (FIC) and on the iron (FIFE) (see chapter II.2.1) , a comparison of $A(tot)_{Sr}$ values from experiments with and without Fe reveals that, in presence of Fe total Sr-release is about factor 4 lower. This indicates that dissolution rates decreased under reducing conditions, thus confirming the observation of Stroes-Gascoyne. However, the rather high release rates of Cs and in particular of the fission gases in the presence of iron are not yet understood.

II.4.5 Behavior of individual radionuclides in the fuel dissolution process

The observed changes in the relative leachability of radionuclides (Figures II.13-II.16) may be rationalized in terms of reaction path considerations. The reaction path describes the change in solution composition and the formation of alteration phases as a function of reaction progress. In Figure II.25 the solution concentrations of various elements in the tests with NaCl solutions in the absence of iron at various S/V ratios are plotted against the reaction progress. Reaction progress is expressed in terms of the mass of fuel dissolved per unit mass of water. Sr-data are used to calculate the dissolved fuel mass, hence, solution concentrations of Sr must follow a straight line when plotted against reaction progress. Our experiments cover more than four orders of difference in reaction progress. Experiments with fuel fragments yield very low reaction progress values, highest reaction progress is obtained when using fuel powders. The concentration ranges observed in the various tests are summarized in Table II.7.

Table II.7: Range of concentrations (molal), observed in corrosion solutions, lower limits for Am, U, Np, Cm and Tc are detection limits

Sr	10^{-10} - 10^{-6}	Cs	10^{-9} - 10^{-5}
U	10^{-8} - 10^{-4}	Pu	10^{-11} - 10^{-7}
Eu	10^{-12} - 10^{-8}	Am	10^{-9} - 10^{-7}
Ru	10^{-10} - 10^{-8}	Np	10^{-9} - 10^{-8}
Sb	10^{-10} - 10^{-7}	Cm	10^{-10} - 10^{-9}
Tc	10^{-7} - 10^{-7}	Ag	10^{-9} - 10^{-6}

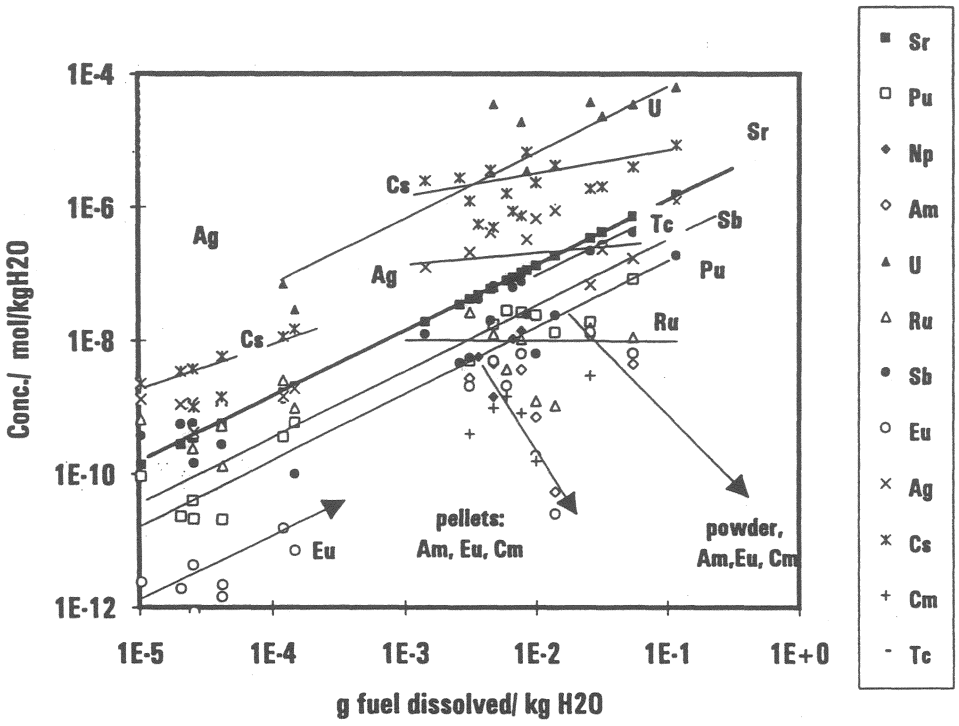

Figure II.25: Solution concentrations of various elements in the tests with NaCl solutions (same data as in Figures II.13-16) plotted against the reaction progress. Reaction progress is expressed in terms of the mass of fuel dissolved per unit mass of water. Sr-data are used to calculate the dissolved fuel mass

The solution concentrations of most elements increase with the proceeding reaction. Exceptions are Ru, whose concentration remains constant after reaching a concentration of 10^{-8} m (solubility?) and the elements Am, Cm and Eu with increasing concentrations at low reaction progress and decreasing concentrations at high reaction progress. Differences in the solution concentrations of the various elements are in part related to the different nuclide inventories in the fuel.

III. SOLUBILITY TESTS WITH UNIRRADIATED UO_2

III.1 Dissolution of UO_2(s) in brines.

In these experiments, the solid phase is an unirradiated crystalline UO_2, most experiments have been carried out using 1 mm of particle size. However, fine powder and pellets were also used.

The specific surface area of the solids were determined by the BET method, using a mixture of 0.1% Krypton by volume in helium as adsorbate. Values for each solid were: pellet (0.000192 m^2g^{-1}); 1 mm particle size (0.0016 m^2g^{-1}) and fine powder less than 10 μm (0.27 m^2g^{-1}).

In all the experiments, we determined the uranium concentration by the SCINTREX laser fluorescence technique[23] according to a method previously[24] to avoid chloride and magnesium interferences.

We have used two different brines and 95% saturated NaCl solution. In Table III.1 the composition and the calculated pH for both brines are shown.

Table III.1: Brines composition in molality units. pH was calculated using the PHRQPITZ computer program

	NaCl-brine	$MgCl_2$-brine
Na^+	6.036	0.48
K^+	0.037	0.57
Mg^{2+}	0.018	4.21
Ca^{2+}	0.021	-
Cl^-	6.036	8.84
SO_4^{2-}	0.058	0.32
Ionic strength	6.25	14.00
pH	7.7	4.7

[23] Robbins J.C, Can. Inst. Min. Mat. Bull. 5/61 (1978) 2
[24] de Pablo J., L. Duro, J. Giménez, J. Havel, M.E. Torrero and I. Casas, Anal. Chim. Acta 264 (1992) 115

III.1.1 Influence of the redox conditions

In these experiments, the influence of the redox conditions on the UO_2 dissolution have been investigated in both brines.

Reducing conditions were obtained by using a hydrogen flux and a Palladium catalyst. Oxidizing conditions were achieved with a mixture of O_2 and N_2, with an oxygen partial pressure of 0.21 atm. The redox potential was measured by means of a platinum wire electrode.

In Figure III.1, the total uranium concentration in solution under reducing conditions for both brines has been plotted as a function of contact time.

It can be seen that there is a relatively fast initial increase of the uranium concentration in solution in both brines. After this initial dissolution, the uranium concentration decreases down to a constant value which shows slight differences depending on the brine. In the NaCl-brine, the uranium concentration is 2.8 10^{-7}molkg^{-1} and in the $MgCl_2$-brine is 3.1 10^{-7} mol kg^{-1}. These constant values seem to indicate that the uranium concentration is controlled by the solubility of a solid phase.

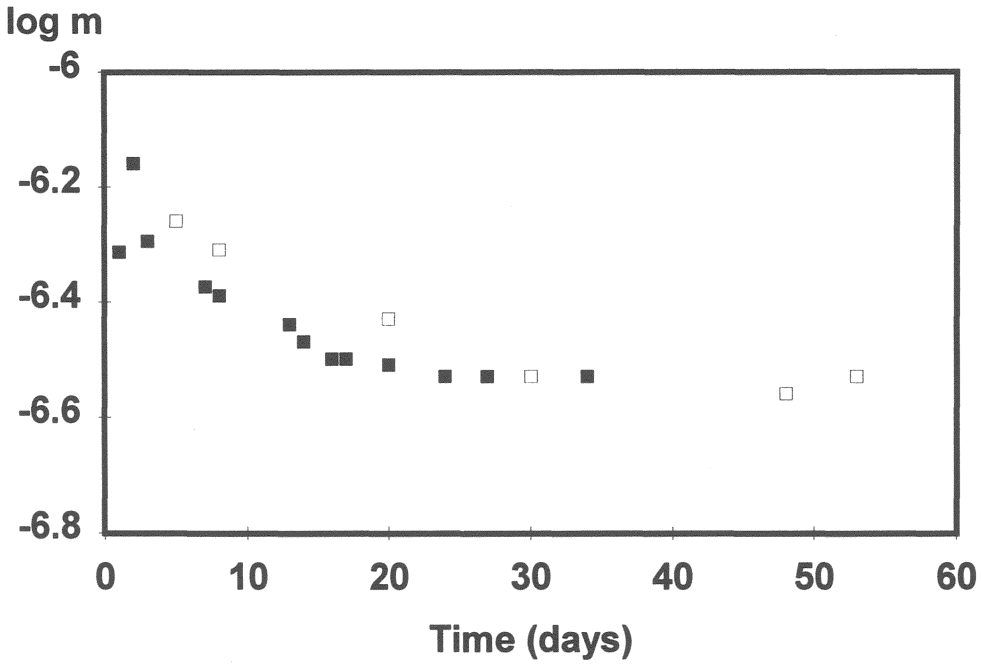

Figure III.1: Dissolution of UO_2 under reducing conditions. (■ : in NaCl-brine; □ in $MgCl_2$-brine).

At the end of the experiments, redox potentials (E_h) were measured in both brines giving similar values that ranged from 0 to 60 mV. At these potentials and pHs and according to the thermodynamic data for uranium[25], we can assume that the stable solid phase is UO_2.

Under oxidizing conditions, results are shown in Figure III. 2, in $MgCl_2$-brine uranium concentration increases slowly during all the experiment (100 days) which indicates that the kinetics of dissolution control this concentration. In NaCl-brine, after 10 days, uranium concentration remains constant, this result points to the possibility that this concentration would correspond to the solubility of a secondary solid phase.

The final solid surface in both brines have been determined by XPS. XPS results have shown that the solid put in contact with the $MgCl_2$-brine had a final composition of $UO_{2.1}$ while the one put in contact with the NaCl-brine brine had a final composition of $UO_{2.4}$. In the $MgCl_2$-brine, the composition of the solid surface in the second stage is close to UO_2 because the dissolution of the oxidized layer is faster than the oxidation of the solid surface. On the other hand, in NaCl-brine, the solid surface is more oxidized probably due to the precipitation of a U(VI)-solid phase.

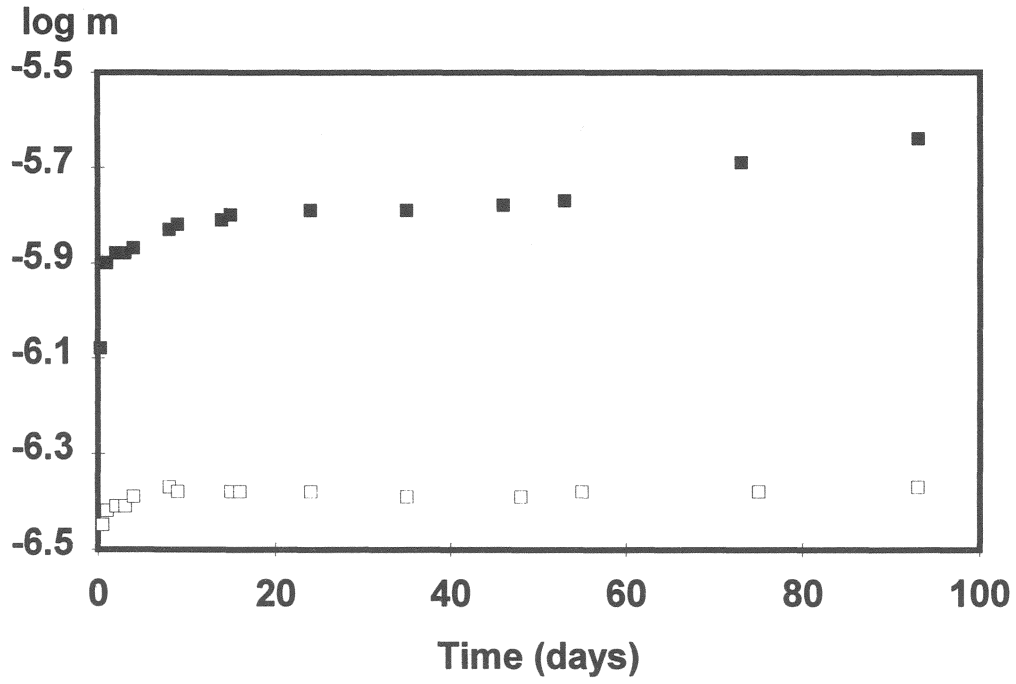

Figure III. 2: Uranium concentration (molality) vs time under oxidizing conditions (21% O_2/N_2). (■ : in $MgCl_2$-brine ; □: in NaCl-brine)

[25] Grenthe I., et al, *Chemical Thermodynamics of Uranium*, (Wanner and Forest Eds.) OECD/NEA 1992

III.1.2 Influence of other oxidants: H_2O_2 and ClO^-

H_2O_2

Following the same treatment used in this work with the spent fuel, solids were washed during 30 days with a saturated 95% NaCl solution. This solution was the same used in the experiments with H_2O_2. In order to avoid the presence of O_2 or CO_2, these experiments were performed bubbling continuously nitrogen through the vessel. Table III.2 shows the different experiments carried out.

Table III.2 Experiments carried out with H_2O_2

Experiment	particle size	$[H_2O_2]$ (mol/L)	S/V (m^{-1})
H1	<10 μm	0.1	1350
H2	1 mm	0.01	8
H3	pellet	0.01	8

In Figures III.3, III.4, and III.5, the results of uranium concentration as function of time for experiments H1, H2 and H3 are shown.

In the three experiments, the uranium concentration behaves similar, there is an initial fast increase during the first days, after this initial stage the uranium concentration remains constant. This concentration is higher when the particle size is smaller. A calculation of hydrogen peroxide concentration when the uranium concentration was constant indicated that hydrogen peroxide had reacted completely.

Dissolution rates were calculated by linear regression taking into account the mass and the surface area of the solids. In experiments H2 and H3, dissolution rates were equal to 1.29 mg $m^{-2}d^{-1}$, while in experiment H1, the dissolution rate was 17.49 mg $m^{-2}d^{-1}$. These values have been compared to those given in the literature in Figure III.6. It should be pointed out that those values were obtained in diluted solutions, however, good agreement can be observed.

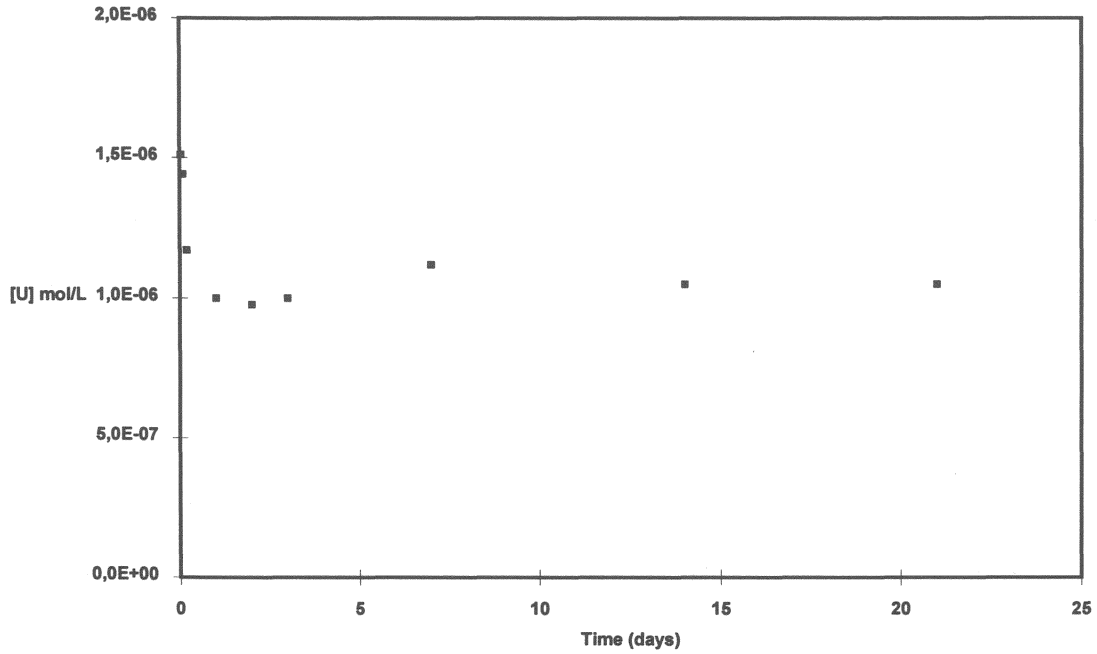

Figure III.3: Uranium concentration *vs* time in experiment H1

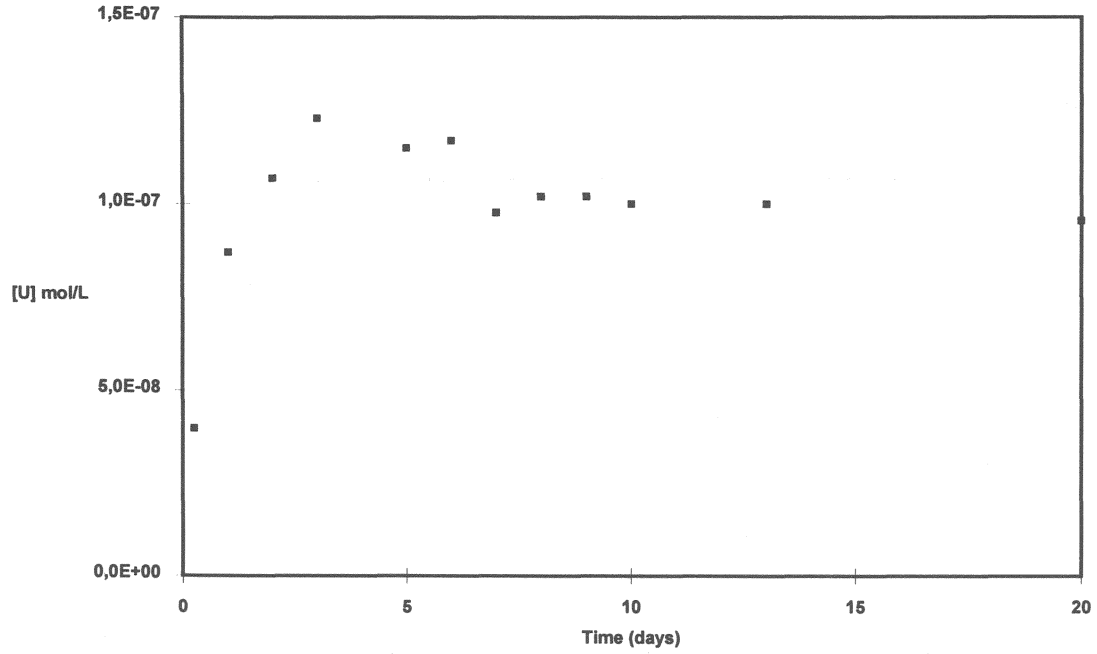

Figure III.4: Uranium concentration *vs* time in experiment H2

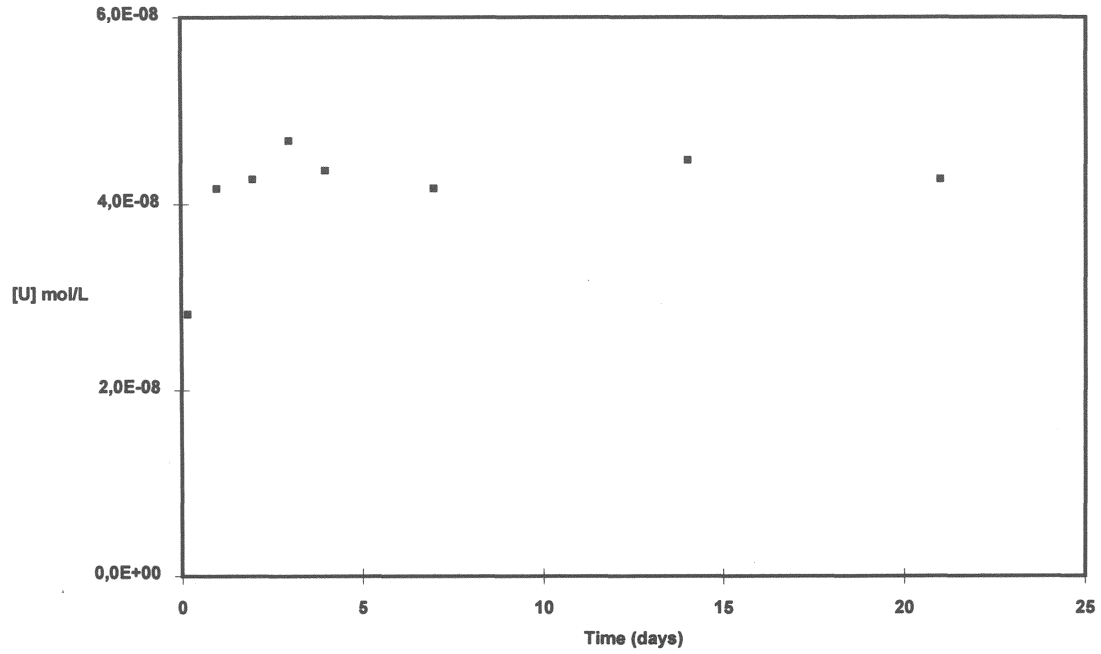

Figure III.5: Uranium concentration *vs* time in experiment H3

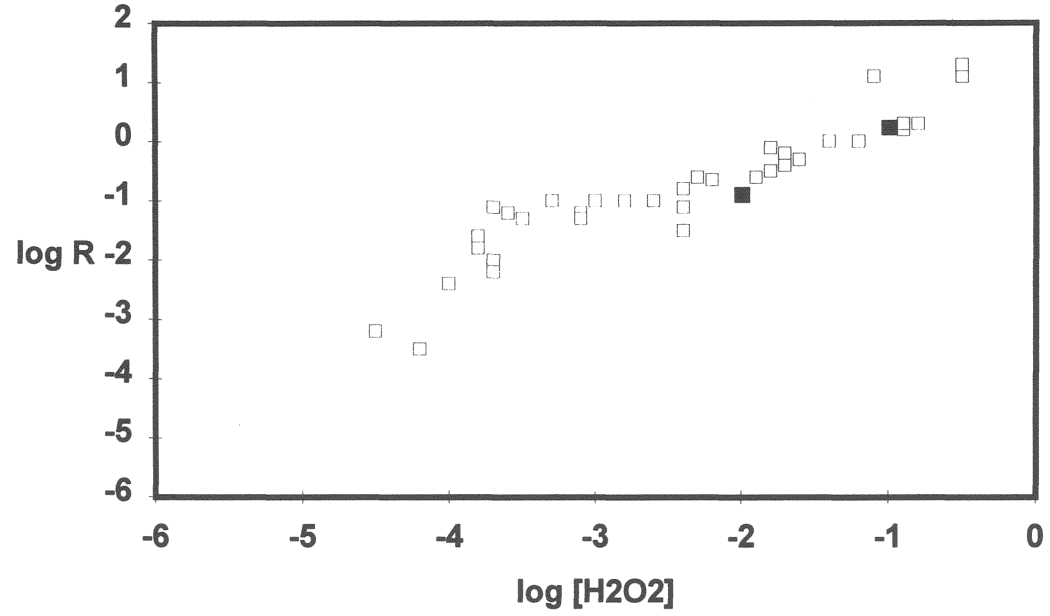

Figure III.6: Dissolution rate ($\mu g\ d^{-1}\ cm^{-2}$) versus H_2O_2 concentration. ■ this work; □ from reference[26].

[26] Shoesmith D. and S. Sunder, J. Nucl. Mater. 190 (1992) 20

ClO^-

In order to study the influence of ClO^- on the UO_2 dissolution, similar experiments to the ones performed with H_2O_2 were carried out. Table III.3 collects the experiments.

Table III.3: Experiments carried out with ClO^-

Experiment	Particle size	$[ClO^-]$ mol/L	solution	S/V (m^{-1})
C1	pellet	0.1	95% NaCl	8
C2	1 mm	0.01	95% NaCl	8
C3	1 mm	0.01	NaCl-brine	33

In Figure III.7, the results of uranium concentration as function of time for experiments C1, C2 and C3 are shown.

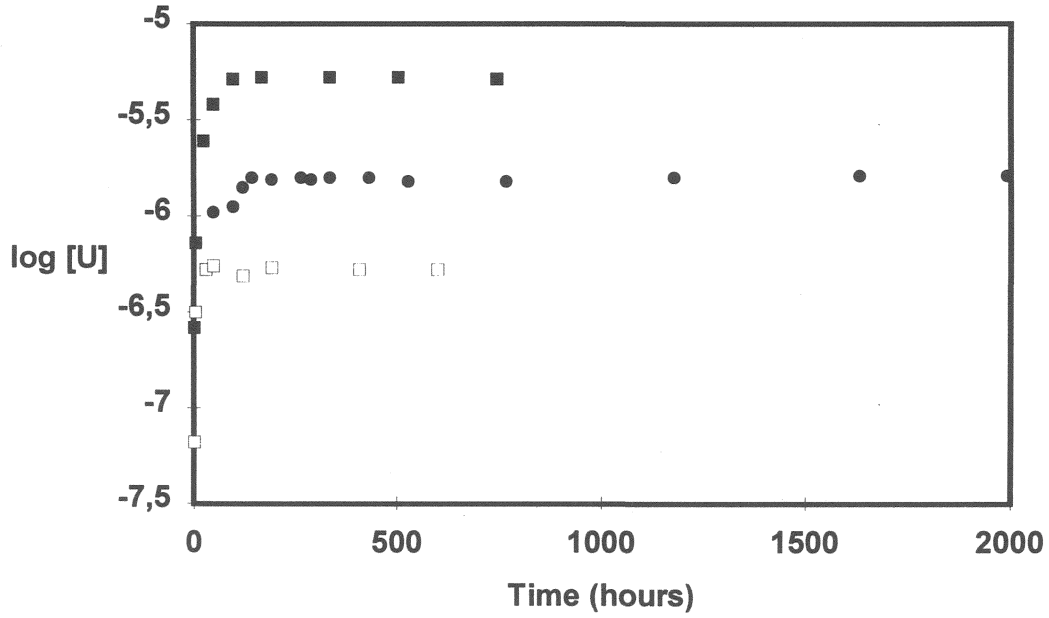

Figure III.7:. Uranium concentration *vs* time: ■ C1 ; □ C2; ● C3.

As it can be observed, the uranium concentration increases during the first days. After this initial behavior, the concentration reaches a steady state. In this case, dissolution rates were also calculated by linear regression. Dissolution rate in experiment C1 was

38.08 mg m^{-2} d^{-1} and in experiments C2 and C3 were very similar and equal to 4.17 mg m^{-2} d^{-1}. The different uranium steady state concentration observed in the experiments seems to indicate that these values are not in equilibrium with the same solid phase. Taking into account that the only difference between experiments C1 and C2 is particle size, we can conclude that kinetics control the uranium concentration in solution.

In this case, dissolution rates could not be compared to literature values. However, we calculated the dependence of dissolution rate on ClO^- concentration, which gave a value equal to 0.96. This value should be taken as a first approximation.

Finally, in Figure III.8, we have plotted dissolution rates in different oxidant media.

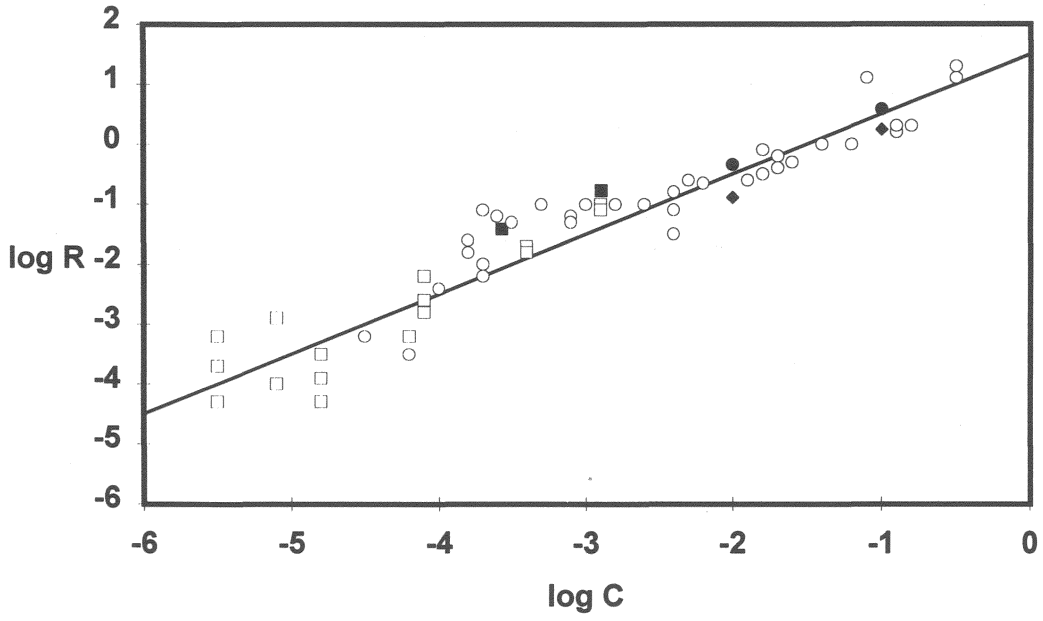

Figure III.8: Dissolution rates as a function of oxidant concentration. ● ClO^- (this work); ◆ H_2O_2 (this work); ■ O_2 (Annual Report 1992); O H_2O_2 (Shoesmith and Sunder 1992) and □ O_2 (Shoesmith and Sunder 1992).

The same general behavior can be observed independent on the oxidant considered. A slope equal to 1 can be assumed, as it is shown in Figure III.8. Therefore, the following general relationship can be written:

$$\log r = \log k + \log [ox.]$$

this equation (with a slope = 1) seems to indicate that the oxidation of the UO_2 (s) is the slowest step of the overall process which would include the oxidation and the dissolution.

III. 1.3 Influence of Iron

The influence of iron on UO_2 dissolution should be considered due to the presence of the canister. Two experiments were carried out, as leachant we used 95% NaCl and nitrogen was continuously bubbling through the experimental vessel. The particle size of the solid was 1 mm and the UO_2 weight and pH in both vessels were the same. In one vessel, we introduced 9 g of iron (particle size less than 10 μm), this experiment is identified in text as F2 and the experiment without iron as F1. The redox potential was monitored in both experiments, in F1 we measured an average of 400 mV and in F2 of -380 mV.

Uranium concentration as a function of time is plotted in Figures III.9 and III.10 As it can be seen, uranium concentration is $\approx 4\ 10^{-8}$ mol/L in both experiments. This value is similar to that obtained bubbling hydrogen and using a Pd catalyst[27]. This fact indicates that anoxic conditions (N_2) and reducing conditions (H_2 or Fe) are enough in this kind of experiments to avoid the oxidation of the solid. All these experiments can be explained taking into account the UO_2 solubility.

In order to study, the effect of both iron and radiolysis products such as H_2O_2 on the UO_2 dissolution, we have added H_2O_2 0.01 mol/L in experiments F1 and F2.

In experiment F1, uranium concentration increases from $2.89\ 10^{-8}$ to $6.45\ 10^{-8}$ mol/L after 15 days. In experiment F2, there is also an increase during the first day from $1.41\ 10^{-8}$ to $5.13\ 10^{-8}$ mol/L but after 15 days, the concentration decreases again up to $1.81\ 10^{-8}$ mol/L.

These results indicate that iron is a good redox buffer even in the presence of radiolytic products. Another important conclusion would be that in these experiments no sorption of uranium onto iron has been observed since uranium concentration in F1 and F2 are very similar.

[27] Torrero M.E., I. Casas, M. Aguilar, J. de Pablo, J. Giménez and J. Bruno, Mat. Res. Soc. Symp. Proc. 212 (1991) 229

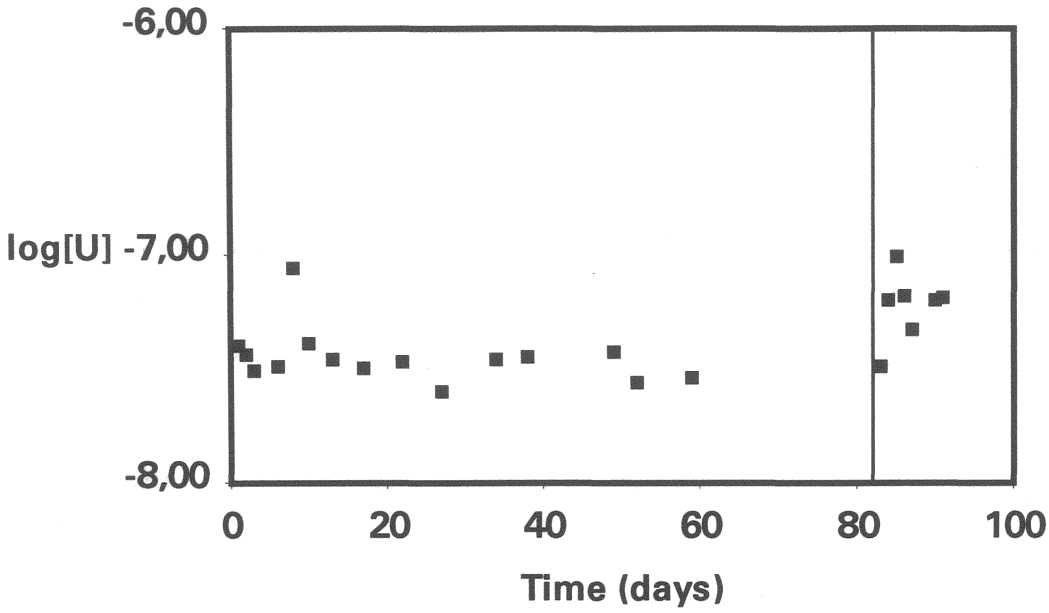

Figure III.9: Uranium concentration *vs* time in experiment F1. After full line introduction of H_2O_2 0.01 mol/L in the vessel

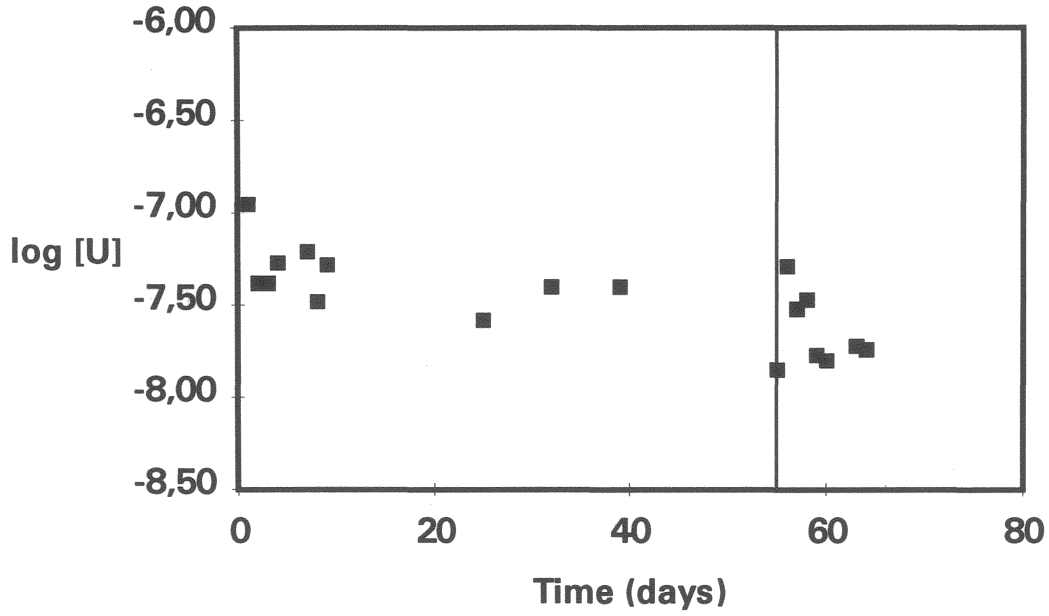

Figure III.10: Uranium concentration *vs* time in experiment F2. After full line introduction of H_2O_2 0.01 mol/L in the vessel

III.1.4 Conclusions

1.- Under reducing conditions, the uranium concentration behavior is independent on the brine composition. The constant uranium concentrations at the end of the experiments agree well with the UO_2 solubility at these conditions calculated by the PHRQPITZ program.

2.- Under oxidizing conditions, different initial dissolution rates are obtained in both brines due to their different pH. A second dissolution rate is obtained in Q-brine but not in the NaCl-brine possibly due to the precipitation of a secondary solid phase in this brine.

3.- The initial dissolution rate increases proportionally to the concentration of oxidants in solution following this equation:

$$R = k\,[Oxidant]$$

The initial dissolution rate does not depend on the S/V ratio used in this study. Results in diluted solutions are similar to those obtained in this work.

4.- The presence of iron reduces the redox potential of the solution and the results are similar to the ones obtained in nitrogen and/or hydrogen. No adsorption of uranium into the Fe powder has been observed.

III.2. Influence of the particle size

In these experiments, unirradiated UO_2 pellets were crashed and sieved in order to obtain different particle size. We used the following particle size ranges: 10-50 μm,100-300μm, 900-1100μm as well as pellets as received has been used.

The leaching solution used in this work was 0.01 mol L^{-1} $NaClO_4$. The pH was adjusted to 8 by adding CO_2-free NaOH solution.

Oxidizing conditions were achieved by using 5% O_2 in N_2 flux. The experiments were carried out at room temperature in Teflon vessels. The pH was measured by a combined glass electrode. The redox potential was recorded continuously by means of a platinum wire, using a Ag/AgCl electrode as a reference.

The different solid phases were put in contact with the test solutions; and aliquots for uranium analysis were taken as a function of time. All the samples were filtered immediately through a 0.22 μm MILLIPORE membrane filter; and uranium concentration was determined by the Scintrex UA-3 laser fluorescence analyzer[23].

The uranium dioxide specific surface area for each solid was determined by the BET method, using a volumetric apparatus that employed a mixture of 0.1% Krypton in helium as adsorbate. Results are shown in the annual EU-Report (1992) of this project[28].

III.2.1 Results

The uranium concentration as a function of contact time is plotted for each solid (100-300 μm, 900-1100 μm and pellet) in Figure III.10. A similar dissolution behavior in all cases is observed. After a relatively fast initial uranium release (first 15 days), the uranium concentration increases very slowly. In addition, the redox potential of the bulk solution is approximately constant during all the experiments.

In the experiment with the smallest particle size (10-50 μm), the UO_2 dissolution differs considerably. In Figure III.11, the uranium concentration and the bulk redox potential are plotted as a function of time. The decrease on uranium concentration during the first days coincides with the decrease observed on the redox potential.

This result could be related to the redox buffer capacity of UO_2. The small particle size would react easily with the oxygen in solution. The decrease of the oxygen in solution leads to a more reducing potentials and consequently, a lower uranium concentration. When the capacity of consuming oxygen is over, both the redox potential and the uranium concentration increase up to values similar to those obtained with the other particle size. This explanation should be studied in more detail because UO_2 could control redox potential in the near field.

---

[28] Grambow, B.; A.Loida, P. Dressler, H. Geckeis, P. Diaz, J. Gago, I. Casas, J. De Pablo, „Reaction of High-Burnup Spent Fuel and UO2 in Salt Solutions" KfK 5377 (1994)

in detail by using X-ray Photoelectron Spectroscopy (XPS) [Annual EU report 1993]. The oxidation/dissolution mechanism proposed is schematized in Figure III.12

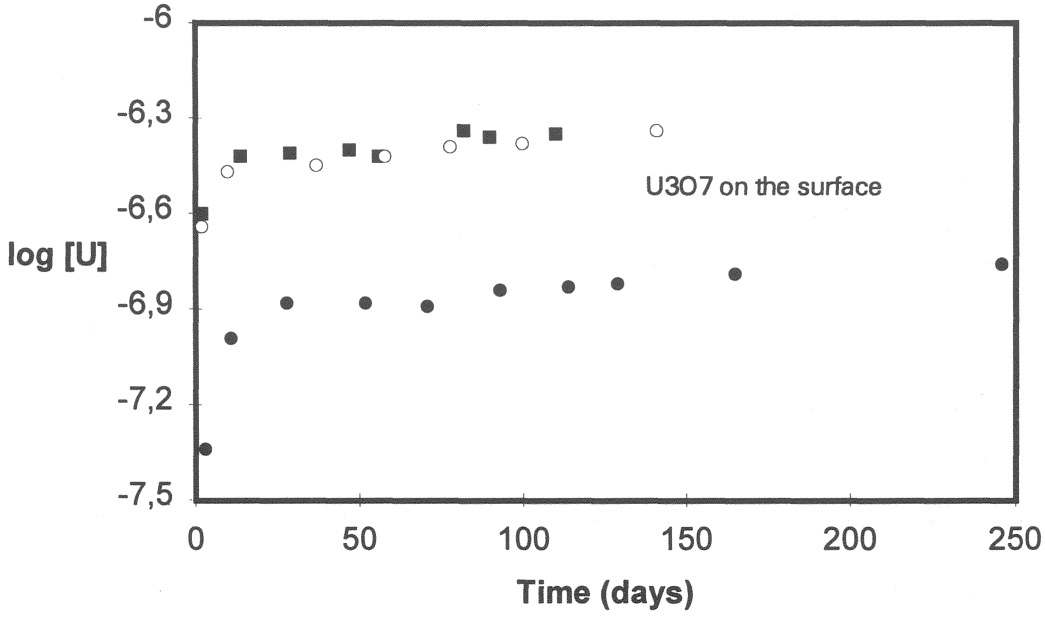

Figure III.10: Uranium concentration *vs* time. ● pellet; ○ 900-1100 μm; ■ 100-300 μm. Oxidizing conditions at pH = 8.

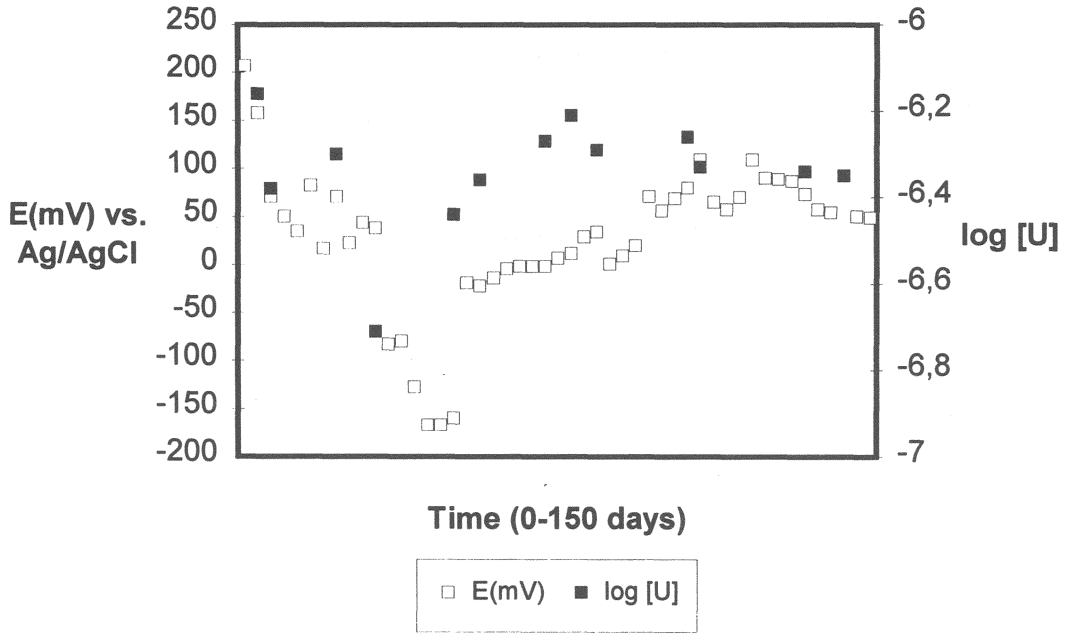

Figure III.11: □ Redox potential and ■ uranium concentration as a function of time. Particle size 10-50 microns.

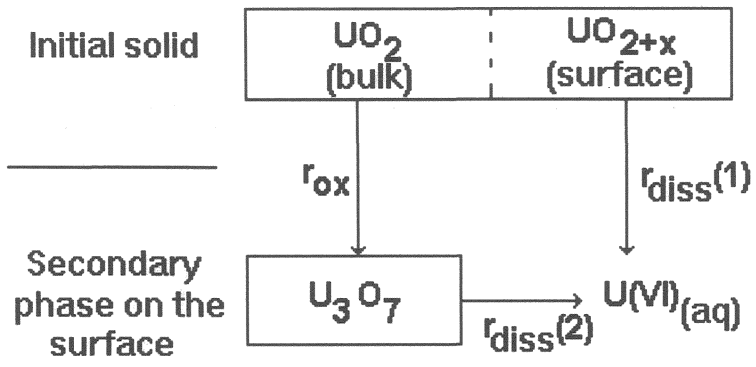

Figure III.12:. Scheme of the mechanism of UO_2 dissolution under oxidizing conditions.

In this Figure, $r_{diss}(1)$ stands for the rapid initial dissolution rate of the initial oxidized solid surface; r_{ox} for the rate at which the UO_2 is oxidized to the U_3O_7 solid surface composition found at pH=8, while $r_{diss}(2)$ represents the dissolution of this secondary solid phase.

In all cases studies in this work, $r_{diss}(1)$ seems to be higher than $r_{diss}(2)$ and r_{ox}. Since $r_{diss}(1)$ indicates a process parallel to the one determined by $r_{ox} + r_{diss}(2)$, the overall dissolution will be in this case determined by the faster reaction.

Once this initial solid surface phase is dissolved, the mechanism goes through the way indicated by $r_{ox} + r_{diss}(2)$, and in this case the experimentally observed dissolution rate will be governed by the slower step. This model may correspond to a simplified mechanism, where other contributions should also be considered (i.e. precipitation of saturated phases, diffusion, ...)in a more detailed mechanism.

The dissolution rates determined in these experiments are collected in the next chapter where all the dissolution rates (UO_2 and spent fuel) are compared.

The mechanism shown in Figure III.12 implies that the dissolution of U_3O_7 should be very slow since the uranium concentration in solution increases slowly (see Figure III.10). This assumption is not clear if we take into account the results observed with spent fuel, spent fuel dissolution rate determined by Sr release is much higher than the ones obtained in these experiments. Because of that, some continuos flow experiments were performed.

In these experiments, we can measure more "elementary" processes, which give release rates more fundamental than the ones obtained from batch experiments.

The experimental flow system used is based on a thin layer reactor[29]. The use of this reactor minimizes the effect of diffusion through the solid.

In Figure III.13, uranium concentration was plotted as a function of time. The uranium concentration decreased at the beginning of the experiment, reaching a steady state after two days. This steady state concentration remained constant during more than 60 days.

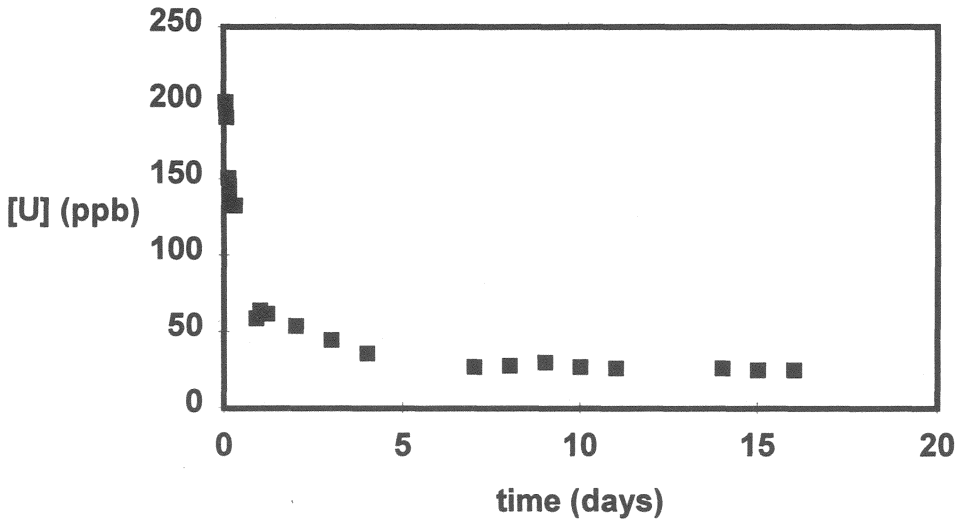

Figure III.13: Uranium concentration as a function of time under oxidizing conditions and pH = 8.

[29] Bruno J., I. Casas and I. Puigdomènech, Geochim. Cosmochim. Acta, 55 (1991) 647

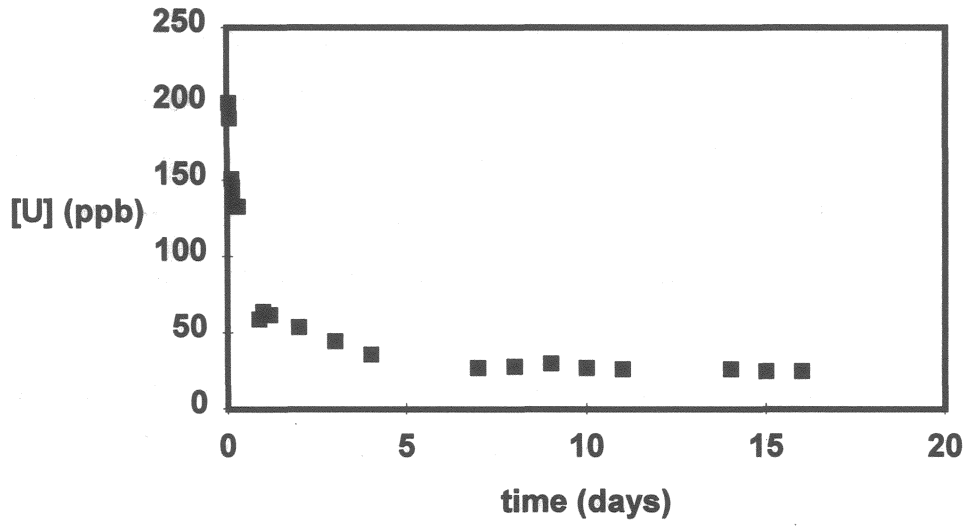

Figure III.13: Uranium concentration as a function of time under oxidizing conditions and pH = 8.

Dissolution rate was calculated using the following expression:

$$r_{diss} = Q\,[U]/S$$

where Q (L/d) is the flow rate, [U] (mol/L) is the uranium concentration and S is the total surface area of the solid enclosed in the reactor (m^2) determined by the BET method.

We have compared dissolution rates in batch and flow experiments at the same conditions, we have also determined the final solid surface in both experiments by using XPS. These values are given in Table III.4.

Table III.4: Comparison of solid surface composition and dissolution rates in batch and flow experiments. Conditions in both experiments were: $NaClO_4$ 0.01 mol/L, 5% O_2 in N_2 and pH=8.

	BATCH	FLOW
SURFACE COMPOSITION	$UO_{2.38}$	$UO_{2.21}$
DISSOLUTION RATE	4.3 E-3 mg/m^2 d	1.9 E-1 mg/m^2 d

Although both surface composition are a little different, the surface determined in the flow experiments is much higher than those obtained in carbonate and the same pH[30] and at

[30] Bruno J., I. Casas, E. Cera, J. de Pablo, J. Giménez and M.E. Torrero, Mat. Res. Soc. Symp. Proc., pp 601 - 608 (1995)

acid pH[31]. This fact seems to indicate that the great difference between dissolution rates shown in Table III.4 must be due to the precipitation of a secondary phase.

This behavior should be studied in more detail because the difference between the uranium concentration and Sr release rates in the spent fuel experiments could be due to this phenomenon. In fact, flow dissolution rates agree much better with those determined in the spent fuel.

III.2.2 Conclusions

1.- The same dissolution rates have been obtained under the same oxidizing conditions and pH independent on particle size: 100-300 μm, 900-1100 μm and pellets. Therefore, BET determinations seem to be enough useful to normalize dissolution rates.

2.- Using a particle size less than the ones mentioned above (10-50 μm), a decrease on uranium concentration and redox potential has been observed. This fact has been related to the redox buffer capacity of UO_2 (s).

3.- The oxidation/dissolution mechanism proposed of UO_2 is based on solid surface evolution.

Acid pH: $\mathbf{UO_2 + UO_{2+x} \Rightarrow UO_2 \Rightarrow U(VI)\ (aq)}$

Basic pH: $\mathbf{UO_2 + UO_{2+x} \Rightarrow U_3O_7 \Rightarrow U(VI)\ (aq)}$

4.- Dissolution rates determined in a continuos flow system are higher than the ones determined in batch. Final solid surface is very similar in both methodologies, this fact point out that other phenomena i.e. uranium precipitation take place in batch experiments.

[31] Casas I., J. Giménez, V. Martí, M.E. Torrero and J. de Pablo, Radiochim. Acta 66/67 (1994) 23

IV. Modeling of the reaction behavior of spent fuel with saline brines.

Due to the long time spans of interest, performance assessment of spent fuel behavior in a repository cannot be based on experimentally oriented studies alone but must be based on investigation of scenaria on how the disposal system may evolve in future and on modeling techniques. Modeling comprises geochemical and reaction path modeling, radiolysis, hydraulic models. etc.. Model development can only occur iterative in conjunction with experimental and natural analogue studies. In the context of the present program some cornerstones of a future overall source term model for saline brines are described. These include: (1) an instant release term for Cs135 and J129, (2) Constraints on fuel matrix dissolution rates, controlling long-term release of soluble elements (Cs, Sr, Tc(VII), Np(V), Sb, and, conservatively, all nuclides for which solubility limits are unknown), (3) Concepts describing the retention of radionuclides (emphasis on actinides) during fuel dissolution, either by coprecipitation, sorption or solubility. Additional effects to be included in modeling, such as potentially fast release from the fuel rim and the effect of iron on reaction rates were discussed in chapter II and will not be repeated here. A model describing the surface oxidation state of dissolving UO_2 has been presented in chapter III and will also not be repeated here.

Relative leachability is function (1) of the competing individual radionuclide release rates from the fuel matrix, the fuel sheath gap, fracture surfaces and from grain boundaries, combined (2) with resorption processes onto the fuel surface or sorption on the Ti/Pd or Ta-liner and (3) with (co-)precipitation processes.

The relative leachability of various radionuclides is assessed by comparison of respective FIAP values. For tests in NaCl solutions in the absence of iron, Figure IV.1 gives the normalized solution concentrations of various radionuclides as a function of reaction progress. Normalized concentrations of the nuclide i are expressed as g fuel/kg water = NL_i*(S/V) (see Chapter II.2.3). They may be interpreted as the hypothetical solution concentration of fuel, if the fuel would dissolve with the same rate than the respective nuclide. Data for Sr are used for calculating reaction progress, similarly in terms of a hypothetical solution concentration of dissolved fuel.

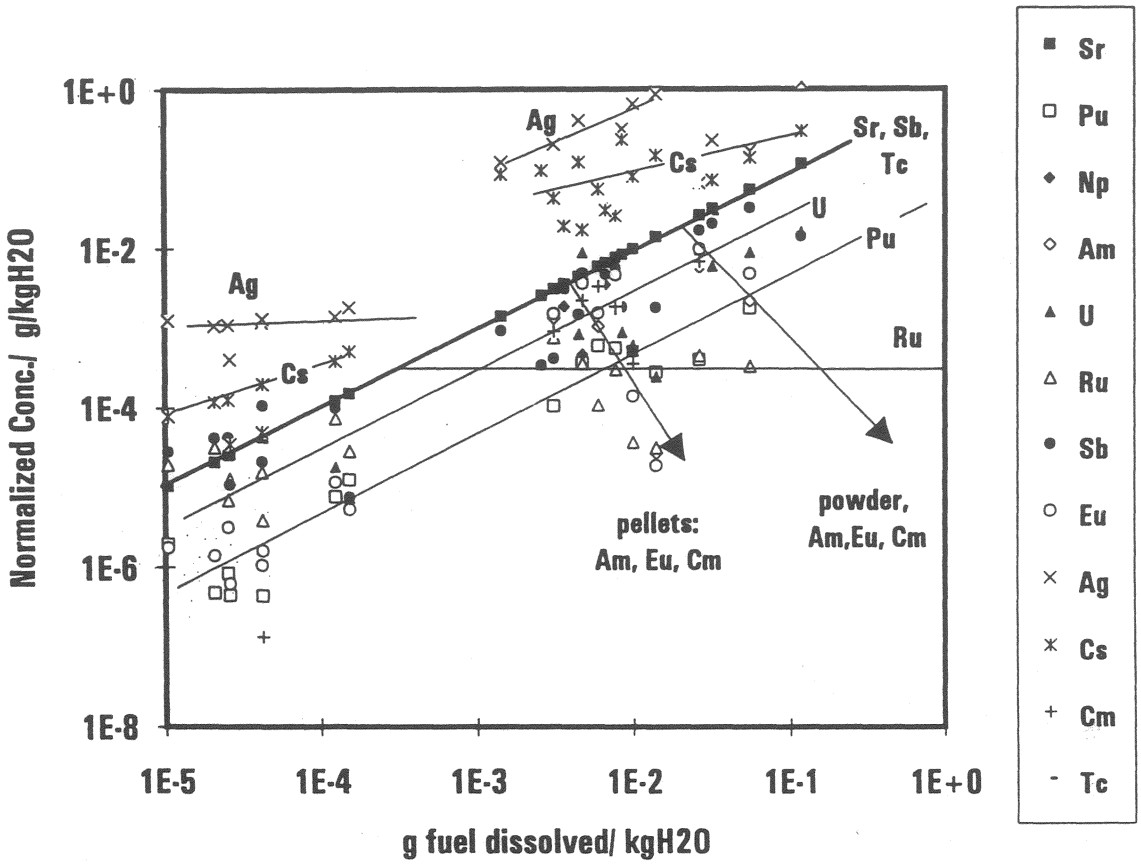

Figure IV.1: Normalized solution concentrations of various elements in the tests with NaCl solutions in the absence of iron (based on concentration data from Figure II.25)

As discussed in chapter II, fuel matrix dissolution rates are calculated from the release rates of Sr90. Elements with normalized solution concentrations similar to those of Sr are released with the same rate, most likely as Sr being controlled by the dissolution rate of the fuel matrix. The kinetics of fuel matrix dissolution seem to control the release rates of Sr, Np, Tc, Sb and the initial release rate of Ru. It is surprising that Ru initially appears to be released by matrix dissolution as this element is contained in the segregated metallic phases. Possibly, there remains a significant fraction of Ru in the fuel matrix and there is only a small fraction in segregated phases. It could also be possible that, due to chloride complexation, the metallic phases dissolve fast in chloride media. In LWR fuel, the metallic phases are rather small (as compared to CANDU fuel for example), and associated high specific surface areas will allow fast dissolution of the metallic phases. If this phases are homogeneously dispersed in the fuel matrix, the rate of matrix dissolution may govern the rate of exposure of new metallic phases

to the solution, and consequently, rates of metallic phase dissolution may become similar to the rates of fuel matrix dissolution.

IV.1 Preferential release of radionuclides: instant release term

In the present context, the term „preferential release" is used for those radionuclides whose release rates (dissolution, gas release) are faster than expected from the rate of fuel matrix dissolution. When normalized solution concentrations (for definition see chapter II.2.3) of a given element are higher than that of Sr, preferential release from fractures, grain boundaries or easily soluble segregated phases is the likely cause. This was observed only for Cs and in some cases for Ag (see Chapter II.4.1 and Figure IV.1). An instantaneous release term[32], in particular for Cs135 and I129, has to be included into source terms for radionuclide release from spent fuel. This instant release term should cover the sum of gap and grain boundary inventories of the fuel and must be determined experimentally.

J129 was not analysed in the present study but results from the literature[33] show that the behavior of J129 is normally rather similar to the behavior of Cs. In few cases inventory normalized initial J129 release was up to a factor 2 higher than release of Cs137[33] whereas in certain other cases it was found to be as much as a factor of 3-4 lower[34]. Considering heterogeneity of the fuel, we may use the Cs137 data of chapter II.4.1 to estimate the J129 gap-release as 2-3% and grain boundary release as 3-4%. The sum was between 4 and 7%. with an average instant release value of about 6% applicable for the two long-term relevant nuclides Cs135 and J129. These values are only valid for the high burnup fuel presently under investigation. More realistic average values for typical LWR fuel to be disposed in a first repository will probably be below 3%.

---

[32] N.Garisto et al. AECL-9892 Atomic Energy of Canada Limited, Whiteshell (1989)
[33] S. Stroes-Gascoyne, L.H. Johnson, D. Sellinger, Nuclear Technology 77 320-330 (1987)
[34] V.M.Oversby, H.F.Shaw, UCID-20926, Lawrence Livermore National Laboratory (1987)

IV.2 Comparison of dissolution rates of spent fuel matrix with those from UO_2 dissolution (data from Chapter II and Chapter III): Effect of radiolysis

A detailed discussion of factors controlling fuel dissolution rates are given in chapter II and respective evaluation of dissolution rates of unirradiated UO_2 is given in chapter III. What remains to be done is a comparison of the reaction rates from the two studies. This comparison also points to the significance of a joint UO_2/spent fuel study.

Sr90 based reaction rates of spent fuel and of UO_2 samples, measured in the project are summarized in Table IV.1, both for static experiments (denoted "B") and for tests with flowing solutions (denoted "F"). In the course of some UO_2 dissolution tests, two rates were measured, an initial rate R and a long-term rate R(2). The experimental conditions are indicated in the table, including the description of the particle size of the samples used, the logarithm of the partial pressures of oxygen ("pO_2") and of CO_2 ("carb"), and the resulting molality of dissolved uranium in solution ("log [U]").

In case of UO_2-dissolution, reaction rates are derived from the measured uranium concentration in solution and the BET-measured sample surface area. The actual reaction rates may have been higher, if part of the dissolved Uranium is reprecipitated into secondary phases which may form in the course of the dissolution reaction. Therefore, only initial reaction rates will be used for a comparison of UO_2 and spent fuel dissolution rates. In tests with flowing solutions, saturation effects with respect to U(VI), and consequently secondary phase formation should be prevented. In case of spent fuel dissolution tests, Sr90-data were used to obtain reaction rates of spent fuel samples. It has been shown in chapter II that Sr-release is governed by the dissolution rate of the fuel matrix. Differences in the fractional release rates of Sr and U therefore describe the extent of secondary phase formation.

Sr based long term rates of dissolution of spent fuel pellets in the absence of carbonate were found to be about a factor of 10 higher than the rate of UO_2 dissolution in flow test. On the other hand, it is reported in the literature[35] that UO_2 dissolution rates may become as high as our spent fuel dissolution rates if exposed to a γ-dose rate of a magnitude (ca. 10000 rad/h). Hence the difference in spent fuel and UO_2 dissolution rates may be explained by radiolysis.

[35] D. Shoesmith, Sunder, SKB report 91/63, 1991

Table IV.1: Comparison of dissolution rates R (initial) and R (2) (long-term) of UO_2 and spent fuel (S.F.) B = static experiments, F = flow tests. Logarithm of the partial pressures of oxygen (pO_2) and of CO_2 (carb), resulting molality of dissolved Uranium in solution (log [U]).

Exp.	Solid	Particle size	pH	pO_2	Other	Ionic Medium	R (mg/m2d)	R (2)	log [U] molal
B	UO_2	100/300(pr)	8	0,05		0,01 $NaClO_4$	0,11	0,00037	-6,4
B	UO_2	900/1100 µm	8	0,05		0,01 $NaClO_4$	0,64	0,0028	-6,4
B	UO_2	Pellet	8	0,05		0,01 $NaClO_4$	0,45	0,0048	-6,8
B	UO_2	100/300 µm	8	0,05		0,01 $NaClO_4$	0,6	0,0043	-6
B	UO_2	100/300 µm	8,5	0,21	0,01 carb.	0,1 NaCl	1,8	1	-3,3
B	UO_2	Pellet	8,5	0,21	0,01 carb.	0,1 NaCl	2,4	1,3	-5,7
F	UO_2	100/300 µm	8,5	0,21	0,01 carb.	0,1 NaCl	3,1		
F	UO_2	100/300 µm	8	0,21		0,1 NaCl	0,18		
B	UO_2	900/1100 µm	6,3	0,05		$MgCl_2$-brine	0,25	0,03	-5,9
B	UO_2	900/1100 µm	6,3	0,21		$MgCl_2$-brine	0,81	0,04	-5,5
B	UO_2	900/1100 µm	6,3	1		$MgCl_2$-brine	1,7	0,09	-5,3
B	UO_2	900/1100 µm	3,8	0,21		$MgCl_2$-brine	1,05		-4,6
B	UO_2	900/1100 µm	7,6	0,21		NaCl-brine	0,59		-6,3
B	UO_2	900/1100 µm	7,6	0,21	0,001 carb	NaCl-brine	1,24		-5,7
B	UO_2	900/1100 µm	7,6	nitrogen		NaCl-brine	0,7		-6,2
B	UO_2	900/1100 µm	7,6	nitrogen	0,01 ClO-	NaCl-brine	2,1		-5,8
B	UO_2	< 10 µm	7,5	nitrogen		NaCl 5m	0,1*		-6,7
B	UO_2	900/1100 µm	6,3	nitrogen		NaCl 5m	1,16*		-7,5
B	UO_2	Pellet (pr)	7,3	nitrogen		NaCl 5m	0,47*		-8
B	UO_2	900/1100 µm	6,6	nitrogen	9 g Fe	NaCl 5m	0,64*		-7,4
B	UO_2	< 10 micr (pr)	7,3	nitrogen	0,1 H_2O_2	NaCl 5m	17,5		-5,9
B	UO_2	900/1100 (pr)	7,8	nitrogen	0,01 H_2O_2	NaCl 5m	1,32		-7,1
B	UO_2	Pellet (pr)	8	nitrogen	0,01 H_2O_2	NaCl 5m	1,27		-7,4
B	S.F.	Pellet	9,2	argon		NaCl 5m	1		-5,4
B	S.F.	Pellet	7,8	argon		NaCl 5m	1		-6
B	S.F.	Pellet	7,3	argon		H_2O	3 to 4		-7,1
B	S.F.	Pellet	7,3	argon		H_2O	3 to 4		-8
B	S.F.	Powder	6,3	argon		NaCl 5m	0,05		-4,2
B	S.F.	Powder	6,6	argon		NaCl 5m	0,05		-4,4
B	S.F.	Pellet	9,6	argon	Fe	NaCl 5m	0,2		-7
B	S.F.	Pellet	9,6	argon	Fe	NaCl 5m	0,1		-7,2
B	S.F.	Fragments	7,2	argon		NaCl 5m	2		-7,3

The potential radiolysis product H_2O_2 has a strong influence on UO_2 dissolution rates above a concentration of 0.001 m (Chapter III). UO_2 dissolution rates in 5 m NaCl solution in the presence of H_2O_2 are similar to reported[35] UO_2-dissolution rates in deionized water at the same H_2O_2 concentration. Hence, the presence of NaCl has a negligible effect on the accelerating effect of H_2O_2 on UO_2 dissolution rates.

On the other hand, it is reported for carbonate media that flow test with UO_2 and with spent fuel[36] give similar results, hence, under these conditions radiolysis appears not to be very effective for accelerating fuel dissolution rates. This different significance of radiolysis may be explained on the basis of the different dissolution rates in presence or absence of carbonate. The high rates in the presence of carbonate (Table IV) may mask any radiolysis effect.

The initial UO_2 dissolution rates are generally similar under static and dynamic conditions, however long-term rates are in most cases lower under static conditions. Hence, the apparent decrease in the UO_2-reaction rates in static tests may be associated to secondary phase formation. The initial UO_2 dissolution rates increase with partial pressure of oxygen and of CO_2 but are only slightly dependent on pH and independent on salinity. Initial dissolution rates of UO_2 under oxidizing conditions are governed by two processes: (1) the dissolution of an oxidized surface film initially present and (2) oxidative dissolution of $UO_{2.0}$. By using flow tests we can distinguish between processes (1) and (2). In the presence of carbonate, short and long-term dissolution rates of UO_2 are rather similar. This is probably an effect of the absence of secondary phase formation caused by increasing solubility of U(VI) solid phases due to carbonate complexation of the dissolved uranyl ion. Consequently UO_2 long-term dissolution rates in carbonate media are similar under static and dynamic conditions[36].

Extremely low apparent long-term dissolution rates (<0.01 mg/m^2d) are only observed with UO_2, not with spent fuel samples. This indicates that the real long-term reaction rate of unirradiated UO_2 may remain much higher but, due to the precipitation of Uranium (VI) containing secondary phases, this continuing reaction cannot anymore be monitored by measuring the uranium concentration in solution. The apparent UO_2 long-term dissolution rates are strongly correlated with the degree of surface oxidation of the dissolving solid. They are highest when oxidation is lowest. Observed are saturation effects or extremely low long-term rates (R(2), Table IV.1) when the surface is oxidized to $UO_{2.33}$. This surface composition of $UO_{2.33}$ is the average composition measured by ESCA (Chapter III) for the outer few nm of the surface region and it may either represent oxidized UO_2 (U_3O_7 etc.) or, for example a thin "schoepite (UO_3*2H_2O) layer" on UO_2. If solubility of this surface film is the limiting

[36] W. Gray, personal communication

condition of its formation, reaction rates shall become zero. Non-zero reaction rates may be expected, if electrochemical dominated surface oxidation states are lower than bulk Eh values.

IV.3 Modeling and discussion of the retention behavior of various radionuclides

Normalized concentrations of radionuclides lower than those of Sr are controlled either by sorption on the Ta or Ti lined container or on the zircalloy cladding, by resorption on the fuel samples, by precipitation or coprecipitation processes or by the dissolution of sparingly soluble phases, segregated during reactor operation in the fuel matrix or at grain boundaries. Among these elements are U, Pu, Am, Cm, Eu and long-term Ru. If sorption, resorption, or dissolution of sparingly soluble segregated phases control release, the solution concentrations should increase with reaction progress, while they should decrease or remain constant in case of a precipitation process controlling release. Coprecipitation may result in increasing, decreasing or constant concentrations with reaction progress, depending on endmember stability and stoichiometric constraints.

In order to rationalize solubility effects, the solution concentrations of radionuclides may be compared with the solubility of potentially precipitating phases.

IV.3.1 Uranium

Uranium is the principal element constituting the fuel matrix. Understanding of the rates of uranium release and of the formation of uranium containing secondary alteration products, therefore, is of high interest for understanding the fuel dissolution process. For quantification of the source term for disposal of spent nuclear fuel important questions are: (1) what is the Uranium concentration in solution and by dissolution or precipitation of which phase it is controlled and (2) whether U saturation has any effect on the release of radionuclides, either by (a) controlling fuel corrosion rates (saturation effects, protective layers etc.), (b) by formation of coprecipitates or (c) by controlling surface redox potentials. Only question (1) is addressed in the present context, and question (2a) is discussed in part in Chapters II. Important are the redox states of uranium in the dissolving phase (IV), the secondary phases (IV or VI) and in solution (IV or VI). In case of non-irradiated material the dissolving phase (UO_2) or its partly oxidized

surface layers (up to $UO_{2.33}$) may become thermodynamically stable under reducing conditions. Radiolysis may prevent reducing conditions to persist at the UO_2 surface of irradiated material.

IV.3.1.1 Dominant redox states of Uranium in solution

The redox states and solution species of uranium have not been analyzed experimentally in the context of the present project. In order to estimate the stability ranges of dominant uranium species and valence states, geochemical calculations were performed, using the code EQ3/6. The electrolyte theory of Pitzer was used to calculate activity coefficients for the dominant solution species, as far as the required binary and ternary interaction coefficients were available. For highly concentrated solutions such as the present 95% saturated NaCl solution, very little is known on the interaction coefficients for the U(IV/VI)/Na/Cl system, except for acid conditions. Under acid conditions, depending on solution Eh either U^{++++} or UO_2^{++} are dominant. The UO_2^{++}/Cl^- system is known[37], binary interaction coefficients are reported by Pitzer and together with a θ value of 0.0231 for Na^+/UO_2^{++} interaction[38], mean trace activity coefficients of uranyl chloride in NaCl solutions were calculated. Chloride complexation is implicitly, not explicitly accounted for. Mean activity coefficients for the binary U^{++++}/Cl system are not known but, for the present estimation, they may be considered identical to respective values of the chemically homologue Th^{++++}/Cl system reported by[39]. The ionic strength dependency of the equilibrium redox reaction in acidic NaCl solution is then given by the mean activity coefficients of HCl, UO_2Cl_2 and UCl_4 in NaCl solution and an E_o value of 269 mV[40] for the U(IV)/U(VI) redox equilibrium at infinite dilution. Both, for U(VI) and for U(IV) chloride complexation is considered implicitly within the numerical values of the mean activity coefficients.

To calculate redox equilibria at neutral to alkaline pH values, hydrolysis reactions, both of U(VI) and of U(IV) needs to be considered. The calculation of the predominance fields of the various hydrolysis species is made for 3 m NaCl solution and a typical total uranium

[37] R.A.Robinson, Lim, J.Chem. Soc. 1840 (1951)
[38] H.T. Kim, W.J. Frederic, J.Chem Eng.Data **33**, 278-83 (1988)
[39] Pitzer K.S., "Theory: Ion Interaction Approach" in Activity Coefficients in Electrolyte Solutions" Vol I, ed. R.M. Pythowicz, CRC Press Inc. Boca Raton, Florida USA (1979)
[40] J. Bruno, I. Grenthe, B. Lagerman, „On the UO_2^{++}/U^{4+} Redox Potential"; Acta Chem. Scand, **44**, 896-901 (1990)

concentration of 10^{-5} m. Under these conditions, polynuclear U(VI) complexes dominate the hydrolysis behavior of the uranyl ion and respective conditional stability constants are given by [41]. The calculated mean activity coefficient of traces of uranyl chloride in NaCl solution are directly compatible with the conditional stability constants given by[41], as both do consider chloride complexation implicitly. For $(UO_2)_3(OH)_7^-$ and $UO_2(OH)_3^-$, stability constants are only available up to Na concentrations of 0.5 m ($NaClO_4$) and since at this ionic strength stability constants are within the error range of the standard state values[42], the latter were used in the calculations.

Data for the ionic strength dependency of the hydrolysis reactions in the Na/U(IV)/Cl-system are not known but may be estimated by analogy to the Na/Th/Cl system reported by Felmy et al.[43]. These authors describe the solubility of $Th(OH)_4(am)$ in 0-3m NaCl solutions quite well with only two solution species: Th^{4+} and $Th(OH)_4(aq)$. Using this model and a β^o_{14} value of -9.0 for $U(OH)_4(aq)$[44] hydrolysis of U(IV) in NaCl solutions may be estimated.

The results of the present calculations of the U(IV)/U(VI)/NaCl/H^+ system are given in terms of an E_h/pH diagram in Figure IV.2. Experimentally determined Eh and pH values of our tests in the absence of iron are included. From Figure IV.2 it can be seen that U(VI) hydrolysis starts at pH values higher than 5, and even at U(tot) concentration in solution as low as 10^{-5} m essentially polynuclear complexes are formed well up to alkaline pH values. Reduction of U(VI) to U(IV) is expected to start at negative E values. For the Eh/pH data of our experiments the results of Figure IV.2 indicate that the dominant solution species in the absence of iron will likely be polynuclear U(VI) hydrolysis species. The measured Eh values are outside of the stability field of UO_2, consequently oxidation of the UO_2 matrix (to U_4O_9, U_3O_7...) is expected. This is confirmed by our ESCA measurements on surfaces of pure UO_2 as reported in Chapter III.

---

[41] H.S. Dunsmore, L.G. Sillen, Acta Chem Scand. **17** 2657-2663 (1963)

[42] „The Chemical Thermodynamics of Uranium", OECD/NEA (1992), I. Grenthe et al. eds. North Holland Publ., Amsterdam.

[43] A.R.Felmy, D. Rai, Radiochimica Acta **48**, 29-35 (1989)

[44] T. Yajima, Y. Kawamura and S. Ueta, „Uranium(IV) solubility and hydrolysis constants under reducing conditions"; Mat. Res. Soc. Symp. Proc. **353**, 1137-1142 (1995)

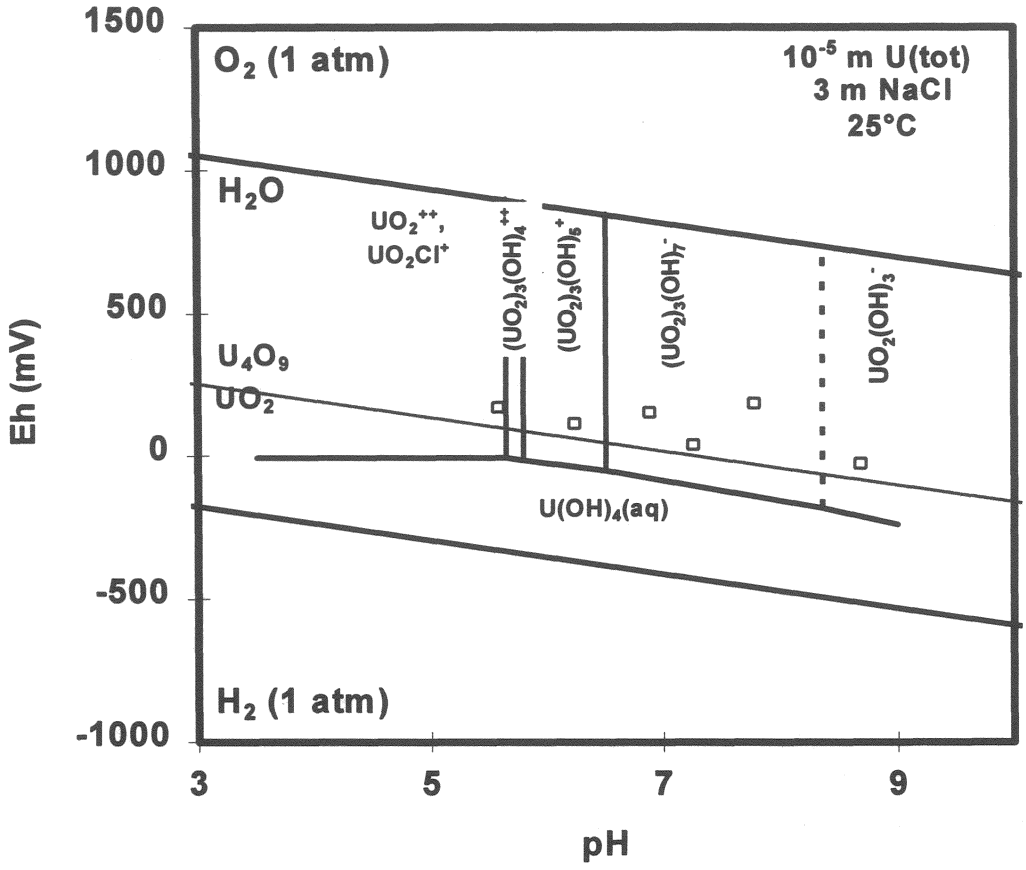

Figure IV.2: Stability fields of various solution species of uranium and stability boundary of UO_2/U_4O_9 at 25°C in 3 m NaCl solutions and experimentally measured Eh and pH values in spent fuel dissolution tests

IV.3.1.2 Solubility controls by secondary U(VI) solid phases

In all spent fuel dissolution experiments, except those using mm sized fuel fragments, U(VI) solution concentrations reach very fast constant values (Figures II.14-II.16). Figure IV.3 gives a plot of the apparent equilibrium values as a function of pH. In our experiments with spent fuel powder in 5 m NaCl solution the U(VI) concentrations were at least a factor of 10 higher than in experiments with fuel pellets at the same pH value. This appears to be a quite common phenomena. The solution concentrations of U(VI) in equilibrium with dissolving UO_2

[45] or spent fuel[46] may vary quite substantially during a long lasting experiment often by as much as a factor of 100 in a similar chemical environment.

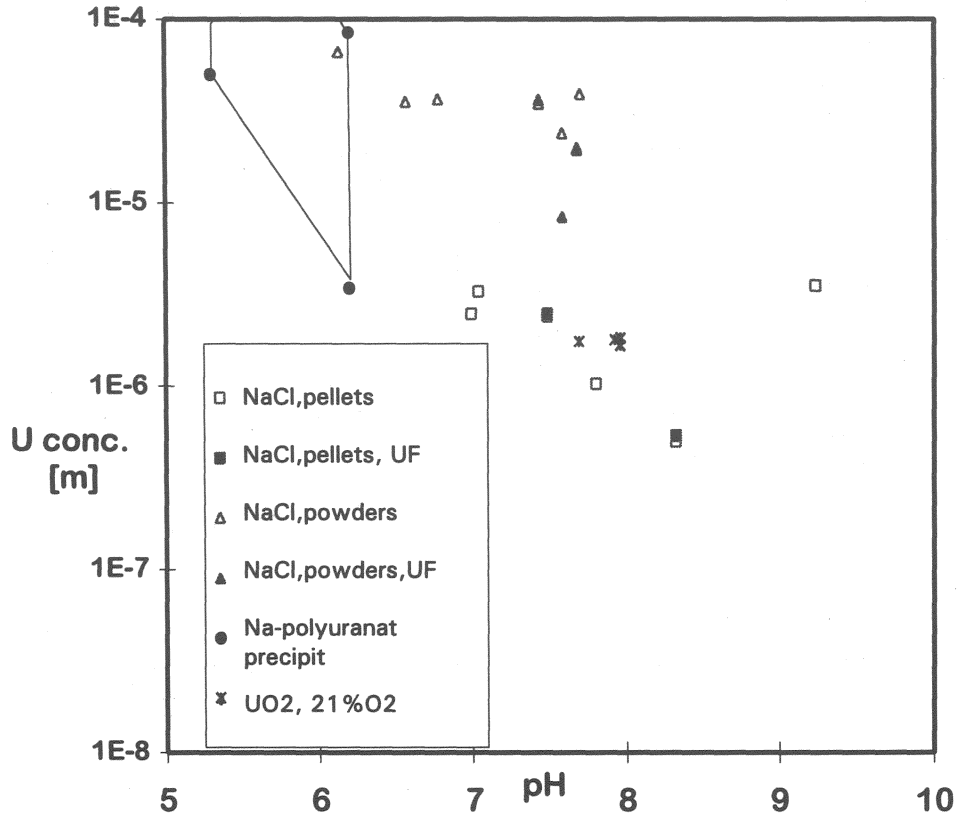

Fig. IV.3: Uranium concentrations obtained in spent fuel dissolution tests in 95% saturated NaCl solutions at 25°C under argon atmosphere in the absence of Fe. Oxidizing reactants are produced by radiolysis Comparison with apparent equilibrium concentrations of uranium in UO_2 dissolution tests in 5 m NaCl solutions (Chapter III), in 21 % O2 atmosphere and comparison with results from precipitation of Na-polyuranates from supersaturation test [Data from[47] : Uranium concentrations after ultra filtration (1.8 nm). Titration of 5 m NaCl solutions with a UO_2Cl_2 at constant pH. Differences in the data sets result from differences in crystallinity].

The experimental data from fuel dissolution tests (Chapter II) are compared with apparent equilibrium concentrations of uranium in UO_2 dissolution tests (pellets) in 5 m NaCl solutions (Chapter III), in 21 % O_2 atmosphere. In an atmosphere with 21% oxygen, only U(VI) species and U(VI) solid phases are stable whereas, lower redox states are instable (see Figure IV.2). Very good agreement is obtained, indicating that even under anoxic conditions (spent fuel dissolution experiments under argon atmosphere) radiolysis produces sufficient oxygen (see chapter II, Table II.3) to provide oxic conditions with respect to redox states of uranium in solution and in solid phases. The close agreement between the solution

[45] K. Ollilla, Nuclear Waste Commission of Finish Power Companies, Report YJT 86-28 (1986)
[46] B. Grambow, SKB Technical Report 89/13 (1989)
[47] Diaz and Grambow, ENRESA Publicacion Tecnica Num. 06/93 (1993)

concentration of uranium encountered in spent fuel dissolution test with respective data from UO_2 dissolution tests may indicate that the same solid phase controls solution concentrations. Figure IV.3. compares also the measured solution concentrations of U as a function of pH with concentrations of U obtained from oversaturated conditions when titrating 5 m NaCl solutions with pure uranyl chloride solutions at various fixed pH values. The oversaturation experiments where performed for a period of three month[48]. The solution concentrations obtained from oversaturated conditions are rather similar to respective values obtained from spent fuel dissolution tests using fuel powder, possibly indicating that similar solid phases (Na-polyuranates, see below) were formed.

Various attempts to identify the solubility controlling phase under oxic or anoxic conditions seemed to indicate that solution concentration show some agreement with the solubility limit of schoepite[51,46,49]. Indeed, in long-term experiments with spent CANDU fuel UO_3*2H_2O (schoepite) was identified by XRD [Stroes-Gascoyne et al. 1986] as alteration product. Schoepite or other uranyl oxide hydrate phases are also an initial alteration product of natural uraninite deposits under oxic conditions[50]. Studies on schoepite solubility show variability in apparent equilibrium concentrations by as much as a factor of 1000 associated mainly to crystallinity and/or particle size[51]. Hence the variability in uranium concentration (Figure IV.3) is not at all surprising. The higher apparent equilibrium concentration of U(VI) in experiments with fuel powder is probably associated with faster approach of supersaturated conditions, resulting in faster precipitation rates with smaller particle sizes and higher solubility. However, schoepite is not the only potential alteration product and a large variety of phases may be formed, depending on the composition of the groundwater. In LWR fuel dissolution test with limited quantities of Tuff water as in the natural alteration of uraninite under oxidizing conditions, not only various uranyl oxide hydrate phases were observed but also silicates etc.[52,50]. Recently, for 5 NaCl solution it has been shown that the stable solid phase is not schoepite but Na-polyuranates[53] and it may very well be expected that this phase is also formed during spent fuel tests and controls the uranium solution concentration in the powder test.

---

[48] P. Diaz Arocas, B. Grambow; „Comportamiento del Combustible Gastado en un Geologico Salino. Quimica del Uranio en Salmueras", CIEMAT, ITN/TR-20/PC-92 (1992)
[49] J. Bruno, R. Forsyth, L.Werme, Mat. Res. Soc. Symp. Proc. **44**, 413-420 (1984)
[50] E. Pearcy, J. Prikryl, W.Murphy and B.Leslie, Appl. Geochemistry, **9**, pp. 713-732 (1994)
[51] M.Torrero, I. Casas, J.Pablo, M.C.A.Sandino, B. Grambow, Radiochmimica Acta **66/67**, 29-35 (1994)
[52] D. Wronkiewics, J. Bates, T. Gerding, E. Veleckis and B. Tani, J. Nucl. Mat. **190**, 107-127 (1992)
[53] P. Diaz and B. Grambow, submitted to Geochimica acta (1995)

IV.3.1.3 Uranium solubility under reducing conditions

The behavior of uranium in spent fuel dissolution tests under reducing conditions may be analyzed using the uranium concentrations in solution (0.45 µm filtered and ultrafiltered „UF") from the test with iron powder being present. The results are given in Figure IV.4. Comparison is made with respective data (see chapter III) from UO_2 dissolution tests (two different particle sizes) in 5 m NaCl solution under an H_2 atmosphere in presence of Pd as a catalyst.

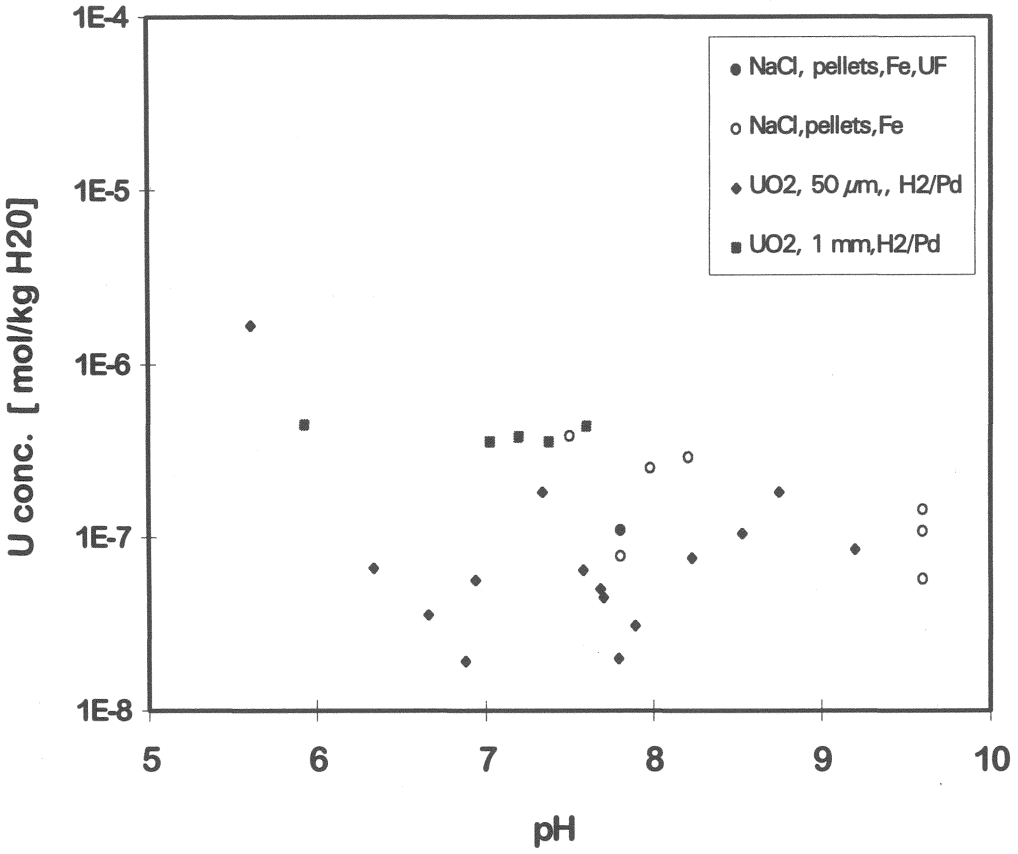

Fig. IV.4: Uranium concentrations in presence of Fe-powder, obtained in spent fuel dissolution tests in 95% saturated NaCl solutions at 25°C under argon atmosphere Reducing conditions obtained by consumption of oxidizing reactants by reaction with Fe.

Fig. IV.4. shows that there is good agreement between the measured solution concentrations of uranium from the spent fuel and UO_2 dissolution tests at two different particle sizes. This good agreement suggests that reducing conditions are indeed achieved in the spent fuel experiments, hence, radiogenic oxidizing reactants are effectively removed from solution by reaction with the iron powder. This is also confirmed by the absence of radiolytic oxygen in spent fuel tests with iron present, observed when analyzing radiolytic gas production (chapter

II). The absence of any clear pH dependency in the solution concentrations of U(tot) between pH 6 and 10 could indicate that uranium concentrations are controlled by UO_2 of $U(OH)_4(s)$ as solid phases in equilibrium with $U(OH)_4(aq)$ as dominant solution complex (see also Figure IV.2, Eh-values in presence of Fe should be similar to the lower stability field boundary of H_2O, hence, $U(OH)_4(aq)$ should be dominant). The scatter in the U-data is too high to allow unambiguous conclusions.

IV.3.2 Solution controls for trivalent actinide and rare earth elements

In general trivalent actinides (Am, Cm) and rare earth elements (Eu, Ce) exhibit similar mobilization behavior upon spent fuel dissolution. It has been shown[54] that below pH 6 the fraction of inventory of Am in the aqueous phase ($FIAP_{Am}$) is similar to the altered fuel mass ($FIAP_{matrix}$) calculated from the solution data of either Sr or Cs. This indicates that below pH 6 Am release is controlled by the alteration rate of the fuel matrix. At higher pH values the ratio $FIAP_{Am}/FIAP_{matrix}$ approached 0.01 to 0.001 indicating retention of Am during spent fuel dissolution. Measured solution concentrations of Am from tests with fuel powders and pellets with and without Fe being present are shown in Figure IV.5 both for filtered and ultrafiltered solution samples.

The results show large scatter, by more than 3 orders of magnitude at a given pH. A possible reason for this scatter is the precipitation kinetics. In Figure IV.6 the dependence of solution concentrations on time is shown, both for 0.45 μm filtered and 18Å ultrafiltered solution samples. The following observations can be made: (1) concentrations of Am generally decrease with time, pointing to the importance of precipitation kinetics. (2) a large fraction of Am is always in the colloidal state, (3) the total concentrations of colloidal Am decreases with time, hence, for the present experimental situation, colloid generation is not a long-term process, (4) Am concentrations of experiments with fuel powders and with pellets become very similar with time, (5) in the presence of Fe, colloidal bound Am concentrations are extremely low and non-colloidal true Am-concentrations are lower than the detection limit. The concentrations approach the ingestion limits for workers (ICRP61, considering 800 L of drinking water per year) thus indicating that an iron based waste package for spent fuel is a very effective barrier against radionuclide release, (6) in all experiments, measured

[54] Loida, A. B. Grambow, H. Geckeis, P. Dressler, Mat. Res Soc. Symp. Proc. **353**, 577-585 (1995)

concentrations of Am solution were orders of magnitude below concentration values which one would expect if Am release would be controlled by the congruent dissolution of the fuel matrix. This indicating that Am is effectively removed from solution. In Figure IV.7 only the long-term concentrations of Am are considered obtained from solution sampling after one year. A much more clear trend in the data can be seen.

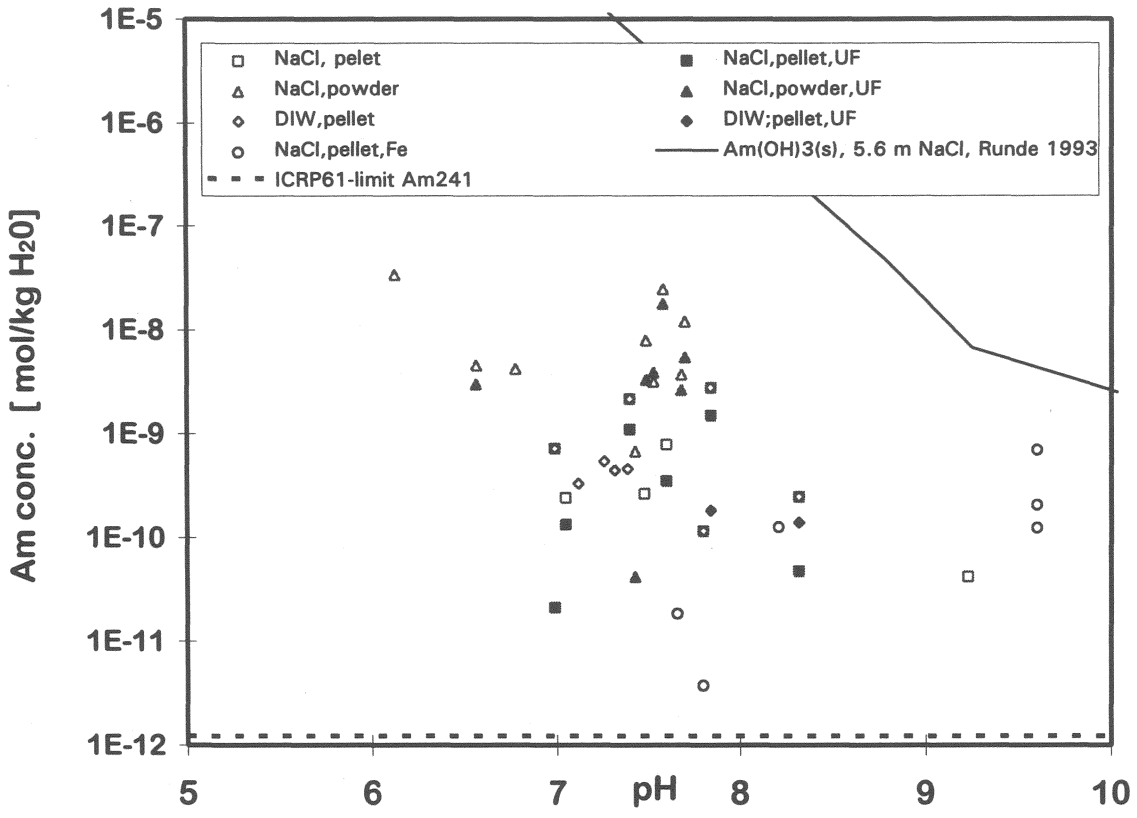

Figure IV.5: Solution concentrations of Am from tests with spent fuel powders and pellets with and without iron being present in 95% saturated NaCl-solution (micro- and ultrafiltrated). Comparison with limit of ingestion for workers (ICRP61) and with the solubility of pure $Am(OH)_3$ in NaCl solutions of similar ionic strengt[h24].

One of the processes which may retain Am is precipitation of secondary phases. The solubility of precipitated Am in carbonate free anaerobic 5 M (5.6 molal) NaCl solutions has been measured by Runde[55]. The solubility controlling phase was assumed to be amorphous $Am(OH)_3(s)$. Adapting a model (based on the electrolyte theory of Pitzer and spectroscopic observations) for the ionic strength dependence of Cm hydrolysis to Am hydrolysis, Fanghänel et al.[56] calculated the solubility of $Am(OH)_3$ in 5.8 m NaCl solutions and obtained good agreement with the data of Runde when using a solubility product at infinite dilution of

[55] Runde, W.; "Zum chemischen Verhalten von drei- und fünfwertigem Americium in salinen NaCl-Lösungen" Dissertation, Technische Universität München, (1993)
[56] Fanghänel, T, J.I. Kim, P. Paviet, R. Klenze, W. Hauser; Radiochimica Acta **66/67** 81-87 (1994)

log K = -28.2. The solubility data of Runde[55] are included in Figures IV.5 and IV.7. Measured concentrations of Am/Eu in spent fuel corrosion solutions are about 5 orders of magnitude lower (Figs. IV.5 and IV.7). One of the reasons for this discrepancy is the possible formation of solid solutions by coprecipitation. The content of other trivalent cations in spent fuel (Nd,

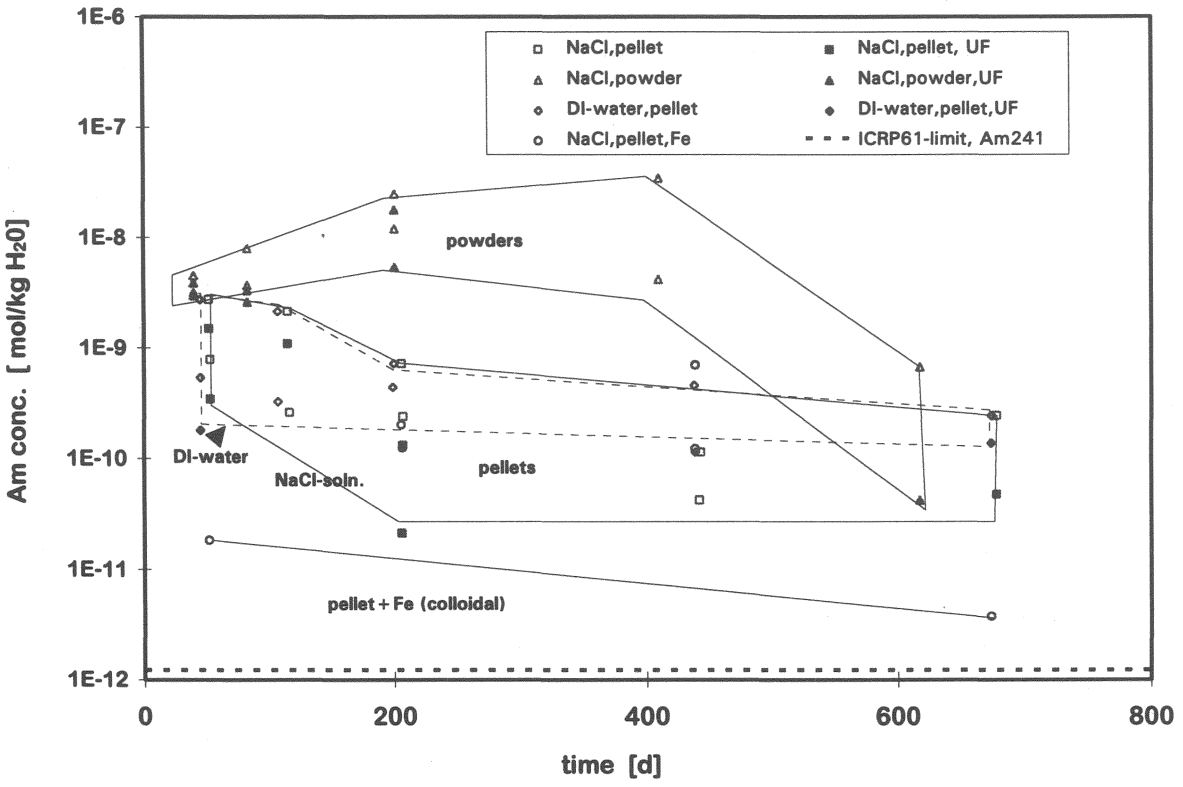

Fig. IV. 6: Time dependency of solution concentrations of Am from tests with spent fuel powders and pellets with and without iron being present in 95% saturated NaCl-solution and in deionized water „DI-water" (0.45 µm micro- and 18 A ultrafiltrated „UF"). If micro- and ultrafiltered solution concentrations deviate substantially, microfiltered solution are considered to represent colloidal Am. The limit for ingestion of workers (ICRP61) is included for estimating radiological impact, considering 800 L water consumption per year.

La, Pr, Sm..) is about 25 times higher than that of Am or Eu. It is rather unlikely that individual $Am(OH)_3$ phases will form. Instead, one expects the formation of solid solutions for example of the general type $(REE;AN)(OH)_3$. Using the most simple solid solution model[57], neglecting mixing entropy and assuming end member activity equal to its mol fraction, the partial solubility product $K_{p,SS}$ of an end member in a solid solution is $K_{p,SS} = x_i K_i$ where x_i and K_i are the mol fraction of the end member and its individual solubility product in the absence of solid solution formation. If a large fraction of the inventory of trivalent actinides and rare earth elements in the altered fuel mass is contained in secondary

[57] Lippmann,F., N.Jahrb.Mineral. Abh., Vol 130, pp.243-263 (1977)

coprecipitates and only a small fraction stays in solution, than Am and REE the mol fraction of these elements in the solid precipitate are governed by their inventory ratio. Consequently, for $K_{p,SS,\ Am(OH)3}$ the value would be about 25 times smaller than $K_{Am(OH)3}$. and a similar decrease in the corresponding equilibrium solution concentrations of Am is expected. This alone cannot explain the difference of five orders of magnitude between solubility of precipitated pure $Am(OH)_3$ and Am "solubility" in spent fuel tests.

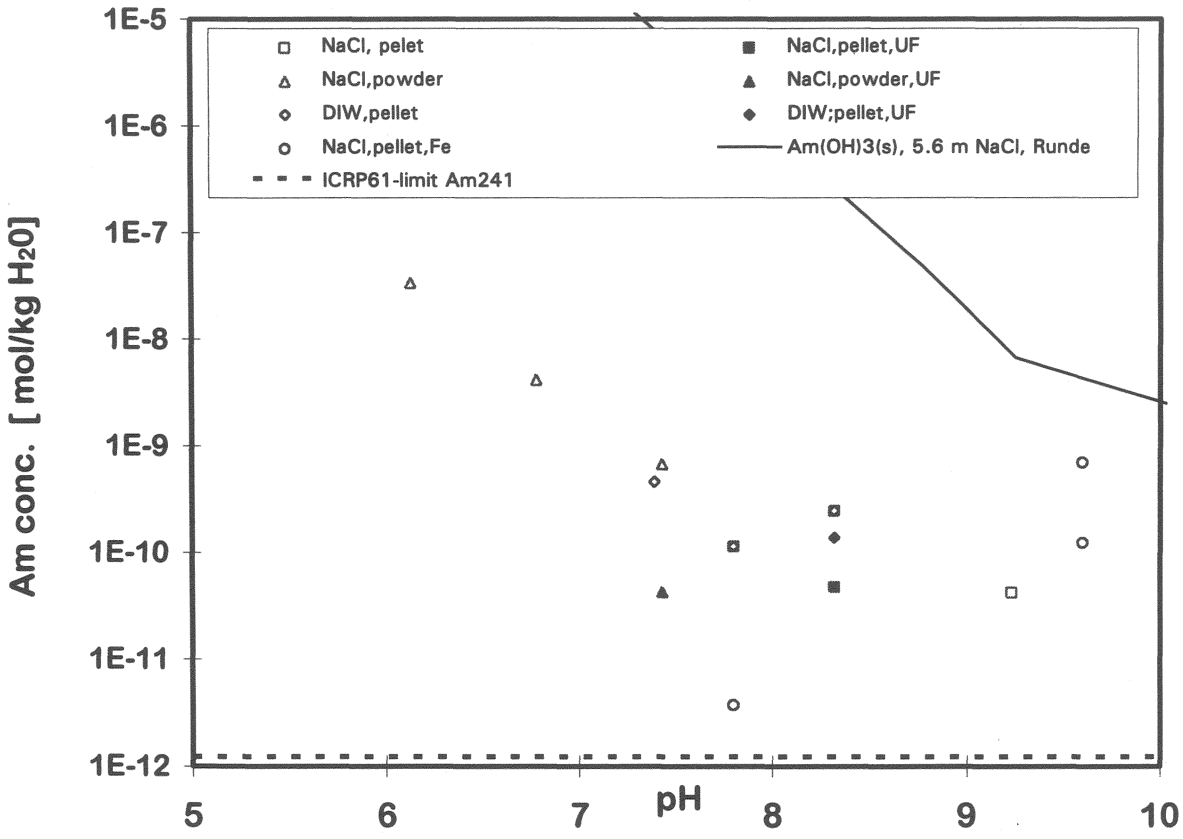

Figure IV.7: Am concentrations in spent fuel dissolution tests in 95% saturated NaCl solutions and in deionized water for contact periods of spent fuel and leachants larger than 400 days. Comparison with ICRP61 limit and with the solubility of pure $Am(OH)_3$ (see Figure IV.5)

Alternatively, Am may coprecipitate with secondary U(VI) phases such as schoepite or polyuranates. In this case, inventory controlled x_i values would be about $6 \cdot 10^{-4}$ (Table I.4) and equilibrium solution concentrations would be about 1500 times lower than pure phase solubility, thus better approaching actually measured data. Coprecipitation of Am with U(VI) secondary phases should be studied to unravel the behavior of trivalent rare earth and actinide

elements to allow prediction of solubility/coprecipitation controlled Am concentrations during spent fuel dissolution.

IV. 3.3 Solution controls for plutonium

The fraction of inventory of Pu dissolved into the aqueous phase (FIAP) has been found in all cases to be lower than that of Sr and in most cases also much lower than that of U. This indicates solution control by the solubility of a precipitating phase, coprecipitation or sorption processes similarly, as suggested by Forsyth et al.[58] for granite groundwater.

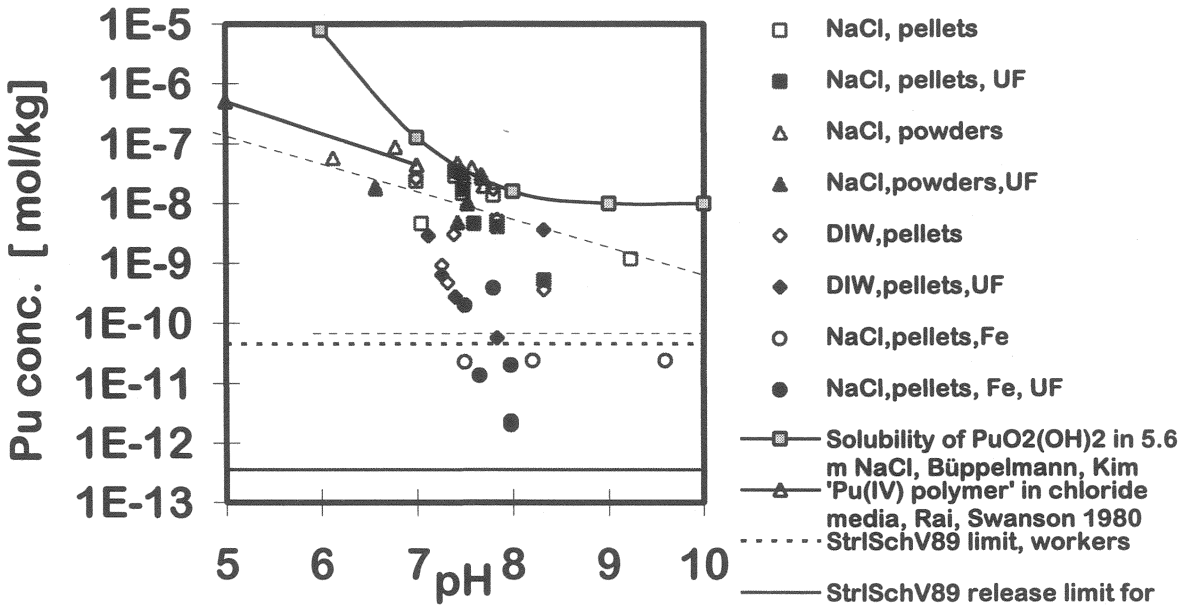

Fig. IV.8: Pu concentrations observed in spent fuel dissolution tests in NaCl solutions and in deionized water „DIW", as a function of pH. 0.45 µm micro and 18A ultrafiltered solutions „UF" are included. Comparison to theoretical solubility of $PuO_2(OH)_2$[63] to the solubility of Pu(IV) polymer in chloride media[64] and to the limits of ingestion given by the German radiation protection rules StrSchV89 (see discussion in text)

For pH values below 4 it has been shown that Pu is released congruently with the dissolving fuel matrix[59]. At higher pH values significant fractions of Pu are retained in secondary solid phases. All measured solution concentrations from our tests remain at least a factor 100 lower than values which one would expect if Pu-release from the fuel would be

[58] Forsyth, R.S., L.O. Werme and J. Bruno, "The Corrosion of Spent Fuel in Synthetic Groundwater", J. Nucl. Mater. 138, 1986, pp. 1-15

[59] A. Loida, B. Grambow, P. Dressler, K. Friese, H. Geckeis, „Chemical Durability of High Burnup LWR-Spent Fuel in Concentrated Salt Solutions", Mat. Res. Soc. Symp. Proc., **333**, 417-424 (1994)

controlled by the dissolution rate of the fuel matrix. Pu concentrations encountered in the various spent fuel dissolution tests are shown as a function of pH in Fig. IV.8 for experiments with fuel powders and pellets with and without iron being present. Included in Fig. IV.8 are curves calculated for solubility controls with respect to either $PuO_2(OH)_2$ or Pu(IV)-polymer as discussed further below. Solubility calculations are complicated by the various possible oxidation states of dissolved Pu which may coexist simultaneously and by the possibility that either Pu(IV) or Pu(VI) solid phases may form. Furthermore, the surface's electrochemical potential may differ substantially from the overall redox potential in solution, which means that a potential gradient will be established and solubility calculations using bulk solution Eh data may be of no use for inferring the saturation state with respect to the dissolving solid.

The valence state of dissolved Pu has not yet been measured. It is rather difficult to predict the redox state of Pu under conditions of redox disequilibrium, governed by the competing effects of radiolysis with coexisting quantities of dissolved hydrogen and oxygen and other redox controlling species and surface redox potential formation. In order to estimate the relative importance of various redox states for our experiment, overall equilibrium was assumed. The stability field data for various Pu species (stability constants of hydrolysis species, E_o values) given by Capdevilla et al.[60] were adapted for 5 m NaCl solutions, with activity coefficient corrections being made on the basis of the electrolyte theory of Pitzer. The necessary binary and ternary interaction coefficients for calculating activity coefficients for the various Pu species in NaCl solutions are not measured but are considered in first approximation identical to the respective coefficients of other actinides of the same valence states. Interaction coefficients for trivalent Pu are taken from the Cm(III)/Cl system[56], for tetravalent Pu interaction coefficients were taken from the Th/Cl system [Felmy et al.[43]], respective coefficients for pentavalent Pu were taken from the Np(V)/Cl system [61] and the coefficients for the plutonyl ion are taken from the UO_2^{2+}/Cl system[37]. The calculated Eh/pH diagram is given in Figure IV.9 together with the measured Eh/pH values from our experiments.

The data in Figure IV.9 suggest for the conditions of our tests that Pu^{3+} or $Pu(OH)_4(aq)$ should be the dominant solution species. However, these calculations are only estimations,

[60] Capdevilla,H., Vitorge,P.,Giffaut,E., Radiochimica Acta 58/59, pp 45-52 (1992)
[61] Neck, V.; Th. Fanghänel and J.I. Kim, Report FZKA 5599, Forschungszentrum Karlsruhe (1995)

and, in particular for $Pu(OH)_4(aq)$ the thermodynamic data are rather uncertain. Moreover, radiation and redox disequilibrium etc. may lead to the formation and persistence of metastable species.

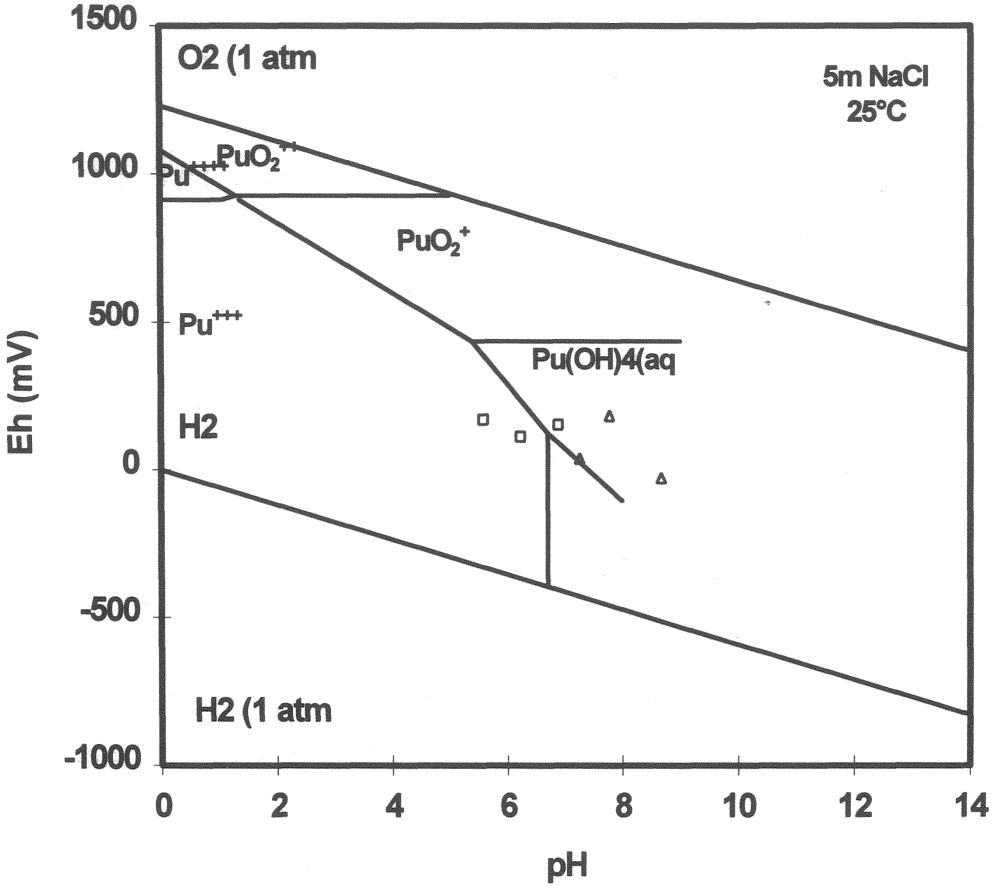

Fig. IV.9:.Estimation of predominances of various Pu-species and valence states as a function of pH and Eh in the absence of carbonate at 25C in 5 m NaCl solution. Included are experimentally measured Eh/pH data for □ spent fuel powders and Δ for pellets, both in the absence of iron (for details see text)

In saline solutions at sufficiently high radiation doses, Pu(VI) is stabilized and lower oxidation states are oxidized by radiolysis[62]. Pu(VI) solubility in carbonate free 5M NaCl solutions has been measured by Büppelmann and Kim[63] and by Pashalidis and Kim[62] at specific alpha activities between 148 and 1665 GBq/L and radiolytically induced Eh values >1000 mV. The solubility limiting phase in the experiments of Pasalidis and Kim[62] was $PuO_2(OH)_2$. Reported experimental Pu concentrations were much higher than calculated solution concentrations based only on hydrolysis and chloride complexation. This increase

[62] Pashalidis, I., and J.I.Kim, ; Institut für Radiochemie der Technischen Universität München, RCM 01092 (1992)

[63] Büppelmann, K. und J.I.Kim; Institut für Radiochemie der Technischen Universität München, RCM 01088 (1988)

was attributed to the formation of Pu(VI) hypochlorite complexes caused by α-radiolysis. For the pH range 6-10 relevant for interpreting our experimental results, the measurements by Pashalidis and Kim[62] and by Büppelmann and Kim[63] yield Pu concentrations which are always > $10^{-6.3}$ m, i.e. much higher than the solution concentrations of Pu encountered in our experiments. This difference may either be attributed to the lower α-radiation doses and associated lower Eh values (in our test the specific α-activity was always <10 GBq/L, Eh values were <0 mV), or Pu concentrations in our tests are not controlled by its individual solubility but by sorption, resorption or by coprecipitation. Measurements of Pu(VI) solubility at low α-doses are nor reported for 5 M NaCl solutions, we use for comparison to our data (included in Fig.. IV.8) the theoretical $PuO_2(OH)_2$ solubility curve calculated by Pashalidis and Kim[62] by only considering hydrolysis and chloride complexation and neglecting radiolysis. It can be seen that measured solution concentrations remain lower than this solubility curve. At the low redox potentials of our tests the solubility controlling phase may alternatively be a Pu(IV) (hydr)oxide. Included in Fig.IV.8 are reported solubility data of Pu(IV) polymer in air saturated chloride media (solubility between PuO_2(cr) and $Pu(OH)_4$(am)) reported by Rai and Swanson[64] with PuO_2^+ as the dominant solution specie. There is a certain tendency for agreement with the release data of spent fuel. However, such solubility equilibrium would be in conflict with the Eh/pH data of our experiments in Fig. IV.9, as $Pu(OH)_4$(aq) should be dominant. As said before, the stability range of this specie is rather uncertain. Also, Pu species may be oxidized radiolytically to PuO_2^+.

Under reducing conditions, i.e. when radiolytically generated oxidizing reactants were consumed by the corroding iron powder, solution concentrations of Pu appear to be much lower, than in the absence of Fe (Figure IV.8). Under these conditions the dominant solution species is either $Pu(OH)_4$(aq) or a trivalent Pu specie. The lack of a pronounced pH dependency may suggest that Pu solubility is controlled by the Pu(IV) polymorph in equilibrium with $Pu(OH)_4$(aq). However, more work is necessary, before solution controls of Pu can be identified unambiguously.

[64] Rai,D., Swanson, J.L., Nucl.Technology, Vol.54, pp 107 - 112 (1981)

ACKNOWLEDGMENT

The authors are very thankful for the hot cell work by **Mr. B. Schweigel** and **Mr. R. Reger** from the Department of Hot Cells (FZK) and of laboratory work by **Mr.N.Müller**, **Mr.W. Müller** and **Mr. R.Gebauer**. Help in analytical work was gratefully obtained by **Mrs. A. Görtzen**, **Mr. K. Friese**, **Mr. F.Geyer** from INE (FZK). For performing of SEM investigations the help of **Mr. R. Pejsa** (Hot Cells/FZK), **Mr. J.Römer** and **Mr. K.Spieler** is gratefully acknowledged.

APPENDIX

Summary of data from spent fuel corrosion tests

Pellets, DI water, 25°C

Pellets + 8,5 g Fe-powder, 95%saturated NaCl-solution, 25°C

Pellets, 95%saturated NaCl-solution, 25°C

Fragments, 95%saturated NaCl-solution, 25°C

Powders, 95%saturated NaCl-solution, 25°C

Pellet, 95%saturated NaCl-solution, 150°C

Table A 1: Activity of leach solutions from spent fuel corrosion tests (Bq/ml)									
Sample:	K 1 (Pellet): 7,335 g (=6,466 g HM)		Solution: DI-water			Starting volume: 200 ml			
	7,319 g at test termination		Temperature: 25 °C			Final volume: 164 ml			
	Washcycles		**Static tests**						**Acid cleaning**
Nuclide	1.Cycl (31d)	2.Cycl (45 d)	1. Sampling	2. Sampling	3. Sampling	4. Sampling	5. Sampling		of the
			121 d (cumul.)	183 d (cumul.)	276 d (cumul.)	514 d (cumul.)	750 d (cumul.)		container
	0,45 µm -filtered		0,45 µm -filtered					1,8 nm-filtered	
RU106	2,26E+02	1,80E+02	1,04E+02	9,60E+01	3,45E+01		<1,86E+1	<1,92E+1	9,85E+02
CS134	2,54E+06	3,34E+05	2,85E+05	6,01E+05	6,91E+05	8,70E+05	7,50E+05	7,32E+05	9,21E+01
CS137	3,38E+06	4,88E+05	5,60E+05	1,06E+06	1,30E+06	1,75E+06	2,04E+06	1,98E+06	2,53E+02
EU154	4,26E+01	2,53E+02	1,17E+02	1,00E+02	9,09E+01	8,36E+01	2,68E+01	8,46E+01	5,48E+02
EU155	4,55E+01	1,36E+02	6,95E+01	5,24E+01	3,91E+01	4,51E+01	<3,54E+0	4,27E+01	2,31E+02
SB125	2,89E+02		4,34E+01	<4,37E-01	2,07E+02	7,21E+01	8,50E+02	8,78E+02	1,48E+02
SR90	4,18E+05	3,25E+04	6,95E+03	1,41E+04	4,17E+04	9,87E+04	7,32E+04	6,92E+04	4,97E+03
CE144	3,63E+02	1,52E+03	5,21E+02	5,11E+02	4,93E+02	8,13E+01	<9,19E+0	3,38E+01	5,15E+02
TC99	<1,48E+00	1,48E+00					7,36E+00	6,93E+00	
AG110M			<8,69E-01	<4,37E-01	<1,21E+01	<4,20E-01	<4,47E+0	<4,61E+0	
AM241	7,96E+01	2,17E+01	8,69E+00	1,05E+01	8,48E+00	7,23E+00	1,04E+00	5,45E+00	1,72E+02
AM243		1,85E+00	1,52E+00	<1,18E+00	<1,21E+00				
NP237		3,70E-02					<2,05E-2	<1,54E-1	
NP239		1,85E+00							
CM244	2,22E+01	2,28E+02	1,78E+02	8,73E+01	8,97E+01	3,92E+01	5,66E+00	2,94E+01	4,40E+02
CM242		6,83E+00	1,52E+00	1,18E+00	1,21E+00	1,54E-01	<7,44E-2	7,68E-02	1,68E+00
PU238	4,07E+01	4,00E+00	1,26E+00	1,66E+00	9,45E-01	2,28E+01	1,81E+01	2,49E+01	3,20E+02
PU239/40	2,89E+01	7,77E-01	2,17E-01	5,68E-01	3,76E-01	3,27E+00	2,29E+00	3,47E+00	4,60E+01
PU241	1,20E+03	1,52E+02				3,79E+02	4,36E+02	4,48E+02	
U	*5,1E-01 µg/ml*	*1,0E+00 µg/ml*			*2,4E-01 µg/ml*	*2,1E-02 µg/ml*	*2,4E-02 µg/ml*	*6,7E-02 µg/ml*	
pH	6,42	4,86	7,69	8,08	7,82	7,37	6,73	6,73	
Eh	264 mV	320 mV	173 mV	195 mV	180 mV	97 mV	195 mV	195 mV	

Table A 2:Release of radionuclides in leach solutions from spent fuel corrosion tests (FIAP: Fraction of inventory in the aequeous phase)									
									*FIC= Fraction
Sample:	K 1 (Pellet):	7,335 g (=6,466 g HM)	Solution: DI-water		Starting volume: 200 ml				of Inventory
		7,319 g at test termination	Temperature: 25 °C		Final volume: 164 ml				on Container
									Wall
	Washcycles		**Static tests**						**Acid cleaning**
Nuclide	1.Cycl (31d)	2.Cycl (45 d)	1. Sampling	2. Sampling	3. Sampling	4. Sampling	5. Sampling		of the container
			121 d (cumul.)	183 d (cumul.)	276 d (cumul.)	514 d (cumul.)	750 d (cumul.)		(FIC*)
	0,45 µm -filtered		0,45 µm -filtered					1,8 nm-filtered	
RU106	2,55E-06	2,51E-06	1,97E-06	1,72E-06	5,81E-07		<6,82E-7	<7,04E-7	4,32E-05
CS134	2,03E-02	2,96E-03	2,94E-03	5,84E-03	6,33E-03	8,61E-03	9,64E-03	9,41E-03	1,50E-06
CS137	1,71E-02	2,50E-03	2,89E-03	5,17E-03	5,96E-03	7,62E-03	8,89E-03	8,62E-03	1,47E-06
EU154	3,46E-06	2,11E-05	1,01E-05	8,18E-06	6,98E-06	6,22E-06	2,09E-06	6,60E-06	5,66E-05
EU155	7,18E-06	2,24E-05	1,22E-05	8,67E-06	6,10E-06	6,99E-06	<6,05E-7	7,30E-06	5,18E-05
SB125	6,06E-05		1,10E-05	<1,04E-07	4,67E-05	1,69E-05	2,41E-04	2,49E-04	5,41E-05
SR90	3,11E-03	2,43E-04	5,26E-05	1,01E-04	2,81E-04	6,30E-04	4,69E-04	4,43E-04	4,25E-05
CE144	4,63E-06	2,55E-05	1,29E-05	1,20E-05	1,09E-05	2,45E-06	<5,69E-7	2,09E-06	3,69E-05
TC99	<6,68E-05	6,68E-05					2,72E-04	2,56E-04	
AG110M			<2,37E-05	<1,12E-05	<2,94E-04	<1,46E-05	<3,55E-4	<3,66E-4	
AM241	4,36E-05	1,11E-05	4,09E-06	4,66E-06	3,55E-06	2,64E-06	3,28E-07	1,72E-06	7,45E-05
AM243		2,27E-05	1,86E-05	<1,36E-05	<1,32E-05				
NP237		6,30E-05					<2,86E-5	<2,15E-4	
NP239		2,27E-05							
CM244	1,55E-06	1,61E-05	1,28E-05	5,92E-06	5,72E-06	2,38E-06	3,49E-07	1,81E-06	3,62E-05
CM242		1,19E-05	5,22E-06	3,82E-06	3,70E-06	8,47E-07	<1,47E-6	1,51E-06	3,42E-05
PU238	3,79E-06	3,73E-07	1,18E-07	1,47E-07	7,89E-08	1,79E-06	1,41E-06	1,93E-06	3,33E-05
PU239/40	1,72E-05	4,63E-07	1,29E-07	3,19E-07	1,99E-07	1,63E-06	1,12E-06	1,69E-06	3,01E-05
PU241	4,65E-06	5,99E-07				1,30E-06	1,53E-06	1,57E-06	
U	1,69E-5	3,31E-05			7,06E-06	5,85E-07	6,51E-07	1,82E-06	2,47E-05
pH	6,42	4,86	7,69	8,08	7,82	7,37	6,73	6,73	
Eh	264 mV	320 mV	173 mV	195 mV	180 mV	97 mV	195 mV	195 mV	

Table A 3: Concentration of radionuclides in leach solutions from spent fuel corrosion tests (mol/L)										
Sample:	K 1 (Pellet): 7,335 g (=6,466 g HM)		Solution: DI-water			Starting volume: 200 ml				
		7,319 g at test termination	Temperature: 25 °C			Final volume: 164 ml				
	Washcycles		Static tests						Acid cleaning	
Nuclide	1.Cycl (31d)	2.Cycl (45 d)	1. Sampling	2. Sampling	3. Sampling	4. Sampling	5. Sampling		of the container	
			121 d (cumul.)	183 d (cumul.)	276 d (cumul.)	514 d (cumul.)	750 d (cumul.)			
	0,45 µm -filtered		0,45 µm -filtered					1,8 nm-filtered		
RU106	2,81E-09	2,77E-09	2,17E-09	2,00E-09	7,19E-10		<9,16E-10	<9,45E-10	4,32E-08	
CS134	1,90E-05	2,77E-06	2,75E-06	5,78E-06	6,65E-06	9,65E-06	1,10E-05	1,07E-05	1,28E-09	
CS137	1,60E-05	2,34E-06	2,70E-06	5,12E-06	6,26E-06	8,53E-06	1,01E-05	9,84E-06	1,25E-09	
EU154	1,52E-10	9,23E-10	4,43E-10	3,80E-10	3,44E-10	3,27E-10	1,12E-10	3,53E-10	2,26E-09	
EU155	3,15E-10	9,80E-10	5,33E-10	4,02E-10	3,00E-10	3,67E-10	<3,24E-11	3,90E-10	2,06E-09	
SB125	3,49E-10	4,83E-38	6,33E-11	<6,37E-13	3,02E-10	1,17E-10	1,70E-09	1,75E-09	2,83E-10	
SR90	1,34E-06	1,05E-07	2,28E-08	4,62E-08	1,37E-07	3,26E-07	2,47E-07	2,34E-07	1,67E-08	
CE144	3,75E-09	2,06E-08	1,05E-08	1,03E-08	9,91E-09	2,37E-09	<5,61E-10	2,06E-09	2,71E-08	
TC99	<2,48E-08	2,48E-08					1,23E-07	1,16E-07		
AG110M			<7,89E-10	<3,96E-10	<1,10E-08	<5,83E-10	<1,44E-8	<1,49E-8		
AM241	2,87E-09	7,32E-10	2,69E-10	3,25E-10	2,63E-10	2,08E-10	2,63E-11	1,38E-10	4,46E-09	
AM243		1,49E-09	1,23E-09	<9,51E-10	<9,78E-10					
NP237		6,18E-09					<3,42E-9	<2,57E-8		
NP239		2,22E-09								
CM244	2,19E-11	2,28E-10	1,81E-10	8,88E-11	9,12E-11	4,05E-11	6,04E-12	3,14E-11	4,66E-10	
CM242		1,68E-10	7,40E-11	5,74E-11	5,90E-11	1,44E-11	<2,54E-11	2,62E-11	4,42E-10	
PU238	5,79E-09	5,70E-10	1,80E-10	2,37E-10	1,35E-10	3,27E-09	2,62E-09	3,60E-09	4,62E-08	
PU239/40	2,62E-08	7,07E-10	1,98E-10	5,16E-10	3,42E-10	2,97E-09	2,08E-09	3,16E-09	4,18E-08	
PU241	7,10E-09	9,15E-10				2,38E-09	2,85E-09	2,93E-09		
U	2,1E-06	4,2E-06			1,01E-06	8,91E-08	1,01E-07	2,82E-07	2,86E-06	
pH	6,42	4,86	7,69	8,08	7,82	7,37	6,73	6,73		
Eh	264 mV	320 mV	173 mV	195 mV	180 mV	97 mV	195 mV	195 mV		

Table A 4: Incremental rates of radionuclide release from spent fuel corrosion tests (FIAP/d)									
Sample:	K 1 (Pellet): 7,335 g (=6,466 g HM)		Solution: DI-water			Starting volume: 200 ml			
		7,319 g at test termination	Temperature: 25 °C			Final volume: 164 ml			
	Washcycles		Static tests						Acid cleaning
Nuclide	1.Cycl (31d)	2.Cycl (45 d)	1. Sampling	2. Sampling	3. Sampling	4. Sampling	5. Sampling		of the container
			121 d (cumul.)	183 d (cumul.)	276 d (cumul.)	514 d (cumul.)	750 d (cumul.)		
	0,45 µm -filtered		0,45 µm -filtered					1,8 nm-filtered	
RU106	8,23E-08	5,59E-08	4,38E-08				<2,89E-9		
CS134	6,55E-04	6,58E-05	6,53E-05	4,95E-05	8,88E-06	1,12E-05	5,05E-06		
CS137	5,53E-04	5,55E-05	6,42E-05	3,94E-05	1,17E-05	8,51E-06	5,96E-06		
EU154	1,12E-07	4,68E-07	2,25E-07						
EU155	2,32E-07	4,97E-07	2,70E-07			5,33E-09			
SB125	1,96E-06		2,44E-07		5,01E-07		9,53E-07		
SR90	1,00E-04	5,41E-06	1,17E-06	8,25E-07	2,00E-06	1,54E-06			
CE144	1,49E-07	5,67E-07	2,88E-07						
TC99	<2,15E-06	1,48E-06					1,15E-06		
AG110M			<5,26E-07		<3,05E-06		<1,44E-6		
AM241	1,41E-06	2,47E-07	9,09E-08	1,28E-08					
AM243		5,04E-07	4,14E-07		<3,90E-09				
NP237		1,40E-06					<1,21E-7		
NP239		5,04E-07							
CM244	4,99E-08	3,57E-07	2,84E-07		1,63E-09				
CM242		2,64E-07	1,16E-07		1,09E-09		<2,69E-9		
PU238	1,22E-07	8,30E-09	2,62E-09	5,70E-10		7,21E-09			
PU239/40	5,54E-07	1,03E-08	2,87E-09	3,18E-09		6,05E-09			
PU241	1,50E-07	1,33E-08				5,47E-09	1,07E-09		
U	5,44E-7	7,35E-07			7,60E-08		3,22E-10		
pH	6,42	4,86	7,69	8,08	7,82	7,37	6,73	6,73	
Eh	264 mV	320 mV	173 mV	195 mV	180 mV	97 mV	195 mV	195 mV	

Table A 5: Activity of leach solutions from spent fuel corrosion tests (Bq/ml)								
Sample:	**K 2** (Pellet): 7,109 g (=6,266 g HM)		Solution: DI-water			Starting volume: 200 ml		
		..... g at test termination	Temperature: 25 °C			Final volume:		
	Washcycles		**Static tests**					**Acid cleaning**
Nuclide	1.Cycl (31d)	2.Cycl (45 d)	1. Sampling	2. Sampling	3. Sampling	4. Sampling	5. Sampling	of the liner
			121 d (cumul.)	183 d (cumul.)	275 d (cumul.)	513 d (cumul.)		container
	0,45 µm -filtered		0,45 µm -filtered					
RU106			1,04E+02		4,20E+01			
CS134	2,69E+06	9,64E+05	5,05E+05	7,19E+05	8,26E+05	9,98E+05		
CS137	2,67E+06	1,48E+06	9,05E+05	1,24E+06	1,50E+06	1,95E+06		
EU154	2,07E+01	3,00E+02	1,17E+02	9,99E+01	2,07E+02	3,29E+02		
EU155		1,67E+02	6,50E+01	5,21E+01	9,93E+01	1,68E+02		
SB125	3,15E+02	7,41E+01	3,90E+01	1,30E+00	1,66E+02	3,87E+02		
SR90	1,10E+05	3,41E+04	1,88E+04	3,28E+04	8,46E+04	1,53E+05		
CE144	4,51E+01	1,37E+03	4,77E+02	5,17E+02	7,10E+02	4,46E+02		
TC99	<1,48E+00							
AG110M			5,63E-01	<4,34E-01	1,19E+01			
AM241	1,76E+02	2,59E+01	1,73E+01	1,06E+01	1,42E+01	1,59E+01		
AM243			6,93E-01	1,17E+00	1,19E+00			
NP237		3,71E-02				3,90E-02		
NP239								
CM244	9,25E+00	1,48E+02	1,53E+02	1,35E+02	1,57E+02	1,08E+02		
CM242		4,45E+00	1,52E+00	1,17E+00	1,19E+00	1,16E+00		
PU238	4,88E+01	9,56E+00	6,50E+00	2,00E+01	3,30E+00	2,09E+01		
PU239/40	2,22E+01	1,11E+00	9,97E-01	3,26E+00	6,17E-01	2,88E+00		
PU241	1,41E+03	3,03E+02				2,93E+02		
U	*2,7E-01 µg/ml*				*1,5E-01 µg/ml*	*3,1E-03 µg/ml*		
pH	6,5	7,26	7,26	7,12	7,32	7,39		
Eh	261 mV	183 mV	182 mV	181 mV	161 mV	110 mV		

Table A 6:Release of radionuclides in leach solutions from spent fuel corrosion tests (FIAP: Fraction of inventory in the aequeous phase)								
Sample:	K 2 (Pellet): 7,109 g (=6,266 g HM)		Solution: DI-water			Starting volume: 200 ml		
	..... g at test termination		Temperature: 25 °C			Final volume:		
	Washcycles		Static tests					Acid cleaning
Nuclide	1.Cycl (31d)	2.Cycl (45 d)	1. Sampling	2. Sampling	3. Sampling	4. Sampling	5. Sampling	of the
			121 d (cumul.)	183 d (cumul.)	275 d (cumul.)	513 d (cumul.)		container
	0,45 µm -filtered		0,45 µm -filtered					
RU106			2,03E-06	7,21E-03	7,29E-07			
CS134	2,22E-02	8,83E-03	5,36E-03	6,26E-03	7,80E-03	1,02E-02		
CS137	1,40E-02	7,82E-03	4,82E-03	8,40E-06	7,09E-03	8,76E-03		
EU154	1,74E-06	2,58E-05	1,04E-05	8,89E-06	1,64E-05	2,53E-05		
EU155		2,83E-05	1,17E-05	3,22E-07	1,60E-05	2,69E-05		
SB125	6,82E-05	1,74E-05	1,02E-05	2,42E-04	3,86E-05	9,38E-05		
SR90	8,43E-04	2,64E-04	1,47E-04	1,25E-05	5,88E-04	1,01E-03		
CE144	5,95E-07	2,38E-05	1,22E-05		1,62E-05	1,38E-05		
TC99	<6,89E-05			1,15E-05				
AG110M			1,58E-05	<4,84E-06	2,97E-04			
AM241	9,98E-05	1,37E-05	8,42E-06	1,40E-05	6,16E-06	5,99E-06		
AM243			8,77E-06		1,34E-05			
NP237		6,52E-05				5,73E-05		
NP239				9,41E-06				
CM244	6,65E-07	1,08E-05	1,13E-05	3,92E-06	1,03E-05	6,78E-06		
CM242		7,97E-06	5,37E-06	1,83E-06	3,74E-06	6,58E-06		
PU238	4,70E-06	9,22E-07	6,29E-07	1,89E-06	2,84E-07	1,69E-06		
PU239/40	1,36E-05	6,83E-07	6,12E-07		3,37E-07	1,48E-06		
PU241	5,65E-06	1,23E-06				1,04E-06		
U	9,21E-6			9,21E-6	4,69E-06	8,83E-08		
pH	6,5	7,26	7,26	7,12	7,32	7,39		
Eh	261 mV	183 mV	182 mV	181 mV	161 mV	110 mV		

Table A 7: Concentration of radionuclides in leach solutions from spent fuel corrosion tests (mol/L)								
Sample:	K 2 (Pellet): 7,109 g (=6,266 g HM)		Solution: DI-water			Starting volume: 200 ml		
	..... g at test termination		Temperature: 25 °C			Final volume:		
	Washcycles		Static tests					Acid cleaning
Nuclide	1.Cycl (31d)	2.Cycl (45 d)	1. Sampling	2. Sampling	3. Sampling	4. Sampling	5. Sampling	of the liner
			121 d (cumul.)	183 d (cumul.)	275 d (cumul.)	513 d (cumul.)		container
	0,45 µm -filtered		0,45 µm -filtered					
RU106			2,16E-09		8,75E-10			
CS134	2,01E-05	8,01E-06	4,87E-06	6,92E-06	7,95E-06	1,11E-05		
CS137	1,27E-05	7,09E-06	4,37E-06	6,01E-06	7,22E-06	9,51E-06		
EU154	7,39E-11	1,10E-09	4,42E-10	3,78E-10	7,81E-10	1,29E-09		
EU155		1,20E-09	4,99E-10	4,00E-10	7,62E-10	1,37E-09		
SB125	3,80E-10	9,69E-11	5,69E-11	1,90E-12	2,42E-10	6,27E-10		
SR90	3,53E-07	1,10E-07	6,14E-08	1,07E-07	2,77E-07	5,06E-07		
CE144	4,67E-10	1,87E-08	9,57E-09	1,04E-08	1,43E-08	1,30E-08		
TC99	<2,48E-08							
AG110M			5,11E-10	<3,94E-10	1,08E-08			
AM241	6,37E-09	8,76E-10	5,37E-10	3,27E-10	4,41E-10	4,58E-10		
AM243			5,59E-10	9,46E-10	9,57E-10			
NP237		6,19E-09				6,51E-09		
NP239								
CM244	9,14E-12	1,48E-10	1,56E-10	1,37E-10	1,59E-10	1,12E-10		
CM242		1,10E-10	7,39E-11	5,71E-11	5,78E-11	1,08E-10		
PU238	6,95E-09	1,36E-09	9,31E-10	2,86E-09	4,72E-10	3,00E-09		
PU239/40	2,02E-08	1,01E-09	9,06E-10	2,96E-09	5,61E-10	2,62E-09		
PU241	8,36E-09	1,83E-09				1,84E-09		
U	1,13E-06				6,48E-07	1,30E-08		
pH	6,5	7,26	7,26	7,12	7,32	7,39		
Eh	261 mV	183 mV	182 mV	181 mV	161 mV	110 mV		

Table A 8: Incremental rates of radionuclide release from spent fuel corrosion tests (FIAP/d)										
Sample:	K 2 (Pellet): 7,109 g (=6,266 g HM)			Solution: DI-water		Starting volume: 200 ml				
		..... g at test termination		Temperature: 25 °C		Final volume:				
	31	45								
	Washcycles		**Static tests**					**Acid cleaning**		
Nuclide	1.Cycl (31d)	2.Cycl (45 d)	1. Sampling	2. Sampling	3. Sampling	4. Sampling	5. Sampling	of the		
			121 d (cumul.)	183 d (cumul.)	275 d (cumul.)	513 d (cumul.)		container		
	0,45 µm -filtered		0,45 µm -filtered							
RU106			4,51E-8		7,92E-09					
CS134	7,16E-04	1,96E-04	1,19E-4	3,46E-05	1,10E-05	1,20E-05				
CS137	4,51E-04	1,74E-04	1,07E-4	2,75E-05	1,30E-05	8,85E-06				
EU154	5,61E-08	5,74E-07	2,31E-7		9,18E-08	4,17E-08				
EU155		6,30E-07	2,61E-7		8,26E-08	4,99E-08				
SB125	2,20E-06	3,86E-07	2,26E-7		4,17E-07	2,42E-07				
SR90	2,72E-05	5,86E-06	3,26E-6	1,67E-06	3,91E-06	1,92E-06				
CE144	1,92E-08	5,29E-07	2,71E-7	1,56E-08	4,78E-08					
TC99	<2,22E-06									
AG110M			<3,5E-7		3,11E-06					
AM241	3,22E-06	3,05E-07	1,87E-7		1,73E-08	8,93E-10				
AM243			1,95E-7	9,23E-08	1,78E-09					
NP237		1,45E-06				2,41E-07				
NP239										
CM244	2,15E-08	2,40E-07	2,52E-7		1,58E-08					
CM242		1,77E-07	1,19E-7		4,99E-10	1,29E-08				
PU238	1,51E-07	2,05E-08	1,40E-8	1,99E-08		6,00E-09				
PU239/40	4,40E-07	1,52E-08	1,36E-8	2,12E-08		4,88E-09				
PU241	1,82E-07	2,74E-08				4,37E-09				
U	2,97E-7				5,09E-08					
pH	6,5	7,26	7,26	7,12	7,32	7,39				
Eh	261 mV	183 mV	182 mV	181 mV	161 mV	110 mV				

Table A 9: Activity of leach solutions from spent fuel corrosion tests (Bq/ml)										
Sample:	**K 3** (Pellet):	6,976 g (=6,149 g HM)	Solution: 95% sat **NaCl**		Starting volume: 200 ml		Acid cleaning solution: 220 ml conc.HNO3			
		6,951 g at test termination	Temperature: 25 °C		Final volume: 164 ml					
	Addition of 8,5 g **Fe-powder** after 2.washcycle									
	Washcycles		**Static tests**						**Acid cleaning**	**Activity**
Nuclide	1.Cycl (30d)	2.Cycl (41 d)	1. Sampling	2. Sampling	3. Sampling	4. Sampling	5. Sampling		of the container	sorbed on 1 g
			123 d (cumul.)	185 d (cumul.)	277 d (cumul.)	509 d (cumul.)	745 d (cumul.)		wall	Fe - powder
	0,45 µm -filtered		0,45 µm -filtered					1,8 nm-filtered		
RU106	6,29E+02	2,85E+02	1,81E+00	<3,70E-01	<1,15E+01	<1,00E+01	<1,85E+01	<1,92E+01		1,21E+04
CS134	1,52E+06	7,46E+05	9,09E+05	1,34E+06	1,89E+06	1,91E+06	1,79E+06	1,90E+06		7,72E+04
CS137	1,99E+06	1,06E+06	1,66E+06	2,37E+06	3,50E+06	3,82E+06	4,89E+06	5,18E+06		2,96E+05
EU154	1,07E+02	7,40E+01	5,55E-01	<3,70E-01	6,54E+00		<2,59E+00	<2,69E+00		1,53E+04
EU155	7,03E+01	4,07E+01	3,70E-01	<3,70E-01	<1,15E+00	<4,00E+00	<3,68E+00	<3,63E+00		6,80E+03
SB125	2,89E+02	5,92E+01	<3,70E-01	<3,70E-01	<1,36E+00	<1,50E+01	<1,37E+01	<1,38E+01		6,31E+03
SR90	4,63E+04	9,45E+03	8,44E+02	5,29E+03	1,05E+04	1,56E+04	1,35E+04	1,54E+04	6,45E+02	2,56E+04
CE144	2,28E+03	5,18E+02	1,59E+00	<3,70E-01	<1,15E+01	<1,00E+01	<9,51E+00	<9,77E+00		1,11E+04
TC99	1,48E+00						<5,92E-02	<6,15E-02		
AG110M	1,48E+02		3,70E-01	<3,70E-01	<1,15E+01	<4,00E+00	<4,44E+00	<4,62E+00		
AM241	9,03E+01	4,44E+00	5,92E-01	<3,70E-01	6,79E+00	2,42E+01	1,48E-01	<7,69E-01	3,16E+01	4,20E+03
AM243	1,15E+00				<1,15E+00					
NP237	4,81E-02	<6,66E-02					<4,63E-02	<3,85E-02	3,38E-02	8,40E-02
NP239	3,70E-01									
CM244	7,92E+01	5,55E+01	2,00E-01		<2,30E-01	1,31E+02	<7,40E-02	6,15E-01	1,37E+02	
CM242	2,96E+00	7,40E-01				1,16E+00	<1,48E-02	<6,92E-02	8,75E-01	
PU238	1,03E+02	3,11E+01	2,96E-02	<2,22E-02	2,64E-02		<5,85E-01	3,30E+00	2,21E+01	4,81E+03
PU239/40	2,33E+01	3,70E+00	1,48E-02	<2,22E-02	2,64E-02		<4,75E-01	4,27E-01	2,80E+00	5,43E+02
PU241	2,35E+03	7,88E+02					<1,40E+01	3,26E+01	2,98E+02	5,48E+04
U	*1,2E+0 ug/mL*			*6,0E-2 ug/mL*	*3,4E-2 ug/mL*	*2,6E-2 ug/mL*	*1,9E-2 ug/mL*	*2,6E-2 ug/mL*	*6,2E-2 ug/mL*	*2,49E+01 ng*
pH	5,8	6,05	7,66	7,98	9,6	9,6	7,8	7,8		
Eh	383 mV	307 mV	180 mV	115 mV	-368 mV	-368 mV	-148 mV	-148 mV		

Table A 10: Release of radionuclides in leach solutions from spent fuel corrosion tests (FIAP: Fraction of inventory in the aeqeous phase)									*	**
									FIC= Fraction	FIFE=Fractn.
Sample:	K 3 (Pellet): 6,976 g (=6,149 g HM)		Solution: 95% sat NaCl			Starting volume: 200 ml			of Inventory	of Inventory
	6,951 g at test termination		Temperature: 25 °C			Final volume: 164 ml			on Container	on Fe-
	Addition of 8,5 g Fe-powder after 2.washcycle								wall	powder
	Washcycles		Static tests						Acid cleaning	Inventory on
Nuclide	1.Cycl (30d)	2.Cycl (41 d)	1. Sampling	2. Sampling	3. Sampling	4. Sampling	5. Sampling		of the con-	8,5 g Fe-powd.
			123 d (cumul.)	185 d (cumul.)	277 d (cumul.)	509 d (cumul.)	745 d (cumul.)		tainer (FIC*)	(FIFE**)
	0,45 µm -filtered		0,45 µm -filtered					1,8 nm-filtered		
RU106	7,47E-06	4,19E-06	3,60E-08	<6,95E-09	<2,34E-07	<2,21E-07	<7,13E-07	<7,40E-07		3,19E-05
CS134	1,28E-02	6,96E-03	9,84E-03	1,37E-02	<1,95E-02	<1,99E-02	2,42E-02	2,57E-02		6,49E-05
CS137	1,06E-02	5,70E-03	9,01E-03	1,22E-02	<1,70E-02	<1,75E-02	2,24E-02	2,37E-02		7,75E-05
EU154	9,17E-06	6,48E-06	5,03E-08	<3,17E-08	<5,36E-07		<2,13E-07	<2,21E-07		7,29E-05
EU155	1,17E-05	7,05E-06	6,81E-08	<6,44E-08	<1,94E-07	<6,52E-07	<6,62E-07	<6,53E-07		7,21E-05
SB125	6,37E-05	1,41E-05	<9,85E-08	<9,31E-08	<3,39E-07	<3,70E-06	<4,09E-06	<4,12E-06		1,15E-04
SR90	3,62E-04	7,45E-05	6,72E-06	3,98E-05	<7,47E-05	<1,05E-04	9,09E-05	1,04E-04	5,80E-06	9,85E-06
CE144	3,06E-05	9,16E-06	4,15E-08	<9,13E-09	<3,20E-07	<3,16E-07	<6,19E-07	<6,36E-07		5,21E-05
TC99	7,02E-05						<2,30E-06	<2,39E-06		
AG110M	1,99E-03		1,06E-05	<1,00E-05	<3,60E-04	<1,46E-04	<3,70E-04	<3,85E-04		
AM241	5,20E-05	2,39E-06	2,93E-07	<1,73E-07	<2,88E-06	<9,29E-06	4,90E-08	<2,55E-07	1,44E-05	7,62E-05
AM243	1,48E-05				<1,32E-05					
NP237	8,62E-05	<1,19E-04					<6,80E-05	<5,66E-05	6,66E-05	7,01E-06
NP239	4,77E-06									
CM244	5,80E-06	4,11E-06	1,51E-08		<1,55E-08	<8,38E-06	<4,80E-09	3,99E-08	1,18E-05	
CM242	3,34E-06	1,35E-06				<6,71E-06	<3,07E-07	<1,43E-06	1,88E-05	
PU238	1,01E-05	3,05E-06	2,92E-09	<2,07E-09	<2,32E-09		<4,78E-08	2,69E-07	2,42E-06	2,24E-05
PU239/40	1,46E-05	2,32E-06	9,27E-09	<1,31E-08	<1,47E-08		<2,44E-07	2,19E-07	1,93E-06	1,58E-05
PU241	9,63E-06	3,27E-06					<5,17E-08	1,20E-07	1,46E-06	1,16E-05
U	4,17E-05			<1,97E-06	<1,07E-06	<7,46E-07	5,27E-07	7,47E-07	2,38E-06	4,03E-05
pH	5,8	6,05	7,66	7,98	9,6	9,6	7,8	7,8		
Eh	383 mV	307 mV	180 mV	115 mV	-368 mV	-368 mV	-148 mV	-148 mV		

Table A 11: Concentration of radionuclides in leach solutions from spent fuel corrosion tests (mol/L)									
Sample:	K 3 (Pellet): 6,976 g (=6,149 g HM)		Solution: 95% sat NaCl			Starting volume: 200 ml			
		6,951 g at test termination	Temperature: 25 °C			Final volume: 164 ml			
	Addition of 8,5 g Fe-powder after 2.washcycle								
	Washcycles		Static tests						Acid cleaning
Nuclide	1.Cycl (30d)	2.Cycl (41 d)	1. Sampling	2. Sampling	3. Sampling	4. Sampling	5. Sampling		of the container
			123 d (cumul.)	185 d (cumul.)	277 d (cumul.)	509 d (cumul.)	745 d (cumul.)		
	0,45 µm -filtered		0,45 µm -filtered					1,8 nm-filtered	
RU106	7,83E-09	4,39E-09	3,77E-11	<7,70E-12	<2,75E-10	<2,78E-10	<9,11E-10	<9,45E-10	
CS134	1,14E-05	6,20E-06	8,76E-06	1,29E-05	<1,95E-05	<2,12E-05	2,63E-05	2,79E-05	
CS137	9,45E-06	5,07E-06	8,02E-06	1,14E-05	<1,70E-05	<1,86E-05	2,43E-05	2,58E-05	
EU154	3,83E-10	2,70E-10	2,10E-12	<1,40E-12	<2,51E-11		<1,08E-11	<1,12E-11	
EU155	4,86E-10	2,94E-10	2,84E-12	<2,84E-12	<9,07E-12	<3,26E-11	<3,36E-11	<3,32E-11	
SB125	3,49E-10	7,73E-11	<5,39E-13	<5,39E-13	<2,09E-12	<2,43E-11	<2,73E-11	<2,75E-11	
SR90	1,49E-07	3,06E-08	2,76E-09	1,73E-08	<3,45E-08	<5,16E-08	4,56E-08	5,20E-08	2,17E-09
CE144	2,36E-08	7,05E-09	3,20E-11	<7,43E-12	<2,77E-10	<2,91E-10	<5,81E-10	<5,97E-10	
TC99	2,48E-08						<9,93E-10	<1,03E-09	
AG110M	6,30E-08		3,36E-10	<3,36E-10	<1,28E-08	<5,55E-09	<1,43E-08	<1,49E-08	
AM241	3,26E-09	1,50E-10	1,83E-11	<1,15E-11	<2,03E-10	<6,96E-10	3,74E-12	<1,95E-11	8,19E-10
AM243	9,25E-10				<9,26E-10				
NP237	8,03E-09	<1,11E-08					<7,73E-09	<6,43E-09	5,64E-09
NP239	4,44E-10								
CM244	7,83E-11	5,55E-11	2,03E-13		<2,35E-13	<1,35E-10	<7,90E-14	6,56E-13	1,45E-10
CM242	4,51E-11	1,82E-11				<1,08E-10	<5,04E-12	<2,36E-11	2,30E-10
PU238	1,47E-08	4,43E-09	4,24E-12	<3,18E-12	<3,79E-12		<8,46E-11	4,77E-10	3,19E-09
PU239/40	2,12E-08	3,36E-09	1,35E-11	<2,02E-11	<2,40E-11		<4,32E-10	3,88E-10	2,55E-09
PU241	1,40E-08	4,75E-09					<9,16E-11	2,13E-10	1,93E-09
U	5,04E-06			<2,52E-07	<1,45E-07	<1,08E-07	7,77E-08	1,10E-07	2,61E-07
pH	5,8	6,05	7,66	7,98	9,6	9,6	7,8	7,8	
Eh	383 mV	307 mV	180 mV	115 mV	-368 mV	-368 mV	-148 mV	-148 mV	

Table A 12: Incremental rates of radionuclide release from spent fuel corrosion tests (FIAP/d)							
Sample:	K 3 (Pellet): 6,976 g (=6,149 g HM)		Solution: 95% sat NaCl		Starting volume: 200 ml		
	6,951 g at test termination		Temperature: 25 °C		Final volume: 164 ml		
	Addition of 8,5 g Fe-powder after 2.washcycle						
	Washcycles		Static tests				
Nuclide	1.Cycl (30d)	2.Cycl (41 d)	1. Sampling	2. Sampling	3. Sampling	4. Sampling	5. Sampling
			123 d (cumul.)	185 d (cumul.)	277 d (cumul.)	509 d (cumul.)	745 d (cumul.)
	0,45 µm -filtered		0,45 µm -filtered				
RU106	2,49E-07	1,02E-07	6,9E-10		2,5E-9	8,6E-12	2,1E-9
CS134	4,26E-04	1,70E-04	1,9E-4	7,16E-05	7,2E-5	6,6E-6	2,0E-5
CS137	3,54E-04	1,39E-04	1,7E-4	5,87E-05	6,0E-5	6,6E-6	2,2E-5
EU154	3,06E-07	1,58E-07	9,7E-10		5,5E-9		9,0E-10
EU155	3,89E-07	1,72E-07	1,3E-9		1,4E-9	2,0E-9	9,1E-11
SB125	2,12E-06	3,45E-07	1,9E-9		2,7E-9	1,5E-8	1,9E-9
SR90	1,21E-05	1,82E-06	1,3E-7	5,40E-07	4,0E-7	1,5E-7	
CE144	1,02E-06	2,23E-07	8,0E-10		3,4E-9	6,9E-11	1,3E-9
TC99	2,34E-06						9,8E-9
AG110M	6,63E-05		<2,0E-7		3,8E-6		9,6E-7
AM241	1,73E-06	5,84E-08	5,6E-9		3,0E-8	2,8E-8	
AM243	4,93E-07				1,4E-7		
NP237	2,87E-06	<2,91E-06					2,9E-7
NP239	1,59E-07						
CM244	1,93E-07	1,00E-07	2,9E-10		1,7E-10	3,6E-8	
CM242	1,11E-07	3,30E-08				2,9E-8	
PU238	3,37E-07	7,45E-08	5,6E-11		4,0E-12		2,0E-10
PU239/40	4,86E-07	5,65E-08	1,8E-10	<7,06E-11	2,5E-11		1,0E-9
PU241	3,21E-07	7,98E-08					2,2E-10
U	1,39E-06			<3,18E-08			
pH	5,8	6,05	7,66	7,98	9,6	9,6	7,8
Eh	383 mV	307 mV	180 mV	115 mV	-368 mV	-368 mV	-148 mV

Table A 13: Activity of leach solutions from spent fuel corrosion tests (Bq/ml)									
Sample:	**K 4** (Pellet): 7,530 g (=6,638 g HM)			Solution: 95% sat **NaCl**		Starting volume: 200 ml			
		..... g at test termination		Temperature: 25 °C		Final volume: ... ml			
	Addition of 9,2 g **Fe-powder** after 2.washcycle								
	Washcycles		**Static tests**					**Acid cleaning**	
Nuclide	1.Cycl (31d)	2.Cycl (42 d)	1. Sampling	2. Sampling	3. Sampling	4. Sampling	5. Sampling	of the container	
			123 d (cumul.)	185 d (cumul.)	280 d (cumul.)	511 d (cumul.)			
	0,45 µm -filtered		0,45 µm -filtered						
RU106	5,33E+02	4,81E+02	<4,24E-01	<4,24E-01	<1,15E+01	<1,69E+01			
CS134	1,50E+06	8,03E+05	1,05E+06	1,62E+06	2,14E+06	1,83E+06			
CS137	1,92E+06	1,16E+06	1,95E+06	2,85E+06	4,01E+06	3,67E+06			
EU154	1,11E+02	1,70E+02	<4,24E-01	<4,24E-01	<1,15E+01	7,04E+00			
EU155	5,55E+01	1,15E+02	<4,24E-01	<4,24E-01	<1,15E+01	<3,37E+00			
SB125	6,51E+02	1,63E+02	<4,24E-01	<4,24E-01	<1,15E+01	<1,26E+01			
SR90	4,70E+04	1,11E+04	2,12E+02	1,16E+03	1,70E+03	5,60E+03			
CE144	2,59E+03	7,03E+02	<4,24E-01	<4,24E-01	<1,15E+01	<8,43E+00			
TC99	<1,48E+00								
AG110M	2,27E+02		<4,24E-01	<4,24E-01	<1,15E+01	<3,37E+00			
AM241	8,55E+01	3,03E+01	<4,24E-01	<4,24E-01	4,03E+00	4,27E+00			
AM243	1,30E+00	1,48E+00		<1,14E+00	<1,15E+00				
NP237	4,81E-02	3,70E-02							
NP239	2,59E-01	1,48E+00							
CM244	7,62E+01	1,81E+02	<2,29E-01	<2,29E-01	<2,29E-01	3,12E+00			
CM242	2,85E+00	4,44E+00				5,08E-02			
PU238	1,82E+02	4,22E+01	<2,54E-03	<2,54E-02	<2,64E-02	6,70E+00			
PU239/40	8,99E+01	5,44E+00	<2,54E-03	<2,54E-02	<2,64E-02				
PU241	5,03E+03	1,27E+03							
U	*1,2E+0 µg/ml*			*9,2E-2 µg/ml*	*6,9E-2 µg/ml*	*1,4E-2 µg/ml*			
pH	5,82	6,03	7,98	7,5	8,21	9,6			
Eh	378 mV	324 mV	115 mV	120 mV	130 mV	-340 mV			

Table A 14: Release of radionuclides in leach solutions from spent fuel corrosion tests								
(FIAP: Fraction of inventory in the aequeous phase)								
Sample:	K 4 (Pellet): 7,530 g (=6,638 g HM)		Solution: 95% sat NaCl			Starting volume: 200 ml		
	..... g at test termination		Temperature: 25 °C			Final volume: ... ml		
	Addition of 9,2 g Fe-powder after 2.washcycle							
	Washcycles		Static tests					Acid cleaning
Nuclide	1.Cycl (31d)	2.Cycl (42 d)	1. Sampling	2. Sampling	3. Sampling	4. Sampling	5. Sampling	of the container
			123 d (cumul.)	185 d (cumul.)	280 d (cumul.)	511 d (cumul.)		
	0,45 µm -filtered		0,45 µm -filtered					
RU106	5,86E-06	6,55E-06	<2,88E-04	<7,37E-09	<1,88E-07	<3,47E-07		
CS134	1,17E-02	6,94E-03	3,91E+02	1,53E-02	1,91E-02	1,76E-02		
CS137	9,49E-03	5,76E-03	3,62E+02	1,35E-02	1,80E-02	1,56E-02		
EU154	8,79E-06	1,38E-05	<1,32E-03	<3,36E-08	<8,58E-07	5,10E-07		
EU155	8,53E-06	1,84E-05	<2,67E-03	<6,83E-08	<1,74E-06	<5,09E-07		
SB125	1,33E-04	3,60E-05	<3,87E-03	<9,88E-08	<2,52E-06	<2,88E-06		
SR90	3,40E-04	8,10E-05	5,78E-02	8,06E-06	1,11E-05	3,48E-05		
CE144	3,22E-05	1,15E-05	<3,79E-04	<9,68E-09	<2,47E-07	<2,47E-07		
TC99	<6,51E-05							
AG110M	2,82E-03		<4,16E-01	<1,06E-05	<2,71E-04	<1,14E-04		
AM241	4,56E-05	1,52E-05	<7,19E-03	<1,84E-07	1,65E-06	1,52E-06		
AM243	1,55E-05	1,77E-05		<1,29E-05	<1,22E-05			
NP237	7,98E-05	6,14E-05						
NP239	3,09E-06	1,77E-05						
CM244	5,17E-06	1,25E-05	<5,91E-04	<1,51E-08	<1,43E-08	1,85E-07		
CM242	2,98E-06	7,51E-06				2,72E-07		
PU238	1,65E-05	3,84E-06	<8,59E-06	<2,19E-09	<2,14E-09	5,13E-07		
PU239/40	5,22E-05	3,16E-06	<5,46E-05	<1,39E-08	<1,36E-08			
PU241	1,91E-05	4,90E-06						
U	3,87E-5			2,79E-6	1,97E-06	3,68E-07		
pH	5,82	6,03	7,98	7,5	8,21	9,6		
Eh	378 mV	324 mV	115 mV	120 mV	130 mV	-340 mV		

Table A 15: Concentration of radionuclides in leach solutions from spent fuel corrosion tests (mol/L)									
Sample:	K 4 (Pellet): 7,530 g (=6,638 g HM)		Solution: 95% sat NaCl			Starting volume: 200 ml			
	..... g at test termination		Temperature: 25 °C			Final volume: ... ml			
	Addition of 9,2 g Fe-powder after 2.washcycle								
	Washcycles		Static tests					Acid cleaning	
Nuclide	1.Cycl (31d)	2.Cycl (42 d)	1. Sampling	2. Sampling	3. Sampling	4. Sampling	5. Sampling	of the container	
			123 d (cumul.)	185 d (cumul.)	280 d (cumul.)	511 d (cumul.)			
	0,45 µm -filtered		0,45 µm -filtered						
RU106	6,63E-09	7,41E-09	<3,26E-07	<8,82E-12	<2,39E-10	<4,69E-10			
CS134	1,12E-05	6,67E-06	3,76E-01	1,56E-05	2,07E-05	2,03E-05			
CS137	9,12E-06	5,54E-06	3,48E-01	1,38E-05	1,94E-05	1,79E-05			
EU154	3,96E-10	6,22E-10	<5,93E-08	<1,60E-12	<4,34E-11	2,75E-11			
EU155	3,84E-10	8,28E-10	<1,20E-07	<3,25E-12	<8,80E-11	<2,74E-11			
SB125	7,87E-10	2,13E-10	<2,29E-08	<6,18E-13	<1,67E-11	<2,04E-11			
SR90	1,51E-07	3,60E-08	2,57E-05	3,79E-09	5,56E-09	1,85E-08			
CE144	2,68E-08	9,57E-09	<3,15E-07	<8,51E-12	<2,30E-10	<2,46E-10			
TC99	<2,48E-08								
AG110M	9,65E-08		<1,42E-05	<3,85E-10	<1,04E-08	<4,68E-09			
AM241	3,08E-09	1,02E-09	<4,86E-07	<1,31E-11	1,25E-10	1,23E-10			
AM243	1,04E-09	1,19E-09		<9,23E-10	<9,25E-10				
NP237	8,03E-09	6,18E-09							
NP239	3,11E-10	1,78E-09							
CM244	7,53E-11	1,81E-10	<8,61E-09	<2,33E-13	<2,33E-13	3,22E-12			
CM242	4,34E-11	1,09E-10				4,74E-12			
PU238	2,59E-08	6,02E-09	<1,35E-08	<3,64E-12	<3,78E-12	9,62E-10			
PU239/40	8,18E-08	4,95E-09	<8,55E-08	<2,31E-11	<2,40E-11				
PU241	2,99E-08	7,68E-09							
U	5,0E-06			3,85E-07	2,89E-07	5,76E-08			
pH	5,82	6,03	7,98	7,5	8,21	9,6			
Eh	378 mV	324 mV	115 mV	120 mV	130 mV	-340 mV			

Table A 16: Incremental rates of radionuclide release from spent fuel corrosion tests (FIAP/d)									
Sample:	K 4 (Pellet): 7,530 g (=6,638 g HM)			Solution: 95% sat NaCl		Starting volume: 200 ml			
		..... g at test termination		Temperature: 25 °C		Final volume: ... ml			
	Addition of 9,2 g Fe-powder after 2.washcycle								
	Washcycles		Static tests					Acid cleaning	
Nuclide	1.Cycl (31d)	2.Cycl (42 d)	1. Sampling	2. Sampling	3. Sampling	4. Sampling	5. Sampling	of the container	
	31	42	123 d (cumul.)	185 d (cumul.)	280 d (cumul.)	511 d (cumul.)			
	0,45 µm -filtered		0,45 µm -filtered						
RU106	1,89E-07	1,56E-07	1,56E-10		1,9E-9	7,4E-10			
CS134	3,77E-04	1,65E-04	2,11E-04	8,6E-5	5,0E-5				
CS137	3,06E-04	1,37E-04	1,96E-04	6,9E-5	5,5E-5				
EU154	2,84E-07	3,29E-07	7,12E-10		8,7E-9				
EU155	2,75E-07	4,38E-07	1,45E-09		1,8E-8				
SB125	4,30E-06	8,57E-07	2,09E-09		2,6E-8	2,3E-9			
SR90	1,10E-05	1,93E-06	3,12E-08	1,1E-7	3,7E-8	1,1E-7			
CE144	1,04E-06	2,74E-07	2,05E-10		2,5E-9	6,7E-11			
TC99	<2,10E-06								
AG110M	9,10E-05		<2,25E-07		2,7E-6				
AM241	1,47E-06	3,61E-07	3,9E-9		1,5E-8				
AM243	4,99E-07	4,21E-07		2,1E-7	3,4E-10				
NP237	2,58E-06	1,46E-06							
NP239	9,97E-08	4,21E-07							
CM244	1,67E-07	2,96E-07	3,2E-10		4,0E-13	7,4E-10			
CM242	9,61E-08	1,79E-07				1,2E-9			
PU238	5,33E-07	9,14E-08	4,6E-12	3,2E-11	8,2E-13	2,2E-9			
PU239/40	1,68E-06	7,51E-08	2,9E-11	2,0E-10	5,2E-12				
PU241	6,15E-07	1,17E-07							
U	1,25E-6			4,5E-8					
pH	5,82	6,03	7,98	7,5	8,21	9,6			
Eh	378 mV	324 mV	115 mV	120 mV	130 mV	-340 mV			

Table A 17: Activity of leach solutions from spent fuel corrosion tests (Bq/ml)									
Sample:	**K 9** (Pellet): 7,430 g (=6,549 g HM)			Solution: 95% sat **NaCl**		Starting volume: 200 ml			
				Temperature: 25 °C		Final volume:			
	Washcycles		**Static tests**					**Acid cleaning**	
Nuclide	1.Cycl (31d)	2.Cycl (42 d)	1. Sampling	2. Sampling	3. Sampling	4. Sampling	5. Sampling	of the liner	
			126 d (cumul.)	189 d (cumul.)	280 d (cumul.)	514 d (cumul.)			
	0,45 µm -filtered		0,45 µm -filtered						
RU106	5,51E+02	5,18E+02	1,18E+02	2,41E+01	1,50E+02	4,58E+01			
CS134	1,67E+06	1,36E+05	2,96E+05	3,38E+05	4,06E+05	7,33E+05			
CS137	2,12E+06	1,86E+05	5,19E+05	5,69E+05	7,35E+05	1,38E+06			
EU154	1,08E+02	1,81E+02	1,52E+02	3,81E+01	1,31E+01				
EU155	6,03E+01	1,15E+02	8,85E+01	2,54E+01	5,93E+00				
SB125	5,14E+02	1,04E+02	1,14E+02	4,23E+01	1,74E+02	2,20E+02			
SR90	3,33E+04	2,48E+03	5,82E+03	1,06E+04	1,81E+04	3,67E+04			
CE144	2,09E+03	9,99E+02	3,37E+01	<4,23E-01	<1,95E+00				
TC99	<1,48E+00								
AG110M	5,74E+01	5,18E+01	1,39E+02	<4,23E-01	3,78E+02	2,58E+02			
AM241	8,51E+01	2,22E+01	2,53E+01	8,46E+00	8,05E+00	<1,46E+00			
AM243	<3,70E-01	<1,48E+00	<1,14E+00	2,62E+00	5,72E+00				
NP237	<3,70E-02	<3,70E-02	<4,21E-03	<4,23E-03					
NP239	<3,70E-01	<1,48E+00	4,21E-01						
CM244	1,14E+02	2,68E+02	9,90E+01	2,62E+01	1,26E+01	3,57E-01			
CM242	4,55E+00	6,83E+00	8,01E-01						
PU238	1,39E+02	5,55E+01	2,74E+01	1,13E+02	3,59E+01	1,13E+01			
PU239/40	4,44E+01	6,66E+00	5,06E+00	1,61E+01	5,04E+00	1,31E+00			
PU241	3,58E+03	1,30E+03	6,39E+02	2,60E+03		1,13E+02			
U	*1,2E+0 µg/ml*			*5,7E-1 µg/ml*	*8,0E-1 µg/ml*	*8,4E-1 µg/ml*			
pH	5,75	5,83	7,6	7,48	7,05	9,23			
Eh	324 mV	295 mV	114 mV	142 mV	136 mV	-215 mV			

Table A 18: Release of radionuclides in leach solutions from spent fuel corrosion tests (FIAP: Fraction of inventory in the aequeous phase)								
Sample:	K 9 (Pellet): 7,430 g (=6,549 g HM)			Solution: 95% sat NaCl		Starting volume: 200 ml		
				Temperature: 25 °C		Final volume:		
	Washcycles		Static tests					Acid cleaning
Nuclide	1.Cycl (31d)	2.Cycl (42 d)	1. Sampling	2. Sampling	3. Sampling	4. Sampling	5. Sampling	of the liner
			126 d (cumul.)	189 d (cumul.)	280 d (cumul.)	514 d (cumul.)		
	0,45 µm -filtered		0,45 µm -filtered					
RU106	6,15E-06	7,15E-06	2,20E-06	4,25E-07	2,87E-06	9,52E-07		
CS134	1,32E-02	1,19E-03	3,01E-03	3,25E-03	3,94E-03	7,16E-03		
CS137	1,06E-02	9,39E-04	2,65E-03	2,74E-03	3,35E-03	5,93E-03		
EU154	8,67E-06	1,49E-05	1,29E-05	3,06E-06	1,01E-06			
EU155	9,39E-06	1,86E-05	1,53E-05	4,14E-06	9,39E-07			
SB125	1,07E-04	2,32E-05	2,84E-05	9,99E-06	4,08E-05	5,10E-05		
SR90	2,44E-04	1,83E-05	4,35E-05	7,47E-05	1,21E-04	2,31E-04		
CE144	2,64E-05	1,66E-05	8,26E-07	<9,79E-09	<5,10E-08			
TC99	<6,59E-05							
AG110M	7,23E-04	8,94E-04	3,74E-03	<1,07E-05	1,11E-02	8,85E-03		
AM241	4,60E-05	1,12E-05	1,18E-05	3,71E-06	3,21E-06	<5,26E-07		
AM243	<4,48E-06	<1,79E-05	<1,38E-05	3,00E-05	6,16E-05	0,00E+00		
NP237	<6,22E-05	<6,22E-05	<7,09E-06	<6,72E-06				
NP239	<4,48E-06	<1,79E-05	5,10E-06					
CM244	7,83E-06	1,86E-05	7,01E-06	1,75E-06	7,99E-07	2,14E-08		
CM242	4,83E-06	1,17E-05	2,71E-06					
PU238	1,28E-05	5,12E-06	2,53E-06	9,91E-06	2,97E-06	8,76E-07		
PU239/40	2,61E-05	3,92E-06	2,97E-06	8,93E-06	2,64E-06	6,43E-07		
PU241	1,38E-05	5,08E-06				3,83E-07		
U	3,92E-5			1,76E-5	2,33E-05	2,29E-05		
pH	5,75	5,83	7,6	7,48	7,05	9,23		
Eh	324 mV	295 mV	114 mV	142 mV	136 mV	-215 mV		

Table A 19: Concentration of radionuclides in leach solutions from spent fuel corrosion tests (mol/L)									
Sample:	K 9 (Pellet): 7,430 g (=6,549 g HM)			Solution: 95% sat NaCl		Starting volume: 200 ml			
				Temperature: 25 °C		Final volume:			
	Washcycles		Static tests					Acid cleaning	
Nuclide	1.Cycl (31d)	2.Cycl (42 d)	1. Sampling	2. Sampling	3. Sampling	4. Sampling	5. Sampling	of the liner	
			126 d (cumul.)	189 d (cumul.)	280 d (cumul.)	514 d (cumul.)			
	0,45 µm -filtered		0,45 µm -filtered						
RU106	6,86E-09	7,98E-09	2,46E-09	5,02E-10	5,02E-10	1,27E-09			
CS134	1,25E-05	1,13E-06	2,85E-06	3,26E-06	3,26E-06	8,13E-06			
CS137	1,01E-05	8,90E-07	2,51E-06	2,75E-06	2,75E-06	6,73E-06			
EU154	3,85E-10	6,62E-10	5,74E-10	1,44E-10	1,44E-10				
EU155	4,17E-10	8,28E-10	6,79E-10	1,95E-10	1,95E-10				
SB125	6,22E-10	1,35E-10	1,66E-10	6,17E-11	6,17E-11	3,56E-10			
SR90	1,07E-07	8,03E-09	1,90E-08	3,46E-08	3,46E-08	1,21E-07			
CE144	2,16E-08	1,36E-08	6,77E-10	<8,49E-12	<8,49E-12				
TC99	<2,48E-08								
AG110M	2,44E-08	3,02E-08	1,26E-07	<3,84E-10	3,84E-10	3,58E-07			
AM241	3,07E-09	7,49E-10	7,84E-10	2,62E-10	2,62E-10	<4,20E-11			
AM243	<2,98E-10	<1,19E-09	<9,18E-10	2,12E-09	2,12E-09				
NP237	<6,18E-09	<6,18E-09	<7,04E-10	<7,06E-10	7,06E-10				
NP239	<4,44E-10	<1,78E-09	5,06E-10						
CM244	1,13E-10	2,68E-10	1,01E-10	2,67E-11	2,67E-11	3,69E-13			
CM242	6,93E-11	1,68E-10	3,90E-11						
PU238	1,97E-08	7,92E-09	3,92E-09	1,62E-08	1,62E-08	1,62E-09			
PU239/40	4,04E-08	6,06E-09	4,60E-09	1,46E-08	1,46E-08	1,19E-09			
PU241	2,13E-08	7,86E-09	3,94E-09		1,60E-08	7,10E-10			
U	5,04E-6			2,40E-6	2,40E-06	3,53E-06			
pH	5,75	5,83	7,6	7,48	7,05	9,23			
Eh	324 mV	295 mV	114 mV	142 mV	136 mV	-215 mV			

Table A 20: Incremental rates of radionuclide release from spent fuel corrosion tests (FIAP/d)									
Sample:	K 9 (Pellet): 7,430 g (=6,549 g HM)			Solution: 95% sat NaCl		Starting volume: 200 ml			
				Temperature: 25 °C		Final volume:			
	Washcycles		Static tests					Acid cleaning	
Nuclide	1.Cycl (31d)	2.Cycl (42 d)	1. Sampling	2. Sampling	3. Sampling	4. Sampling	5. Sampling	of the liner	
	31	42	126 d (cumul.)	189 d (cumul.)	280 d (cumul.)	514 d (cumul.)			
	0,45 µm -filtered		0,45 µm -filtered						
RU106	1,98E-07	1,70E-07	4,2E-8		2,7E-8				
CS134	4,25E-04	2,83E-05	5,7E-5	6,4E-6	9,6E-6	1,5E-5			
CS137	3,43E-04	2,24E-05	5,0E-5	3,8E-6	8,4E-6	1,2E-5			
EU154	2,80E-07	3,55E-07	2,4E-7						
EU155	3,03E-07	4,44E-07	2,9E-7						
SB125	3,44E-06	5,53E-07	5,4E-7		3,4E-7	5,5E-8			
SR90	7,88E-06	4,36E-07	8,2E-7	5,3E-7	5,6E-7	5,0E-7			
CE144	8,50E-07	3,95E-07	1,6E-8		4,6E-10				
TC99	<2,13E-06								
AG110M	2,33E-05	2,13E-05	<7,1E-5		1,2E-4				
AM241	1,49E-06	2,68E-07	2,2E-7						
AM243	<1,44E-07	<4,26E-07	2,6E-7	2,7E-7	3,7E-7				
NP237	<2,01E-06	<1,48E-06	1,3E-7	3,7E-10					
NP239	<1,44E-07	<4,26E-07	9,6E-8						
CM244	2,53E-07	4,43E-07	1,3E-7						
CM242	1,56E-07	2,79E-07	5,1E-8						
PU238	4,12E-07	1,22E-07	4,8E-8	1,2E-7					
PU239/40	8,42E-07	9,32E-08	5,6E-8	9,7E-8					
PU241	4,44E-07	1,21E-07				1,6E-9			
U	1,26E-6			2,8E-7	7,3E-8	4,5E-9			
pH	5,75	5,83	7,6	7,48	7,05	9,23			
Eh	324 mV	295 mV	114 mV	142 mV	136 mV	-215 mV			

Table A 21: Activity of leach solutions from spent fuel corrosion tests (Bq/ml)

Sample:	**K 10** (Pellet): 7,369 g (=6,496 g HM)		Solution: 95% sat **NaCl**			Starting volume: 200 ml			
		7,366 g at test termination	Temperature: 25 °C			Final volume: 164 ml			
	Washcycles		**Static tests**						**Acid cleaning**
Nuclide	1.Cycl (32d)	2.Cycl (42 d)	1. Sampling	2. Sampling	3. Sampling	4. Sampling	5. Sampling		of the liner
			126 d (cumul.)	189 d (cumul.)	280 d (cumul.)	516 d (cumul.)	752 d (cumul.)		
	0,45 µm -filtered		0,45 µm -filtered					1,8 nm-filtered	
RU106	4,66E+02	3,22E+02	1,27E+03	1,79E+02	5,99E+01	4,16E+01	<4,74E+3	<2,68E+3	9,60E+01
CS134	1,61E+06	7,29E+05	1,46E+05	1,94E+05	2,74E+05	4,65E+05	1,28E+06	1,49E+06	6,35E+01
CS137	2,06E+06	1,06E+06	2,56E+05	3,34E+05	4,79E+05	8,80E+05	3,57E+06	4,25E+06	1,79E+02
EU154	1,04E+02	6,29E+01	5,48E+02	5,58E+02	4,97E+01	7,02E+00	<2,36E+2	<7,01E+0	5,13E+01
EU155	4,55E+01	4,07E+01	3,42E+02	3,09E+02	2,08E+01		<7,46E+1	<9,76E+0	2,03E+01
SB125	5,18E+02	7,40E+01	5,06E+01		5,78E+01	2,13E+02	2,02E+03	1,18E+03	8,50E-01
SR90	2,85E+04	4,07E+03	1,27E+04	2,42E+04	4,06E+04	6,09E+04	7,20E+05	7,85E+05	7,10E+03
CE144	2,59E+03	2,07E+02	1,14E+03	2,66E+01	<1,16E+01	6,89E+01	5,33E+02	3,18E+02	1,20E+02
TC99	<1,48E+00						1,10E+01	1,15E+01	
AG110M	9,62E+01		2,32E+02	<4,23E+00	7,40E+02	6,94E+02	2,02E+02	1,01E+02	
AM241	4,92E+01	1,48E+01	3,19E+01	6,89E+01	4,62E+01	3,98E+00	2,00E+01	1,29E+00	5,64E+01
AM243	<3,70E-01		2,05E+00	<1,14E+00	4,62E+00				
NP237	4,81E-02	3,70E-02	<4,22E-03	<4,23E-03			<1,57E-1	2,97E-01	
NP239	<3,70E-01		9,11E-01						
CM244	1,17E+02	6,83E+01	3,96E+02	1,45E+03	1,53E+02	8,76E+00	8,95E+01	3,27E+00	9,96E+02
CM242	2,85E+00	1,14E+00	4,39E+00	1,94E+01	1,16E+00	1,54E-01	<3,70E-1	<3,44E-2	2,97E+00
PU238	1,30E+02	2,66E+01	3,71E+01	2,35E+02	1,80E+02	1,18E+02	3,04E+02	3,10E+01	3,16E+02
PU239/40	3,44E+01	3,11E+00	5,48E+00	3,13E+01	2,61E+01	1,49E+01	5,22E+01	5,28E+00	4,47E+01
PU241	2,98E+03	5,99E+02				2,20E+03	8,57E+03	8,28E+02	
U	*1,2E+0 µg/ml*				*5,9E-1 µg/ml*	*2,5E-1 µg/ml*	*8,2E+0 µg/ml*	*8,7E+0 µg/ml*	*7,6E-1 µg/ml*
pH	6,42	4,86	7,84	7,4	6,99	7,8	8,32	8,32	
Eh	264 mV	320 mV	141 mV	140 mV	127 mV	- 148 mV	- 4 mV	- 4 mV	

Table A 22: Release of radionuclides in leach solutions from spent fuel corrosion tests (FIAP: Fraction of inventory in the aequeous phase)									
Sample:	K 10 (Pellet): 7,369 g (=6,496 g HM) 7,366 g at test termination		Solution: 95% sat NaCl Temperature: 25 °C			Starting volume: 200 ml Final volume: 164 ml			*FIC= Fraction of Inventory in Container
	Washcycles		Static tests						Acid cleaning
Nuclide	1.Cycl (32d)	2.Cycl (42 d)	1. Sampling	2. Sampling	3. Sampling	4. Sampling	5. Sampling		of the container
			126 d (cumul.)	189 d (cumul.)	280 d (cumul.)	516 d (cumul.)	752 d (cumul.)		FIC*
	0,45 µm -filtered		0,45 µm -filtered					1,8 nm-filtered	
RU106	5,24E-06	4,48E-06	2,38E-05	3,19E-06	1,00E-06	8,72E-07	<6,75E-7	<7,44E-7	4,19E-06
CS134	1,28E-02	6,44E-03	1,49E-03	1,88E-03	2,50E-03	4,58E-03	1,36E-02	1,66E-02	1,03E-06
CS137	1,04E-02	5,39E-03	1,32E-03	1,62E-03	2,19E-03	3,81E-03	1,19E-02	1,48E-02	1,04E-06
EU154	8,42E-06	5,22E-06	4,71E-05	4,53E-05	3,80E-06	5,20E-07	<1,98E-7	<2,09E-7	5,28E-06
EU155	7,14E-06	6,67E-06	5,95E-05	5,10E-05	3,23E-06		<5,72E-7	<6,18E-7	4,53E-06
SB125	1,08E-04	1,67E-05	1,28E-05		1,30E-05	4,98E-05	1,38E-04	1,39E-04	3,09E-07
SR90	2,11E-04	3,03E-05	9,54E-05	1,73E-04	2,72E-04	3,87E-04	3,57E-04	4,02E-04	6,04E-05
CE144	3,29E-05	3,47E-06	2,81E-05	6,22E-07	<2,54E-07	2,06E-06	1,58E-06	2,48E-06	8,55E-06
TC99	<6,65E-05						4,05E-04	4,24E-04	
AG110M	1,22E-03		6,29E-03	<1,08E-04	1,78E-02	2,40E-02	1,87E-02	1,95E-02	
AM241	2,68E-05	7,55E-06	4,15E-05	3,05E-05	9,64E-06	1,45E-06	3,04E-06	5,90E-07	2,43E-05
AM243	<4,51E-06		2,50E-05	<1,32E-05	5,02E-05				
NP237	8,16E-05	6,28E-05	<7,15E-06	<6,78E-06			<3,85E-5	1,13E-05	
NP239	<4,51E-06		1,11E-05						
CM244	8,13E-06	4,79E-06	2,83E-05	9,75E-05	9,69E-06	5,30E-07	1,82E-09	2,00E-08	8,15E-05
CM242	3,04E-06	1,97E-06	1,50E-05	6,27E-05	3,52E-06	8,43E-07	<1,45E-7	<4,80E-7	6,03E-05
PU238	1,20E-05	2,48E-06	3,46E-06	2,08E-05	1,50E-05	9,22E-06	1,95E-07	2,82E-07	3,27E-05
PU239/40	2,04E-05	1,84E-06	3,25E-06	1,75E-05	1,38E-05	7,38E-06	4,25E-08	3,99E-07	2,91E-05
PU241	1,15E-05	2,36E-06				7,53E-06	1,97E-07	1,67E-07	
U	3,95E-5				1,73E-5	6,73E-6	3,21E-06	3,45E-06	2,75E-5
pH	6,42	4,86	7,84	7,4	6,99	7,8	8,32	8,32	
Eh	264 mV	320 mV	141 mV	140 mV	127 mV	- 148 mV	- 4 mV	- 4 mV	

Table A 23: Concentration of radionuclides in leach solutions from spent fuel corrosion tests (mol/L)										
Sample:	K 10 (Pellet): 7,369 g (=6,496 g HM)		Solution: 95% sat NaCl			Starting volume: 200 ml				
		7,366 g at test termination	Temperature: 25 °C			Final volume: 164 ml				
	Washcycles		Static tests						Acid cleaning	
Nuclide	1.Cycl (32d)	2.Cycl (42 d)	1. Sampling	2. Sampling	3. Sampling	4. Sampling	5. Sampling		of the liner	
			126 d (cumul.)	189 d (cumul.)	280 d (cumul.)	516 d (cumul.)	752 d (cumul.)			
	0,45 µm -filtered		0,45 µm -filtered					1,8 nm-filtered		
RU106	5,80E-09	4,96E-09	2,63E-08	3,73E-09	1,25E-09	1,16E-09	<9,11E-10	<1,00E-9	4,21E-09	
CS134	1,21E-05	6,06E-06	1,40E-06	1,87E-06	2,64E-06	5,16E-06	1,56E-05	1,91E-05	8,81E-10	
CS137	9,79E-06	5,07E-06	1,24E-06	1,61E-06	2,31E-06	4,29E-06	1,36E-05	1,70E-05	8,86E-10	
EU154	3,71E-10	2,30E-10	2,07E-09	2,11E-09	1,88E-10	2,74E-11	<1,06E-11	<1,12E-11	2,11E-10	
EU155	3,15E-10	2,94E-10	2,62E-09	2,38E-09	1,60E-10		<3,07E-11	<3,32E-11	1,81E-10	
SB125	6,26E-10	9,67E-11	7,38E-11		8,43E-11	3,45E-10	9,75E-10	9,79E-10	1,63E-12	
SR90	9,16E-08	1,32E-08	4,14E-08	7,93E-08	1,33E-07	2,01E-07	1,89E-07	2,13E-07	2,39E-08	
CE144	2,68E-08	2,82E-09	2,29E-08	5,35E-10	<2,32E-10	2,01E-09	1,56E-09	2,46E-09	6,32E-09	
TC99	<2,48E-08						1,84E-07	1,93E-07		
AG110M	4,09E-08		2,11E-07	<3,84E-09	6,72E-07	9,63E-07	7,64E-07	7,96E-07		
AM241	1,78E-09	5,00E-10	2,74E-09	2,14E-09	7,16E-10	1,15E-10	2,45E-10	4,76E-11	1,46E-09	
AM243	<2,98E-10		1,65E-09	<9,21E-10	3,73E-09					
NP237	8,03E-09	6,18E-09	<7,04E-10	<7,06E-10			<4,62E-9	1,36E-09		
NP239	<4,44E-10		1,09E-09							
CM244	1,16E-10	6,83E-11	4,03E-10	1,47E-09	1,55E-10	9,05E-12	3,16E-14	3,48E-13	1,06E-09	
CM242	4,33E-11	2,80E-11	2,14E-10	9,45E-10	5,63E-11	1,44E-11	<2,52E-12	<8,35E-12	7,81E-10	
PU238	1,84E-08	3,80E-09	5,31E-09	3,37E-08	2,58E-08	1,69E-08	3,66E-10	5,28E-10	4,56E-08	
PU239/40	3,13E-08	2,83E-09	4,99E-09	2,84E-08	2,38E-08	1,36E-08	7,95E-11	7,47E-10	4,07E-08	
PU241	1,77E-08	3,62E-09				1,38E-08	3,69E-10	3,13E-10		
U	5,04E-6				2,48E-6	1,03E-6	5,00E-07	5,38E-07	3,19E-06	
pH	6,42	4,86	7,84	7,4	6,99	7,8	8,32	8,32		
Eh	264 mV	320 mV	141 mV	140 mV	127 mV	- 148 mV	- 4 mV	- 4 mV		

Table A 24: Incremental rates of radionuclide release from spent fuel corrosion tests (FIAP/d)

Sample:	**K 10** (Pellet): 7,369 g (=6,496 g HM)		Solution: 95% sat **NaCl**			Starting volume: 200 ml			
	7,366 g at test termination		Temperature: 25 °C			Final volume: 164 ml			
	Washcycles		**Static tests**						**Acid cleaning**
Nuclide	1.Cycl (32d)	2.Cycl (42 d)	1. Sampling	2. Sampling	3. Sampling	4. Sampling	5. Sampling		of the liner
			126 d (cumul.)	189 d (cumul.)	280 d (cumul.)	516 d (cumul.)	752 d (cumul.)		
	0,45 µm -filtered		0,45 µm -filtered					1,8 nm-filtered	
RU106	1,64E-07	1,07E-07	4,6E-7						
CS134	4,01E-04	1,53E-04	2,9E-5	7,5E-6	8,0E-6	9,5E-6	3,8E-5		
CS137	3,25E-04	1,28E-04	2,5E-5	5,9E-6	7,3E-6	7,5E-6	3,4E-5		
EU154	2,63E-07	1,24E-07	9,1E-7	1,2E-8					
EU155	2,23E-07	1,59E-07	1,1E-6				2,4E-9		
SB125	3,38E-06	3,98E-07	2,5E-7		1,4E-7	1,6E-7	3,8E-7		
SR90	6,59E-06	7,23E-07	1,8E-6	1,3E-6	1,2E-6	5,6E-7			
CE144	1,03E-06	8,26E-08	5,4E-7			7,7E-9			
TC99	<2,08E-06						1,7E-6		
AG110M	3,82E-05		<1,2E-4		2,0E-4	3,1E-5			
AM241	8,39E-07	1,80E-07	8,0E-7				6,9E-9		
AM243	<1,41E-07		4,8E-7		4,2E-7				
NP237	2,55E-06	1,49E-06	1,4E-7	2,4E-10			1,6E-7		
NP239	<1,41E-07		2,1E-7						
CM244	2,54E-07	1,14E-07	5,4E-7	1,1E-6					
CM242	9,50E-08	4,69E-08	2,9E-7	7,7E-7					
PU238	3,75E-07	5,90E-08	6,7E-8	2,8E-7					
PU239/40	6,37E-07	4,39E-08	6,3E-8	2,3E-7					
PU241	3,61E-07	5,61E-08				3,2E-8			
U	1,23E-6				1,9E-7				
pH	6,42	4,86	7,84	7,4	6,99	7,8	8,32	8,32	
Eh	264 mV	320 mV	141 mV	140 mV	127 mV	- 148 mV	- 4 mV	- 4 mV	

Table A 25: Activity of leach solutions from spent fuel corrosion tests (Bq/ml)								
Sample:	**F 3** (Fragment): 0,020 g (=0,018 g HM)		Solution: 95% sat **NaCl**			Starting volume: 200 ml		
			Temperature: 25 °C			Final volume: 164 ml		
	Washcycles		**Static tests**					**Acid cleaning**
Nuclide	1.Cycl (33d)	2.Cycl (43 d)	1. Sampling	2. Sampling	3. Sampling	4. Sampling	5. Sampling	of the liner
			125 d (cumul.)	188 d (cumul.)	279 d (cumul.)	513 d (cumul.)	749 d (cumul.)	
	0,45 µm -filtered		0,45 µm -filtered					
RU106		1,37E+01	2,56E+01	5,28E+01	2,01E+02	9,12E+01	2,73E+01	1,50E+02
CS134	7,59E+03	4,37E+02	1,83E+02	5,02E+02	1,11E+03	2,01E+03	4,27E+03	4,81E+02
CS137	6,66E+03	5,18E+02	2,98E+02	7,18E+02	1,19E+03	2,33E+03	6,28E+03	1,25E+03
EU154	3,06E+00		3,84E-01	5,07E-01	5,73E-01	4,00E+00	<9,01E-01	8,53E+01
EU155			2,13E-01	3,80E-01	9,86E-02	3,00E+00	<1,17E+00	3,54E+01
SB125		4,81E+00	2,56E+00	5,07E+00	1,26E+01	1,10E+01	2,90E+01	1,04E+01
SR90	8,14E+03	9,62E+01	1,71E+02	8,44E+01	1,72E+02	4,99E+02	2,03E+03	1,02E+04
CE144	5,81E+01		5,12E-01	3,38E-01	<1,1E+01	<8,0E-01	<3,44E+00	1,20E+02
TC99	1,48E+00						3,02E-01	
AG110M		3,70E+00	1,36E+00	1,22E+00	1,26E+00	1,06E+00	<2,27E+00	
AM241	5,18E+01		4,26E-01	4,22E-01	<1,3E-01	8,6E-01	2,27E-01	2,46E+01
AM243								
NP237							<5,87E-02	
NP239								
CM244	2,59E-01				<5,7E-02		3,78E-01	1,23E+02
CM242	1,37E-02						<1,51E-02	2,24E-01
PU238	5,92E-01		8,40E-02	6,75E-02	6,88E-02	1,39E+00	3,83E+00	7,40E+01
PU239/40			2,21E-02	2,53E-02	2,29E-02	2,20E-01	3,75E-01	1,50E+01
PU241	5,55E+00	2,96E+01	5,30E+00			6,4E+01	1,55E+02	
U	*4,0E-1 µg/ml*					*1,3E-2 µg/ml*	*5,8E-2 µg/ml*	*2,6E-1 µg/ml*
pH	4,92	5,22	8,15	7,89	7,28	7,18	7,8	
Eh	368 mV	309 mV	125 mV	156 mV	195 mV	-78 mV	-148 mV	

Table A 26: Release of radionuclides in leach solutions from spent fuel corrosion tests (FIAP: Fraction of inventory in the aequeous phase)								
								*FIC= Fraction
Sample:	F 3 (Fragment): 0,020 g (=0,018 g HM)			Solution: 95% sat NaCl		Starting volume: 200 ml		of Inventory
				Temperature: 25 °C		Final volume: 164 ml		in Container
	Washcycles		Static tests					Acid cleaning
Nuclide	1.Cycl (33d)	2.Cycl (43 d)	1. Sampling	2. Sampling	3. Sampling	4. Sampling	5. Sampling	of the liner
			125 d (cumul.)	188 d (cumul.)	279 d (cumul.)	513 d (cumul.)	749 d (cumul.)	(FIC*)
	0,45 µm -filtered		0,45 µm -filtered					
RU106		7,40E-05	1,77E-04	3,46E-04	1,39E-03	7,04E-04	3,67E-04	2,41E-03
CS134	2,23E-02	1,46E-03	6,92E-04	1,79E-03	3,95E-03	7,29E-03	2,01E-02	2,88E-03
CS137	1,24E-02	9,72E-04	5,65E-04	1,28E-03	2,02E-03	3,72E-03	1,00E-02	2,67E-03
EU154	9,13E-05		1,21E-05	1,51E-05	1,64E-05	1,09E-04	<2,58E-05	3,23E-03
EU155			1,37E-05	2,31E-05	5,77E-06	1,71E-04	<7,34E-05	2,91E-03
SB125		4,08E-04	2,38E-04	4,45E-04	1,09E-03	9,47E-04	3,02E-03	1,39E-03
SR90	2,22E-02	2,65E-04	4,74E-04	2,22E-04	4,27E-04	1,17E-03	4,77E-03	3,20E-02
CE144	2,72E-04		4,66E-06	2,91E-06	<1,1E-04	<8,8E-06	<7,81E-05	3,15E-03
TC99	2,45E-02						4,10E-03	
AG110M		2,56E-02	1,36E-02	1,16E-02	1,33E-02	1,35E-02	<6,60E-02	
AM241	1,04E-02		7,36E-05	6,89E-05	<1,9E-05	1,2E-04	2,62E-05	3,91E-03
AM243	1,66E-28							
NP237							<3,01E-02	
NP239								
CM244	6,62E-06				<1,4E-06		8,55E-06	3,71E-03
CM242	5,39E-06						<1,09E-04	1,67E-03
PU238	2,02E-05		2,89E-06	2,19E-06	2,11E-06	4,00E-05	1,09E-04	2,82E-03
PU239/40			4,83E-06	5,23E-06	4,46E-06	4,01E-05	6,72E-05	3,60E-03
PU241	7,92E-06	4,30E-05	7,85E-06			8,0E-05	2,00E-04	
U	4,85E-03					1,32E-04	5,76E-04	3,44E-03
pH	4,92	5,22	8,15	7,89	7,28	7,18	7,8	
Eh	368 mV	309 mV	125 mV	156 mV	195 mV	-78 mV	-148 mV	

Table A 27: Concentration of radionuclides in leach solutions from spent fuel corrosion tests (mol/L)								
Sample:	F 3 (Fragment): 0,020 g (=0,018 g HM)		Solution: 95% sat NaCl			Starting volume: 200 ml		
			Temperature: 25 °C			Final volume: 164 ml		
	Washcycles		Static tests					Acid cleaning
Nuclide	1.Cycl (33d)	2.Cycl (43 d)	1. Sampling	2. Sampling	3. Sampling	4. Sampling	5. Sampling	of the liner
			125 d (cumul.)	188 d (cumul.)	279 d (cumul.)	513 d (cumul.)	749 d (cumul.)	
	0,45 µm -filtered		0,45 µm -filtered					
RU106		2,22E-10	5,32E-10	1,10E-09	4,69E-09	2,53E-09	1,34E-09	6,58E-09
CS134	5,68E-08	3,72E-09	1,77E-09	4,84E-09	1,13E-08	2,23E-08	6,27E-08	6,67E-09
CS137	3,16E-08	2,48E-09	1,44E-09	3,47E-09	5,78E-09	1,14E-08	3,12E-08	6,19E-09
EU154	1,09E-11		1,45E-12	1,92E-12	2,20E-12	1,56E-11	<3,76E-12	3,51E-10
EU155			1,64E-12	2,92E-12	7,75E-13	2,44E-11	<1,07E-11	3,16E-10
SB125		6,41E-12	3,73E-12	7,39E-12	1,92E-11	1,78E-11	5,78E-11	1,99E-11
SR90	2,62E-08	3,12E-10	5,58E-10	2,76E-10	5,66E-10	1,65E-09	6,85E-09	3,43E-08
CE144	6,00E-10		1,03E-11	6,78E-12	<2,7E-10	<2,3E-11	<2,10E-10	6,32E-09
TC99	2,48E-08						5,06E-09	
AG110M		2,33E-09	1,24E-09	1,11E-09	1,36E-09	1,47E-09	<7,32E-09	
AM241	1,87E-09		1,32E-11	1,31E-11	<3,8E-12	2,5E-11	5,74E-12	6,38E-10
AM243								
NP237							<9,80E-09	
NP239								
CM244	2,56E-13				<5,9E-14		4,03E-13	1,30E-10
CM242	2,08E-13						<5,15E-12	5,89E-11
PU238	8,42E-11		1,20E-11	9,67E-12	9,86E-12	2,00E-10	5,54E-10	1,07E-08
PU239/40			2,01E-11	2,30E-11	2,09E-11	2,00E-10	3,41E-10	1,36E-08
PU241	3,30E-11	1,79E-10	3,27E-11			4,0E-10	1,01E-09	
U	1,68E-06					5,46E-08	2,43E-07	1,08E-06
pH	4,92	5,22	8,15	7,89	7,28	7,18	7,8	
Eh	368 mV	309 mV	125 mV	156 mV	195 mV	-78 mV	-148 mV	

Table A 28: Incremental rates of radionuclide release from spent fuel corrosion tests (FIAP/d)									
Sample:	F 3 (Fragment): 0,020 g (=0,018 g HM)			Solution: 95% sat NaCl		Starting volume: 200 ml			
				Temperature: 25 °C		Final volume: 164 ml			
	Washcycles		Static tests					Acid cleaning	
Nuclide	1.Cycl (33d)	2.Cycl (43 d)	1. Sampling	2. Sampling	3. Sampling	4. Sampling	5. Sampling	of the liner	
	33	43	125 d (cumul.)	188 d (cumul.)	279 d (cumul.)	513 d (cumul.)	749 d (cumul.)		
	0,45 µm -filtered		0,45 µm -filtered						
RU106		1,72E-06	3,6E-6	2,8E-6	1,2E-5				
CS134	6,74E-04	3,39E-05	1,4E-5	1,8E-5	2,5E-5	1,5E-5	5,5E-5		
CS137	3,76E-04	2,26E-05	1,2E-5	1,2E-5	8,9E-6	7,8E-6	2,7E-5		
EU154	2,77E-06		2,5E-7	5,8E-8	2,3E-8	4,0E-7			
EU155			2,8E-7	1,6E-7		7,1E-7			
SB125		9,49E-06	4,8E-6	3,5E-6	7,3E-6		8,9E-6		
SR90	6,73E-04	6,16E-06	9,7E-6		2,4E-6	3,3E-6	1,5E-5		
CE144	8,25E-06		9,5E-8		1,2E-6		2,9E-7		
TC99	7,42E-04						1,7E-5		
AG110M		5,96E-04	<2,8E-4		2,6E-5	4,5E-6	2,2E-4		
AM241	3,16E-04		1,5E-6			4,2E-7			
AM243	5,04E-30								
NP237							1,3E-4		
NP239									
CM244	2,01E-07				1,5E-8		3,6E-8		
CM242	1,63E-07						4,6E-7		
PU238	6,13E-07		5,9E-8		4,6E-10	1,6E-7	3,0E-7		
PU239/40			9,8E-8	1,1E-8		1,5E-7	1,2E-7		
PU241	2,40E-07	1,00E-06	1,6E-7			3,4E-7	5,1E-7		
U	1,47E-04					5,6E-7	1,9E-6		
pH	4,92	5,22	8,15	7,89	7,28	7,18	7,8		
Eh	368 mV	309 mV	125 mV	156 mV	195 mV	-78 mV	-148 mV		

Table A 29: Activity of leach solutions from spent fuel corrosion tests (Bq/ml)									
Sample:	F 4 (Fragment): 0,008 g (=0,007 g HM)			Solution: 95% sat NaCl		Starting volume: 200 ml			
				Temperature: 25 °C		Final volume: ...ml			
	Washcycles		**Static tests**					**Acid cleaning**	
Nuclide	1.Cycl (33d)	2.Cycl (43 d)	1. Sampling	2. Sampling	3. Sampling	4. Sampling	5. Sampling	of the liner	
			125 d (cumul.)	188 d (cumul.)	279 d (cumul.)	516 d (cumul.)			
	0,45 µm -filtered		0,45 µm -filtered						
RU106		7,40E+00	2,12E+01	3,14E+01	<1,2E+01	3,51E+01			
CS134	2,52E+03	2,13E+02	2,21E+02	5,17E+02	9,86E+02	1,55E+03			
CS137	2,63E+03	2,40E+02	2,08E+02	4,66E+02	7,69E+02	3,05E+03			
EU154		1,37E-01	2,25E-01	6,36E-01	1,15E+00	1,83E+00			
EU155			<4,2E-01	<4,2E-01	3,81E-01	2,26E+00			
SB125		1,55E+00	1,32E+00	3,39E+00	5,19E+00	<8,30E-01			
SR90	4,07E+02	3,33E+01	1,06E+02	4,24E+01	1,04E+02	6,14E+02			
CE144			<4,2E-01	<4,2E-01	<1,2E+01	<8,3E-01			
TC99	1,48E+00								
AG110M		7,40E-01	4,67E-01	1,44E+00	1,3E+00	1,37E+00			
AM241	5,18E+01	<3,70E-01	<4,2E-01	<4,2E-01	<1,2E+01	4,10E-01			
AM243									
NP237									
NP239									
CM244	1,71E-01				<5,8E-02				
CM242	6,83E-03								
PU238			6,37E-02	2,92E-01	1,27E-01	2,94E+00			
PU239/40			2,34E-02	1,02E-01	4,38E-02	7,59E-01			
PU241	4,44E+00	2,29E+02				1,29E+01			
U	*4,0E-1 µg/ml*					*5,8E-3 µg/ml*			
pH	5,51	5,25	8,1	7,6	7,28	7,02			
Eh	308 mV	330 mV	109 mV	150 mV	195 mV	-92 mV			

Table A 30: Release of radionuclides in leach solutions from spent fuel corrosion tests (FIAP: Fraction of inventory in the aequeous phase)								
Sample:	F 4 (Fragment): 0,008 g (=0,007 g HM)		Solution: 95% sat NaCl			Starting volume: 200 ml		
			Temperature: 25 °C			Final volume: ...ml		
	Washcycles		Static tests					Acid cleaning
Nuclide	1.Cycl (33d)	2.Cycl (43 d)	1. Sampling	2. Sampling	3. Sampling	4. Sampling	5. Sampling	of the liner
			125 d (cumul.)	188 d (cumul.)	279 d (cumul.)	516 d (cumul.)		
	0,45 µm -filtered		0,45 µm -filtered					
RU106		9,12E-05	3,68E-04	5,13E-04	<1,8E-04	6,77E-04		
CS134	1,85E-02	1,70E-03	2,08E-03	4,61E-03	8,28E-03	1,41E-02		
CS137	1,22E-02	1,12E-03	9,85E-04	2,08E-03	3,24E-03	1,22E-02		
EU154		1,04E-05	1,78E-05	4,75E-05	8,12E-05	1,25E-04		
EU155			<6,8E-05	<6,4E-05	5,44E-05	3,21E-04		
SB125		3,19E-04	3,06E-04	7,44E-04	1,07E-03	<1,79E-04		
SR90	2,77E-03	2,28E-04	7,37E-04	2,78E-04	6,41E-04	3,60E-03		
CE144			<9,7E-06	<9,1E-06	<2,3E-04	<2,3E-05		
TC99	6,12E-02							
AG110M		1,12E-02	1,17E-02	3,40E-02	2,8E-02	4,37E-02		
AM241	2,60E-02	<1,76E-04	<1,8E-04	<1,7E-04	<4,4E-03	1,37E-04		
AM243								
NP237								
NP239								
CM244	1,09E-05				<3,4E-06			
CM242	6,72E-06							
PU238			5,48E-06	2,37E-05	9,70E-06	2,12E-04		
PU239/40			1,28E-05	5,25E-05	2,13E-05	3,46E-04		
PU241	1,58E-05	8,28E-04				4,07E-05		
U	1,21E-02					1,47E-04		
pH	5,51	5,25	8,1	7,6	7,28	7,02		
Eh	308 mV	330 mV	109 mV	150 mV	195 mV	-92 mV		

Table A 31: Concentration of radionuclides in leach solutions from spent fuel corrosion tests (mol/L)									
Sample:	F 4 (Fragment): 0,008 g (=0,007 g HM)			Solution: 95% sat NaCl		Starting volume: 200 ml			
				Temperature: 25 °C		Final volume: ...ml			
	Washcycles		Static tests					Acid cleaning	
Nuclide	1.Cycl (33d)	2.Cycl (43 d)	1. Sampling	2. Sampling	3. Sampling	4. Sampling	5. Sampling	of the liner	
			125 d (cumul.)	188 d (cumul.)	279 d (cumul.)	516 d (cumul.)			
	0,45 µm -filtered		0,45 µm -filtered						
RU106		1,10E-10	4,42E-10	6,53E-10	<2,4E-10	9,75E-10			
CS134	1,88E-08	1,73E-09	2,13E-09	4,98E-09	9,49E-09	1,72E-08			
CS137	1,25E-08	1,14E-09	1,01E-09	2,25E-09	3,72E-09	1,49E-08			
EU154		4,98E-13	8,51E-13	2,40E-12	4,36E-12	7,15E-12			
EU155			<3,3E-12	<3,3E-12	2,92E-12	1,84E-11			
SB125		2,00E-12	1,92E-12	4,94E-12	7,57E-12	<1,34E-12			
SR90	1,31E-09	1,08E-10	3,48E-10	1,39E-10	3,40E-10	2,03E-09			
CE144			<8,5E-12	<8,5E-12	<2,3E-10	<2,4E-11			
TC99	2,48E-08								
AG110M		4,07E-10	4,24E-10	1,31E-09	1,2E-09	1,90E-09			
AM241	1,87E-09	<1,26E-11	<1,3E-11	<1,3E-11	<3,6E-10	1,18E-11			
AM243									
NP237									
NP239									
CM244	1,69E-13				<5,9E-14				
CM242	1,04E-13								
PU238			9,12E-12	4,17E-11	1,82E-11	4,22E-10			
PU239/40			2,12E-11	9,25E-11	3,99E-11	6,90E-10			
PU241	2,64E-11	1,38E-09				8,11E-11			
U	1,68E-06					2,44E-08			
pH	5,51	5,25	8,1	7,6	7,28	7,02			

Table A 32: Incremental rates of radionuclide release from spent fuel corrosion tests (FIAP/d)									
Sample:	F 4 (Fragment): 0,008 g (=0,007 g HM)			Solution: 95% sat NaCl		Starting volume: 200 ml			
				Temperature: 25 °C		Final volume: ...ml			
	Washcycles		Static tests					Acid cleaning	
Nuclide	1.Cycl (33d)	2.Cycl (43 d)	1. Sampling	2. Sampling	3. Sampling	4. Sampling	5. Sampling	of the liner	
	33	43	125 d (cumul.)	188 d (cumul.)	279 d (cumul.)	516 d (cumul.)			
	0,45 µm -filtered		0,45 µm -filtered						
RU106		2,12E-06	7,5E-6	2,6E-6		2,2E-6			
CS134	5,59E-04	3,95E-05	4,3E-5	4,2E-5	4,3E-5	2,7E-5			
CS137	3,70E-04	2,61E-05	2,0E-5	1,8E-5	1,4E-5	3,9E-5			
EU154		2,42E-07	3,6E-7	4,9E-7	4,0E-7	2,1E-7			
EU155			1,4E-6			1,1E-6			
SB125		7,41E-06	6,2E-6	7,2E-6	4,1E-6				
SR90	8,41E-05	5,31E-06	1,5E-5		4,2E-6	1,3E-5			
CE144			2,0E-7		2,5E-6				
TC99	1,86E-03								
AG110M		2,60E-04	<2,4E-4	3,6E-4		7,3E-5			
AM241	7,89E-04	<4,09E-06	3,7E-6		4,7E-5				
AM243									
NP237									
NP239									
CM244	3,31E-07				3,7E-8				
CM242	2,04E-07								
PU238			1,1E-7	2,9E-7		8,5E-7			
PU239/40			2,6E-7	6,4E-7		1,4E-6			
PU241	4,80E-07	1,93E-05				1,7E-7			
U	3,68E-04					6,2E-7			
pH	5,51	5,25	8,1	7,6	7,28	7,02			

Table A 33: Activity of leach solutions from spent fuel corrosion tests (Bq/ml)										
Sample:	**P 1 (Powder)**: 2,9 g (=2,556 g HM)			Solution: 95% sat **NaCl**		Starting volume: 200 ml				
				Temperature: 25 °C		Final volume: 164 ml				
	Ultrasonic cleaning of		**Washcycle**	**Static tests**						**Acid cleaning**
Nuclide	**18,942 g** (=16,681 g HM)		(40 d)	1. Sampling	2. Sampling	3. Sampling	4. Sampling	5. Sampling		of the
	powder in 200 ml DIW			80 d (cumul.)	123 d (cumul.)	241 d (cumul.)	449 d (cumul.)	657 d (cumul.)		container
	0,45 µm -filtered			0,45 µm -filtered					1,8 nm-filtered	
RU106	6,92E+03	6,29E+03	8,51E+02	5,99E+02	5,01E+02	7,42E+02	4,08E+02	4,74E+03	2,68E+03	4,78E+03
CS134	4,03E+06	5,11E+06	5,77E+04	5,73E+04	8,50E+04	2,03E+05	4,03E+05	1,28E+06	1,49E+06	2,89E+04
CS137	6,03E+06	7,66E+06	1,10E+05	1,03E+05	1,55E+05	3,97E+05	8,28E+05	3,57E+06	4,25E+06	1,07E+05
EU154	2,75E+02	2,85E+02	2,90E+02	1,32E+03	1,68E+03	3,55E+03	1,66E+03	2,36E+02	<7,01E+00	5,48E+03
EU155	1,50E+02	1,35E+02	1,45E+02	7,51E+02	9,12E+02	1,69E+03	7,43E+02	7,46E+01	<9,76E+00	1,58E+03
SB125	9,25E+02	8,14E+02	1,22E+03	5,99E+02	7,05E+02	2,06E+03	3,54E+03	2,02E+03	1,18E+03	1,20E+03
SR90	8,88E+04	1,33E+05	1,42E+04	1,91E+04	3,14E+04	1,07E+05	2,22E+05	7,20E+05	7,85E+05	2,96E+05
CE144	1,11E+03	9,99E+02	7,40E+02	2,18E+03	8,50E+02	1,51E+02	7,90E+01	5,33E+02	3,18E+02	6,89E+03
TC99	<1,48E+00				<2,97E+00			1,22E+01	1,41E+01	
AG110M			4,81E+01	<4,28E-01	<4,25E-01	7,61E+01	1,24E+02	2,02E+02	1,01E+02	
AM241	3,26E+01	2,59E+01	4,07E+01	1,45E+02	1,18E+02	3,87E+02	1,45E+02	2,00E+01	1,29E+00	1,06E+03
AM243	<3,70E-01	3,70E-01		2,31E+01	6,31E+00	6,47E+01				
NP237				8,55E-03	8,50E-02		4,48E-01	1,57E-01	2,97E-01	
NP239	<3,70E-01	3,70E-01								
CM244	2,07E+02	2,22E+02		9,59E+02	8,08E+02	2,95E+03	1,33E+03	8,95E+01	3,27E+00	5,66E+04
CM242	5,92E+00	5,55E+00		1,27E+01	6,89E+00	2,92E+01	1,00E+01	3,70E-01	<3,44E-02	1,23E+02
PU238	1,33E+02	1,25E+02	1,48E+02	1,07E+02	1,62E+02	1,11E+02	5,67E+02	3,04E+02	3,10E+01	3,49E+04
PU239/40	2,11E+01	2,00E+01	2,74E+01	1,92E+01	2,93E+01	2,11E+01	9,49E+01	5,22E+01	5,28E+00	5,70E+03
PU241	3,89E+03	3,74E+03		2,58E+03	4,74E+03		1,15E+04	8,57E+03	8,28E+02	1,08E+06
U	*1,5E+1 µg/ml*			*8,4E+0 µg/ml*	*4,6E+0 µg/ml*	*9,3E+0 µg/ml*	*8,7E+0 µg/ml*	*8,2E+0 µg/ml*	*8,7E+0 µg/ml*	*1,5E+2 µg/ml*
pH		4,86	4,86	6,57	7,68	7,7	6,78	7,43	7,34	
Eh		320 mV	320 mV	335 mV	171 mV	150 mV	-75 mV	-75 mV	- 75 mV	

Table A 34: Release of radionuclides in leach solutions from spent fuel corrosion tests (FIAP: Fraction of inventory in the aequeous phase)										*FIC= Fraction of Inventory on Container wall
Sample:	**P 1 (Powder)**: 2,9 g (=2,556 g HM)			Solution: 95% sat **NaCl**		Starting volume: 200 ml				
				Temperature: 25 °C		Final volume: 164 ml				
	Ultrasonic cleaning of		**Washcycle**	**Static tests**						**Acid cleaning**
Nuclide	**18,942 g** (=16,681 g HM)		(40 d)	1. Sampling	2. Sampling	3. Sampling	4. Sampling	5. Sampling		of the container (FIC*)
	powder in 200 ml DIW			80 d (cumul.)	123 d (cumul.)	241 d (cumul.)	449 d (cumul.)	657 d (cumul.)		
	0,45 µm -filtered			0,45 µm -filtered					1,8 nm-filtered	
RU106	3,03E-05	3,41E-05	4,07E-05	2,86E-05	2,26E-05	3,16E-05	2,17E-05	2,48E-04	1,40E-04	5,30E-04
CS134	1,25E-02	1,76E-02	1,50E-03	1,49E-03	2,09E-03	4,70E-03	1,01E-02	3,15E-02	3,66E-02	1,19E-03
CS137	1,19E-02	1,52E-02	1,43E-03	1,35E-03	1,91E-03	4,61E-03	9,11E-03	3,86E-02	4,59E-02	1,57E-03
EU154	8,65E-06	9,20E-06	6,33E-05	2,87E-04	3,47E-04	6,90E-04	3,13E-04	4,36E-05	<1,30E-06	1,43E-03
EU155	9,16E-06	8,61E-06	6,41E-05	3,32E-04	3,82E-04	6,65E-04	2,91E-04	2,87E-05	<3,76E-06	8,96E-04
SB125	7,53E-05	7,16E-05	7,82E-04	3,84E-04	4,27E-04	1,17E-03	2,10E-03	1,18E-03	6,88E-04	1,11E-03
SR90	2,56E-04	3,87E-04	2,73E-04	3,66E-04	5,68E-04	1,82E-03	3,59E-03	1,14E-02	1,25E-02	6,40E-03
CE144	5,50E-06	6,51E-06	4,65E-05	1,37E-04	5,04E-05	8,44E-06	6,01E-06	3,98E-05	2,38E-05	1,25E-03
TC99	<2,59E-05				<3,21E-04			1,14E-03	1,32E-03	
AG110M			3,31E-03	<2,95E-05	<2,76E-05	4,67E-03	1,09E-02	1,74E-02	8,72E-03	
AM241	6,92E-06	5,15E-06	4,85E-05	1,73E-04	1,33E-04	4,10E-04	1,34E-04	1,81E-05	1,17E-06	1,16E-03
AM243	<1,76E-06	1,76E-06		7,17E-04	1,85E-04	1,79E-03				
NP237				3,69E-05	3,46E-04		1,61E-03	5,55E-04	1,05E-03	
NP239	<1,76E-06	1,76E-06								
CM244	5,60E-06	6,07E-06		1,74E-04	1,39E-04	4,77E-04	2,05E-04	1,35E-05	4,94E-07	1,18E-02
CM242	2,46E-06	3,74E-06		1,10E-04	5,65E-05	2,26E-04	1,39E-04	5,05E-06	<4,70E-07	6,34E-03
PU238	4,81E-06	4,54E-06	3,51E-05	2,54E-05	3,64E-05	2,34E-05	1,13E-04	5,93E-05	6,05E-06	9,17E-03
PU239/40	4,87E-06	4,61E-06	4,12E-05	2,90E-05	4,17E-05	2,82E-05	1,19E-04	6,45E-05	6,52E-06	9,44E-03
PU241	5,86E-06	5,72E-06		2,63E-05	4,57E-05		1,00E-04	7,32E-05	7,07E-06	1,27E-02
U	1,92E-04			7,06E-04	3,64E-04	6,90E-04	6,10E-04	5,63E-04	5,94E-04	1,34E-02
pH		4,86	4,86	6,57	7,68	7,7	6,78	7,43	7,34	
Eh		320 mV	320 mV	335 mV	171 mV	150 mV	-75 mV	-75 mV	- 75 mV	

Table A 35: Concentration of radionuclides in leach solutions from spent fuel corrosion tests (mol/L)										
Sample:	**P 1 (Powder)**: 2,9 g (=2,556 g HM)			Solution: 95% sat **NaCl**		Starting volume: 200 ml				
				Temperature: 25 °C		Final volume: 164 ml				
	Ultrasonic cleaning of		**Washcycle**	**Static tests**						**Acid cleaning**
Nuclide	**18,942 g** (=16,681 g HM)		(40 d)	1. Sampling	2. Sampling	3. Sampling	4. Sampling	5. Sampling		of the container
	powder in 200 ml DIW			80 d (cumul.)	123 d (cumul.)	241 d (cumul.)	449 d (cumul.)	657 d (cumul.)		
	0,45 µm -filtered			0,45 µm -filtered					1,8 nm-filtered	
RU106	1,32E-08	1,48E-08	1,77E-08	1,25E-08	1,04E-08	1,54E-08	1,13E-08	1,32E-07	7,44E-08	2,10E-07
CS134	4,63E-06	6,50E-06	5,56E-07	5,52E-07	8,18E-07	1,96E-06	4,47E-06	1,42E-05	1,65E-05	4,01E-07
CS137	4,39E-06	5,61E-06	5,31E-07	4,98E-07	7,49E-07	1,92E-06	4,04E-06	1,74E-05	2,07E-05	5,27E-07
EU154	1,50E-10	1,59E-10	1,10E-09	4,98E-09	6,36E-09	1,34E-08	6,49E-09	9,22E-10	<2,74E-11	2,26E-08
EU155	1,59E-10	1,49E-10	1,11E-09	5,76E-09	7,00E-09	1,30E-08	6,05E-09	6,07E-10	<7,94E-11	1,41E-08
SB125	1,71E-10	1,63E-10	1,78E-09	8,73E-10	1,03E-09	3,00E-09	5,73E-09	3,27E-09	1,91E-09	2,30E-09
SR90	4,38E-08	6,61E-08	4,66E-08	6,26E-08	1,03E-07	3,49E-07	7,34E-07	2,38E-06	2,60E-06	9,95E-07
CE144	1,76E-09	2,08E-09	1,49E-08	4,38E-08	1,71E-08	3,03E-09	2,30E-09	1,55E-08	9,27E-09	3,63E-07
TC99	<3,80E-09				<4,99E-08			2,05E-07	2,36E-07	
AG110M		3,30E-36	4,37E-08	<3,88E-10	<3,86E-10	6,91E-08	1,72E-07	2,80E-07	1,40E-07	
AM241	1,80E-10	1,34E-10	1,26E-09	4,51E-09	3,66E-09	1,20E-08	4,17E-09	5,76E-10	3,71E-11	2,74E-08
AM243	<4,57E-11	4,57E-11		1,87E-08	5,09E-09	5,22E-08				
NP237				1,43E-09	1,42E-08		7,48E-08	2,62E-08	4,96E-08	
NP239	<6,81E-11	6,81E-11								
CM244	3,14E-11	3,40E-11		9,76E-10	8,22E-10	3,00E-09	1,37E-09	9,25E-11	3,38E-12	6,00E-08
CM242	1,38E-11	2,10E-11		6,19E-10	3,35E-10	1,42E-09	9,34E-10	3,46E-11	<3,21E-12	3,23E-08
PU238	2,90E-09	2,74E-09	2,12E-08	1,53E-08	2,32E-08	1,59E-08	8,14E-08	4,37E-08	4,45E-09	5,03E-06
PU239/40	2,94E-09	2,78E-09	2,49E-08	1,75E-08	2,67E-08	1,92E-08	8,63E-08	4,75E-08	4,80E-09	5,18E-06
PU241	3,54E-09	3,45E-09		1,59E-08	2,92E-08		7,23E-08	5,39E-08	5,20E-09	6,99E-06
U	9,66E-06			3,55E-05	1,93E-05	3,89E-05	3,67E-05	3,45E-05	3,64E-05	6,14E-04
pH		4,86	4,86	6,57	7,68	7,7	6,78	7,43	7,34	
Eh		320 mV	320 mV	335 mV	171 mV	150 mV	-75 mV	-75 mV	- 75 mV	

Table A 36: Incremental rates of radionuclide release from spent fuel corrosion tests (FIAP/d)									
Sample:	**P 1 (Powder)**: 2,9 g (=2,556 g HM)			Solution: 95% sat **NaCl**		Starting volume: 200 ml			
				Temperature: 25 °C		Final volume: 164 ml			
	Ultrasonic cleaning of		**Washcycle**	**Static tests**					**Acid cleaning**
Nuclide	**18,942 g** (=16,681 g HM)		(40 d)	1. Sampling	2. Sampling	3. Sampling	4. Sampling	5. Sampling	of the liner
	powder in 200 ml DIW			80 d (cumul.)	123 d (cumul.)	241 d (cumul.)	449 d (cumul.)	657 d (cumul.)	
	0,45 µm -filtered			0,45 µm -filtered					
RU106			1,02E-06	7,2E-7		8,7E-8		1,1E-6	
CS134			3,76E-05	3,7E-5	1,6E-5	2,3E-5	2,7E-5	1,0E-4	
CS137			3,59E-05	3,4E-5	1,5E-5	2,4E-5	2,3E-5	1,4E-4	
EU154			1,58E-06	7,2E-6	1,8E-6	3,1E-6			
EU155			1,60E-06	8,3E-6	1,6E-6	2,6E-6			
SB125			1,96E-05	9,6E-6	1,5E-6	6,5E-6	4,8E-6		
SR90			6,82E-06	9,2E-6	5,2E-6	1,1E-5	9,0E-6	3,8E-5	
CE144			1,16E-06	3,4E-6				1,6E-7	
TC99				0,0E+0	7,5E-6			5,5E-6	
AG110M			8,28E-05	<7,4E-7		3,9E-5	3,1E-5	3,2E-5	
AM241			1,21E-06	4,3E-6		2,4E-6			
AM243				1,8E-5		1,4E-5			
NP237				9,2E-7	7,2E-6		7,8E-6		
NP239									
CM244				4,3E-6		2,9E-6			
CM242				2,8E-6		1,5E-6			
PU238			8,77E-07	6,3E-7	2,9E-7		4,4E-7		
PU239/40			1,03E-06	7,2E-7	3,3E-7		4,5E-7		
PU241							4,8E-7		
U				1,8E-5		2,9E-6			
pH		4,86	4,86	6,57	7,68	7,7	6,78	7,43	
Eh		320 mV	320 mV	335 mV	171 mV	150 mV	-75 mV	-75 mV	

Table A 37: Activity of leach solutions from spent fuel corrosion tests (Bq/ml)

Sample:	**P 2 (Powder)**: 2,95 g (=2,600 g HM)			Solution: 95% sat **NaCl**		Starting volume: 200 ml			
				Temperature: 25 °C		Final volume: ... ml			
	Ultrasonic cleaning of		**Washcycle**	**Static tests**					**Acid cleaning**
Nuclide	**18,942 g** (=16,681 g HM)		(40 d)	1. Sampling	2. Sampling	3. Sampling	4. Sampling	5. Sampling	of the liner
	powder in 200 ml DIW			80 d (cumul.)	123 d (cumul.)	241 d (cumul.)	449 d (cumul.)	657 d (cumul.)	
	0,45 µm -filtered			0,45 µm -filtered					
RU106	6,92E+03	6,29E+03		5,95E+02	4,87E+02	8,30E+02	4,83E+03		
CS134	4,03E+06	5,11E+06	4,2E+04	6,50E+04	9,96E+04	2,22E+05	8,76E+05		
CS137	6,03E+06	7,66E+06	7,4E+04	1,15E+05	1,81E+05	4,28E+05	1,78E+06		
EU154	2,75E+02	2,85E+02	5,2E+02	9,51E+02	1,57E+03	5,96E+03	1,11E+04		
EU155	1,50E+02	1,35E+02		5,16E+02	9,11E+02	2,72E+03	4,99E+03		
SB125	9,25E+02	8,14E+02		3,82E+02	5,80E+02	2,40E+03	1,70E+03		
SR90	8,88E+04	1,33E+05	1,2E+04	1,47E+04	2,69E+04	1,30E+05	5,09E+05		
CE144	1,11E+03	9,99E+02	9,8E+02	1,27E+03	3,86E+02	5,84E+02	3,30E+03		
TC99	<1,48E+00				<2,97E+00	1,85E+01			
AG110M				<4,25E-01	<4,24E-01	2,20E+02	9,67E+02		
AM241	3,26E+01	2,59E+01		1,02E+02	2,56E+02	8,22E+02	1,19E+03		
AM243	<3,70E-01	3,70E-01		4,59E+01	2,29E+01	6,36E+01			
NP237				3,40E-02	6,35E-02		2,27E-01		
NP239	<3,70E-01	3,70E-01							
CM244	2,07E+02	2,22E+02		8,64E+02	1,25E+03	6,93E+03	1,27E+04		
CM242	5,92E+00	5,55E+00		1,03E+01	1,37E+01	8,56E+01	1,19E+02		
PU238	1,33E+02	1,25E+02		6,37E+01	1,74E+02	2,34E+02	3,75E+02		
PU239/40	2,11E+01	2,00E+01		1,10E+01	2,92E+01	4,39E+01	6,25E+01		
PU241	3,89E+03	3,74E+03					7,42E+03		
U	*1,5E+1 µg/ml*					*5,7E+0 µg/ml*	*1,6E+1 µg/ml*		
pH		4,86	4,86	7,53	7,49	7,58	6,13		
Eh		320 mV	320 mV	171 mV	135 mV	156 mV	-17 mV		

Table A 38: Release of radionuclides in leach solutions from spent fuel corrosion tests (FIAP: Fraction of inventory in the aequeous phase)										
									FIC= Fraction	
Sample:	**P 2 (Powder)**: 2,95 g (=2,600 g HM)			Solution: 95% sat **NaCl**		Starting volume: 200 ml			of Inventory	
				Temperature: 25 °C		Final volume: ... ml			in Container	
	Ultrasonic cleaning of		**Washcycle**	**Static tests**					**Acid cleaning**	
Nuclide	**18,942 g** (=16,681 g HM)		(40 d)	1. Sampling	2. Sampling	3. Sampling	4. Sampling	5. Sampling	of the liner	
	powder in 200 ml DIW			80 d (cumul.)	123 d (cumul.)	241 d (cumul.)	449 d (cumul.)	657 d (cumul.)		
	0,45 µm -filtered			0,45 µm -filtered						
RU106	3,03E-05	3,41E-05		2,79E-05	2,16E-05	3,89E-05	2,53E-04			
CS134	1,25E-02	1,76E-02	9,9E-04	1,66E-03	2,41E-03	5,35E-03	2,15E-02			
CS137	1,19E-02	1,52E-02	9,4E-04	1,47E-03	2,19E-03	4,91E-03	1,93E-02			
EU154	8,65E-06	9,20E-06	1,1E-04	2,04E-04	3,18E-04	1,15E-03	2,05E-03			
EU155	9,16E-06	8,61E-06		2,25E-04	3,75E-04	1,08E-03	1,92E-03			
SB125	7,53E-05	7,16E-05		2,41E-04	3,45E-04	1,40E-03	9,93E-04			
SR90	2,56E-04	3,87E-04	2,2E-04	2,77E-04	4,79E-04	2,18E-03	8,08E-03			
CE144	5,50E-06	6,51E-06	5,0E-05	7,87E-05	2,25E-05	3,72E-05	2,47E-04			
TC99	<2,59E-05				<3,14E-04	1,85E-03				
AG110M				<2,88E-05	<2,71E-05	1,57E-02	8,36E-02			
AM241	6,92E-06	5,15E-06		1,19E-04	2,83E-04	8,31E-04	1,08E-03			
AM243	<1,76E-06	1,76E-06		1,40E-03	6,59E-04	1,73E-03				
NP237				1,44E-04	2,54E-04		8,03E-04			
NP239	<1,76E-06	1,76E-06								
CM244	5,60E-06	6,07E-06		1,54E-04	2,11E-04	1,11E-03	1,92E-03			
CM242	2,46E-06	3,74E-06		8,82E-05	1,11E-04	8,43E-04	1,63E-03			
PU238	4,81E-06	4,54E-06		1,49E-05	3,84E-05	4,85E-05	7,32E-05			
PU239/40	4,87E-06	4,61E-06		1,64E-05	4,09E-05	5,79E-05	7,73E-05			
PU241	5,86E-06	5,72E-06					6,34E-05			
U	1,92E-04					4,15E-04	1,08E-03			
pH		4,86	4,86	7,53	7,49	7,58	6,13			
Eh		320 mV	320 mV	171 mV	135 mV	156 mV	-17 mV			

Table A 39: Concentration of radionuclides in leach solutions from spent fuel corrosion tests (mol/L)										
Sample:	**P 2 (Powder)**: 2,95 g (=2,600 g HM)			Solution: 95% sat **NaCl**		Starting volume: 200 ml				
				Temperature: 25 °C		Final volume: ... ml				
	Ultrasonic cleaning of		**Washcycle**	**Static tests**					**Acid cleaning**	
Nuclide	**18,942 g** (=16,681 g HM)		(40 d)	1. Sampling	2. Sampling	3. Sampling	4. Sampling	5. Sampling	of the liner	
	powder in 200 ml DIW			80 d (cumul.)	123 d (cumul.)	241 d (cumul.)	449 d (cumul.)			
	0,45 µm -filtered			0,45 µm -filtered						
RU106	1,32E-08	1,48E-08		1,24E-08	1,01E-08	1,94E-08	1,34E-07			
CS134	4,63E-06	6,50E-06	3,7E-07	6,26E-07	9,59E-07	2,26E-06	9,71E-06			
CS137	4,39E-06	5,61E-06	3,6E-07	5,54E-07	8,74E-07	2,08E-06	8,68E-06			
EU154	1,50E-10	1,59E-10	1,9E-09	3,60E-09	5,93E-09	2,28E-08	4,34E-08			
EU155	1,59E-10	1,49E-10		3,96E-09	6,99E-09	2,14E-08	4,06E-08			
SB125	1,71E-10	1,63E-10		5,57E-10	8,46E-10	3,64E-09	2,75E-09			
SR90	4,38E-08	6,61E-08	3,8E-08	4,81E-08	8,82E-08	4,26E-07	1,68E-06			
CE144	1,76E-09	2,08E-09	1,6E-08	2,56E-08	7,74E-09	1,36E-08	9,62E-08			
TC99	<3,80E-09				<4,97E-08	3,10E-07				
AG110M		3,30E-36		<3,86E-10	<3,85E-10	2,36E-07	1,34E-06			
AM241	1,80E-10	1,34E-10		3,16E-09	7,94E-09	2,47E-08	3,42E-08			
AM243	<4,57E-11	4,57E-11		3,70E-08	1,85E-08	5,13E-08				
NP237				5,67E-09	1,06E-08		3,79E-08			
NP239	<6,81E-11	6,81E-11								
CM244	3,14E-11	3,40E-11		8,79E-10	1,27E-09	7,09E-09	1,31E-08			
CM242	1,38E-11	2,10E-11		5,03E-10	6,69E-10	5,41E-09	1,11E-08			
PU238	2,90E-09	2,74E-09		9,12E-09	2,49E-08	3,35E-08	5,39E-08			
PU239/40	2,94E-09	2,78E-09		1,00E-08	2,66E-08	4,00E-08	5,68E-08			
PU241	3,54E-09	3,45E-09					4,66E-08			
U	9,66E-06					2,38E-05	6,64E-05			
pH		4,86	4,86	7,53	7,49	7,58	6,13			
Eh		320 mV	320 mV	171 mV	135 mV	156 mV	-17 mV			

Table A 40: Incremental rates of radionuclide release from spent fuel corrosion tests (FIAP/d)									
Sample:	**P 2 (Powder)**: 2,95 g (=2,600 g HM)			Solution: 95% sat **NaCl**		Starting volume: 200 ml			
				Temperature: 25 °C		Final volume: ... ml			
	Ultrasonic cleaning of		**Washcycle**	**Static tests**					**Acid cleaning**
Nuclide	**18,942 g** (=16,681 g HM)		(40 d)	1. Sampling	2. Sampling	3. Sampling	4. Sampling	5. Sampling	of the liner
	powder in 200 ml DIW		40	80 d (cumul.)	123 d (cumul.)	241 d (cumul.)	449 d (cumul.)		
	0,45 µm -filtered			0,45 µm -filtered					
RU106				7,0E-7		1,6E-7	1,0E-6		
CS134			2,5E-05	4,2E-5	1,9E-5	2,6E-5	7,9E-5		
CS137			2,4E-05	3,7E-5	1,9E-5	2,4E-5	7,0E-5		
EU154			2,7E-06	5,1E-6	2,9E-6	7,2E-6	4,7E-6		
EU155				5,6E-6	3,8E-6	6,1E-6	4,4E-6		
SB125				6,0E-6	2,7E-6	9,1E-6			
SR90			5,4E-06	6,9E-6	5,1E-6	1,5E-5	2,9E-5		
CE144			1,2E-06	2,0E-6		1,4E-7	1,0E-6		
TC99					7,3E-6	1,3E-5			
AG110M				<7,2E-7		1,3E-4	3,3E-4		
AM241				3,0E-6	4,0E-6	4,8E-6	1,4E-6		
AM243				3,5E-5		9,4E-6			
NP237				3,6E-6	2,8E-6		3,9E-6		
NP239									
CM244				3,9E-6	1,5E-6	7,7E-6	4,2E-6		
CM242				2,2E-6	6,4E-7	6,3E-6	4,0E-6		
PU238				3,7E-7	5,7E-7	1,1E-7	1,3E-7		
PU239/40				4,1E-7	5,9E-7	1,6E-7	1,1E-7		
PU241							3,0E-7		
U						3,5E-6	3,3E-6		
pH		4,86	4,86	7,53	7,49	7,58	6,13		
Eh		320 mV	320 mV	171 mV	135 mV	156 mV	-17 mV		

Table A 41: Activity of leach solutions from spent fuel corrosion tests (Bq/ml)								
Sample:	**K 13** (Pellet):	7,878 g (=6,937 g HM)			Solution: 95% sat **NaCl**		Starting volume: 200 ml	
		7,882 g at test termination			Temperature: 150 °C		Final volume: .... ml	
	Washcycles		**Static tests**			**Acid cleaning**		
Nuclide	1.Cycl (63d)	2.Cycl (0,16 d	1. Sampling	2. Sampling		of the liner		
			61 d (cumul.)	173 d (cumul.)				
	0,45 µm -filtered		0,45 µm -filtered		1,8 nm-filtered			
RU106				<1,12E+1	<1,30E+1			
CS134	3,05E+06	1,05E+03	9,25E+04	1,55E+05	1,55E+5			
CS137	7,06E+06	2,53E+03	2,00E+05	3,78E+05	3,77E+5			
EU154		1,00E+00		<1,45E+0	<1,73E+0			
EU155				<2,12E+0	<2,51E+0			
SB125		4,80E+00	5,00E+01	3,83E+01	<5,63E+0			
SR90	3,40E+05	3,00E+02	2,20E+04	2,75E+04	2,63E+4			
CE144				<5,39E+0	<6,37E+0			
TC99	<3,01E-2			<5,95E-2	<6,93E-2			
AG110M				<3,72E+0	<4,33E+0			
AM241	2,39E+02	4,00E+00	1,56E+03	1,49E-01	9,53E-1			
AM243								
NP237			3,00E-01	<1,49E-2	<8,66E-3			
NP239								
CM244				<7,44E-2	1,04E+0			
CM242				<2,23E-2	<1,73E-2			
PU238	3,00E+01	7,50E+01	3,30E+01	1,67E+00	7,82E+0			
PU239/40	1,00E+01	8,00E+00	8,00E+00	7,64E-01	1,13E+0			
PU241				4,20E+01	8,56E+01			
U				1,71E-2 ug/mL	3,20E-2 ug/mL			
pH mess	5,94		6,08		5,78			
Eh	331 mV		312 mV		xx mV			

Table A 42: Release of radionuclides in leach solutions from spent fuel corrosion tests (FIAP: Fraction of inventory in the aequeous phase)								
Sample:	**K 13** (Pellet): 7,878 g (=6,937 g HM)				Solution: 95% sat **NaCl**		Starting volume: 200 ml	
		7,882 g at test termination			Temperature: 150 °C		Final volume: .... ml	
	Washcycles		**Static tests**			**Acid cleaning**		
Nuclide	1.Cycl (63d)	2.Cycl (0,16 d	1. Sampling	2. Sampling		of the liner		
			61 d (cumul.)	173 d (cumul.)				
	0,45 µm -filtered		0,45 µm -filtered		1,8 nm-filtered			
RU106				<4,43E-7	<5,14E-7			
CS134	4,13E-2	7,11E-06	1,25E-03	2,15E-03	2,15E-3			
CS137	3,48E-2	6,23E-06	9,85E-04	1,78E-03	1,77E-3			
EU154		4,36E-08		<1,22E-7	<1,46E-7			
EU155				<3,91E-7	<4,64E-7			
SB125		7,32E-07	1,53E-05	1,17E-05	<1,73E-6			
SR90	2,46E-3	1,09E-06	1,59E-04	1,90E-04	1,82E-4			
CE144				<3,60E-7	<4,26E-7			
TC99	1,27E-6			<2,38E-6	<2,77E-6			
AG110M				<3,19E-4	<3,71E-4			
AM241	8,84E-5	7,40E-07	5,77E-04	5,07E-08	3,24E-7			
AM243								
NP237			4,76E-04	<2,25E-5	<1,31E-5			
NP239								
CM244				<4,95E-9	6,93E-8			
CM242				<4,74E-7	<3,68E-7			
PU238	2,64E-6	3,30E-06	2,91E-06	1,40E-07	6,56E-7			
PU239/40	5,55E-6	2,22E-06	4,44E-06	4,03E-07	5,96E-7			
PU241				1,59E-07	3,25E-07			
U				5,01E-7 ug/mL	9,37E-7 ug/mL			
pH mess	5,94		6,08		5,78			
Eh	331 mV		312 mV		xx mV			

Table A 43: Concentration of radionuclides in leach solutions from spent fuel corrosion tests (mol/L)								
Sample:	**K 13** (Pellet):	7,878 g (=6,937 g HM)			Solution: 95% sat **NaCl**		Starting volume: 200 ml	
		7,882 g at test termination			Temperature: 150 °C		Final volume: .... ml	
	Washcycles		**Static tests**			**Acid cleaning**		
Nuclide	1.Cycl (63d)	2.Cycl (0,16 d	1. Sampling	2. Sampling		of the liner		
			61 d (cumul.)	173 d (cumul.)				
	0,45 µm -filtered		0,45 µm -filtered		1,8 nm-filtered			
RU106				<5,51E-10	<6,40E-10			
CS134	4,15E-05	1,43E-08	1,26E-06	2,27E-06	2,27E-6			
CS137	3,49E-05	1,25E-08	9,89E-07	1,88E-06	1,87E-6			
EU154		4,10E-12		<6,05E-12	<7,22E-12			
EU155				<1,94E-11	<2,30E-11			
SB125		9,05E-12	9,43E-11	7,64E-11	<1,12E-11			
SR90	1,14E-06	1,01E-09	7,39E-08	9,28E-08	8,88E-8			
CE144				<3,29E-10	<3,89E-10			
TC99	5,05E-10			<9,98E-10	<1,16E-9			
AG110M				<1,20E-8	<1,40E-8			
AM241	6,25E-09	1,05E-10	4,08E-08	3,77E-12	2,41E-11			
AM243								
NP237			5,01E-08	<2,49E-9	<1,45E-9			
NP239								
CM244				<7,94E-14	1,11E-12			
CM242				<7,60E-12	<5,90E-12			
PU238	4,33E-09	1,08E-08	4,76E-09	2,41E-10	1,13E-9			
PU239/40	9,09E-09	7,28E-09	7,28E-09	6,95E-10	1,03E-9			
PU241				2,75E-10	5,60E-10			
U				7,18E-8 ug/mL	1,34E-7 ug/mL			
pH mess	5,94		6,08		5,78			
Eh	331 mV		312 mV		xx mV			

Table A 44: Incremental rates of radionuclide release from spent fuel corrosion tests (FIAP/d)								
Sample:	**K 13** (Pellet): 7,878 g (=6,937 g HM)				Solution: 95% sat **NaCl**		Starting volume: 200 ml	
	7,882 g at test termination				Temperature: 150 °C		Final volume: .... ml	
	Washcycles		**Static tests**			**Acid cleaning**		
Nuclide	1.Cycl (63d)	2.Cycl (0,16 d	1. Sampling	2. Sampling		of the liner		
	63		61 d (cumul.)	173 d (cumul.)				
	0,45 µm -filtered		0,45 µm -filtered		1,8 nm-filtered			
RU106				4,0E-9				
CS134	6,56E-4		2,1E-5	1,9E-5				
CS137	5,52E-4		1,6E-5	1,6E-5				
EU154				1,1E-9				
EU155				3,5E-9				
SB125			2,5E-7	1,0E-7				
SR90	3,90E-5		2,6E-6	1,7E-6				
CE144				3,2E-9				
TC99				2,1E-8				
AG110M				2,8E-6				
AM241	1,40E-6		9,5E-6	4,5E-10				
AM243								
NP237			7,8E-6	2,0E-7				
NP239								
CM244				4,4E-11				
CM242				4,2E-9				
PU238	4,19E-8		4,8E-8	1,2E-9				
PU239/40	8,81E-8		7,3E-8	3,6E-9				
PU241				1,4E-9				
U				4,5E-9				
pH mess	5,94		6,08	5,78				
Eh	331 mV		312 mV	xx mV				